The Study of Senescent Pathology in *Caenorhabditis elegans*

Ann F. Gilliat

Department of Genetics, Evolution and Environment

University College London

PhD Thesis

Declaration

I, Ann F. Gilliat, confirm that the work presented in this thesis is my own. Where information has been derived from other sources, I confirm that this has been indicated in the thesis.

……..

Ann F. Gilliat

Abstract

The aim of this work is to identify the biological mechanisms of ageing, which remain poorly understood. One model organism widely used by biogerontologists is *C. elegans*. Here lifespan is, one assumes, a function of life limiting senescent pathologies. However, the cause of senescent pathologies and the identity of those pathologies that limit life are unclear. Therefore the main goals of my PhD were to understand where senescent pathologies come from and to identify the pathologies that limit worm lifespan. Using Nomarski microscopy, pathology within various tissues of the germline and soma was examined during ageing. The *C. elegans* intestine is the major somatic organ and is a likely location for lethal, senescent pathology. It undergoes major atrophy during ageing, which is demonstrated here to be driven by intestinal biomass conversion into yolk. To determine the pathology state at death, we performed necropsy analysis on the corpses of elderly worms. This revealed that the majority of early deaths occurred with an enlarged pharynx, reflecting severe bacterial infection. Combining survival and pathology data into a new pathology-centred approach has allowed new insights to be obtained into the determinants of late life disease and lifespan.

It has long been widely believed that ageing was caused by molecular damage. However the recently proposed hyperfunction theory, which is related to the antagonistic pleiotropy theory, suggests that a major contributory cause of ageing is actually quasi-programmes. These are biological programmes essential for early-life fitness that continue to operate in a non-adaptive fashion in older organisms, such as intestinal biomass conversion to yolk. Thus hyperfunction may contribute to the development of age-related pathologies, some of which will cause death.

Impact statement

Thanks to numerous breakthroughs in medical science over the last century, we are now living longer than ever. Unfortunately this has also resulted in many diseases that were once relatively rare, such as Alzheimer's, becoming prevalent in our population. Therefore treatments or cures for these diseases are urgently needed. However a great frustration for medical professionals when treating the elderly is that when one ageing related ailment is alleviated, others may subsequently emerge. Thus old people need to repeatedly return to hospital for treatment. A more efficient approach would be to treat a central mechanism of ageing to delay multiple age-related pathologies in tandem.

In support of this, findings from biogerontology using animal models suggests the possibility that one could combat many age-related diseases at once by treating ageing itself. However a more realistic idea proposed recently is that during ageing an array of pathologies develop, with mutliple underlying causes, some of which are potentially life limiting (Gems 2015). Interventions that inhibit mechanisms that result in lethal age-related pathology, particularly those that generate multiple life limiting pathologies, will cause large extensions to lifespan, such as those seen in animal models, by suppressing senescent polymorbidity. However to intervene in and delay age-related pathology, one ideally needs to know what biological mechanisms cause them. For obvious reasons, studying ageing in humans is laborious and time consuming. Therefore short-lived model organisms, in which genetic manipulation is relatively straightforward, have been employed. This has revealed signalling pathways that modulate ageing, including the insulin/IGF-1 signalling (IIS) pathway and the TOR pathway. These include targets for drugs which proved able to extend lifespan and improve late life health in a range of animal models, including mice (Harrison et al. 2010; Kenyon 2010). Thus model organisms can help us to understand and to treat ageing.

My work has focused on the study of senescent pathology in *C. elegans*, in particular what causes them and which of them cause death. For the latter we used necropsy analysis, which identified a lethal pharyngeal pathology ('P death') that occurs in a subpopulation of shorter-lived worms (Zhao et al., 2017). By combining mortality and pathology data, mortality could be deconvolved to reveal how different interventions that alter lifespan affect the timing and prevalence of P death. This can give indications of conserved mechanisms that promote age-related pathology, which could give clues about the origins of pathology in ageing humans. For example, both P death in worms and osteoarthritis in elderly humans are promoted by mechanical damage in early life (Davies et al. 2016; Zhao et al., 2017). Thus, age-related disease in both humans and *C. elegans* can be promoted by conserved etiologies. This validates *C. elegans* as a powerful tool to study senescent pathologies.

Dedicated to Mum, Dad and Gareth.

Whose love and support have made this all possible.

Acknowledgements

I would like to take the opportunity to thank everyone who has been involved in supporting me and contributing to my PhD.

Firstly I would like to show my appreciation for the following members of the Gems' laboratory: Marina Ezcurra, Yuan Zhao, Alexandre Benedetto, Catherine Au, Evgeniy Galimov, Jennifer Tullet, Filipe Cabreiro, Michele Riesen, Thanet Sornda, Hongyuan Wang, Yila de la Guardia and Carina Kern. Thank you for all the help both within the laboratory and with personal guidance over the last few years. I would also like to thank my collaborators Matthias Ziehm and Zachary Pincus whose expertise added essential insights into my work.

I have been fortunate to share an office with many wonderful people, including Danny Filer, Sahar Emran, Jorge Castillo Quan, Fiona Kerr, Oyinkansola Adesakin and bonus member Thomas Moens. Thank you for all the laughter and conversation that created such a positive atmosphere to work in. I would also like to thank all the members of the Institute of Healthy Ageing, UCL and my second supervisor Nazif Alic for useful discussions and advice throughout my PhD.

I am hugely grateful to Wellcome and the UCL impact award for providing the funding needed to complete this work.

A special thank you to my partner, Gareth Jones, who provided indispensable emotional support over the last few years. Thank you for all the cups of tea when I needed them most.

Finally I owe a huge amount of gratitude to my supervisor David Gems, whose guidance has proved invaluable. I am very grateful for his open door policy, allowing me to seek his help or advice whenever I needed it.

Abbreviations

C. elegans	*Caenorhabditis elegans*
CFU	Colony forming unit
Daf-c	Dauer constitutive
Daf-d	Dauer defective
DG	Distal gonad
DR	Dietary restriction
DTC	Distal tip cell
FdUMP	Fluorodeoxyuridine monophosphate
FUDR	5-fluoro-2'-deoxyurdine
GFP	Green fluorescent protein
GP	Germ cell proliferation
IIS	Insulin/IGF-1 signalling
L1-4	Larval stages 1 – 4
NGM	Nematode growth media
n.s.	Not significant
OP50-RFP	*E. coli* OP50 expressing DsRed
PA	Physiological apoptosis
PG	Proximal gonad
P death	Death with pharyngeal infection
p death	Death with pharyngeal atrophy
RFP	Red fluorescent protein
RNAi	RNA-mediated interference
ROS	Reactive oxygen species
S.D.	Standard deviation
SEM	Standard error of the mean
SIA	Stress-induced apoptosis
SOD	Superoxide dismutase
TEM	Transmission electron microscopy
TOR	Target of rapamycin
Uno-o	Unfertilised oocyte overproducer
WT	Wild-type
YP	Yolk protein

Table of contents

Abstract……3

Impact Statement……..4

Acknowledgements……..7

Abbreviations……8

Table of contents……..9

List of figures and tables……..14

Chapter 1 Introduction 19

1.1 Introduction to ageing 19

1.1.1 Treating ageing as a disease 20

1.1.2 Evolutionary theories of ageing 21

1.2 The biological mechanisms of ageing 23

1.2.1 Ageing as the result of molecular damage 24

1.2.2 The disposable soma theory 26

1.2.3 The hyperfunction theory..... 27

1.2.4 Hyperfunction and age-related pathology 30

1.3 *Caenorhabditis elegans* as a model organism..... 32

1.3.1 *C. elegans* life cycle 35

1.3.2 *C. elegans* anatomy 36

1.3.3 *C. elegans* nomenclature 39

1.4 Ageing research using *C. elegans* 40

1.4.1 Pathways involved in ageing in *C. elegans* 41

1.4.2 Hyperfunction as a possible cause of senescent pathology in *C. elegans*..... 45

1.4.3 Lethal pathology in ageing *C. elegans* 47

1.5 Consolidating ageing theories..... 49

1.6 Aims 51

Chapter 2 Materials and Methods..... 54

2.1 *C. elegans* maintenance and methods..... 54

2.1.1 Stock maintenance 54
2.1.2 List of *C. elegans* strains 55
2.1.3 Elimination of contamination 56
2.1.4 Synchronizing populations 57
2.1.5 Survival and necropsy analysis 57
2.1.6 Individual liquid culture 58
2.1.7 RNA-mediated interference 59
2.2 Bacterial methods 59
2.2.1 Preparation of bacterial cultures 59
2.2.2 Inhibition of bacterial growth 60
2.3 Staining methods 61
2.3.1 DAPI staining 61
2.3.2 SYTO 12/13 staining 61
2.4 Microscopy 62
2.5 Preparation for imaging 62
2.5.1 Microscope systems 62
2.5.2 Electron microscopy 63
2.5.3 Measuring the pathology state of *C. elegans* tissues 64
2.5.4 Uterine tumours 64
2.5.5 Gonad atrophy 64
2.5.6 Intestinal atrophy and lumen distension 65
2.5.7 Yolky/lipid pools 66
2.5.8 Pharyngeal pathology 66
2.5.9 Tracking pathology in individual worms 67
2.6 Measuring pharyngeal function 68
2.6.1 Pharyngeal pumping rate 68
2.6.2 Serotonin assay 68
2.7 Statistics 68
2.8 Reagents 69

Chapter 3 The development and impact of pathologies in the *C. elegans* germ line 71
3.1 Part 1: Investigating the effect of *C. elegans'* uterine tumours on mortality 71

3.2 Introduction 71
3.2.1 *C. elegans* uterine tumours as a model for mammalian tumours 73
3.2.2 Manipulating uterine tumour growth 73
3.3 Results 77
3.3.1 Mating delays development of uterine tumours in wild-type hermaphrodites 77
3.3.2 FUDR can decrease uterine tumour size in wild-type and in the *mdl-1* mutant 79
3.3.3 Uterine tumours do not affect lifespan 83
3.3.4 Uterine tumours become infected with *E. coli* in aged *C. elegans* 85
3.4 Discussion 92
3.4.1 Uterine tumours are not a life-limiting pathology in *C. elegans* 92
3.4.2 Uterine tumours of aged worms become infected with *E. coli*94
3.4.3 *C. elegans* as a model for benign mammalian tumours 98
3.5 Part 2: Altering apoptosis levels changes the rate of gonad disintegration in *C. elegans* hermaphrodites 102
3.6 Introduction to the structure of the *C. elegans* gonad 102
3.6.1 Apoptosis in *C. elegans* germline 104
3.6.2 The role of apoptosis in the germline of the *C. elegans* hermaphrodite 106
3.6.3 Degeneration of the *C. elegans* gonad due to apoptotic run-on 107
3.7 Results 110
3.7.1 Increasing apoptosis in hermaphrodites accelerates gonad disintegration 110
3.7.2 Decreasing physiological apoptosis reduces accelerated gonad disintegration 112
3.7.3 Inhibition of apoptosis in post-reproductive hermaphrodites suppresses gonad degeneration 115
3.7.4 Feminization does not induce gonad disintegration in males 117

3.7.5 Endoreduplication contributes to oocyte hypertrophy 119
3.8 Discussion 122
3.8.1 Run-on of physiological apoptosis contributes to gonad disintegration..... 122
3.8.2 The balance with germ cell proliferation 123

Chapter 4 Intestinal biomass conversion to yolk causes age-related intestinal atrophy in *C. elegans* 126
4.1 Introduction to the *C. elegans* intestine..... 126
4.1.1 The intestine as a site of life-limiting pathology 127
4.1.2 Obstacles to analysing intestinal atrophy 129
4.1.3 Bacterial proliferation as a possible cause of intestinal atrophy 130
4.2 Results 132
4.2.1 The *C. elegans* hermaphrodite intestine undergoes rapid atrophy during early ageing 132
4.2.2 The biomass conversion theory 139
4.2.3 Males do not accumulate lipid pools during ageing..... 141
4.2.4 The male intestine does not undergo atrophy 145
4.2.5 Feminised males undergo intestinal atrophy..... 149
4.2.6 Intestinal atrophy in feminised males is not due to proliferative *E. coli* 154
4.2.7 Blocking yolk production does not reduce intestinal atrophy in feminised males 157
4.2.8 Autophagy promotes intestinal biomass conversion to yolk 159
4.2.9 Later yolk production increases reproductive fitness 161
4.3 Discussion 164
4.3.1 Autophagy-dependent biomass conversion causes intestinal atrophy 164
4.3.2 Intestinal atrophy as a life-limiting pathology in *C. elegans*. 167

Chapter 5 Pharyngeal infection is a life-limiting pathology in ageing *C. elegans* 170
5.1 Introduction to the *C. elegans* pharynx 170

5.1.1 Age-related functional decline and tissue degeneration in the pharynx 171
5.1.2 Studying age-related pharyngeal pathology 173
5.2 Results 176
5.2.1 Pharyngeal pathology increases with age and correlates with lifespan 176
5.2.2 Early deaths are associated with pharyngeal swelling 180
5.2.3 Two forms of death explain mortality deceleration in ageing *C. elegans* populations 182
5.2.4 Bacterial infection is the primary cause of pharyngeal swelling 183
5.2.5 Pharyngeal infection is associated with a sudden decline in function 189
5.2.6 Mechanical damage may promote pharyngeal infection 191
5.2.7 Evidence of wound healing in the pharyngeal cuticle as defence against bacterial infection 200
5.3 Discussion 204
5.3.1 Latent infection may lead to P death in ageing *C. elegans* . 204
5.3.2 Deconvolving mortality to solve the mysteries of ageing 207

Chapter 6 Conclusions 209

Appendix 1: Statistics……212
Appendix 2: Publications……216
Bibliography……257

List of figures and tables

Chapter 1:

Figure 1.1. The oxidative damage theory of ageing. 25
Figure 1.2. The hyperfunction theory of ageing. 28
Figure 1.3. Ageing results in the generation of multiple pathologies. 31
Figure 1.4. The *C. elegans* life cycle. 36
Figure 1.5. The *C. elegans* male and hermaphrodite. 37
Figure 1.6. The structure of the *C. elegans'* pharynx. 38
Figure 1.7. Structure of the *C. elegans* hermaphrodite intestine. 38
Figure 1.8. The insulin/IGF-1 signalling pathway in *C. elegans*. 42
Figure 1.9. TOR-centric model for the hyperfunction theory of ageing. .. 44
Figure 1.10. Age-related pathology caused by hypertrophy in *C. elegans*. 46
Figure 1.11. Death fluorescence in *C. elegans*. 48

Chapter 3

Figure 3.1. Ageing of the *C. elegans* hermaphrodite reproductive system. 72
Figure 3.2. The uterus pathology scoring system. 76
Figure 3.3. The effect of mating on uterine tumour growth in *C. elegans* hermaphrodites. 78
Figure 3.4. The effect of FUDR on tumour formation in wild-type *C. elegans*. 80
Figure 3.5. The effect of FUDR on tumour formation in wild-type and *mdl-1(tm311)* mutant *C. elegans*. 82
Figure 3.6. The effect of 50μM FUDR on tumour formation in wild-type and *mdl-1(tm311)*. 83
Figure 3.7. No effect on lifespan by 50μM FUDR in wild-type and *mdl-1(tm311) C. elegans*. 84
Figure 3.8. Invasion of the *C. elegans* uterus by *E. coli* OP50. 86
Figure 3.9. The effect of different conditions on bacterial invasion of the uterus in *C. elegans*. 88
Figure 3.10. Initial invasion of *E. coli* into the uterus near the vulva. 91
Figure 3.11. Progression of bacterial infection of uterine tumours. 96

Figure 3.12. Germline tumours in *C. elegans* hermaphrodites. 99
Figure 3.13. The structure of the *C. elegans'* gonad. 103
Figure 3.14. The apoptotic pathway in *C. elegans*. 105
Figure 3.15. The *C. elegans* gonad scoring system. 108
Figure 3.16. Gonad degeneration in ageing wild-type *C. elegans* hermaphrodites at 20°C. 109
Figure 3.17. Accelerated gonad degeneration in *C. elegans* mutants with elevated apoptosis levels at 25°C. 111
Figure 3.18. Suppression of accelerated gonad degeneration in *gld-1(op236)* mutants. 113
Figure 3.19. Accelerated gonad degeneration in *gld-1(op236)* does not require *cep-1*-dependent apoptosis. 114
Figure 3.20. Blocking apoptosis in post-reproductive hermaphrodites prevents further gonad degeneration. 116
Figure 3.21. Partial feminization of males induces germline apoptosis but not gonad atrophy. 118
Figure 3.22. The effect of FUDR on percentage of hypertrophic oocytes. 120
Figure 3.23. The effect of FUDR on percentage of hypertrophic nuclei in terminal oocytes. 121
Figure 3.24. Quasi-programmed physiological apoptosis and declining germ cell proliferation lead to gonad disintegration. 125
Table 3.1. The distribution of uterine status scores in wild-type worms aged on various FUDR concentrations……..80
Table 3.2. Uterine status scores in wild-type and *mdl-1(tm311)* aged on various FUDR concentrations……..82

Chapter 4:

Figure 4.1. Age-related degeneration in the *C. elegans* intestine. 128
Figure 4.2. Scoring intestinal atrophy. 130
Figure 4.3. Age-related changes to the *C. elegans* intestine in *glp-4* mutants. 133
Figure 4.4. Intestinal atrophy in *oxIs144*[INX-16::GFP, *lin-15*+] *C. elegans*. 135

Figure 4.5. Intestinal lumen distension in *oxIs144*[INX-16::GFP, *lin-15*+] 136
Figure 4.6. Accelerated atrophy at intestinal cell boundaries.. 137
Figure 4.7. Loss of fluorescence of *E. coli* OP50-RFP in the intestinal lumen during ageing. 139
Figure 4.8. The biomass conversion theory.. 141
Figure 4.9. Lipid pools in wild-type male *C. elegans*. 142
Figure 4.10. Measuring yolky/lipid pools in *C. elegans*. 142
Figure 4.11. Lipid pool scores in ageing wild-type male and hermaphrodite *C. elegans*..... 144
Figure 4.12. Intestinal atrophy and lumen dilation in ageing wild-type hermaphrodites and males in liquid culture. 147
Figure 4.13. Intestinal atrophy and lumen dilation in ageing wild-type hermaphrodites and males on plates.. 148
Figure 4.14. Lipid pool accumulation in feminized *mab-3(mu15)* males. E 150
Figure 4.15. Intestinal atrophy in feminized *mab-3(mu15)* males.. 151
Figure 4.16. Lipid pool accumulation and intestinal atrophy in *mab-3(e1240)* males. 152
Figure 4.17. Intestinal atrophy and lumen dilation in *mab-3(e1240)* males. 153
Figure 4.18. Lumen dilation in *mab-3(mu15)* males during ageing..... 154
Figure 4.19. Yolky pool accumulation and intestinal atrophy is not affected by antibiotic treatment in *mab-3(mu15)* mutant males. 155
Figure 4.20. Antibiotic treatment does not prevent lumen dilation in *mab-3(mu15)* mutants males. 156
Figure 4.21. The effect of *vit-5,6* RNAi on yolk accumulation and intestinal atrophy in *mab-3(mu15)* males. 158
Figure 4.22. The process of autophagy. 160
Figure 4.23. The effects of mating on yolk accumulation and intestinal atrophy in wild-type hermaphrodites. 162
Figure 4.24. Intestinal atrophy as a cause of death in ageing *C. elegans*. 169

Chapter 5:

Figure 5.1. The grinder of the *C. elegans* pharynx. 171
Figure 5.2. The pharynx pathology scoring system.. 174
Figure 5.3. Pharyngeal pathology in *C. elegans* corpses. 176
Figure 5.4. Age-related changes to the *C. elegans* pharynx in wild-type hermaphrodites. 177
Figure 5.5. Tracking development of age-related pathologies in individual worms.. 179
Figure 5.6. Early death in *C. elegans* is associated with pharyngeal swelling and reduced lifespan (P death). 181
Figure 5.7. Mortality rate deceleration in ageing *C. elegans* populations. 183
Figure 5.8. Bacterial infection causes pharyngeal swelling. 185
Figure 5.9. Evidence from electron microscopy of bacterial invasion of the pharynx. 187
Figure 5.10. Blocking bacterial proliferation prevented P death and extended lifespan. 188
Figure 5.11. Bacterial infection is associated with a sudden decline in pharyngeal function..... 190
Figure 5.12. The effect of carbenicillin treatment on the correlation between pharyngeal function and lifespan. 191
Figure 5.13. Uterine tumour infection in worms with infected pharynxes. 192
Figure 5.14. Bacterial infection in different cell types within the pharynx. 193
Figure 5.15. Evidence from electron microscopy that bacterial infection starts near the grinder.. 194
Figure 5.16. The effect on lifespan and the occurrence of P death of initially growing worms on non-proliferating bacteria. 195
Figure 5.17. The effect of feeding powdered glass on *C. elegans* longevity and pharyngeal infection. 196
Figure 5.18. The effects of serotonin exposure until mid-life on longevity, pharyngeal infection and pharyngeal pumping rate.. 198

Figure 5.19. The effects of serotonin exposure, only in mid-life, on longevity, pharyngeal infection and pharyngeal pumping rate..... 199
Figure 5.20. Lowering pharyngeal pumping rate reduces the level of P death. 200
Figure 5.21. Pharyngeal pumping rate on day 1 of adulthood of P and p death worms. 201
Figure 5.22. Evidence of scarring in the *C. elegans* pharynx..... 203
Figure 5.23. A proposed mechanism for the development of P death.. 206
Table 5.1. Correlations between life span and pathology severity..... 179

Chapter 6: Conclusions

Table 6.1. The possible causes of pathologies examined in this study.. 211

Appendix 1. Statistics

Table A.1. Survival statistics for wild-type and *mdl-1* treated with FUDR from L4. ……212
Table A.2 Survival statistics for growing wild-type worms on non-dividing ……...212
Table A.3. Survival statistics for maintaining wild-type worms on non-dividing ……213
Table A.4. Survival statistics for worms fed ground glass. …….214
Table A.5. Survival statistics for worms treated with serotonin……..214
Table A.6. Survival statistics for the *eat-2* mutant. ……214
Table A.7 Two-way ANOVA statistics for the effect of vit-5,6 RNAi on lipid pool scores during ageing in mab-3(mu15) and him-5(e1490) males and hermaphrodites…….214
Table A.8 Two-way ANOVA statistics for the effect of vit-5,6 RNAi on intestinal atrophy during ageing in mab-3(mu15) and him-5(e1490) males and hermaphrodites…….215

Chapter 1 Introduction

1.1 Introduction to ageing

Ageing or senescence can be defined as the gradual decline in fitness and emergence of age-related pathologies with increasing chronological age. It is something everyone has sadly witnessed in their older relatives and friends, where it cruelly strips away both cognitive and physical wellbeing, leaving individuals in a state of decay for the remainder of their lives. However science has still not been able to definitively explain how and why we age. To add to the enigma it seems possible that in some animals, such as famously in *Hydra vulgaris*, ageing can be avoided altogether (Martínez 1998). Moreover, ageing can occur at a very slow rate, such as in tubeworms belonging to the *Lamellibrachia* genus, which can live for around 250 years (Bergquist et al. 2000). However evolutionary biology and laboratory research to identify longevity mechanisms has begun to reveal the mysteries of ageing.

Ageing has become more prevalent over the last hundred years as advances in sanitation and medicine during the 20th Century resulted in large increases in life expectancy, particularly in the developed world. This led to an increase in the occurrence of age-related diseases, such as cardiovascular disorders, cancer, dementia and arthritis. The care of elderly people is therefore becoming an increasing burden on public healthcare resources. Thus treatments are needed for these conditions to reduce the burden of late-life disease. One possible approach is to understand and treat the ageing process.

1.1.1 Treating ageing as a disease

The notion of treating ageing does have it critics. For a condition to be considered appropriate for treatment it must be considered a disease and historically ageing has been viewed as a normal and natural process. For example the bioethicist Leon Kass stated that ageing is a biological process that should be looked upon as entirely separate from disease (Kass 1985). Whether or not ageing should be classed as natural does not diminish the suffering it causes older people and thus it is right to try to intervene in its progression. On the other hand, society often encourages us to not just endure ageing but to actually celebrate it. For example, the charity Age UK currently has an interview with the actress Julie Walters on its website discussing why she is “embracing ageing”. This is an example of how society propagates a confused view of old age. It is true that an increase in calendar age can have various benefits to an individual, such as an amassing of knowledge and retirement. However by over-emphasising this aspect of ageing, we conceal the abhorrent reality of senescence and the pathologies it causes. Presumably, she does not embrace senescence. In truth, elderly people often experience long periods of ill health. This in turn has resulted in the widely reported crisis in late life care and overburdening of the NHS.

Currently, research into age-related diseases is fragmented, with each being individually studied by different parts of the scientific community. However it would be more productive to unite scientists to study the main risk factor for all these conditions, which is ageing. If we could treat and therefore decelerate ageing we could hopefully delay the emergence of many age-related diseases and give people longer, healthier lives.

To treat ageing, we must understand the biological processes that cause it. For decades, biogerontologists have mostly attempted to reveal these mechanisms by studying the effects of interventions on life span. However this ignores the core component of the ageing phenotype, which is pathology. Pathology is what causes sickness and suffering, and of

course death, in ageing humans. Yet those studying ageing using model organisms, such as *Caenorhabditis elegans*, have largely ignored it. The work described in this thesis focuses on the study and development of age-related pathology in *C. elegans*. Additionally I emphasise the importance of investigating pathology development in conjunction with survival analysis, a practice we have called mortality deconvolution (Zhao et al. 2017). This has allowed the relationship between pathology and mortality in *C. elegans* to be unravelled, helping to make sense of the sometimes complex, and previously enigmatic shapes of survival curves and mortality profiles.

1.1.2 Evolutionary theories of ageing

Billions of years of evolution have resulted in the remarkable array of organisms we now have on Earth. Natural selection has ensured that beneficial genes remain enriched in populations, allowing species to continuously adapt to changing environments. However despite this, ageing appears to be ubiquitous, as most species we know of experience ageing in some form. Even bacteria can exhibit ageing; cells that inherit older cellular material during division have a lower proliferative capacity (Stewart et al. 2005). This is despite the fact that selection should favour individuals that are fitter and fertile for longer. How has ageing, which is a wholly deleterious trait, been able to slip through the stringent process of natural selection? Various evolutionary theories have offered an explanation to this conundrum.

An early theory proposed by Alfred Russel Wallace in the 1860s was that ageing exists because it benefits the species (Partridge & Gems 2002). In wild populations, where resources are finite, ageing ousts older individuals allowing resources to be liberated for their fitter and more fertile offspring. However there are several issues with this theory. Firstly, it does not acknowledge that ageing is relatively rare in wild populations, with the majority of organisms dying from extrinsic hazards, such as

predation or disease (Kirkwood & Austad 2000). Secondly, natural selection mostly works towards the benefit of an individual rather than the species or group. Therefore one would expect selfish cheats who do not age to have a selective advantage over their altruistic fellows, yet such individuals do not exist (Partridge & Gems 2002). Finally this theory assumes that there are already aged individuals within a population that are suitable for removal, it does not explain where they came from.

So why does ageing exist at all? Inspiration came from an unlikely source: Huntington's disease. This is a dominant, inherited neurodegenerative disorder in humans where symptoms only begin to emerge from around 30 years old. This means individuals can reproduce successfully before they become disabled by their condition. As reproduction has occurred and the genes have already been inherited by the next generation, natural selection is unable to completely eliminate the disease from the population (Haldane 1941). Based on this deduction, Haldane proposed that late-acting mutations, that only exhibit their deleterious effect post-reproduction, are not strongly selected against. Over time such mutations accumulate in populations and eventually result in ageing. This would have little effect on fitness in the wild, as most organisms will die from extrinsic hazard before the effects of these mutations are expressed in later-life. Thus fitness is mainly a function of reproductive output in early life, with late life health being of little importance to fitness (Gems 2015). However the majority of humans living in the developed world today inhabit an environment where extrinsic hazards are greatly reduced. This has allowed these deleterious mutations to exhibit their late life effects, resulting in an increased prevalence of age-related diseases.

Over the years this initial theory proposed by Haldane has been built upon and refined. The mutation accumulation theory proposed that ageing emerges because the force of natural selection to eliminate unfavourable characteristics declines with chronological age, even if a species displays no biological ageing. This is because organisms will die

from extrinsic hazards and therefore there will always be more organisms at younger ages than older ages (Medawar 1952). The antagonistic pleiotropy theory based on these ideas proposed that given that mutations can be highly pleiotropic, those that are beneficial in young organisms but have negative impacts in older organisms can be acted on positively by natural selection and therefore not eliminated from the population but incorporated into the gene pool. This is because organisms will reproduce and pass on their genes to the next generation before the negative impacts of the mutation become apparent and prevent them from doing so (Williams 1957). Additionally, recent theory has argued that factors other than extrinsic mortality also contributes to the age decline in selection, for example the low frequency of older adults in an expanding population (Abrams 1993).

While these evolutionary theories, particularly antagonistic pleiotropy, may help us to understand why ageing is so prevalent, it does not reveal the biological mechanisms that cause it. For that we must study the mechanistic theories of ageing.

1.2 The biological mechanisms of ageing

The underlying processes that cause ageing still remain largely a mystery, despite decades of research and discussion. Evolutionary theory implies that ageing is not programmed because genes should not exist that have the sole purpose of self-sabotage. However there is now a plethora of studies that show mutations of individual genes can cause substantial increases in lifespan (Kenyon 2010). This implies that ageing is in fact programmed by genes, which seemingly conflicts with evolutionary theory. One approach to try to resolve this apparent paradox is to consider the mechanisms of ageing by which such life shortening genes act. These remain poorly understood, though there are various candidate mechanisms and theories. Here two theories are discussed: the molecular damage theory and the more recent hyperfunction theory.

1.2.1 Ageing as the result of molecular damage

The idea that molecular damage causes ageing for many years focused in particular on oxidative damage. It originates from the 1950s when Harman suggested that free radicals, which are often highly reactive molecules due to an unpaired election (e.g superoxide $O_2^{\bullet -}$), cause widespread molecular damage leading to cellular dysfunction and subsequently ageing (Harman 1956). Later the theory expanded to include a broader group of potentially damaging molecules, referred to as reactive oxygen species (ROS), including non-radicals such as hydrogen peroxide H_2O_2, and was then often referred to as the oxidative damage theory (Sohal & Weindruch 1996) (Figure 1.1). ROS exist within healthy cells as they are produced, for example, during normal respiration. Upon being generated it is suggested they immediately begin causing a wide array of damage within cells, including oxidation of DNA and carbonylation of proteins (Stadtman 1992). Unrepaired damage then accumulates gradually over time, and upon reaching a certain level, an organism will start to exhibit all the symptoms of ageing. Consistent with this, levels of oxidative damage do increase with age (Orr & Sohal 1994; Sohal et al. 1995b). The theory also predicts that interventions that lower ROS levels should reduce this damage and consequently extend lifespan. This could be achieved by administering dietary antioxidants like vitamin E, or by experimentally overexpressing antioxidant enzymes like superoxide dismutase (SOD) or catalase, which together convert superoxide to water and oxygen in a two step reaction.

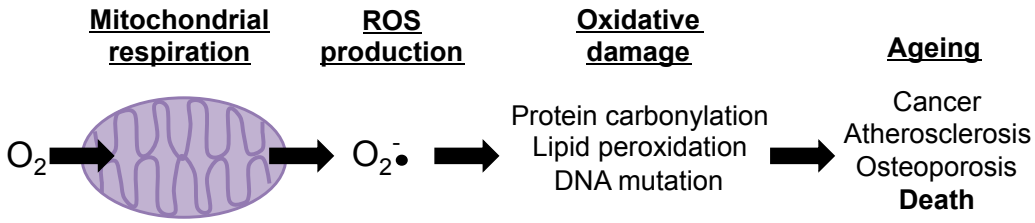

Figure 1.1. The oxidative damage theory of ageing. Normal respiration in mitochondria generates reactive oxygen species (ROS). This causes damage to various macromolecules within the cell. This damage gradually accumulates throughout life, resulting in the characteristic symptoms of ageing. (Adapted from (Doonan et al. 2008)).

Initially many papers appeared that provided evidence to support this theory. For example overexpression of SOD in *Drosophila melanogaster* increased lifespan (Sun et al. 2002; Sun & Tower 1999) and protein carbonyl levels increase as the flies get older (Orr & Sohal 1994). Longer-lived fly species also have lower levels of ROS than shorter-lived species (Sohal et al. 1995a). For example in gerbils, ROS production increased during ageing and correlated with increased oxidative damage to numerous internal organs (Sohal et al. 1995b).

However, more recently numerous findings have been reported that contradict the ROS theory. For example ROS are not only damaging molecules but also have essential functions within cells. For example, H_2O_2 is a signalling molecule involved in initiating a number of cellular mechanisms including differentiation (Veal et al. 2007). Moreover the presence of antioxidant enzymes suggests that cells are highly capable of managing ROS and repairing oxidative damage, with evolution presumably acting to improve these protective mechanisms as needed. It is possible there is a decline in enzymatic activity with age; however SOD levels actually increased in gerbils during ageing in a wide range of tissues, though this is certainly not always the case (Sohal et al. 1995b).

There are now many studies that suggest ROS may only play a small part or make no contribution to the overall ageing process. For example it has been shown overexpressing SOD and/or catalase in mice has no effect on lifespan (Pérez et al. 2009). Furthermore in *C. elegans* deletion of both

sod-2 and *sod-3* did not cause an increase in lifespan, despite causing hypersensitivity to oxidative stress (Doonan et al. 2008). Moreover, deletion of all five *sod* genes did not shorten *C. elegans* lifespan (Van Raamsdonk & Hekimi 2012). Perhaps most significantly clinical trials of antioxidant supplements have mostly failed to slow ageing (Howes 2006). In one study, antioxidants actually increased the incidence of lung cancer in individuals who had a high risk of developing the disease (Omenn et al. 1996). There is also confusion as papers have been published that show different results for the same experiment. For example vitamin E has been shown to both increase *C. elegans* lifespan (Harrington & Harley 1988) and also have no effect (Adachi & Ishii 2000). Here a potential problem is publication bias, as previously noted (Blagosklonny 2008). Papers with positive data that support the oxidative damage theory tend to be published in higher impact journals while studies with negative data that oppose the theory are published in lower impact journals or may remain unpublished.

The balance of evidence does not support the view that oxidative damage is the main driver of ageing. One possibility is that damage does a play a role in ageing, but there are many different types of damage that can occur within a cell, e.g glycation of proteins. Therefore oxidative impact may just be a small proportion of a much wider array of damage (Gems & Doonan 2009). It is also possible that molecular damage is not the main cause of the ageing process and its accumulation is simply correlative, with ageing being caused by another entirely different primary mechanism. There is enough doubt over the role of molecular damage during ageing that new theories should now be contemplated.

1.2.2 The disposable soma theory

A proposal that combined evolutionary theory and the molecular damage theory, is the disposable soma theory suggested by Tom Kirkwood (Kirkwood 1977). The central concepts of this theory are that molecular

damage is the primary cause of ageing and that protection against this damage is very costly. In a wild population, where resources are finite, Kirkwood stated that organisms have to resolve where these limited assets are most needed. As evolution favours reproductive success, so it will encourage the funnelling of resources towards the germline and reproductive output. An individual will therefore prioritise the formation of biomass that will promote reproductive fitness, such as the production of eggs, energy dense yolk and milk. In addition, repair of damage within the germline, which is immortal, will have precedence over somatic maintenance to ensure the continued viability of progeny for boundless generations. In contrast, the soma is only given sufficient resources to assure survival for long enough to allow for reproduction to occur. As the soma only receives a baseline of maintenance, damage gradually accumulates within it, causing ageing (Kirkwood & Austad 2000).

1.2.3 The hyperfunction theory

One alternative theory that has been proposed relatively recently by Mikhail Blagosklonny examines the role of hyperfunction (i.e the excessive activity of biological processes in a mature adult due to wild-type gene action) in ageing (Blagosklonny 2008; Blagosklonny 2006). Blagosklonny notes that ageing appears to act much like a programmed process. For example, ageing results in similar patterns of pathology between individuals of the same species, such as atherosclerosis, arthritis and osteoporosis – all common age-related pathologies in humans. Furthermore the fact that individual genes can be manipulated to control ageing in model organisms provides more evidence ageing is somehow a programmed process. Yet the evolutionary theory of ageing states ageing cannot be programmed because no system should develop with the sole purpose of causing deterioration and death. Therefore surely the only alternative is the accumulation of random molecular damage? Or is there another explanation?

Blagosklonny suggests that while molecular damage does accumulate with age, it does not have an effect on mortality because such damage would be random and not produce the uniformity we see in age-related pathologies within a species (Blagosklonny 2006; Blagosklonny 2008). Instead he proposes quasi-programmes cause ageing (Blagosklonny 2006). By this he means that ageing is genetically programmed, yet does not involve an adaptive programme (note that "programme" here has two distinct meanings). Thus essential processes that promote fitness, health and reproduction can be called programmes when they are functioning during youth. However, when they continue to act in older organisms when they are no longer needed they become known as quasi-programmes (Figure 1.2). This would explain some intriguing results, such as the fact that reducing the level of ribosomal protein S6 kinase, which results in reduced protein synthesis, extended lifespan in *C. elegans* (Hansen et al. 2007). Development of pathologies resulting from hyperfunction would presumably require continued protein synthesis and thus reducing it should extend lifespan. It is important to note that a quasi-programme is not a defective programme; it is simply the continuation of a programme in a way that no longer promotes fitness.

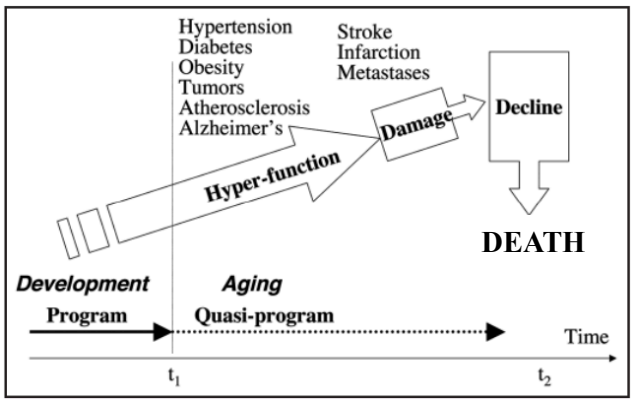

Figure 1.2. The hyperfunction theory of ageing. During development, programmes function to promote fitness in the organism. Once development is complete (t_1), the programme continues to function when it is no longer needed and becomes a quasi-programme. These quasi-programmes lead to a variety of age-related pathologies caused by hyperfunction. Hyperfunction will then lead to damage (including molecular damage) and decline in the organism, eventually resulting in death (t_2) (Image from (Blagosklonny 2006)).

Quasi-programmes will lead to overgrowth and eventually an array of pathologies caused by hyperfunction. A metaphor to describe this is to imagine you are cooking your Sunday roast in the oven. You turn on the oven to cook the meat within so you can eat it. Once the meat has been cooked, the programme is complete and you no longer need the oven turned on. However failure to switch off the oven will result in a burnt dinner. The oven has not malfunctioned, it is doing exactly what you set it to do, and it was simply not switched off at the appropriate time. Therefore the turned on oven became a quasi-programme once the meat begins to overcook, resulting in a ruined dinner.

The hyperfunction theory can fit well with the evolutionary theory of ageing, especially in regards to antagonistic pleiotropy, which is in many ways its foundation. Growth and development in youth requires the activation of nutrient sensing pathways. These pathways have evolved to respond rapidly to food intake to utilise resources efficiently. This makes sense in a wild environment where food supply may be erratic and a young animal would need to respond robustly to nutrient intake to ensure rapid and coordinated growth, and reproduction. However in an older animal the forces of natural selection are weaker, so the nutrient sensing pathways would not be switched off. These activated pathways cause continued operation of quasi-programmes, e.g through continued biosynthesis, in older organisms leading to the development of age-related pathologies. This implies that ageing is to a large extent a quasi-programmed process, rather than one caused by system failure and random damage accumulation. It is merely the result of the continued action of signalling pathways and the resulting consequences of this.

1.2.4 Hyperfunction and age-related pathology

It would be expected that age-related pathologies caused by hyperfunction would be robust and not be the result of a failure of function. This is because they are caused by biological quasi-programmes. There are many examples of age-related pathologies in humans that could be driven by quasi-programmes. For example, osteoporosis is a bone disorder that results in a low bone mass and an increased risk of bone fractures. To maintain its architecture and strength, bone needs to be constantly renewed. Osteoclasts are cells that resorb bone and during ageing they become over-activated and apoptosis resistant (Glantschnig et al. 2003). The signals that stimulate the osteoclasts are not operating incorrectly, but in older individuals there is no mechanism to switch them off. Atherosclerosis is associated with excessive platelet clumping and over activation of the inflammatory response (Shapiro & Fazio 2016). Cancer is a disease of overgrowth, with no evidence that tumour cells in the elderly exhibit a loss of function phenotype. These are just a few examples of many that demonstrate that diseases of ageing may not be the result primarily of damage but the result of hyperfunction, which produces pathologies that subsequently cause damage during ageing.

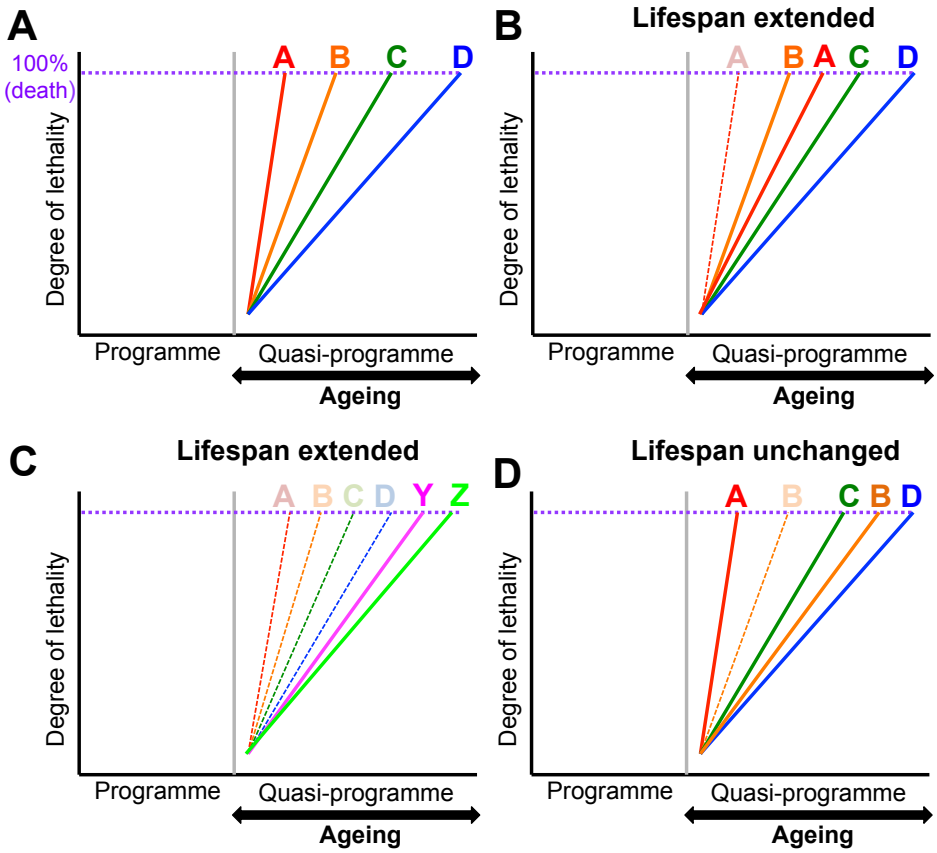

Figure 1.3. Ageing results in the generation of multiple pathologies. (A) During normal development in a young individual, no ageing pathologies develop. When biological programmes (developmental, reproductive or reparative) are no longer needed but remain switched on, they become quasi-programmes. These drive the formation of various pathologies (A-D), with pathology A progressing fastest and becoming the first to reach the lethal threshold. Thus pathology A causes death. **(B)** If pathology A is treated, then lifespan is extended until pathology B limits life. **(C)** If an intervention suppresses multiple senescent pathologies, the lifespan of these long-lived individuals may now be limited by new pathologies (Y,Z). **(D)** If an intervention treats pathology B (e.g uterine tumours in *C. elegans*), which is currently not lethal, then lifespan will be unaltered as it is still limited by pathology A.

To understand more about hyperfunction and its role during ageing in both humans and model organisms we need to identify age-related pathologies that are the result of hyperfunction. If we can understand how these pathologies develop by identifying the quasi-programmes involved, we could attempt to intervene to prevent or slow down their progression. Often a human will die from a single major senescent pathology; therefore this pathology will likely develop faster and become life threatening before the others (Figure 1.3A). If this pathology was treated before it became lethal the individual would live longer but ultimately die from another, slower developing pathology (Figure 1.3B). Therefore to

achieve major gains in human health in later life we need to identify quasi-programmes that cause multiple pathologies and block the programme once it has been completed but before it becomes a quasi-programme and starts to cause pathologies. Lifespan extending interventions may simply cause the development of the same pathologies to be delayed or perhaps an entirely new set of pathologies will emerge (Figure 1.3C,D). A possibility is that if we treated all hyperfunction related pathologies we would be left with a situation where lifespan was now limited by the accumulation of molecular damage, such that antioxidants would be the answer to an even longer life (Blagosklonny 2008).

1.3 *Caenorhabditis elegans* as a model organism

In the early 1960s, Sydney Brenner proposed the nematode *C. elegans* as a suitable model for the study of many biological processes, with his particular interest at the time being neurobiology (Brenner 1974). Since then *C. elegans* has been extensively studied, resulting in it having its entire genome sequenced (Consortium 1998) and the fate of every cell during development identified (Sulston & Horvitz 1977). In 2002, Brenner's work with *C. elegans* contributed to him being one of the recipients of the Nobel Prize for Medicine, an acknowledgement of how important *C. elegans* now is within scientific research.

C. elegans is a small nematode worm, found in putrid fruit and soil in the wild. When fully grown it is only about 1mm long, thus making storage of large populations easy. Worms can be maintained in the laboratory on agar plates or within liquid culture. In the wild they feed on a range of bacteria (Dirksen et al. 2016), though in standard laboratory conditions they are fed the bacterium *Escherichia coli* OP50, a strain that is an uracil auxotroph and so forms thin bacterial lawns, making the worms easier to observe. Conveniently on plates, worms can be identified using a low power dissecting scope. One major advantage of *C. elegans* is that they are transparent, so under high magnification with Nomarski optics, the

cells and internal organs can be examined without the need for dissection. This is a particularly useful feature for studies of pathology.

Worms have a compact genome consisting of five autosomal chromosomes, ~100 million base pairs and ~21,000 protein coding genes, of which nearly 40% are anticipated to have an ortholog in humans (Shaye & Greenwald 2011). There are two sexes, hermaphrodites and males, which are determined by the number of sex chromosomes. Hermaphrodites possess two (XX) and males only have one (XO) (Corski et al. 2015). Hermaphrodites generate several hundred sperm during development and then irreversibly switch to oocyte production during adulthood (Corski et al. 2015). Thus hermaphrodites can self-fertilise, with each individual producing up to 300 progeny, which are all genetically identical to each other and their mother (Corski et al. 2015). This allows for large, clonal populations to be easily generated, a useful tool when experiments require maintaining large numbers of different mutants. In standard laboratory conditions, males occur at a very low rate and make up only about 0.1% of the population (Corski et al. 2015). Stressful conditions, such as high temperature, increase male generation due to non-disjunction of the X chromosome (Lints & Hall 2009a). Therefore in the more stressful conditions experienced in the wild, males may be more common. Males can mate with hermaphrodites, prolonging the hermaphrodite reproductive output and producing a population with equal proportions of both sexes. Mating can be utilised for strain constructions, for example of double mutants. For all of these reasons, *C. elegans* is both a convenient and powerful model organism.

For many years researchers employed a forward genetics approach with *C. elegans*, where mutations are generated via exposure to mutagens such as ethyl methanesulphonate (Brenner 1974). Mutants with a phenotype of interest can then be selected and subsequent analysis should reveal the underlying mutated genes. Nowadays, most studies instead use reverse genetics approaches, which involve altering levels of gene expression and analysing the subsequent effects on the worm

phenotype. This approach has been made easier by advances in technology and access to the fully sequenced *C. elegans* genome.

A revolutionary method for reverse genetics was RNA mediated interference (RNAi), which was discovered in *C. elegans* and was the subject of the 2008 Nobel Prize for Medicine. It was observed that injection (Fire et al. 1998), soaking (Tabara et al. 1998) and ingestion (Timmons & Fire 1998) of double stranded RNA (dsRNA) by worms caused complementary mRNA levels to be reduced. When dsRNA enters a cell it is bound by the Dicer complex, which contains DCR-1, an enzyme that cleaves dsRNA into small interfering RNAs (siRNAs). siRNAs are then processed into single strands by RDE-1, allowing them to bind to complementary mRNAs and initiate their degradation (Zhuang & Hunter 2011). *C. elegans* is particularly suitable for RNAi treatment for a couple of reasons. Firstly, ingestion is a very simple method to induce RNAi. Worms are fed dsRNA expressing *E. coli*, generally the HT115 strain as it has impaired RNA degradation (Timmons et al. 2001). Secondly, when worms take up dsRNA, it is automatically disseminated throughout much of the body, resulting in systemic knock down of the gene of interest (Fire et al. 1998). Perhaps one of the most advantageous features of RNAi is the ability to knock down genes at particularly points in development, especially useful for when mutations cause embryonic lethality. This could also allow for exploration of the hyperfunction theory of ageing, as RNAi could be used to switch off a programme before it becomes a quasi-programme and thus inhibit the development of age-related pathology.

Another progressive reverse genetics approach that works well in *C. elegans* is CRISPR. This system utilises the DNA cleavage enzyme Cas9 to insert sequences specifically into target genes within the genome, forever changes the organism's genotype (Dickinson & Goldstein 2016).

1.3.1 *C. elegans* life cycle

C. elegans has a fast life cycle, developing from an egg to a fertile adult in approximately 65hrs at 20°C (Figure 1.4). When conditions are agreeable, the worms will pass through four larval stages (L1-L4) before becoming a fertile adult, with each transition requiring a moult (Cassada & Russell 1975). However when conditions are less favourable, worms are able to become dauer larvae, an alternative L3 larval stage (Figure 1.4). The decision to become dauer begins at the L1 larval stage is triggered by a combination of different factors. A high population density results in the accumulation of a pheromone that can trigger and maintain the dauer stage (Golden & Riddle 1982). Low food and high temperature also promote the appearance of dauer larvae (Golden & Riddle 1984). Under such conditions, L1 larvae develop into a pre-dauer stage called L2d. If the stressful circumstances persist then L2d larvae become dauers. Dauers have a number of distinct characteristics amongst the *C. elegans* development stages. They are very thin but have a reinforced cuticle, which gives them resistance to external stressors such as acid exposure (Cassada & Russell 1975). They have greatly reduced movement and their pharynx does not pump (Cassada & Russell 1975). In fact, their alimentary canal seals itself, with the mouth closing entirely (Cassada & Russell 1975; Riddle et al. 1981). Notably, the dauer stage is very long lived and can survive for up to 70 days (Klass & Hirsch 1976). Once favourable conditions are restored, the dauer stage is exited and worms develop into normal adults. Intriguingly, the length of time spent as dauer has no effect on adult lifespan, suggesting that dauers are a non-ageing stage (Klass & Hirsch 1976). An alternative possibility is that dauers do senesce, but rejuvenate upon dauer exit (Houthoofd et al. 2002).

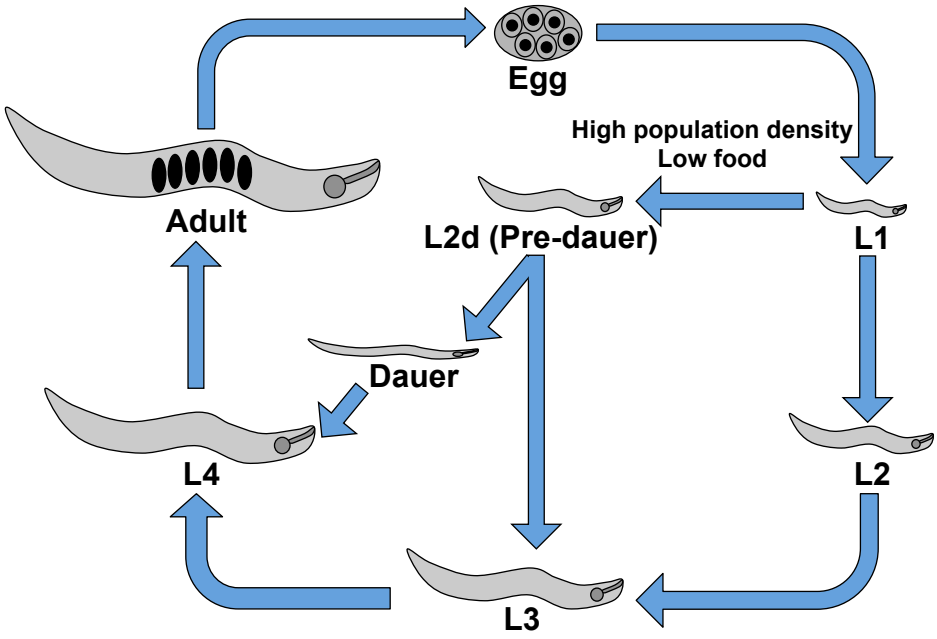

Figure 1.4. The *C. elegans* life cycle. Eggs are laid and hatch to form L1 larvae. When resources are plentiful, L1 larvae can go through several moults and larval stages (L2-L4) until they become self-fertilising adults. However, if L1 larvae experience stress, such as high population density or low food, they can enter a pre-dauer larval stage (L2d). If the stressful conditions cease, then normal development can resume. However if they persist, then L2d larvae can form dauers, a long-lived stage capable of surviving for several months. Once favourable conditions are restored, dauers progress through development to form normal, young adults.

1.3.2 *C. elegans* anatomy

Despite being so small, *C. elegans* does possess a complex anatomy with multiple tissue types and organs. Both the hermaphrodite and the smaller male possess an outer tube of body wall, which includes a sturdy outer cuticle (Figure 1.5) (Altun & Hall 2009c) and body wall muscle which contracts and relaxes to generate a wave-like swimming or crawling movement (Altun & Hall 2009c). Neurons also form part of this outer tube and are mostly located in the head and tail (Altun & Hall 2009c).

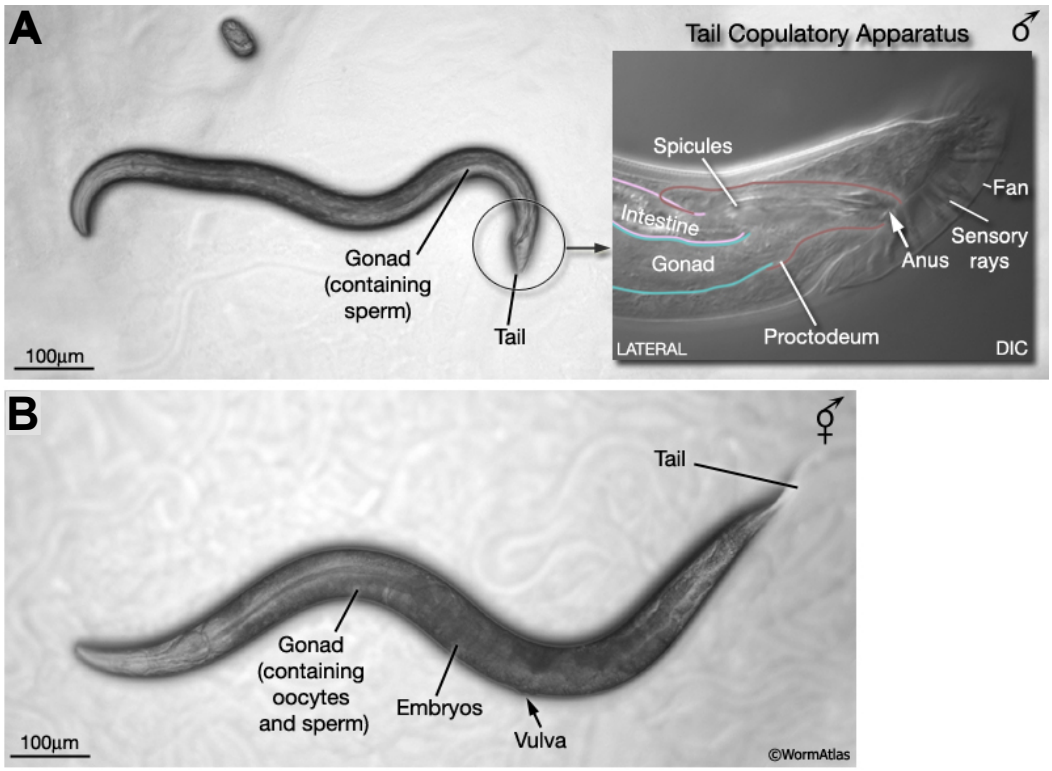

Figure 1.5. The *C. elegans* male and hermaphrodite. (A) The male is smaller and thinner than the hermaphrodite. The apparatus for copulation is located in the tail and comprises of a fan containing sensory rays, which are used to search for the vulva, and spicules, which help to anchor the male to the hermaphrodite during mating. Development of these features can distinguish males relatively early in larval development. **(B)** The hermaphrodite has a thinner tail and a vulva located towards the center on the ventral side. (Image from (Lints & Hall 2009a).

Within the body cavity are the alimentary canal and gonad. The pharynx resides at the anterior end of the alimentary canal and is primarily made up of muscle cells, but also contains epithelial, marginal, gland and neuronal cells (Figure 1.6) (Altun & Hall 2009b). Bacteria are pumped through the anterior portion of the pharynx down into the terminal bulb, where they are macerated before entering the intestine. The intestine is comprised of 20 polyploid cells arranged mostly into paired rings, though with one quadrant at the anterior end (Figure 1.7) (Altun & Hall 2009a). Food passes through the lumen of the intestine as the connecting muscles contract, before being defecated through the anus at the posterior end.

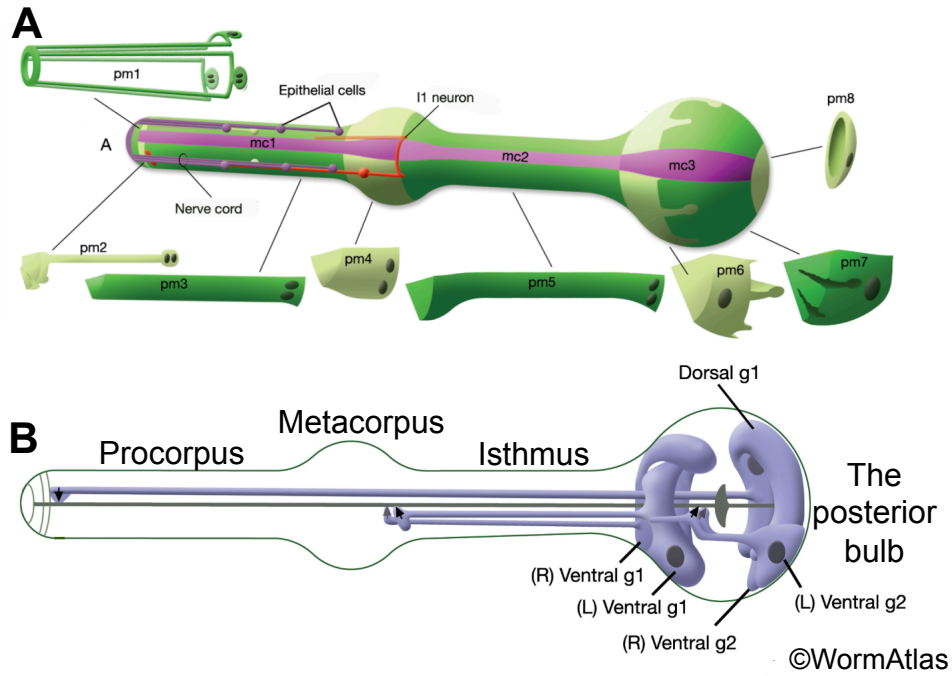

Figure 1.6. The structure of the *C. elegans'* pharynx. (A) The pharynx contains twenty muscle cells that make up eight muscle segments (pm1 – 8) and nine marginal cells that make up three marginal cell segments (mc1 – 3). The marginal cells lie in between the muscle cells and provide additional structural strength. **(B)** The pharynx also has two classes of gland cells: three g1 cells and two g2 cells. These cells have openings into the pharyngeal lumen, with g1 cells having long protrusions that open into the lumen in the metacorpus, whereas g2 cells open directly into the lumen within the posterior bulb of the pharynx. Bacteria are ground down by the grinder inside the posterior bulb, before entering the intestine. (Image from (Altun & Hall 2009b)).

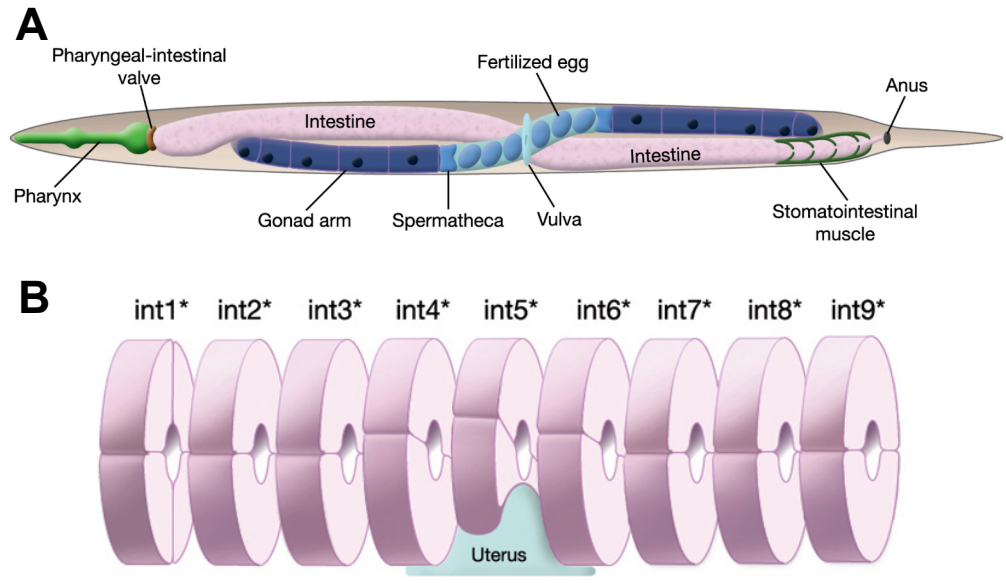

Figure 1.7. Structure of the *C. elegans* hermaphrodite intestine. (A) The intestine (pink) is anchored to the pharynx (green), by the pharyngeal-intestinal valve (dark brown), and to the anus. It has to bend around the gonad (blue); therefore one section of the intestine will lie on top of the gonad and the other underneath. **(B)** The intestine is made up of 20 large epithelial cells. The majority of these cells form pairs to form intestinal rings (int2 – 9). The exception is the most anterior ring, int1, which is composed of four cells. (Image from (Altun & Hall 2009a)).

The hermaphrodite gonad is composed of two reflexed arms that each contain a distal and a proximal region. A somatic sheath encloses the germ cells, which develop into oocytes down the proximal arm. At the proximal end, oocytes are fertilised by sperm within the spermatheca and then enter the uterus. Stimulation of the vulva muscles results in the eggs being laid (Lints & Hall 2009d). The male gonad only has one arm, which solely creates sperm. Spermatids are stored in the seminal vesicle to await copulation (Lints & Hall 2009c). The posterior end of males is not just composed of the excretory portion of the intestine, but also contains the apparatus needed for mating. This consists of a fan-like structure containing sensory rays and additional muscles (Altun & Hall 2009c). Males will utilise these to search the hermaphrodite cuticle for the vulva and then use spicules within their tail to anchor themselves before ejaculation.

1.3.3 *C. elegans* nomenclature

Working with *C. elegans* requires adherence to a well defined genetic nomenclature, which is described in detail on the website, WormBase. When a strain is generated, it should be assigned a unique strain number, consisting of a number preceded by two or three uppercases letters. The letter code identifies the laboratory where the strain was produced. For example CF80 is a strain from Cynthia Kenyon's group.

Genes are given a three or four letter name, written in lower case italics, followed by a number. The name can be derived in a number of different ways. Most are named after a phenotype that mutation of the gene causes. For example, mutation in *glp-4* causes abnormal germline proliferation. They can also be named based on the predicted protein identity or homologs that have already been named in other model organisms, e.g *sir-2.1* was named after yeast SIR2. The protein encoded by a gene is non-italicised and in capital letters, for example GLP-4.

Different alleles also have unique codes. Again they consist of a number preceded by a laboratory-specific letter code. This is written in italics and in brackets after the gene name. For example *glp-4(bn2)* tells us this allele originates from Susan Strome's group. A wild-type allele is indicated by the + symbol within brackets. A heterozygote has the allele code followed by a /+, for example *glp-4(bn2)*/+. After this there is either a roman numeral or X to indicate on which chromosome the gene is found, for example *glp-4(bn2)* I is found on chromosome I. In rare cases the allele code may be followed by mtDNA to indicate the gene is expressed by the mitochondria.

If a mutation is introduced by genetic engineering techniques, the information is enclosed inside square brackets. If a gene encoding a fluorescent protein, such as GFP, has been fused to a gene, the gene name is followed by two colons and the fluorescent protein gene, e.g ::*gfp*. The transgene also possesses the laboratory-specific allele code and additional information to distinguish those that are either extrachromosomal arrays or chromosomally inserted by using the codes Ex and Is respectively. For example *zcIs4[hsp-4::gfp]* tells us that this transgene is integrated and will produce HSP-4 fused to GFP. This nomenclature allows the provenance of *C. elegans* strains to be clearly specified and will be used throughout this thesis.

1.4 Ageing research using *C. elegans*

For decades *C. elegans* has been used as a model organism by biogerontologists. Aside from all the previously mentioned advantages, *C. elegans* also has a very short lifespan of only 2-3 weeks. This means experiments can be completed much faster than in other longer-lived model organisms, such as fruit flies, zebrafish or mice. Importantly, they also show several of the typical symptoms of human ageing, such as a decline in fertility and motility, and increases in tissue degeneration and

mortality. Thus, *C. elegans* has become a convenient and widely used tool for exploring the biological mechanisms of ageing.

1.4.1 Pathways involved in ageing in *C. elegans*

In 1983 Michael Klass published the results of a forward genetic screen, where he had discovered a small number of mutants with increased lifespans (Klass 1983). Tom Johnson then identified one of these mutants as *age-1(hx546)* (Friedman & Johnson 1988). Another significant discovery was that of *daf-2* mutants by Donald Riddle (Riddle 1988). The *daf* genes control the formation of dauer larvae and *daf-2* mutants are dauer constitutive (Daf-c), in that they form dauers even in favourable conditions (Riddle 1988). Cynthia Kenyon studied the lifespan of temperature sensitive *daf-2* mutants. These mutants were moved to the non-permissive temperature later in development so that they would not arrest as dauers, but instead grow into adulthood. These *daf-2* mutants had a lifespan approximately double that of wild-type (Kenyon et al. 1993). Furthermore, the *daf-2(e1370*) adult appeared virtually normal at 20°C, in terms of growth, feeding and fecundity (Kenyon et al. 1993). This lifespan extension was found to require the activity of the dauer defective (Daf-d) gene *daf-16*, suggesting in wild-type worms DAF-16 activity promotes longevity (Kenyon et al. 1993). Later work established that all of the previously mentioned proteins have homologs in humans. AGE-1 is a homolog of the catalytic subunit of phosphoinositide 3-kinase (PI3K) (Morris et al. 1996). DAF-2 is a homolog of the insulin and IGF-1 receptors (Kimura et al. 1997). DAF-16 is a homolog of a forkhead transcription factor (Ogg et al. 1997; Lin et al. 1997). These genes encode part of an evolutionarily conserved signalling pathway called the insulin/IGF-1 signalling (IIS) pathway (Figure 1.8).

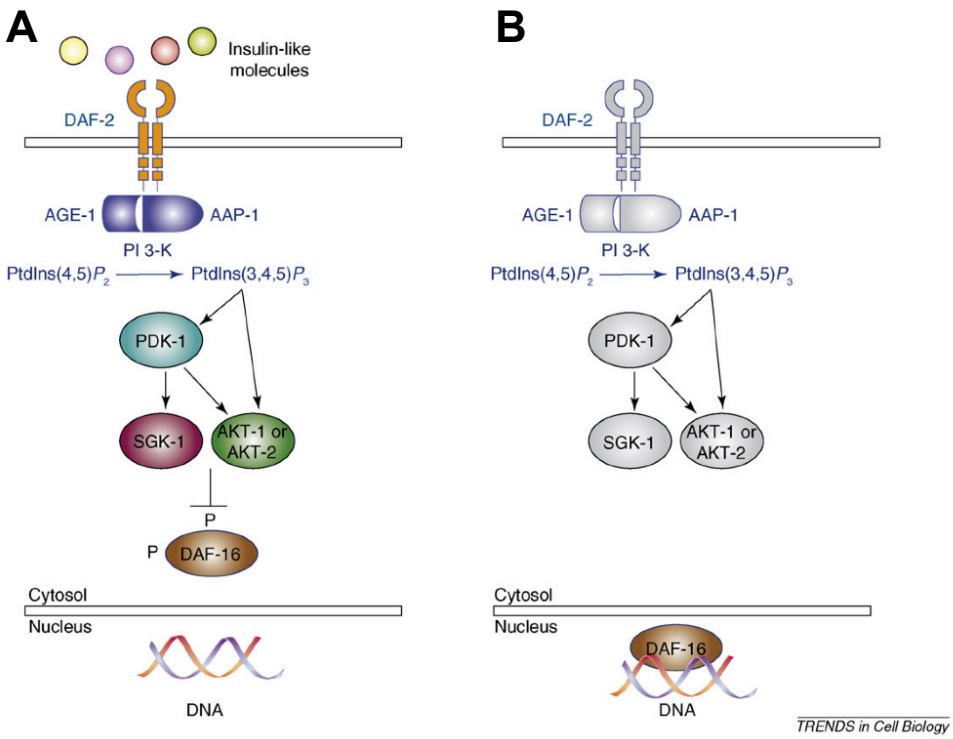

Figure 1.8. The insulin/IGF-1 signalling pathway in *C. elegans*. (A) When the DAF-2 receptor binds its ligand it initiates a signalling cascade. This starts by DAF-2 activating phosphoinositide 3-kinase (PI3K) that phosphorylates phosphatidylinositol 4,5-bisphosphate (PIP_2) to phosphatidylinositol 3,4,5-triphosphate (PIP_3). PIP_3 then stimulates 3-phosphoinositide-dependent kinase-1 (PDK-1) that activates several serine/threonine kinases including AKT and SGK-1. These kinases then phosphorylate the forkhead transcription factor DAF-16. This causes DAF-16 to be retained in the cytosol and thus inactivates it. **(B)** When DAF-2 does not bind its ligand, this kinase cascade does not occur so DAF-16 is unphosphorylated. In this state, DAF-16 can enter the nucleus and bind its target genes. (Image from (Mukhopadhyay & Tissenbaum 2007)).

Mutation of genes within the IIS pathway was also found to affect longevity in higher organisms. For example mutation of *chico*, the insulin receptor substrate in flies, caused a lifespan extension (Clancy et al. 2001). Furthermore lifespan was extended in both male and female *Igf1r*/+ (insulin-like growth factor type 1 receptor) mice (Holzenberger et al. 2003). This confirms that the control of longevity by this pathway is also evolutionarily conserved.

As the importance of IIS in the regulation of ageing became clear, the downstream targets of the transcription factor DAF-16 that could directly affect ageing were sought, in order to discover the nature of the ageing process. However DAF-16 is predicted to control expression of thousands

of genes that are involved in a wide range of activities, from the heat shock response to the immune system (Tullet 2015). The search was further complicated by the discovery that IIS can also modulate the activity of the transcription factors SKN-1 and HSF-1, which widened the net of possible downstream targets (Tullet et al. 2008; Chiang et al. 2012). However many genes that are controlled by IIS and also have a role in ageing have now been identified. For example *spp-1*, which encodes an anti-microbial protein, and *gst-4*, which encodes a protein involved in detoxification, are both upregulated and required for longevity in *daf-2* mutants (Murphy et al. 2003). DAF-16 can activate expression of *hsp-16*, a heat shock protein, which is also required for the lifespan extension of *daf-2* mutants (Hsu et al. 2003). Therefore a pattern is emerging of reduced IIS leading to increased expression of genes involved in various stress responses. Thus insights have been gained about how IIS may be controlling ageing.

Another evolutionary conserved nutrient sensing pathway that has been shown to modulate ageing in *C. elegans* is the TOR (target of rapamycin) pathway. An increase in nutrients activates the TOR pathway and subsequently increases protein synthesis and growth (Blagosklonny 2008). Importantly, a reduction in TOR signalling increases lifespan in *C. elegans* (Vellai et al. 2003; Jia et al. 2004). This effect on longevity is conserved, as mice fed the TOR inhibitor rapamycin also had an extended lifespan (Harrison et al. 2010). The relationship between the effects on ageing of the two main longevity pathways, TOR and IIS, is not completely understood but it seems that they can operate together or independently to modulate longevity. For example, the extended lifespan of the *daf-2(e1370)* mutant was not lengthened by a reduction of TOR signalling (Vellai et al. 2003). This suggests the two pathways act together to regulate ageing. On the other hand, the increased longevity induced by a reduction in TOR signalling does not require DAF-16 activity (Vellai et al. 2003). This implies the two pathways can also operate separately to control longevity.

Dietary restriction, defined as a reduction of food without starvation, has long been known to extend lifespan in a wide range of animals including rats and *C. elegans* (McCay et al. 1935; Klass 1977). In *C. elegans*, the longevity induced by DR does not require DAF-16 activity, suggesting DR does not utilise the IIS pathway (Lakowski & Hekimi 1998). So how does DR cause an increase in lifespan? An increase in nutrients triggers the TOR pathway, while a decrease inhibits it. Thus the TOR pathway seemed a likely candidate for the mediator of DR-induced longevity in *C. elegans* (Walker et al. 2005). In support of this, reducing TOR signalling did not increase the longevity of a *C. elegans* DR mutant (Hansen et al. 2007). Due to its ability to respond robustly to nutrient signals to stimulate growth, Blagosklonny proposes that TOR has a pivotal role in ageing driven by hyperfunction (Blagosklonny 2008). He proposes TOR signalling continues after development, when it may no longer be needed, resulting in hyperfunction and age-related pathology (Figure 1.9) (Blagosklonny 2008). Thus inhibitors of the TOR pathway, such as rapamycin, may be critical anti-ageing drugs in the future.

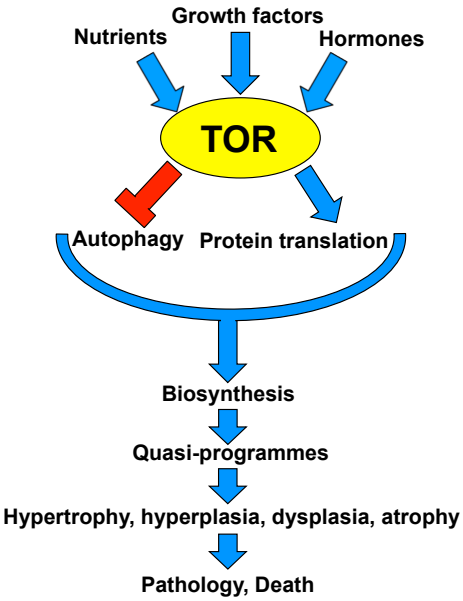

Figure 1.9. TOR-centric model for the hyperfunction theory of ageing. The TOR pathway is stimulated by food uptake, growth factors and hormones. It can cause various effects that activate biosynthesis including activating protein translation and inhibiting autophagy. During ageing, the biomass will increase, resulting in a hypertrophic phenotype. This will eventually cause damage and the development of lethal age-related pathology. (Image adapted from (Blagosklonny 2008; Gems & de la Guardia 2013)).

1.4.2 Hyperfunction as a possible cause of senescent pathology in *C. elegans*

If the hyperfunction theory of ageing is valid then at least some age-related pathologies in *C. elegans* should be the result of quasi-programmes. Certainly there are a number of pathologies that develop in ageing worms that are potentially driven by hyperfunction (Figure 1.10) (Gems & de la Guardia 2013). For example, the body wall cuticle enlarges during ageing, apparently due to run-on of collagen production (Figure 1.10A) (Herndon et al. 2002). Neurons develop additional protrusions during ageing (Figure 1.10B) (Tank et al. 2011). Oily yolk pools accumulate in the body cavity of old worms (Figure 1.10D) (Garigan et al. 2002; Herndon et al. 2002; McGee et al. 2011). Yolk is produced by the intestine to nourish developing oocytes. However the occurrence of these pools suggests yolk production is not switched off after self sperm depletion. This abundance of extracellular yolk may cause the ectopic deposition of lipid seen in other areas of the body, such as the muscle, which could disrupt tissue function (Figure 1.10C) (Herndon et al. 2002). The germline also undergoes extensive changes during ageing. Once reproduction ceases, oocyte production continues, causing an accumulation of oocytes along the proximal arm of the gonad (Jud et al. 2007). Unfertilised oocytes also build up in the uterus, where they undergo endoreduplication leading to the development of uterine tumours (Figure 1.10E) (Golden et al. 2007). The distal gonad arm atrophies and disintegrates during ageing (Figure 1.10D) (Garigan et al. 2002; Luo et al. 2010; Hughes et al. 2011). This appears to be driven by quasi-programmed apoptosis of germ cells: germline apoptosis contributes to oocyte development during the reproductive period but continues to operate in late life causing pathology (de la Guardia et al. 2016).

Therefore there are an abundance of age-related pathologies in *C. elegans* that either are or could be the result of hyperfunction.

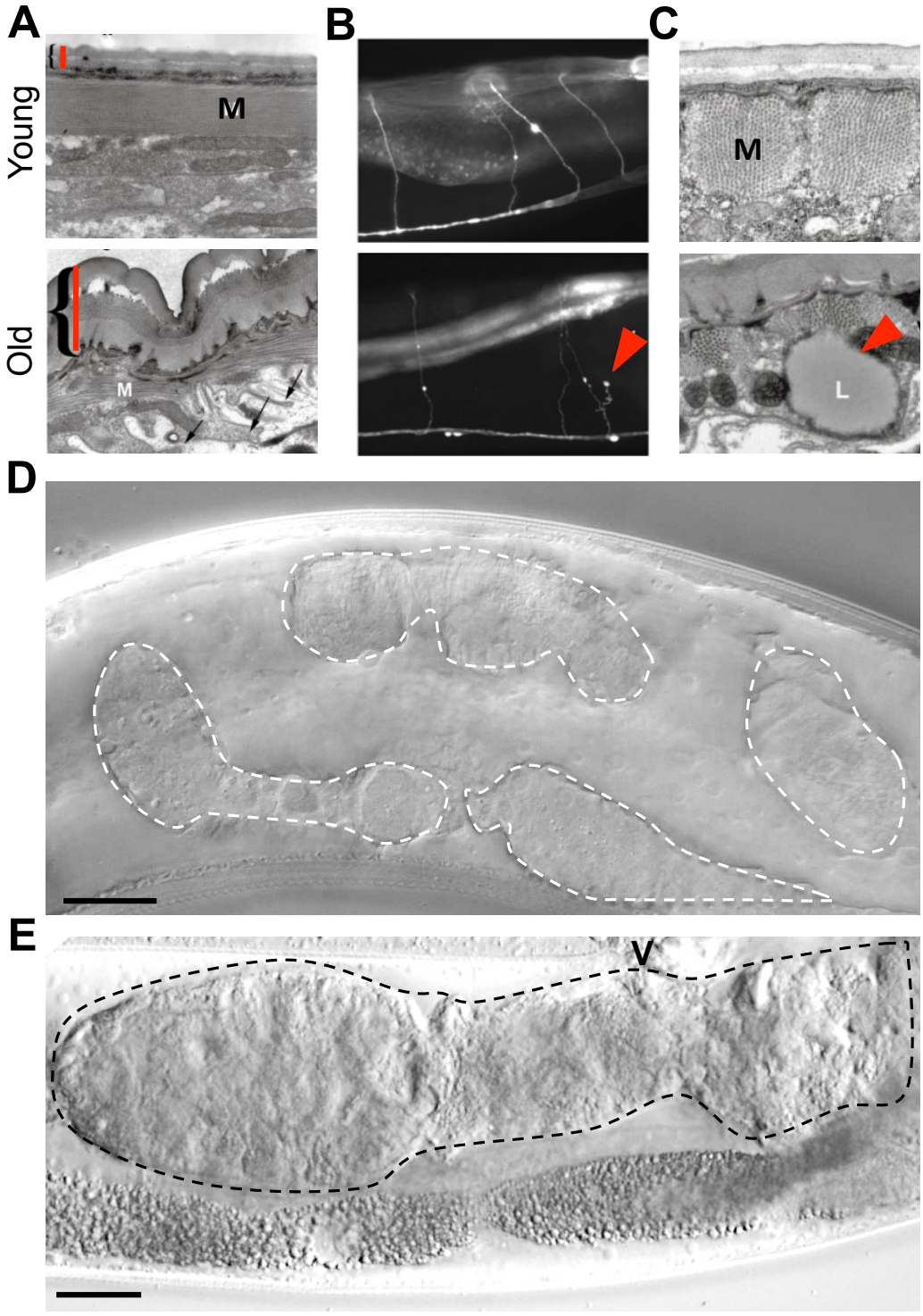

Figure 1.10. Age-related pathology caused by hypertrophy in *C. elegans*. (**A**) Day 18 worm with severe thickening of the body wall cuticle (red line). Muscle, M. (Image from (Herndon et al. 2002)). **(B)** Day 15 worm with evidence of neuronal branching (red arrow) (Image from (Tank et al. 2011)). **(C)** Day 18 worm with ectopic lipid (L) deposition (red arrow) in muscle (M) (Image from (Herndon et al. 2002)). **(D)** Day 11 worm with a disintegrated gonad (fragments outlined in white). Also note the yolky pools that fill the entire body cavity (Scale bar 20μm). **(E)** Day 12 worm with a large tumour (outlined in black) within the uterus. Vulva, V. (Scale bar 20μm).

1.4.3 Lethal pathology in ageing *C. elegans*

What do worms die of (i.e what age-related disease is lethal)? This is a deceptively simple question that surprisingly remains unanswered. To solve this mystery, one must identify the organ of the worm most likely to develop life-limiting pathology. The intestine is an obvious candidate, as it is by far the largest somatic organ in the worm and carries out multiple functions, including yolk synthesis (Altun & Hall 2009a). Furthermore it shows age-related decline, including atrophy of the intestinal cells, degradation of their nuclei and loss of microvilli (McGee et al. 2011). A major clue that indicates the intestine could have a key role in *C. elegans* mortality is that it has been shown in *daf-16; daf-2* mutants that restoration of *daf-16* specifically in the intestine is sufficient to extend lifespan by 50-60% (Libina et al. 2003), though it does not fully restore *daf-2* longevity. Furthermore in the long lived sterile mutant *mes-1(bn7)*, where longevity is *daf-16* dependent, expression of *daf-16* specifically in the intestine of the *daf-16; mes-1* mutant could wholly restore longevity (Libina et al. 2003). This demonstrates that DAF-16 activity in the intestine is at least partially responsible for *daf-2* longevity and could completely account for the longevity seen in germ-line deficient mutants.

There is also evidence that intestinal necrosis is involved in the death of the worm (Coburn et al. 2013). The intestine contains autofluorescent lysosome-related organelles called gut granules that fluoresce blue under UV light. It was long assumed that these gut granules contained lipofuscin because lipofuscin also emits blue fluorescence when exposed to UV light (Jung et al. 2007). Lipofuscin is an aggregate of damaged lipids and proteins that accrues during mammalian ageing and its presence has been used as evidence for the importance of molecular damage during ageing (Jung et al. 2007). However it was discovered in *C. elegans* that blue fluorescence does not increase during ageing, which

one would expect if blue fluorescence were caused by a gradual increase in lipofuscin. In fact levels stay constant until only a few hours before death, where there is a sudden and large increase in blue fluorescence (Figure 1.11) (Coburn et al. 2013). This phenomenon was named death fluorescence and was seen in worms that died from both stress and old age, showing it to be a general feature of death, whatever the cause. Death fluorescence also developed in a clear pattern, where it starts at the anterior end of the intestine and moves all the way along until it reaches the posterior end. This blue fluorescence was then identified as being produced by anthranilic acid derivatives (Coburn et al. 2013). Levels of anthranilic acid derivatives do not suddenly increase at death but their fluorescence is quenched while they are inside the acidic environment of the gut granule. When the membrane of the gut granule is compromised, the anthranilic acid derivatives are dequenched as the pH increases. Therefore death fluorescence is a marker of necrotic death, which is stimulated by a wave of Ca^{2+} influx. This wave of death then spreads along the intestine from anterior to posterior. Ca^{2+} is able to activate various enzymes, including phospholipases and proteases, which promote necrosis. Thus necrotic cell death within the intestine occurs during death in *C. elegans*, presumably contributing to it.

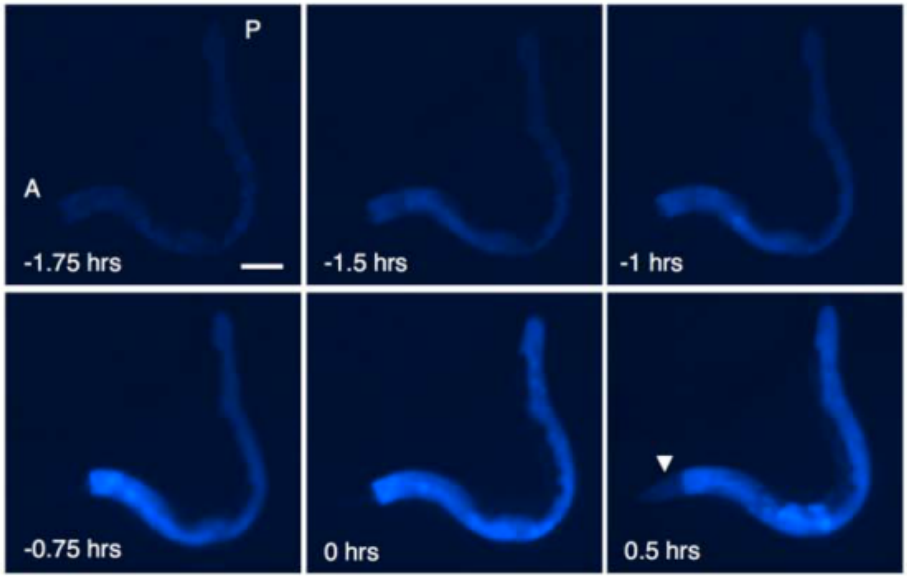

Figure 1.11. Death fluorescence in *C. elegans*. A wave of blue fluorescence spreads from the anterior (A) to the posterior (P) end of the intestine in a worm that has died from old age. This phenomenon is closely associated with death (0 hrs). (Scale bar 50μm). (Image from (Coburn et al. 2013)).

While there is substantial evidence that the intestine is a site of life limiting pathology, it seems unlikely to be the only organ that can develop a pathology that contributes to death in the worm. Firstly intestinal *daf-16* expression does not fully restore *daf-2* longevity in a *daf-16; daf-2* mutant (Libina et al. 2003). Therefore *daf-16* expression in another tissue could be required for full reestablishment of *daf-2* lifespan. Secondly, the necrotic wave in the intestine implies that necrosis contributes to death, however when necrosis is inhibited in *C. elegans* this does not result in a lifespan extension (Coburn et al. 2013). This suggests ageing causes other life limiting pathologies that develop alongside intestinal pathology.

Another possible site of lethal pathology is the pharynx, which has also been observed to undergo major age-related deterioration, losing both structural integrity and functional capacity during ageing (Chow et al. 2006; Huang et al. 2004). Furthermore bacteria accumulate in the pharyngeal lumen and can invade into the pharyngeal tissue of aged worms (Garigan et al. 2002; McGee et al. 2011). Perhaps the most compelling evidence that the pharynx may harbour a life-limiting pathology is that the period of pharyngeal function was found to be a predictor of lifespan, with the longest lived worms sustaining pharyngeal function for longer (Huang et al. 2004). Additionally the necrotic wave in the intestine often begins at the anterior end, close to the pharynx (Coburn et al. 2013). This could suggest that in old worms, an age-related pathology in the pharynx somehow initiates necrosis in the intestine. Overall it seems likely that, as in humans, there are multiple causes of death in ageing *C. elegans*.

1.5 Consolidating ageing theories

Two mechanistic theories of ageing have been introduced in this section: the molecular damage theory and the hyperfunction theory. It might seem

at first that these two theories are distinct and therefore surely only one can be true. However it is possible the two could be interlinked, complicating our understanding of the biological mechanisms that drive ageing. Ageing results in a wide range of phenotypes. While it is possible there is one central process driving the development of all age-related pathologies, a more realistic idea is that they are the result of several different mechanisms. While these mechanisms could act independently there are a number of examples that suggest hypertrophy and molecular damage could interact to drive development of pathology. For example stimulation of TOR, which has been proposed to have a key role in the hyperfunction theory (Blagosklonny 2008), can also cause increased levels of ROS (Kim et al. 2005). Therefore while TOR may cause a hypertrophic phenotype, it could also be causing increased levels of molecular damage in tandem. In addition some hypertrophic pathologies are also linked to increased levels of oxidative damage. For example myocardial infarction is associated with both hypertrophy of cardiac muscle cells but also with an increased amount of lipid peroxidation (Blagosklonny 2008; Cracowski et al. 2002). In such scenarios it is possible that both hyperfunction and molecular could initiate and/or exacerbate the development of the pathology.

For our studies we have chosen to use the model organism *C. elegans* to test the hyperfunction theory of ageing. As listed in section 1.4.2, there are several pathologies in *C. elegans* that could be caused by hyperfunction. However as *C. elegans* has a short growth cycle and a huge reproductive output in a small period of time, it is likely to favour a state of overgrowth to fuel this production. Furthermore they may not be capable of accumulating large levels of molecular damage as they only live for a few weeks. In contrast, humans have a very different life history and are obviously more complex than *C. elegans*. The vast array of pathologies in ageing humans is likely to be due to a number of different causes. Some may be driven predominantly by hyperfunction, for example overactivation of osteoblasts can lead to osteoporosis (Glantschnig et al. 2003). On the other hand, damage to DNA can cause

gene mutations, which in certain cases could lead to excess cellular proliferation and subsequently cancer. Therefore molecular damage could have a more significant role in human ageing. A challenge for future researchers will be to determine how different mechanisms could interact to produce age-related pathologies.

1.6 Aims

C. elegans has been used in numerous studies of ageing, but only a very small number have analysed pathology in the ageing worm (Herndon et al. 2002; McGee et al. 2011; Golden et al. 2007). Therefore there is only a limited knowledge about age-related pathology in *C. elegans*, including how senescent pathologies develop and which are the cause of death. The primary aims of my PhD were to analyse the pattern of progression of various age-related pathologies, explore the possible role of quasi-programmes as etiology and determine which might be the cause of death in ageing *C. elegans*.

A huge advantage of using the worm for this work is that, due to its transparency, Nomarski microscopy can be utilised to examine the internal tissues in live or dead animals, without the need to perform dissection. To evaluate the level of deterioration in various tissues, pathology scores were generated using previously described criteria (de la Guardia et al. 2016; Riesen et al. 2014), and ones more recently developed by Marina Ezcurra. This revealed that while various pathologies develop and worsen during ageing, only two examined during this study seem to be lethal: intestinal atrophy and pharyngeal infection.

The *C. elegans* germline undergoes various age-related changes. The uterus swells dramatically as large tumours develop within it (McGee et al. 2012; Golden et al. 2007). These tumours appear to develop in all wild-type hermaphrodites and are a striking age-related pathology that may cause mortality. In chapter 3.1 we show that various interventions,

including treatment with the anti-cancer drug 5-fluorodeoxyuridine (FUDR), can block uterine tumour development. However we then demonstrate that uterine tumours are not life limiting. Furthermore we identify a novel age-related pathology, bacterial infection of uterine tumours. Previous work in our group by Y. de la Guardia showed that gonad disintegration could be the result of quasi-programmed apoptosis (de la Guardia et al. 2016). In chapter 3.2, we provide additional evidence to support this theory by showing that altering the levels of germline apoptosis can change the extent of gonad disintegration.

It is clear the hermaphrodite intestine deteriorates dramatically during ageing, in particular it experiences major atrophy (McGee et al. 2011; Herndon et al. 2002; Garigan et al. 2002). In chapter 4 we collect morphometric data to obtain a better understanding of the dynamics and pattern of age-related intestinal atrophy. Furthermore, we provide evidence intestinal atrophy is the result of the intestine metabolising its own biomass to fuel quasi-programmed yolk production. The pharynx was the final tissue I examined during this project. In chapter 5 we used necropsy analysis to show that a subpopulation of *C. elegans* die early with an enlarged pharynx, which is caused by bacterial infection. We also provide evidence that this infection may be promoted by mechanical senescence (Zhao et al., 2017).

Throughout this project I have been fortunate to collaborate with many individuals. The work in chapter 3.1 contributed to the published work of Riesen et al., 2014, while chapter 3.2 was done in cooperation with Y. de la Guardia and much of it is now published in de la Guardia et al., 2016 (See papers in Appendix 2). The underlying mechanisms of intestinal atrophy, discussed in chapter 4, would not have been known without the insights gained by M. Ezcurra, T. Sornda and A. Benedetto (Ezcurra et al., 2017, unpublished). The study of pharyngeal infection in chapter 5 became a truly collaborative work, requiring contributions from a number of colleagues. I would like in particular to acknowledge and thank Y. Zhao, with whom I worked in partnership with on this project, leading us

to co-author the paper Zhao et al., 2017 (See paper in Appendix 2). In some places throughout this thesis, I have presented work performed by others to allow for a complete narrative. Whenever this is the case, full acknowledgement is given and I thank them for their involvement.

Chapter 2 Materials and Methods

2.1 *C. elegans* maintenance and methods

2.1.1 Stock maintenance

For normal maintenance worms were generally kept at 20°C on 60mm Petri plates containing nematode growth medium (NGM). These had been seeded with 100µl of *E. coli* OP50 to provide a food supply. To ensure the population did not starve, several adult hermaphrodites were regularly transferred to fresh plates to initiate a new population. Worms were transferred using a worm pick made with a platinum wire. The pick was heated in a Bunsen burner flame briefly to sterilise it, before it was used to transfer worms. A population of worms can also be maintained by chunking. This is where a flame-sterilised scalpel is used to cut out a piece of agar that is then placed on a fresh plate.

The male *C. elegans* is not usually abundant in populations but hermaphrodites can be induced to produce more males by heat shock. L4 hermaphrodites were placed at 30°C for 5-6hrs and then maintained at 20°C. Their progeny should contain some males. These can then be selected and used to create a male stock for experiments, with around 10-15 males for every 4 hermaphrodites, to ensure copious mating occurs. For experiments on plates, males were kept at a low population density of 5 per plate, due to the lifespan lowering effect of large numbers of males (Gems & Riddle 2000; Maures et al. 2014).

For long-term storage, populations from several starved plates were collected into a solution of 1:1 freezing medium and M9 buffer. Aliquots can then be kept at -80°C, for many years if need be. When strains are required, they can be thawed and pipetted onto fresh NGM plates. If the

original freeze was successful, a large number of L1 larvae should have survived and in a few days, grow into fertile adults.

2.1.2 List of *C. elegans* strains

The vast majority of strains were obtained from Caenorhabditis Genetics Center (CGC), at the University of Minnesota. Some strains were kindly supplied to us from individual laboratories, and are indicated as such. The wild-type strain used was the N2 male stock from the CGC, except for chapter 5 where the CGC N2 hermaphrodite stock was used.

Strain name	Genotype
AH102	*lip-1(zh15)* IV
BC12677	*dpy-5(e907)* I*; sIs11111*[*rCesC32F10.8::GFP* + *pCeh361*]
BC12754	*dpy-5(e907)* I; *sIs12567*[*rCesC07H6.3::GFP* + *pCeh361*]
BC16329	*dpy-5(e907)* I; *sEx16329*[*rCesF20B10.1::GFP* + *pCeh361*]
CB3168	*him-1(e879)* I; *mab-3(e1240)* II
CF80	*mab-3(mu15)* II; *him-5(e1490)* V
DA464	*eat-5(ad464)* I
DA493	*phm-3(ad493)* III
DA521	*egl-4(ad450)* IV (previously *eat-7*)
DA522	*eat-13(ad522)* X
DA591	*unc-10(ad591)* X
DA597	*phm-2(ad597)* I
DA606	*eat-10(ad606)* III
DA698	*unc-36(ad698)* III
DA1110	*eat-18(ad1110)* I
DA1116	*eat-2(ad1116)* II
DR466	*him-5(e1490)* V
EG3234	*oxIs144*[*inx-16::GFP*, *lin-15*+]
GA1200	*mdl-1(tm311)* X
GA1801*	*lip-1(gt448)* IV

GA1802*	*ced-9(n1653ts)* III
GA1803[+]	*gld-1(op236)* I; *ced-3(n717)* IV
JK560	*fog-1(q253)* I
JK4563	*gld-1(q126sd)* I/*hT2* [*bli-4(e937) let-?(q782) qIs48*] (I;III)
MT1522	*ced-3(n717)* IV
NQ828[&]	*qnEx446*[*Pabu-1:mCherry*; *Pabu-1:abu-1::sfGFP; rol-6(d)*; *unc-119(+)*]
NQ829[&]	*qnEx447*[*Ppqn-2:mCherry; Ppqn-2:pqn-2::sfGFP; rol-6(d); unc-119(+)*]
SS104	*glp-4(bn2)* I
TG34	*gld-1(op236)* I

*Provided by Anton Gartner

[+]Provided by Björn Schumacher

[&]Provided by David Raizen

2.1.3 Elimination of contamination

To reduce the chances of contamination on plates, plates were only opened near the presence of a flame. Regardless, plates can sometimes become contaminated with either fungus or non-*E. coli* bacteria. To remove fungus, worms were transferred to a non-contaminated plate and allowed to crawl around so they moved away from any spores that had been transferred with them. Worms were then transferred again to a fresh plate. To remove bacterial contamination a solution of 1:1 1M NaOH and 5% bleach was made. A drop of this was added to a fresh NGM plate and several adult hermaphrodites were placed in the drop. This kills everything except the eggs, which are protected by their eggshell. The majority of L1 larvae will not emerge until the bleach solution has soaked into the plate and hence escape death.

2.1.4 Synchronizing populations

Individuals that were at the L4 larva stage were selected from a mixed population of worms to obtain an age-synchronized group. When large numbers of individuals were needed, an egg lay or large scale bleaching was performed. The latter method was also used when eggs needed to be sterile. For an egg lay, 8 adult hermaphrodites were left on a plate to lay eggs for approximately 6 hours at 20°C. The adults were then removed and the eggs kept at 20°C to hatch. L4 larvae were then selected for experiments. For a large scale bleaching, a substantial number of adult hermaphrodites were rinsed into a 15ml falcon tube using M9 buffer. The tube was centrifuged at 3000rpm for 2 minutes. The majority of the supernatant was removed, leaving only 1ml. 300µl of 1:1 solution 10% bleach and 4M NaOH was added. The tube was agitated vigorously and examined regularly under a dissecting scope. Once the cuticle of the adults had dissolved and the eggs had been released, the tube was filled with M9 buffer to terminate the reaction. The eggs were then centrifuged at 3000rpm for 2 minutes and the supernatant removed. The pellet was resuspended in fresh M9. This was performed three times to remove any remnants of the bleach solution. Eggs were then pipetted onto plates and allowed to hatch and grow at 20°C. L4 larvae were then selected for experiments.

2.1.5 Survival and necropsy analysis

For survival assays worms were kept at around 25-35 per plate. If the DNA and RNA synthesis inhibitor 5-fluorodeoxyuridine (FUDR) was used to block progeny production, it was added to the plates the day before the L4 worms were picked. This was to allow it to diffuse throughout the plate. Most survival assays were then scored three times a week for dead worms. For necropsy assays, scoring was performed more regularly to reduce corpse decomposition. Corpses were then collected and prepared for microscopy. A dead worm was one that did not respond to a poke by a

worm pick to the head, body or tail. Sometimes worms had to be censored if they had crawled up the wall and desiccated; if eggs had hatched internally; if the intestine had ruptured through the vulva; or if the plate had become contaminated.

For worms exposed to glass powder for necropsy analysis, glass plates were prepared as follows. Glass frit was obtained from www.warm-glass.co.uk. To purify smaller glass particles, the powder was separated by gravity for 1 minute in 40ml 30% glycerol in a 50ml falcon tube. Only the top third of the solution was retained and again separated by gravity in glycerol. This was done 4 times to obtain a solution of micro glass particles. This was then centrifuged for 5 minutes at 3000rpm, the supernatant removed and the pellet resuspended in M9. This was done three times to wash away the glycerol. The solution was then autoclaved and allowed to cool before 300µl of it was added to a plate with a well-established bacterial lawn. Plates were then allowed to dry overnight before worms were introduced.

2.1.6 Individual liquid culture

To study male ageing in *C. elegans* in the absence of male-male interactions that reduce lifespan, males can be cultured individually using the following liquid culture method developed by D. McCulloch (McCulloch & Gems 2003). OP50 was grown in 200ml OP50 medium overnight at 37°C in a shaker. This solution was then centrifuged at 4100rpm for 15 minutes and resuspended in 150ml S medium, that had been kept at 4°C. The bacterial count of the solution was determined by doing serial dilutions plated onto LB plates. The required range was 1-5 x 10^9 cells ml^{-1} to ensure there was sufficient food for optimum lifespan and progeny production. This liquid medium was then divided into 20ml aliquots and stored at 4°C. Aliquots were streaked on agar plates and if a contaminant grew the aliquot was disposed of. 50µl of this culture was then added to each well in a 96 U-well plate, except for the outer wells

that contained milliQ water to act as an evaporation buffer. Males and hermaphrodites were then removed from agar plates at the L4 stage and placed individually into the wells. The plates were wrapped in parafilm and placed in sealed boxes with a cup of water to prevent the wells from drying out. Worms were could be transferred out of wells for microscopy using a hook shaped pick.

2.1.7 RNA-mediated interference

HT115 is the *E. coli* strain used for RNAi experiments in *C. elegans*. RNAi clones were collected from the Ahringer library (owned by Richard Poole, UCL) and then stored at -80°C. Clones were streaked onto LB plates containing the antibiotics ampicillin (50µg/ml) and tetracycline (10µg/ml) and grown up overnight at 37°C. A single colony was then selected and grown in LB broth with only ampicillin in a 37°C shaker overnight. The bacteria were pelleted in a centrifuge at 4100rpm for 15 minutes and then the supernatant was removed before the pellet was resuspended in a solution of LB devoid of antibiotic. Cultures were then stored at 4°C.

IPTG plates were made by adding 1ml of 1M IPTG for every 1L of NGM media. These plates were then seeded with 200µl of the appropriate HT115 clone. The bacteria were grown on the plates for a couple of days before being used immediately.

2.2 Bacterial methods

2.2.1 Preparation of bacterial cultures

E. coli OP50 was streaked on a LB plate from a frozen stock provided by the CGC. A single colony was selected with a sterile loop and used to inoculate 100ml OP50 culture solution. This was left overnight in a 37°C

shaker and then stored at 4°C. Bacterial stocks were replenished approximately every two weeks.

A strain of *E. coli* OP50 that emitted red fluorescence (OP50-RFP) was kindly generated for me by M. Ezcurra. She transformed *E. coli* with the pRZT3 plasmid, kindly sent to us by J.F Rawls of Duke University, Durham. This plasmid contained genes for tetracycline resistance and DsRed, whose expression was regulated by a constitutive *lac* promoter**.** OP50-RFP for streaked onto a LB plate containing 10µg/ml tetracycline. A single colony was selected and grown in LB solution, also containing tetracycline. This was allowed to grow overnight in a 37°C shaker. The stock was then centrifuged at 4100rpm for 15 minutes and the supernatant removed. The bacterial pellet was then resuspended in fresh, antibiotic-free LB solution and stored at 4°C.

2.2.2 Inhibition of bacterial growth

Bacterial growth was inhibited using either antibiotic treatment or UV exposure, as previously described (Garigan et al. 2002; Gems & Riddle 2000). For antibiotic treatment, NGM plates were seeded with 100µl OP50 and left to grow at room temperature for two days. A 500mM solution of carbenicillin was made up fresh for each experiment in MilliQ water and then 80µl of it was added to each plate to give a final concentration of 4mM carbenicillin. Plates were allowed to dry overnight and then worms were transferred onto plates at the L4 stage, unless otherwise specified. Carbenicillin-treated plates not immediately used for experiments were stored at 4°C until required.

For UV-killing, NGM plates were seeded with 80µl OP50, which was allowed to grow overnight at 20°C. In the morning, a Stratagene UV stratalinker 2400 was sterilised by running it empty for 10 minutes. Plates and their upturned lids were then placed inside for 30 minutes. UV-killed bacteria were then streaked onto a LB plate. If no colonies grew, this

affirmed the protocol had been successful. Sterile eggs, obtained from large scale bleaching, were pipetted onto the plates and allowed to grow until L4 stage, when they were selected for experiments.

2.3 Staining methods

2.3.1 DAPI staining

DAPI (4',6-diamidino-2-phenylindole) emits blue fluorescence and associates with DNA. It has been used extensively to stain *C. elegans* and the following method is based on previous work (Francis et al. 1995). Worms were picked into M9 in a 1.5ml tube and centrifuged at 3000rpm for 2 minutes. The supernatant was removed and 200µl methanol, which was cooled at -20°C, was added. Tubes were kept on ice for 5 minutes, but agitated at regular intervals. The methanol was removed and worms were washed in M9 before being centrifuged again. 200µl DAPI (500ng/ml) was added and the tube was placed in darkness for 30 minutes. M9 was added before worms were centrifuged again and the supernatant removed. Worms were then pipetted onto a NGM plate and prepared for microscopy.

2.3.2 SYTO 12/13 staining

SYTO12 is a vital dye previously used to stain apoptotic cells in *C. elegans* (Gumienny et al. 1999), while SYTO13 has been previously shown to stain *Microbacterium nematophilum* in the worm, where it causes an infection in the rectum (Nicholas & Hodgkin 2004). Both emit a green fluorescence that can be seen using a GFP filter cube. The following method is based off this previous work, but was adapted by A. Benedetto. A square of parafilm was adhered to a microscopy slide and an imprint was formed on it by using the round end of a pencil. A drop of 15µM SYTO13 or 33µM SYTO12 was pipetted into this impression.

Around 10 worms were placed in the droplet, along with some bacteria that had been scraped from the plate, to ensure the worms did not starve. Slides were placed in a covered container that had been partially filled with water. This was to prevent the dye from bleaching and to ensure the worms were protected from desiccation. The container was then placed at 25°C for 4 hours. Worms were then picked out of the drop and placed onto a seeded NGM plate. This had to be done quickly, before the drop dries out. Thus it is recommended to only have one drop per slide. For SYTO12 staining, worms were left for around 30 minutes before they were imaged to allow any dye taken up by the intestine to be flushed out. For SYTO13 experiments, worms were imaged immediately.

2.4 Microscopy

2.5 Preparation for imaging

For both Nomarski and confocal microscopy, live adult worms were placed on 2% agar pads inside a 5µl drop of 0.2% levamisole, an anaesthetic. A cover slip was then gently placed onto the pad and worms were imaged immediately. In some cases, nail varnish was wiped around the coverslip to seal the slides.

2.5.1 Microscope systems

Nomarski images of worms were collected on a Zeiss Axioskop^2 plus microscope with a Hamamatsu ORCA-ER digital camera C4742-95 using Volocity 6.3 (Mac version) software to take the images. For fluorescence images the following filter cubes were used: DAPI cube (excitation range 350 – 380nm, emission >420nm), FITC/GFP cube (excitation range 450 – 490nm, emission 515 – 565nm) and Rhodamine cube (excitation range 540 – 552nm, emission >590nm). The default setting for gain in Volocity is 0 and this was unchanged throughout experiments. Exposure time was

altered as it was optimised for each animal, however the following ranges were generally used: RFP 20-50ms, GFP 250 – 500ms and for DAPI (for *C. elegans* autofluorescence) 100-200ms.

To collect image stacks, a Zeiss Axio Observer microscope was used that was connected to a LSM-710 confocal system. Images were obtained using Zen 2009 software (Windows version) and then exported into Volocity 6.3 (Mac version) for further analysis.

2.5.2 Electron microscopy

We used protocol 8 developed by Dave Hall from WormBook to prepare our worms for electron microscopy (Shaham 2006), with assistance from M. Turmaine. Worms were grown on OP50-RFP until day 8 at 20°C and then sorted into groups based on pharyngeal pathology. Worms were picked onto unseeded plates, into a drop of M9, in an attempt to wash off excess bacteria. A small hole was then cut out of an agar pad on a microscope slide using a scalpel. A drop of fixing solution (2.5% glutaraldehyde, 1% paraformaldehyde in 0.1M sucrose and 0.05M cacodylate) was added to the hole and a worm picked into it. The worm was then decapitated using a 30g needle and the heads were collected into a tube of fixing solution, where they remained for at least 2 hours. The heads then went through several steps of washes and fixes before being mounted into agarose blocks, which are used for sectioning. Sections were collected and examined under low magnification until the posterior bulb of the pharynx was reached. At this point, a diamond blade was used to collect 70nm sections, which were transferred to a copper mesh and stained with lead citrate. The sections were examined using a Joel 1010 transition electron microscope and images were collected by Gatan Imaging Software in TIFF format.

2.5.3 Measuring the pathology state of *C. elegans* tissues

Images used for these pathology screens were Nomarski images obtained at either x400 or x630 magnification, unless otherwise stated. Image J or Volocity 6.3 software (Mac versions) were used to perform any necessary measurements. To prevent bias when qualitative scores were generated, images were randomly sorted and blinded using scrambling software developed by Peter Rennert (de la Guardia et al. 2016). I would like to thank M. Riesen, Y. de la Guardia, Y. Zhao, C. Yang and M. Ezcurra who developed the majority of the following protocols that I adopted for my studies.

2.5.4 Uterine tumours

The following qualitative scoring system was used to determine the pathology state of the uterus (Riesen et al. 2014). A class 1 worm shows no tumours and the eggs are well organised within the uterus. In class 2 there is some disorder and unfertilised oocytes have started to accumulate within the uterus. Class 3 worms have developed small tumours while class 4 worms have larger tumours. Class 5 worms have huge tumours that have filled the entire body cavity. The cross-sectional area of the tumours could also be measured from images collected at x100 magnification.

2.5.5 Gonad atrophy

The following qualitative scoring system was used to determine the extent of gonad atrophy (de la Guardia et al. 2016). A class 1 worm has a healthy gonad, with both gonad arms filling the body cavity. In class 2, the gonad arms have started to thin. In class 3 the thinning has worsened to such an extent a breakage appears unavoidable. In class 4, gonad fragmentation has occurred, while in class 5 the gonad has deteriorated to the point it can no longer be identified.

2.5.6 Intestinal atrophy and lumen distension

Initially I tried to measure the entire cross-sectional area of the intestine and the lumen. To do this I collected three images of each worm taken at x100 magnification; a brightfield image, a gut auto-fluorescence image and a RFP image. Images were then overlaid in Volocity 6.3 software and the cross-sectional area of the entire intestine was measured using both the brightfield and gut auto-fluoresence image as a guide. Next the area of the RFP was measured which, as these worms had been fed OP50-RFP, was hoped to represent the intestinal lumen area. To obtain the cross-sectional area of the intestine, the lumen value was subtracted from the overall area.

We found there to be some problems using this method. Firstly, when the lumen was very narrow, it was virtually impossible to draw around it to measure the area accurately. Secondly, the fluorescent bacteria produced a strong signal in young worms but at older ages the fluorescence sometimes disappeared. Even if the bacteria were still fluorescing in these older worms, the red fluorescence from the intestinal cytoplasm was often of a similar brightness to the luminal fluorescence. This made it difficult to distinguish between the intestinal cytoplasm and lumen.

Therefore I decided to adopt the method that had been developed by M. Ezcurra to get a score for the level of intestinal atrophy and lumen distension. At a point in the posterior intestine, the lumen, intestine and worm body diameter was measured. A lumen score was obtained using the following formula: (lumen diameter/body diameter) x 100. An intestine score was obtained using the following formula: ((intestine diameter – lumen diameter)/body diameter) x 100.

2.5.7 Yolky/lipid pools

The yolky/lipid pool area within the body cavity and the total body cavity area in the field of view were both measured. A lipid/yolky pool score was obtained using the following formula: (yolk area/body area) x 100.

2.5.8 Pharyngeal pathology

Due to our heightened interest in pharyngeal pathology, we used a number of different methods to analyse the ageing pharynx.

Qualitative scoring system

Class 1 pharynxes have a smooth outline and the radial muscle lines are clearly visible. In class 2, the outline of the pharynx becomes uneven, the radial muscle lines are starting to fade and small cavities or blisters appear. By class 3 the pharynx starts to show clear signs of ageing. It will have one of the following features: bacterial accumulation in the lumen, complete loss of radial muscle lines, or large cavities or blisters. Class 4 worms will show at least two of these features. Class 5 worms contain a posterior pharyngeal bulb that is barely recognisable or grossly swollen.

Tracking pharyngeal size in individual worms

11 – 15 worms were placed individually onto plates at the L4 stage. Worms were then imaged three times a week at x200 magnification until their death. As we wanted to track these worms into very old age, the worms had to be imaged *in situ* on agar plates without anaesthetic. This was because the trauma of being mounted onto an agar pad or being exposed to anaesthetic could easily cause the death of a fragile, old worm. Instead worms were immobilised by placing them on ice for around 10-15 minutes until they stopped moving. A Nomarski image was taken of the pharynx and the area of the posterior bulb measured. A control set of worms was kept to ensure the imaging process did not have an effect on lifespan.

Necropsy analysis

Corpses of worms from a survival assay were collected onto an unseeded NGM plate. They could then be examined for evidence of pharyngeal swelling using a Nikon SMZ645 microscope. If further analysis was required or measurements needed to be taken, corpses were mounted onto agar pads and high magnification Nomarski images collected.

Bacterial load

Extracted pharynxes from day 10 or 11 worms, which has been grown at 20°C, were washed in M9 buffer and then pulverised until the entire tissue had broken apart. A serial dilution was performed and plated onto LB plates to allow the colony forming units to be counted.

2.5.9 Tracking pathology in individual worms

Marina Ezcurra developed the following method to obtain high magnification images of worms throughout their life span. Worms were placed onto individual NGM plates. At various time points, up until day 18 at 20°C, the worms were prepared for Nomarski microscopy. Images of a range of tissues were collected. Each worm was mounted onto an agar pad, under a slightly raised cover slip, which was supported on each side by a stack of two cover slips. This was to prevent the coverslip crushing a fragile, elderly worm. A PE120 Peltier stage was set to 4°C before the slide was placed onto it. At this temperature worms were immobile, which made it easier to obtain higher quality images. To retrieve worms, M9 was pipetted under the cover slip. The cover slip was then removed and the worm hooked out of the solution and returned to its NGM plate. A control set of worms was kept to ensure the imaging process did not have an effect on lifespan.

2.6 Measuring pharyngeal function

2.6.1 Pharyngeal pumping rate

Worms that were dwelling on the bacterial lawn were tracked with a Nikon SMZ645 microscope. The total pharyngeal pumps within 15 seconds were recorded using a clicker counter. This was then done twice more to obtain three values from which a mean was calculated. Pharyngeal pumps per minute was then determined.

2.6.2 Serotonin assay

Serotonin hydrochloride was dissolved in a solution of 0.1M HCl, to give a concentration of 250mg/ml serotonin. 100µl of this was then added topically to a NGM plate with an established bacterial lawn, to give a final concentration of 12mM serotonin. Control plates had 100µl of 0.1M HCl added topically to give a final concentration of 1mM HCl. The plates were allowed to dry overnight before worms were transferred onto them. Pharyngeal pumping rate was calculated as above and measured both in worms on the bacterial lawn and those residing away from it.

2.7 Statistics

To compare qualitative pathology scores (e.g gonad atrophy, uterine tumours, pharyngeal pathology), the non-parametric Wilcoxon-Mann-Whitney test was used in JMP 11 and then corrected for multiple comparisons.

For single comparisons, a two-tailed Student's *t* test was performed using Microsoft Excel. If analysis required multiple comparisons the data was analysed in either JMP 11 or Graphpad Prism 6. A one-way ANOVA was performed to analyse a single factor to determine if there were any

statistically significant differences in the data. If the ANOVA result was significant, a Tukey HSD was carried out to obtain the statistical comparisons between all the groups. For two factors a two-way ANOVA was used, followed by a Tukey HSD or Sidak's test if the two-way ANOVA indicated a significant interaction.

Significant correlations between pathology state on a certain day and eventual life span were obtained using linear regression in GraphPad Prism.

Data from survival assays were analysed using the log-rank test in either JMP 11 or Graphpad Prism. To deconvolve lifespan graphs into P and p deaths, each was plotted by censoring the other form of death and the entire standard censors from the whole population. The same was done when calculating mortality rate, which was performed in GraphPad Prism. To determine if there was a significant slope change in mortality rate, two separate linear regressions were performed on data before and after day 11. Graphpad Prism was then used to determine if there was a significant difference between these two slopes.

2.8 Reagents

Name	Recipe (per 1 litre of reagent)
Freezing medium	6.8g KH_2PO_4, 5.85g NaCl, 300ml 100% glycerol in total of 1L water. Autoclave to sterilise, then add 300µl of sterile 1M $MgSO_4$.
IPTG plates	3g NaCl, 17g agar, 2.5g bactopeptone in total of 1L of water. Autoclave to sterilise. Cool to approximately 55°C then add the following sterile solution: 25ml 1M KH_2PO_4, 1ml 1M $CaCl_2$, 1ml 1M $MgSO_4$, 1ml 5mg/ml cholesterol (in 100% ethanol), 1ml 1M IPTG.

LB broth/plates + antibiotics	25g LB broth powder (Fisher Scientific)/17g agar in total of 1L water. Autoclave to sterilise. Cool to approximately 55°C then add 1ml 50mg/ml ampicillin and/or 2ml 10mg/ml tetracycline.
M9 buffer	5g NaCl, 7g $Na_2HPO_4.2H_2O$, 3g KH_2PO_4, 0.25g $MgSO_4.7H_2O$ in total of 1L water. Autoclave.
NGM plates	3g NaCl, 17g agar, 2.5g bactopeptone in total of 1L of water. Autoclave to sterilise. Cool to approximately 55°C then add the following sterile solutions: 25ml 1M KH_2PO_4, 1ml 1M $CaCl_2$, 1ml 1M $MgSO_4$, 1ml 5mg/ml cholesterol (in 100% ethanol).
OP50 broth	5g tryptone, 2.5g yeast extract in total of 1L water. Autoclave to sterilise.
S basal	5.85g NaCl, 1g K_2HPO_4, 6g KH_2PO_4, 1ml 5mg/ml cholesterol (in 100% ethanol) in total of 1L water. Autoclave to sterilise.
S medium	3ml 1M $CaCl_2$, 3ml 1M $MgSO_4$, 10ml 1M potassium citrate, 10ml trace metals solution in 1L S basal. All solutions should be sterilised before mixing.
Trace metals solution	0.69g $FeSO_4.7H_2O$, 0.2g $MnCl_2.4H_2O$, 0.26g $ZnSO_4.7H_2O$, 0.025g $CuSO_4.5H_2O$, 1.86g disodium EDTA in total of 1L water. Autoclave to sterilise.

Chapter 3 The development and impact of pathologies in the *C. elegans* germ line

3.1 Part 1: Investigating the effect of *C. elegans'* uterine tumours on mortality

3.2 Introduction

During the first 3-4 days of adulthood the *C. elegans* hermaphrodite can produce approximately 300 progeny through self-fertilisation. During this time healthy, viable oocytes develop and move down each proximal arm of the gonad and are fertilised in the spermatheca. Once all the sperm have been depleted unfertilised oocytes will continue to be expelled via the vulva for several more days, with reproduction still possible if additional sperm are supplied via mating. Eventually ovulation ceases and oocytes stack up along the proximal arm of the gonad (Jud et al. 2007) before the gonad undergoes atrophy and disintegration (de la Guardia et al. 2016). Unfertilised oocytes that remain in either the uterus or distal to the spermatheca then start to degenerate; they can shrink (Luo et al. 2010) or become hypertrophic (de la Guardia et al. 2016) with cavities forming between cells (Luo et al. 2010). They also start to undergo nuclear endoreduplication (McGee et al. 2012) and eventually develop into large uterine tumours that contain large quantities of DNA (Golden et al. 2007) (Figure 3.1). Earlier studies have refrained from calling them tumours, preferring instead to describe them as clusters (Luo et al. 2010), masses (Golden et al. 2007) or growths (McGee et al. 2012). However we propose that calling them tumours is the most precise definition, where tumour refers to an accumulation of cells. Therefore I shall use the term tumour in regards to this pathology throughout this

thesis. Note this is in contrast with mammalian tumours that occur due to cell proliferation rather than accumulation.

The first appearance of these tumours coincides with the end of reproduction (day 4 at 20°C) and they ultimately develop in all ageing wild-type hermaphrodites. While the tumours are primarily made of polyploid oocytes there is also evidence they contain other components, including yolk (McGee et al. 2012), various secreted proteins (Zimmerman et al. 2015) and lipids within the oocytes (Wang et al. 2017, unpublished).

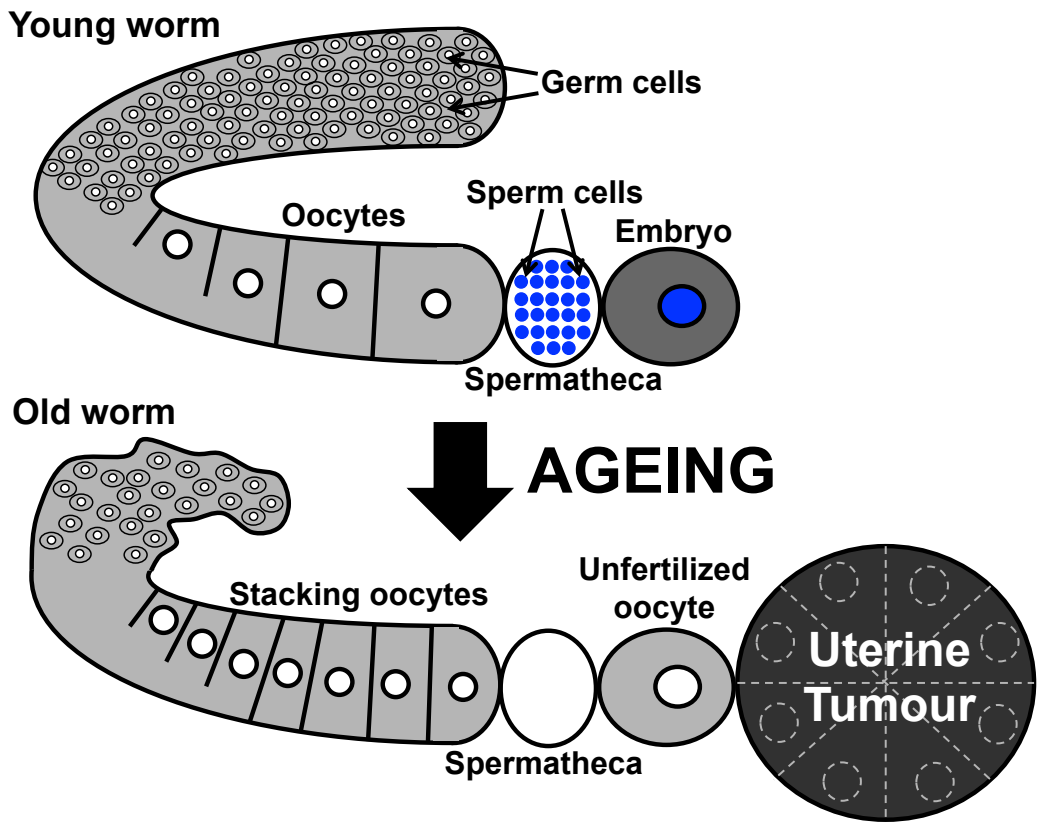

Figure 3.1. Ageing of the *C. elegans* hermaphrodite reproductive system. In young worms, the gonad is healthy with oocytes being fertilized within the spermatheca. Fertilized oocytes go on to form eggs that are eventually expelled through the vulva. In older animals, the sperm supply is exhausted and unfertilized oocytes begin to stack up along the proximal arm. This means unfertilized oocytes start to undergo nuclear endoreduplication, with those within the uterus ultimately forming uterine tumours.

3.2.1 *C. elegans* uterine tumours as a model for mammalian tumours

In mammals both malignant and benign tumours are major age-related pathologies, with cancer being a significant cause of late life mortality. *C. elegans'* uterine tumours are quite different from malignant mammalian tumours. The latter are caused by mutations that result in uncontrolled cell proliferation, leading to the formation of a tumour. These tumours can eventually become metastatic, where cancerous cells spread throughout the body. In contrast, *C. elegans'* tumours are formed by increases in size, apparently unrelated to mutations, and there is no evidence that they can invade other tissues. However they could be viewed as a good model for benign tumours. For example there are parallels to mammalian ovarian teratomas, which are usually benign and are also derived from unfertilised oocytes (Ulbright 2005).

It is unclear whether the uterine tumours impair worm health. However their substantial size does result in compression of the intestine that might cause disruption to nutrient absorption and metabolism. Furthermore in the long-lived mutants *daf-2* and *sma-2* uterine tumours are suppressed (Luo et al. 2009; Luo et al. 2010), though in *daf-2* mutants the uterine tumours can develop later in life (McGee et al. 2012). This raises the possibility that uterine tumours could limit lifespan in wild-type worms. Given the major impact tumours can have on late-life health in mammals, we set out to establish if uterine tumours contribute to mortality in *C. elegans*.

3.2.2 Manipulating uterine tumour growth

The *mdl-1* gene in *C. elegans* encodes a protein homologous to mammalian MAD transcription factors (Yuan et al. 1998). In mammals, these act as growth inhibitors by antagonising the MYC transcription factors, which are often upregulated in cancerous tumours (Yuan 1998).

MAD acts as a tumour suppressor, competing with MYC to form heterodimers with the MAX transcription factors, which can then bind to DNA (Yuan et al. 1998). MYC/MAX heterodimers generally turn on gene expression and promote cell proliferation and growth. In contrast, MAD/MAX heterodimers generally turn off gene expression and are upregulated in terminally different cells (Yuan et al. 1998). *C. elegans* also has a homolog for MAX, which is encoded by *mxl-1* and can form heterodimers with MDL-1. However the *C. elegans* genome does not possess any *myc*-like genes (Yuan et al. 1998; Riesen et al. 2014), perhaps because the somatic tissue is post-mitotic so there is no need for extensive control of cell proliferation.

mdl-1 was identified as a potential direct target of DAF-16 (Schuster et al. 2010), and this was then confirmed (Riesen et al. 2014). As DAF-16 is the transcription factor required for longevity in *daf-2* mutants, this suggests that MDL-1 activity could promote *daf-2* mutant longevity. In agreement with this hypothesis, mutation of *mdl-1* decreased lifespan in both a wild-type and *daf-2(m577)* background (Riesen et al. 2014) and *mdl-1* RNAi was able to reduce *daf-2(mu150)* lifespan (Murphy et al. 2003).

The *mdl-1(tm311) C. elegans* mutant contains a putative null deletion allele and is the strain we decided to use for our experiments. It does not have detectable abnormal somatic growth but shows abnormalities in germline proliferation (Riesen et al. 2014). It lays an increased number of unfertilised oocytes, referred to as the Uno-o (unfertilised oocyte overproducer) phenotype, and also has increased oocyte stacking in the proximal arm of the gonad (Riesen et al. 2014). As endoreduplicating, unfertilised oocytes that persist inside the uterus result in tumour development it was not surprising that *mdl-1*, with its increased oocyte production, also had accelerated tumour development (Riesen et al. 2014). Interestingly, it has also been shown that MDL-1 can act downstream of DAF-16 in the germline. *gld-1* mutants develop lethal, hyperproliferative germline tumours that are distinct from uterine tumours

(Francis et al. 1995). Knockdown of *daf-2* can suppress these tumours, but *mdl-1* RNAi in these worms causes an increase in germ cell number (Pinkston-Gosse & Kenyon 2007). Thus, MDL-1 can suppress growth of the germline and delay uterine tumour development in *C. elegans*.

This all fits with a familiar pattern, that many genes that affect ageing also affect growth, in this case in the germline. Therefore we hypothesised that the *mdl-1* mutant could be shortening lifespan by accelerating tumour development that causes mortality. We decided to test whether reduction or total inhibition of tumour development could increase lifespan in wild-type or *mdl-1* worms. We used 5-fluorodeoxyuridine (FUDR), an anti-cancer drug used in humans, to see if it could block tumour development and extend lifespan. FUDR works by inhibiting DNA and RNA synthesis. FUDR is metabolised into FdUMP that can inhibit thymidylate synthase, an enzyme crucial for DNA synthesis (Bijnsdorp et al. 2007). Other FUDR metabolites can also become incorporated into DNA and RNA, impairing normal synthesis and function (Longley et al. 2003). Therefore FUDR should be able to block endoreduplication in unfertilised oocytes and thus prevent tumour formation. Consistent with this, high doses of FUDR prevent both the development of DNA masses and the dramatic increase in genome copy number seen in ageing *C. elegans* (Golden et al. 2007). In regards to longevity, it has been reported that FUDR does not increase wild-type lifespan (Gandhi et al. 1980; Hosono 1978; Hosono et al. 1982; Van Raamsdonk & Hekimi 2011). However, it is not known whether the FUDR concentrations used were sufficient to block tumour formation. Moreover, one study did report an extension of lifespan at a high concentration of FUDR (400μM) (Angeli et al. 2013), which suggests that in certain conditions uterine tumours could be lethal.

To study uterine tumour development we created a qualitative uterine pathology scoring system that ranked the status of the uterus from class 1-5. Score 1-2 denotes no tumour while scores 3-5 indicate a tumour is present, with higher scores representing larger tumours (Figure 3.2).

Using this scoring system we set out to establish whether FUDR could inhibit tumour development and if so, whether it could also extend lifespan. Some of the data and discussion from this section were published in Riesen et al., 2014.

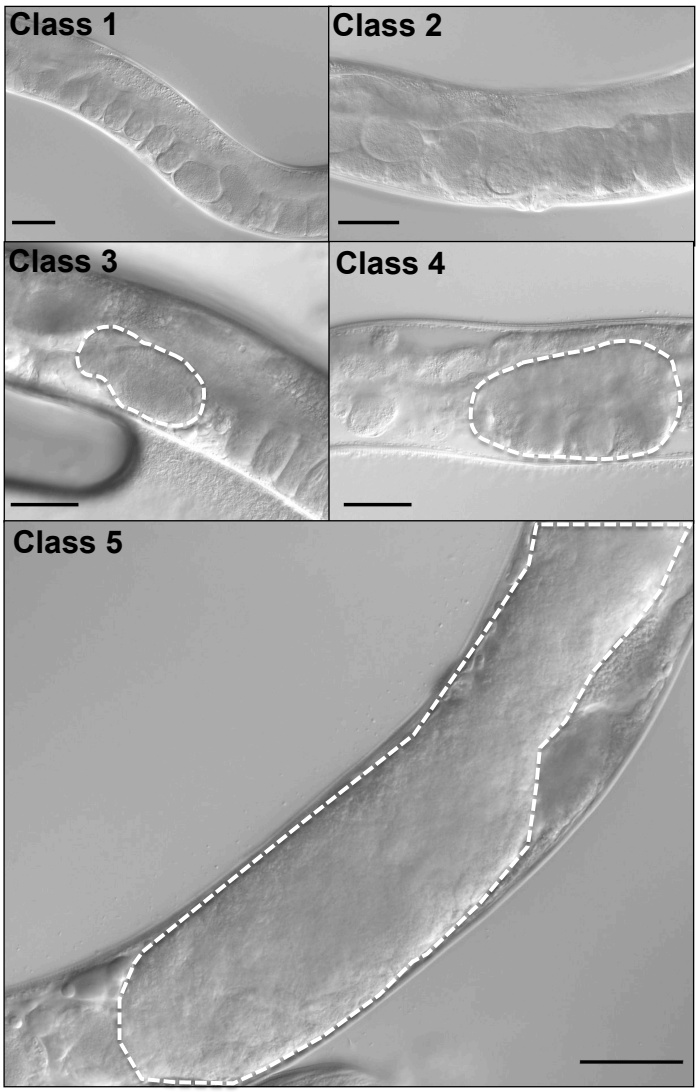

Figure 3.2. The uterus pathology scoring system. All images were taken at x400 magnification and are of wild-type worms. Class 1 denotes a healthy uterus, containing well-organised eggs. Class 2 denotes a mildly abnormal uterus, with unfertilised oocytes present. Classes 3 – 5 indicate that tumours have developed. Class 3 denotes small sized tumours and class 4 medium sized tumours. In class 5 the tumour has become so large it fills the mid-section of the worm. (Scale bar = 40μm).

3.3 Results

3.3.1 Mating delays development of uterine tumours in wild-type hermaphrodites

Hermaphrodites generate a finite amount of sperm during the L4 larval stage (L'Hernault 1997). We hypothesised that uterine tumour development is triggered by sperm depletion, which occurs around day 4 of adulthood. Oocyte production then shifts from being a programme to a quasi-programme in the post-reproductive hermaphrodite. Unfertilised oocytes then accumulate in the uterus and undergo endoreduplication, resulting in uterine tumours. Mated hermaphrodites have additional sperm, allowing more oocytes to be fertilised (Ward & Carrel 1979). Therefore mating could delay uterine tumour growth in hermaphrodites.

To test this hypothesis we placed individual L4 hermaphrodites on plates with three L4 males and allowed them to mate for several days. On day 4 of adulthood, plates were screened for successful mating. Only hermaphrodites that produced approximately 50% male progeny were retained. These worms were transferred away from the males and kept in hermaphrodite-only groups for the remainder of the experiment. On day 1, 4, 7, 11 and 14 Nomarski images of the uteri were taken and scored. These were then compared to the scores from unmated hermaphrodites. Mating caused a significant reduction in uterine tumour development on days 4 and 7 (Figure 3.3). However by day 11, tumour growth in mated worms had reached the same levels as in unmated worms. Presumably this reflects male sperm depletion. At this point unfertilised oocytes will start to accumulate in the uterus, eventually resulting in uterine tumours. There is also an apparent catch-up effect, with more rapid tumour growth between days 7 and 11 in mated hermaphrodites. This pattern was observed in both trials. Perhaps male sperm stimulates hermaphrodites to produce more oocytes. Thus, once male sperm is depleted, oocytes

accumulate more rapidly in the uterus, causing accelerated uterine tumour development.

This demonstrates mating hermaphrodites in early life can delay the formation of uterine tumours, seemingly by allowing fertilization to continue for longer. However once sperm is depleted, subsequent tumour growth occurs more rapidly and reaches the same level as in unmated hermaphrodites. Additionally, mating is not a suitable intervention to see how tumour growth contributes to mortality for several reasons. Most importantly, mating hermaphrodites drastically reduces their lifespan (Shi & Murphy 2014; Gems & Riddle 1996). This could be because in mated hermaphrodites eggs often hatch within the mother, resulting in matricide. (Luo et al. 2009; Pickett & Kornfeld 2013). Mating also causes severe damage to the cuticle around the vulva, which could compromise its protection against the external environment (Woodruff et al. 2014). Finally it has also been shown that males release pheromones that shorten life span (Maures et al. 2014). What is needed is a means to reduce uterine tumour development, which does not reduce life span.

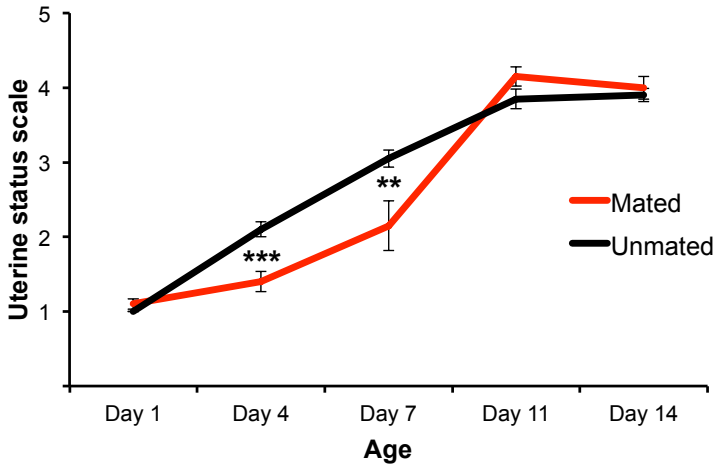

Figure 3.3. The effect of mating on uterine tumour growth in *C. elegans* hermaphrodites. Hermaphrodites were exposed to males at 20°C from L4 until day 4 of adulthood. Mating delayed uterine tumour development until day 11. Data mean±s.e.m, combined from two trials. (p<0.01 **, p<0.001*** Wilcoxon-Mann-Whitney test versus unmated hermaphrodites of the same age. n=20 per time point per condition).

3.3.2 FUDR can decrease uterine tumour size in wild-type and in the *mdl-1* mutant

We attempted to block tumour development using 5-fluorodeoxyuridine (FUDR), an inhibitor of DNA and RNA synthesis that is used in the treatment of colorectal cancers (Aitlhadj & Stürzenbaum 2010). It has been used in work with *C. elegans* for many years to inhibit progeny production to make it easier to maintain synchronised populations of adults (Gandhi et al. 1980; Mitchell & Stiles 1979). When worms are placed onto FUDR at a young age it can cause developmental defects, such as a protruding vulva phenotype (Pvl) (Gandhi et al. 1980). If worms were not exposed to FUDR until L4 the majority do not develop Pvl and have a normal appearance. A previous study found that FUDR could inhibit the development of DNA masses found in uterine tumours (Golden et al. 2007). Therefore we decided to determine whether this drug could reduce overall uterine tumour growth in both wild-type and *mdl-1* worms and whether this could cause an increase in lifespan.

FUDR was added topically to NGM plates with an established *E. coli* lawn and left to diffuse into the plate overnight. Wild-type L4 worms were transferred to FUDR plates and maintained at 20°C for the rest of their lifespan. We selected the following range of FUDR concentrations to study initially: 10μM, 25μM and 50μM. On days 1, 4, 8 and 12 of adulthood Nomarski images of the uteri from 10 worms were collected and then scored (Figure 3.4). On day 4 some worms grown without FUDR had already started to develop small tumours. By day 8, worms grown on 10μM and 25μM were also starting to develop tumours, whereas tumour development was still blocked in worms on 50μM (Table 3.1). By day 12 all worms grown without FUDR had large tumours but both 25μM and 50μM were able to significantly reduce tumour development, though 50μM was more effective than 25μM (p<0.001). Throughout the experiment 10μM FUDR did not have a significant impact on tumour development but the higher concentrations of FUDR were able to reduce tumour size in a dose-dependent manner. Therefore 50μM

FUDR was the most effective dose in this trial because it blocked the appearance of uterine tumours in 90% of day 12 worms, whereas 90% of worms on 25μM FUDR still developed tumours at that age.

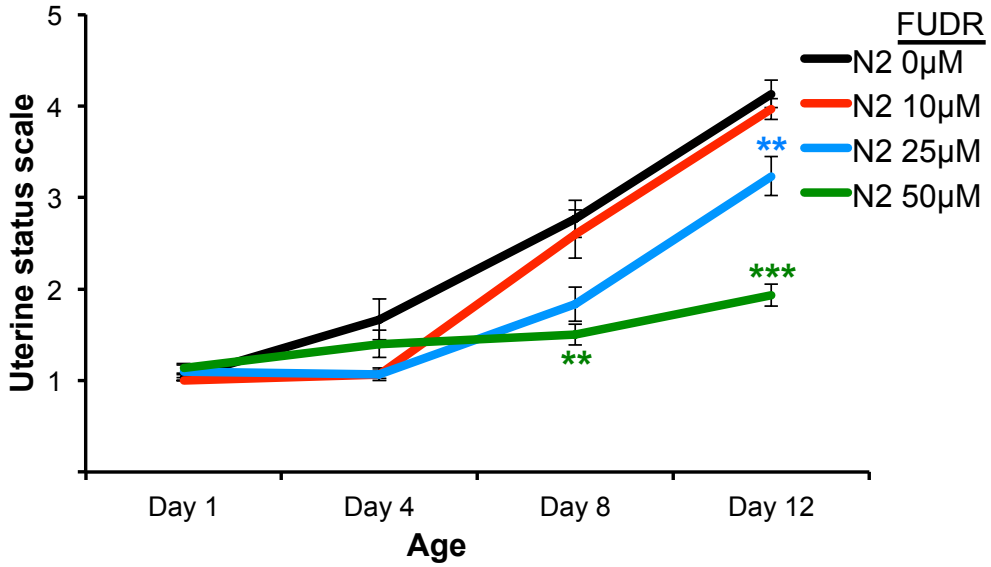

Figure 3.4. The effect of FUDR on tumour formation in wild-type *C. elegans*. Worms were placed on FUDR plates from L4 stage onwards and maintained at 20°C. FUDR decreases uterine tumour formation in a dose-dependent manner in wild-type worms. Data mean±s.e.m ($p<0.01$ **, $p<0.001$*** Wilcoxon-Mann-Whitney test versus 0μM FUDR of the same age. To adjust for multiple comparisons $p<0.01$ was considered to be significant. See table below for sample sizes.).

Age	Uterine status scale																			
	N2 0μM FUDR					N2 10μM FUDR					N2 25μM FUDR					N2 50μM FUDR				
	1	2	3	4	5	1	2	3	4	5	1	2	3	4	5	1	2	3	4	5
Day 1	10	0	0	0	0	10	0	0	0	0	9	1	0	0	0	10	0	0	0	0
Day 4	5	3	2	0	0	9	1	0	0	0	10	0	0	0	0	7	3	0	0	0
Day 8	0	5	3	2	0	0	6	3	1	0	4	4	2	0	0	5	5	0	0	0
Day 12	0	0	0	7	3	0	0	1	8	1	0	1	6	3	0	1	8	1	0	0

Table 3.1. The distribution of uterine status scores in wild-type worms aged on various FUDR concentrations. Scores of 3 and above indicate the presence of a tumour

Next we tested another range of FUDR concentrations, which included a higher dose, to see if this could completely eliminate tumour development in day 12 wild-type adults. We also decided to include *mdl-1* in this trial to see if the same concentration of FUDR could reduce tumour development in both strains. FUDR plates and worms were prepared as described above. Nomarski images were gathered on days 1, 4, 8 and 12 of adulthood and images of the uteri then scored. The results for wild-type were similar to those of the previous experiment (Figure 3.5, Table 3.2A).

In this experiment we were not able to show that *mdl-1* significantly increases the rate of uterine tumour development (Figure 3.6). It is possible that larger sample sizes or perhaps looking at a time point between day 4 and day 8 could have recreated the significant effect of *mdl-1*. For *mdl-1,* 25μM and 50μM FUDR were capable of significantly reducing uterine tumour development on day 8 ($p<0.004$ for both). 50μM was also more effective than 25μM at reducing tumour development consistently on day 12 ($p<0.004$) (Figure 3.5). 75μM was not significantly more effective than 50μM on any of the time points in either strain. In fact, on day 8, 50μM was more effective than 75μM in *mdl-1* ($p<0.004$). However it should be noted that in *mdl-1*, 50% of worms still developed tumours by day 12 on 50μM FUDR. Though the majority of these tumours were small, 50μM FUDR was no longer able to significantly reduce tumour development in *mdl-1* on day 12 (Table 3.2B, Figure 3.6). This implies the effect of FUDR may start to diminish in later life, allowing tumour growth to occur. This could be due either to the breakdown or metabolism of FUDR or because the tumours develop resistance to it. Finally on 50μM FUDR, there was no significant difference between wild-type and *mdl-1* on any of the days examined (Figure 3.6), meaning as well as tumour development being reduced, any differences in the rate of tumour development between the two genotypes had been removed. Thus, FUDR is an effective drug to block uterine tumour development in *C. elegans*, with 50μM being the minimum concentration in this study to get a major inhibition of tumour development in later life.

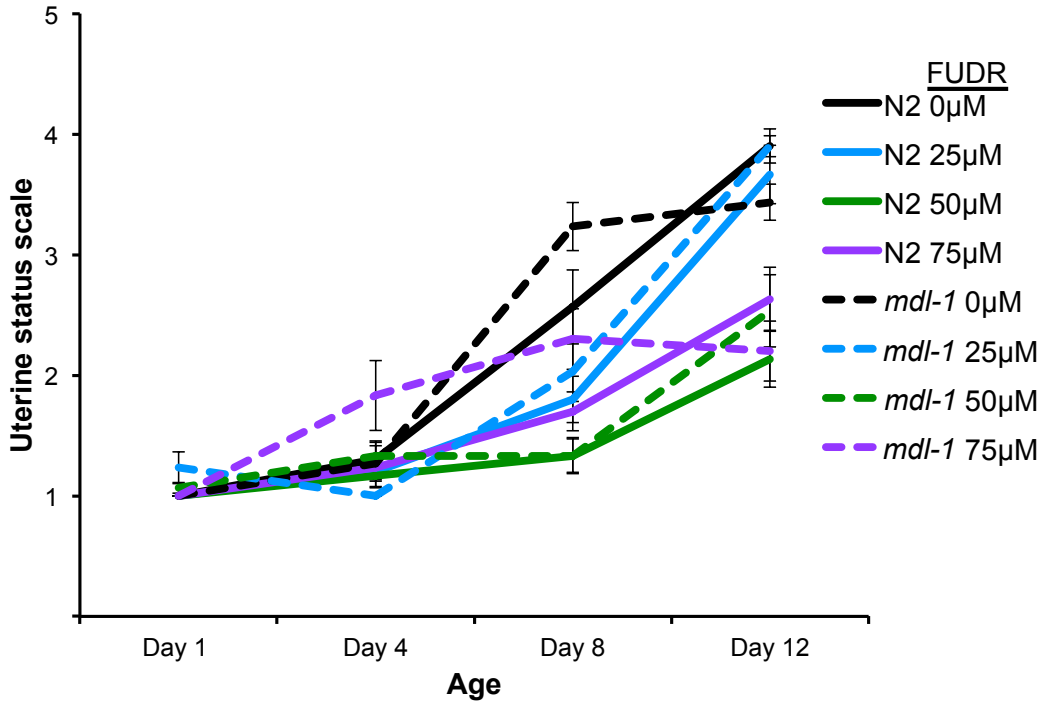

Figure 3.5. The effect of FUDR on tumour formation in wild-type and *mdl-1(tm311)* mutant *C. elegans*. Worms were placed on FUDR plates from L4 stage onwards and maintained at 20°C. FUDR decreases uterine tumour formation in both wild-type and *mdl-1* worms. 50μM FUDR was the optimum dose for reducing tumour development in both strains. Data mean±s.e.m. (Day 12 data can be found in Riesen et al., 2014). (Wilcoxon-Mann-Whitney test. To adjust for multiple comparisons $p<0.004$ was considered to be significant. For sample sizes see table below).

A

Age	Uterine status scale																			
	N2 0μM FUDR					N2 25μM FUDR					N2 50μM FUDR					N2 75μM FUDR				
	1	2	3	4	5	1	2	3	4	5	1	2	3	4	5	1	2	3	4	5
Day 1	10	0	0	0	0	10	0	0	0	0	10	0	0	0	0	10	0	0	0	0
Day 4	8	2	0	0	0	8	2	0	0	0	8	2	0	0	0	9	1	0	0	0
Day 8	2	1	5	2	0	3	5	2	0	0	6	4	0	0	0	4	5	1	0	0
Day 12	0	0	1	9	0	0	1	2	6	1	1	8	0	1	0	0	8	0	2	0

B

Age	Uterine status scale																			
	mdl-1 0μM FUDR					*mdl-1* 25μM FUDR					*mdl-1* 50μM FUDR					*mdl-1* 75μM FUDR				
	1	2	3	4	5	1	2	3	4	5	1	2	3	4	5	1	2	3	4	5
Day 1	10	0	0	0	0	9	1	0	0	0	10	0	0	0	0	10	0	0	0	0
Day 4	7	3	0	0	0	10	0	0	0	0	7	3	0	0	0	3	5	1	1	0
Day 8	0	1	4	5	0	2	5	3	0	0	7	3	0	0	0	0	6	3	1	0
Day 12	0	0	5	5	0	0	0	1	9	0	2	3	3	2	0	2	6	1	1	0

Table 3.2. Uterine status scores in wild-type and *mdl-1(tm311)* aged on various FUDR concentrations. (A) Wild-type **(B)** *mdl-1(tm311)*. Scores of 3 and above indicate the presence of a tumour (Day 12 data can be found in Riesen et al., 2014).

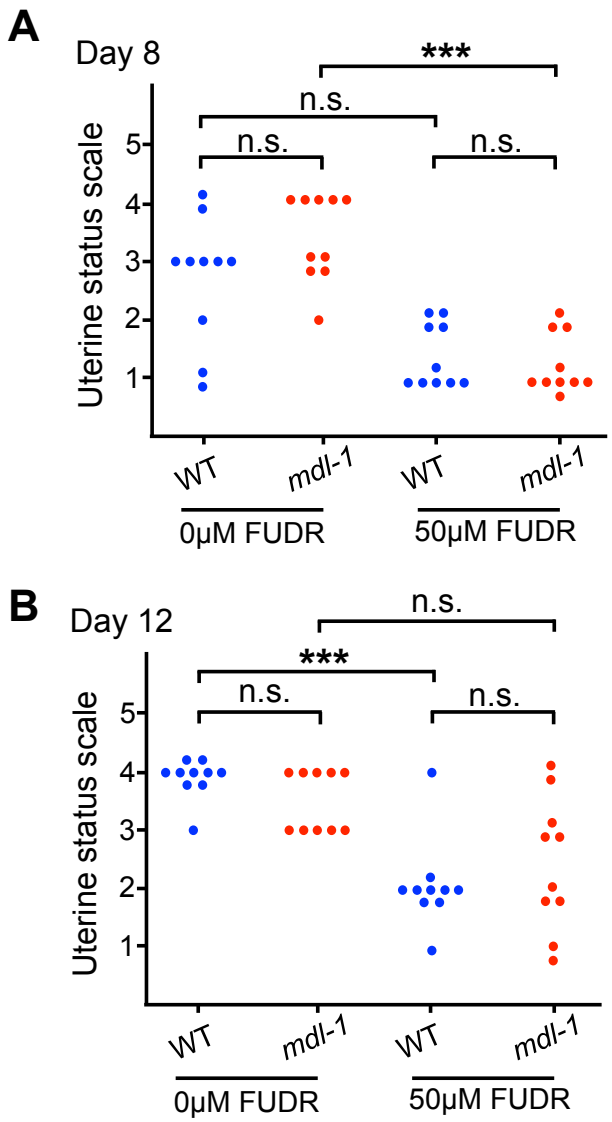

Figure 3.6. The effect of 50μM FUDR on tumour formation in wild-type and *mdl-1(tm311)*. **(A)** Day 8 **(B)** Day 12. Each dot represents a single worm. Scores of 3 and above indicate the presence of a tumour. (p<0.004 **, p<0.001*** Wilcoxon-Mann-Whitney test. To adjust for multiple comparisons p<0.004 was considered to be significant. For sample sizes see table 3.2). (Day 12 data can be found in Riesen et al., 2014).

3.3.3 Uterine tumours do not affect lifespan

As described in the introduction to this section, the majority of published data shows FUDR does not affect lifespan even at relatively high concentrations (Hosono et al. 1982), suggesting uterine tumours are unlikely to limit life span in wild-type worms. However it remains possible that accelerated tumour development, as seen in the short-lived *mdl-1* mutant (Riesen et al. 2014), reduces lifespan.

To address this, we transferred wild-type and *mdl-1* L4 stage worms onto 50μM FUDR plates and recorded survival at 20°C. We found that *mdl-1* shortened lifespan, as previously shown at 25°C (Riesen et al. 2014). However in two trials, 50μM FUDR did not extend lifespan in either strain (Figure 3.7, Table A.1). It was possible that FUDR may not be able to inhibit tumour development in later life as we have shown uterine tumour development is suppressed on day 8 on 50μM FUDR in *mdl-1* but not by day 12. As the mean lifespan of *mdl-1,* with or without FUDR was ~12 days, its possible that tumour growth in both conditions could start to limit life (Table A.1). Nevertheless this demonstrates that uterine tumours do not limit lifespan under standard culture conditions in wild-type worms. Additionally, uterine tumours are unlikely to be limiting lifespan in *mdl-1* worms where their formation is accelerated. This implies uterine tumours do not contribute to age-related mortality in worms, at least under the conditions tested here.

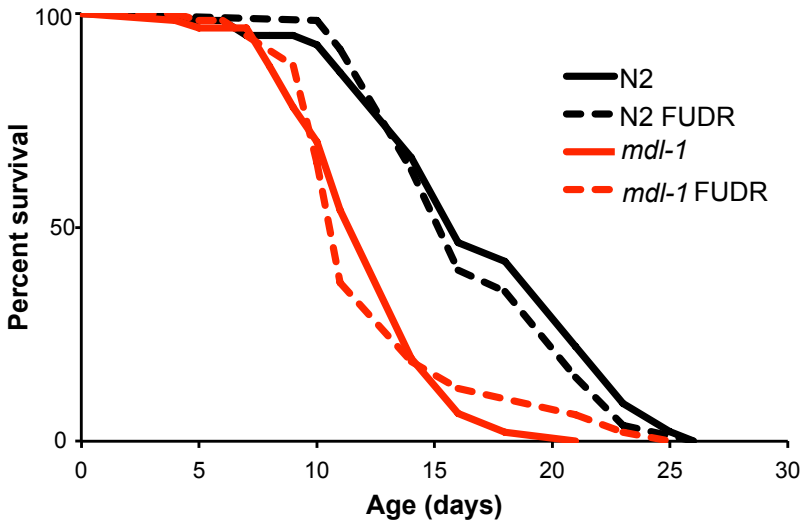

Figure 3.7. No effect on lifespan by 50μM FUDR in wild-type and *mdl-1(tm311)* *C. elegans*. Data from one representative trial. For survival statistics and sample sizes see Appendix table A.1. (Data can be found in Riesen et al., 2014).

3.3.4 Uterine tumours become infected with *E. coli* in aged *C. elegans*

During the course of investigation of intestinal pathology, I serendipitously discovered a new element of the pathology of uterine tumours: their infection with bacteria. To study bacterial accumulation in the lumen of the *C. elegans'* intestine by *E. coli* (Garigan et al. 2002) we used *E. coli* OP50 that contained a plasmid that expressed the red fluorescent protein DsRed (OP50-RFP) (kindly provided by J.F. Rawls, Duke University, originally from W. Bitter, Vrije University) (van der Sar et al. 2003). The plasmid also contained a gene for tetracycline resistance, thus bacteria had to be grown in the presence of antibiotics. However as our objective was to study bacterial pathogenicity, bacteria raised on tetracycline was then resuspended in broth containing no antibiotic. This was to ensure that when the bacteria were growing on NGM plates, their growth was not impeded by the presence of antibiotics.

NGM plates inoculated with OP50-RFP were confirmed to be fluorescent before worms were transferred onto them. Worms for experiments were grown on OP50-RFP from egg. During pilot studies we noticed that the uterine tumours of aged worms often exhibited strong red fluorescence (Figure 3.8A). 45% of wild-type worms had red fluorescence in their tumours by day 9 when grown at 25°C (Figure 3.9A) and in some cases this fluorescence was seen throughout the entire tumour (Figure 3.8A). While weak red autofluorescence has been observed in the uterine tumours of aged worms grown on standard OP50 (Wang et al. 2017, unpublished), the red fluorescence we observed in worms grown on OP50-RFP was of a much higher intensity. This suggested that *E. coli* invades and proliferates within uterine tumours.

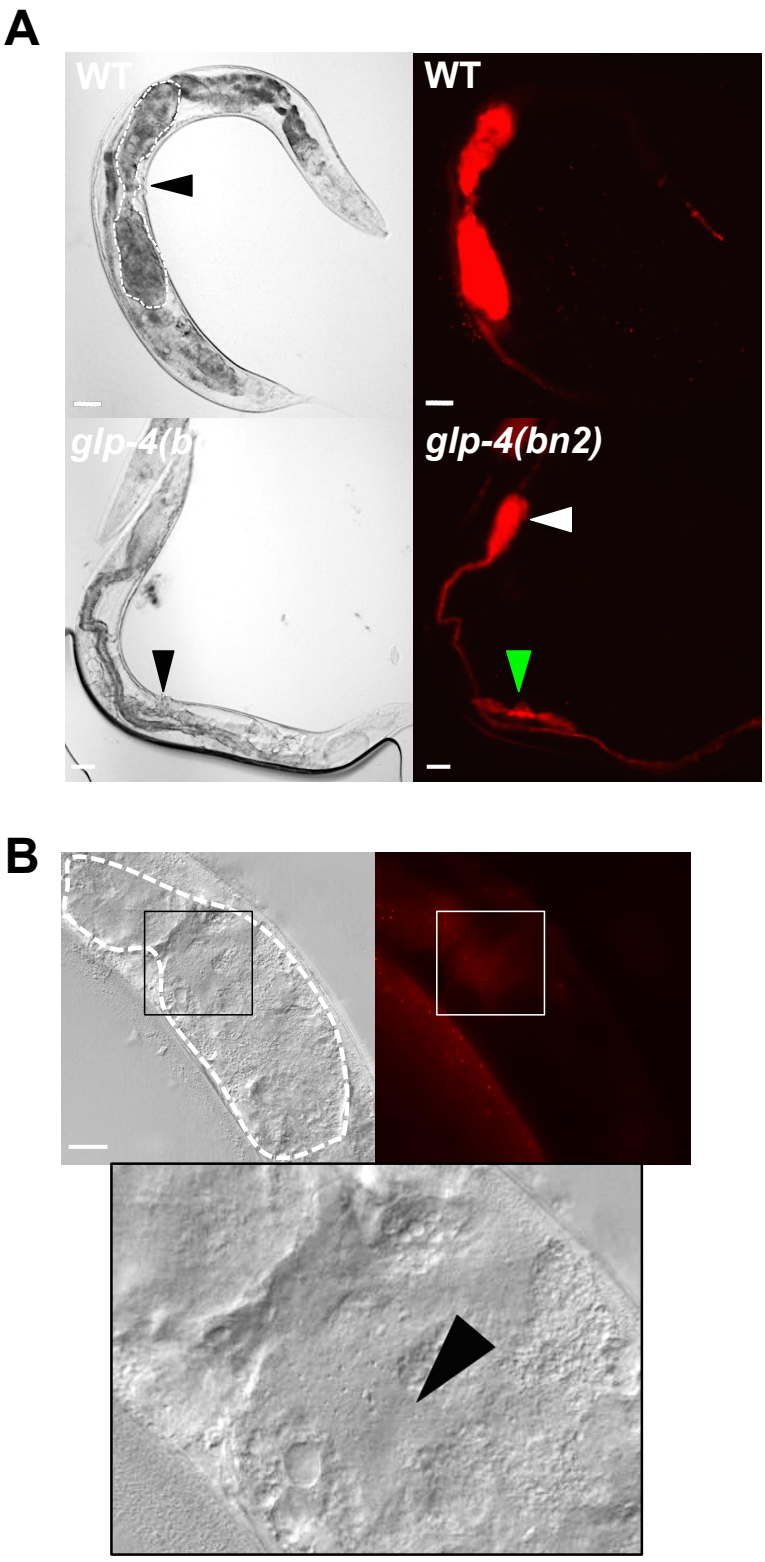

Figure 3.8. Invasion of the *C. elegans* uterus by *E. coli* OP50. (A) x100 brightfield and fluorescent images of day 9 wild-type and *glp-4(bn2)* worms grown at 25°C. Top: tumours in wild-type are outlined in white and emit red fluorescence. Bottom: in *glp-4(bn2)* worms, the uterus emits red fluorescence (green arrow) and *E. coli* accumulation is seen in the anterior intestine (white arrow). (Scale bar 20µm). **(B)** x400 brightfield and fluorescent images of a day 14 wild-type worm grown at 20°C. The tumour is outlined in white with an area emitting red fluorescence and resembling densely packed is bacteria indicated (black arrow). (Scale bar 20µm).

We wanted to confirm that bacteria were actually present within the tumours. It was a possibility that RFP from digested OP50-RFP could be transported out of the intestine and become incorporated into the tumours. Brightfield and fluorescent images of the uterine tumours taken at high magnification were examined. This revealed that regions that exhibited strong red fluorescence also showed a grainy appearance resembling packed bacteria (Figure 3.8B). This provides further evidence that bacterial cells are the cause of the red fluorescence in the uterus.

To see if bacterial proliferation was necessary for this apparent infection, we tested whether antibiotic treatment of OP50-RFP could protect the worms from uteri invasion. The antibiotic carbenicillin was added topically to NGM plates as previously described (Garigan et al. 2002). Worms were grown on OP50-RFP with or without carbenicillin from egg. Worms were grown to L4 at 15°C and then shifted to 25°C. Both a brightfield and a fluorescence image was taken of ~10 worms on days 1, 3, 6 and 9. Images were then scored for the presence of red fluorescence within the uterus. Our results show that the uteri of all wild-type worms on day 1 and 3 remained un-invaded. On day 6 and 9 ~45% of control worms had red fluorescence in their tumours and this was completely suppressed by carbenicillin treatment (Figure 3.9A).

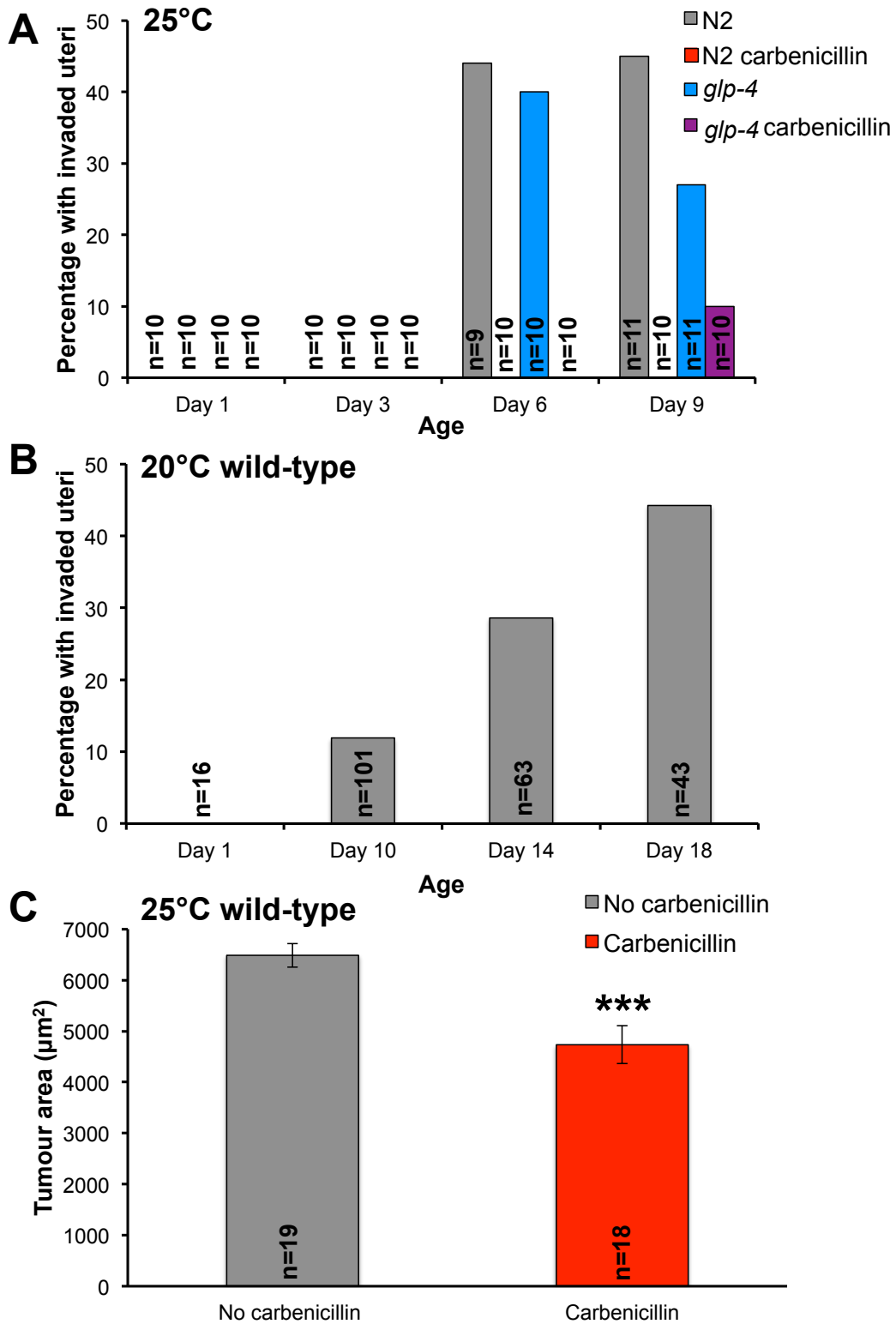

Figure 3.9. The effect of different conditions on bacterial invasion of the uterus in *C. elegans*. (A) Uteri invasion in wild-type and *glp-4(bn2)* worms, grown with and without the antibiotic carbenicillin at 25°C. **(B)** Uteri invasion in wild-type worms grown at 20°C. **(C)** Cross-sectional uterine tumour area in day 9 wild-type worms, grown with and without the antibiotic carbenicillin at 25°C. (p<0.001*** Student's t test versus control). (Sample sizes on graphs).

To confirm this invasion also occurred under more standard culture conditions and to see if there was any temperature dependence, I examined worms grown at 20°C. Worms were examined on days 1, 10, 14 and 18 of adulthood. While red fluorescence was seen in the uteri of these worms, it developed at a much slower rate than at 25°C (Figure 3.9B). For example by day 10 only ~12% of worms had invaded uteri compared to ~45% at 25°C on day 6. In fact, not until day 18 at 20°C did the fraction of worms with invaded uteri reach ~45%. These data show that development of this pathology is closely linked to temperature. This could be because at higher temperatures the bacteria are able to proliferate faster and thus colonise the uterus more rapidly. On the other hand, it has been shown that worms grown at higher temperatures age faster and have a shorter life span (Klass 1977). Potentially the mechanisms that protect young worms from bacterial invasion of the uterus could undergo age-related deterioration faster at 25°C, resulting in more rapid bacterial infection.

I tested whether the presence of tumours was necessary for uterine infection. We used *glp-4* worms which do not develop tumours at 25°C (Riesen et al. 2014). If *glp-4* worms are raised from egg at 25°C they are long lived (Riesen et al. 2014). Therefore we raised worms on OP50-RFP with or without carbenicillin at 15°C and then switched them to 25°C at L4 because *glp-4* worms raised in these conditions do not develop tumours but are not long lived (McElwee et al. 2004). This was because we wanted to ensure we were only examining how the absence of tumours affected this apparent infection; long lived *glp-4* could have longevity mechanisms activated that protect them from bacterial invasion, factors that are independent of the inhibition of tumour development. On day 6 and 9 a proportion of both wild-type and *glp-4* worms had red fluorescent uteri and this was largely prevented by carbenicillin treatment (Figure 3.9A). However 10% of *glp-4* worms on plates with carbenicillin also started to show uterine red fluorescence by day 9. This could be because as *glp-4* worms are sterile they were not transferred as frequently as wild-

type. Therefore as they remained on the same carbenicillin plates for longer it is possible the carbenicillin had started to degrade, allowing some bacterial proliferation to occur.

Finally I explored whether bacterial growth within uterine tumours contributes to their growth. Tumour size was measured in aged wild-type worms grown with or without carbenicillin present. Tumour area was measured instead of using the uterine scoring system so that more subtle differences in tumour size could be detected. This was because it was anticipated that bacterial growth might have a relatively minor effect on uterine tumour size. Wild-type worms grown on carbenicillin did show a significant reduction in tumour size, with a decrease of ~27% (Figure 3.9C), suggesting that bacterial infection does indeed contribute to tumour growth. Subsequent work showed that antibiotics slow development of a wide range of senescent pathologies (Ezcurra, unpublished). Therefore it is unclear if this protection against tumour growth is due to an inhibition of bacterial proliferation within the tumours or whether it is the result of a general protection against a range of pathologies.

These results show that proliferating *E. coli* is capable of invading both the uteri and tumours of aged worms. It is likely that *E. coli* first invades through the vulva of old worms, as this is the nearest opening to the external environment. In support of this, we often saw red fluorescence in worms only in the area just within the vulva (Figure 3.10). Furthermore there is evidence that the vulva undergoes an age-related decline (Leiser et al. 2016; Pickett & Kornfeld 2013), which could result in it no longer being an effective barrier to the external environment.

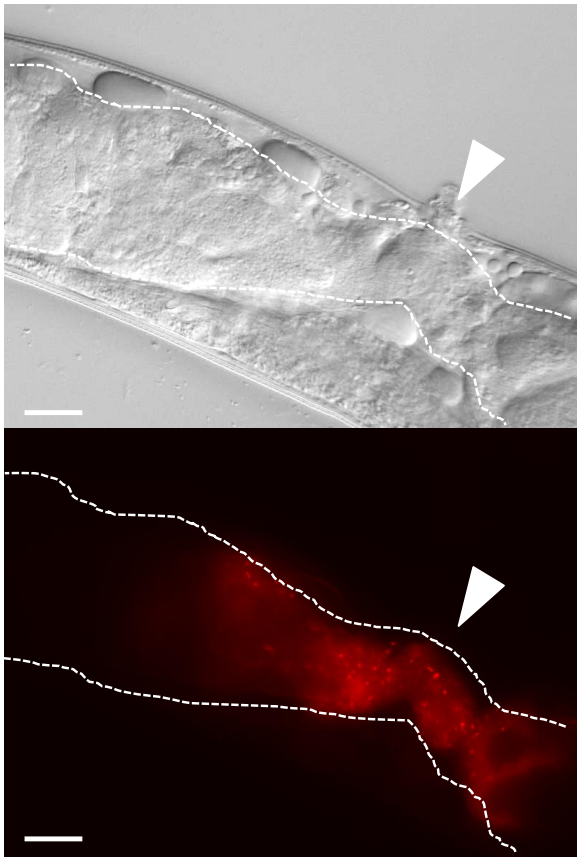

Figure 3.10. Initial invasion of *E. coli* into the uterus near the vulva. Representative x400 brightfield and fluorescent images of a day 18 wild-type worm grown at 20°C with uterine tumours outlined in white. Red fluorescence is strongest near the vulva (white arrow). Fluorescence intensity decreases with distance from the vulva. (Scale bar 20μm).

Uterine tumours present a rich source of nutrients for bacterial proliferation. Unfertilised oocytes take up yolk during their development. Vitellogenins are the protein portion of yolk and when VIT-2 is tagged with GFP, strong green fluorescence is seen within the tumours (Wang et al. 2017, unpublished). Tumours are also lipid rich, perhaps reflecting deposition of yolk lipid (Wang et al. 2017, unpublished). Thus uterine tumours appear to be full of yolk, which likely provides a rich food source for *E. coli*.

3.4 Discussion

3.4.1 Uterine tumours are not a life-limiting pathology in *C. elegans*

We have shown in this study that the anti-cancer drug FUDR can suppress uterine tumour development in *C. elegans* in both wild-type, and *mdl-1* mutants where their development is accelerated. FUDR worked in a dose-dependent manner in both cases up to 50μM, which was sufficient to largely prevent tumour growth in both wild-type and *mdl-1*. However this concentration did not extend lifespan in either genotype. It remains possible that 50μM FUDR is mildly toxic to the worms; in one trial it did slightly reduce wild-type lifespan (Table A.1). Such toxicity could cause a reduction in life span that masks the beneficial effects of tumour suppression. However given that it is widely reported FUDR has no effect on wild-type lifespan (Gandhi et al. 1980; Hosono 1978; Hosono et al. 1982; Van Raamsdonk & Hekimi 2011), even at higher doses than we tested here, it seems unlikely that 50μM FUDR is life-shorteningly toxic. Furthermore as FUDR primarily works through blocking DNA synthesis, the post-mitotic somatic cells of *C. elegans* should be largely unaffected by FUDR, with the drug exerting most of its influence on the mitotic germ line. However FUDR can also disrupt RNA synthesis (Longley et al. 2003) so it remains possible it could impede transcription in somatic tissue resulting in a toxic effect.

However our data is consistent with other studies that show that removal of uterine tumours do not have an affect on life span. The temperature sensitive mutant *glp-4(bn2)* is sterile at 25°C because germ cell proliferation is blocked and thus it does not produce any oocytes. When it is grown until L4 at 15°C and then switched to 25°C it still becomes a sterile adult (Beanan & Strome 1992) but its lifespan remains similar to wild-type (McElwee et al. 2004). Furthermore it was shown that this temperature shift was sufficient to totally block uterine tumour formation in *glp-4*, in both a wild-type and *mdl-1* background (Riesen et al. 2014).

Despite this tumour suppression, *glp-4; mdl-1* mutants raised until L4 at 15°C and then switched to 25°C still had a lifespan that was much the same as *mdl-1* (Riesen et al. 2014). Furthermore removing the whole gonad via laser ablation, which should completely prevent uterine tumours from forming, did not increase lifespan in wild-type worms (Hsin & Kenyon 1999). This demonstrates that in *C. elegans*, uterine tumours are not a life-limiting pathology, even when their growth is accelerated, as in *mdl-1* mutants.

Uterine tumours develop in all ageing wild-type hermaphrodites. Yet surprisingly in the conditions we tested, we have demonstrated they are a bystander pathology and do not limit lifespan, much like skin wrinkling and greying hair in humans. Given that they are not lethal to worms, further study of them could be seen as unnecessary. However tumours, particularly cancerous ones, are major causes of death during ageing in humans. Therefore by understanding the origins of senescent tumours in *C. elegans*, new insights may be gained into the development of cancerous tumours in humans, paving the way for future treatments.

Even if they are not lethal in *C. elegans*, it remains unclear how they affect worm health, something that is harder to measure than changes to life span but could be considered more important. They are a gross, abnormal pathology so it seems unlikely they are not detrimental in some way to worm health. It remains possible in conditions that we have not yet studied that tumours are life-limiting. For example, removal of only the germline via laser ablation caused an increase in wild-type lifespan (Hsin & Kenyon 1999). It is also still uncertain what long-lived *daf-2* mutants die of. They also develop uterine tumours as they age (M. Ezcurra, unpublished) and removal of either the whole gonad or just the germline via laser ablation in *daf-2(e1370)* mutants caused further increases to lifespan (Hsin & Kenyon 1999). This raises the possibility that uterine tumours may be a life-limiting pathology in *daf-2* mutants and in wild-type grown in certain conditions. If yes, then 50μM FUDR should increase *daf-2* mutant lifespan.

In this study we have shown that conditions predicted to block endoreduplication in unfertilised oocytes in the uterus reduced tumour growth. Yet it is possible that the endoreduplication in oocytes is not the only cause of uterine tumour growth. The tumours also incorporate various other components, including yolk (McGee et al. 2012), which is secreted from the intestine, and other proteins such as ULE-2,-3,-4,-5, which are secreted from the toroidal cells of the uterus (Zimmerman et al. 2015). Interestingly RNAi of vitellogenins, the protein portion of yolk, extends lifespan (Murphy et al. 2003). Furthermore RNAi of *ule-2,-3,-4,-5* simultaneously also increases lifespan (Zimmerman et al. 2015). This shows that these proteins are detrimental to life span. One possibility is that uterine tumours do actually shorten life, but it is the yolk or ULE proteins in them that cause this; hence suppressing tumour growth does not extend lifespan.

In the case of males, uterine tumours clearly do no limit life, since males do not develop them, nor any other form of germline tumour (Golden et al. 2007). Therefore everything studied in this section is sex-specific in regards to the hermaphrodite. What *C. elegans* males die from is also still unknown.

3.4.2 Uterine tumours of aged worms become infected with *E. coli*

In approximately half of aged, wild-type *C. elegans* grown on *E. coli* expressing RFP, red fluorescence was seen within the uterine tumours. Possibly RFP from *E. coli* in the lumen of the gut is somehow transported out of the intestine and incorporated into the uterine tumours. However this seems unlikely as antibiotic treatment prevented this tumour fluorescence, despite fluorescent bacteria still being observed in the intestine of these worms. This suggests bacteria are present in the uterine tumours and that bacterial proliferation needs to take place for this invasion to occur. Transmission electron microscopy (TEM) of red

fluorescent tumours would confirm unequivocally that there are bacteria present.

The red fluorescence in the tumours was often brightest near the vulva and becomes weaker more distally in the tumour (Figure 3.10). Given the vulva is an opening into the external environment, this suggests that bacteria invade through the vulva. In support of this, bacteria were observed in the uterus of elderly worms near the vulva using TEM (McGee et al. 2011). Presumably in younger worms, where no bacteria are seen within the uterus, the vulva acts as an effective barrier, but some worms lose this ability during ageing. One study defined a phenotype called Avid (age-associated vulva integrity defects), where the intestine protrudes out of the vulva (Leiser et al. 2016). This condition primarily starts to occur during middle age, which is when bacterial invasion of the uterus is observed. Additionally, it has been shown that the vulval muscles in aged worms no longer respond robustly to serotonin, which would normally make them contract (Pickett & Kornfeld 2013). This is thought to be due to a loss of vulval muscle integrity. One way to test whether a defective vulva is the route of bacterial invasion would be to mate hermaphrodites. Mating damages the vulva (Woodruff et al. 2014) and should therefore increase the percentage of infected uteri or at least cause earlier appearance of infection. Using sterile males would be ideal as additional egg laying may force invading *E. coli* out of the vulva. On the other hand, in young worms bacterial invasion could be prevented by an immune response within the uterus. In aged worms this response could undergo decline and may no longer be able to inhibit bacterial growth.

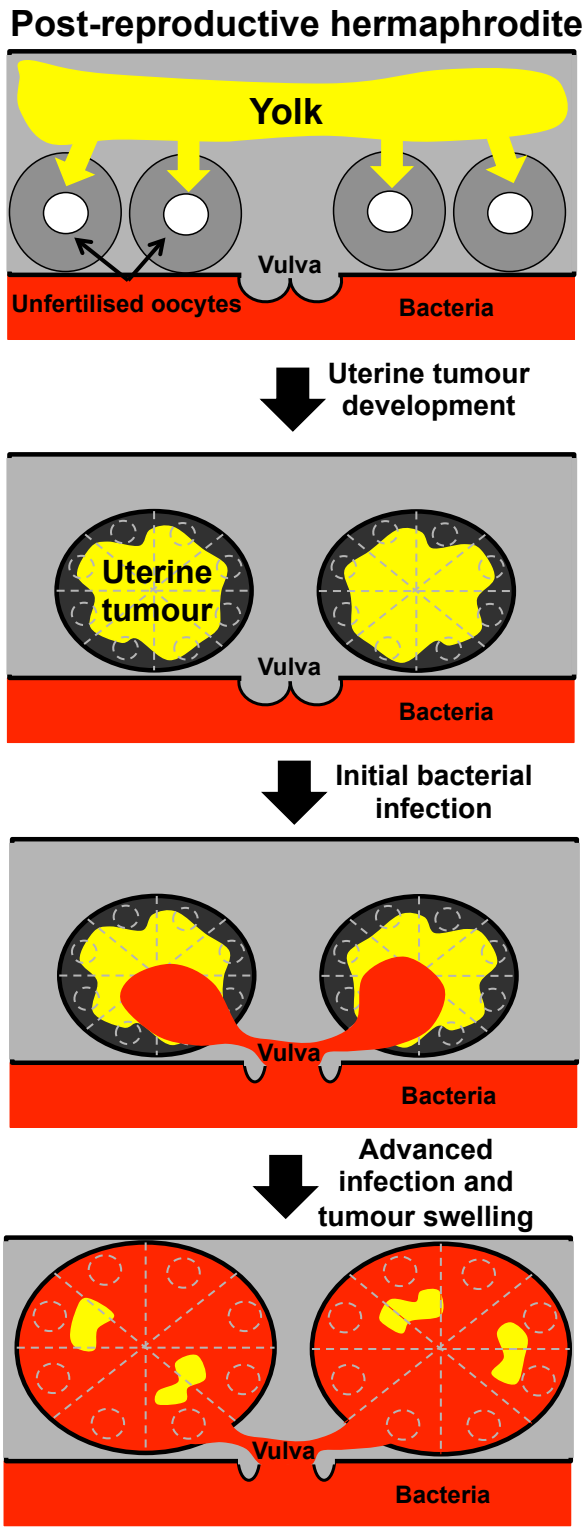

Figure 3.11. Progression of bacterial infection of uterine tumours. Unfertilised oocytes accumulate in the uterus and take up yolk from the body cavity. Endoreduplication in the oocytes drives the formation of uterine tumours, which are rich in yolk. During ageing the vulva weakens and is no longer an effective barrier against the external environment. This allows bacteria to invade into the uterine tumours. A possibility is that the bacteria are nourished by yolk, allowing them to proliferate throughout the tumours. *E. coli* proliferation within tumours may cause them to increase in size.

Presumably once bacteria have entered the uterus they can utilise nutrients within the tumour to proliferate and colonise the tumours (Figure 3.11). Yolk in particular would provide a rich source of nourishment for the bacteria. It is possible that bulk growth of *E. coli* within tumours increases tumour size. This would require bacterial biomass to accommodate more space than the yolk biomass it metabolised. As yolk is an energy rich storage material, this is plausible. Therefore *E. coli* proliferation should increase tumour size. However it is unclear whether this is actually the case. To attempt to answer this question, I compared the size of tumours with and without red fluorescence. While I did not see a difference in size (data not shown), this trial had a small sample size and did not differentiate between levels of infection. Antibiotic treatment prevented uterus invasion and reduced tumour size by around a quarter (Figure 3.9A,C). Furthermore axenic culture conditions, where worms are grown without any bacteria present, also reduced uterine tumour growth (McGee et al. 2012). This suggests bacteria could contribute to tumour growth. However both conditions extend life span and this could reflect in an overall reduction in pathology development in several tissues. In addition, axenic conditions also cause a general slowing of growth that could affect uterine tumours (Szewczyk et al. 2003). Nevertheless it remains possible bacterial proliferation within uterine tumours does contribute to their growth.

In humans the relationship between bacteria and cancer progression has been studied for decades. In some instances, bacteria appear to initiate or drive malignant alterations. For example, colorectal cancer is often associated with an abundance of *Streptococcous bovis/gallolyticus* and *Fusobacterium sp*, which are thought to trigger and drive cancer progression by causing persistent inflammation (Cummins & Tangney 2013; Kostic et al. 2012). As in *C. elegans*, the initial infection of tumours is sometimes thought to be opportunistic, as the anaerobic conditions and excess nutrients within tumours provide an optimum environment for the growth of certain bacteria (Cummins & Tangney 2013). Interestingly, bacterial infection of tumours is not necessarily detrimental to the host.

Post-operative infection in lung cancer actually improved patient survival (Ruckdeschel et al. 1972), perhaps because bacteria compete for nutrients, secrete toxic proteins or help to initiate immune responses against tumour cells. Given that certain bacterial species have an affinity for particular cancers (Cummins & Tangney 2013), genetically engineered bacteria are now being created as future anti-cancer therapies (Baban et al. 2010). These bacteria can either secrete tumour-suppressor proteins or act as vectors to deliver therapeutic genes via plasmids to cancerous cells (Baban et al. 2010). As *C. elegans* tumours have now been shown to be susceptible to bacterial invasion, they could be used as a model to study this pathology or to test new bacteria-based anti-cancer therapies. However caution should be adopted, as *C. elegans* tumours are fundamentally different from mammalian tumours. For example they are the result of cell accumulation rather than proliferation and there is no metastasis or angiogenesis. In addition we are unaware whether *C. elegans* tumours are hypoxic like many mammalian tumours. Thus further investigation of the composition and environment of *C. elegans* tumours is required before they can be used as model for bacterial invasion of mammalian tumours.

3.4.3 *C. elegans* as a model for benign mammalian tumours

The ability of somatic cells to undergo mitotic division is a major evolutionary advantage in youth as it allows for tissues to be renewed or repaired. However a disadvantage is that an organism becomes more vulnerable to developing cancer in later life. Malignant tumours often have a number of the following characteristics: loss of cell cycle control; apoptosis resistance; invasion of nearby tissue; activation of angiogenesis and metastasis. All of these attributes mean these tumours can significantly disrupt normal tissue function. While it is still uncertain exactly why we become more susceptible to cancer as we become older, there is no doubt cancer is a major cause of death in the elderly. This means there is a huge amount of research focused on developing cancer treatments and cures, leading to the need for suitable model organisms.

In adult *C. elegans* all somatic cells are post-mitotic and are therefore incapable of dividing. Consequently, *C. elegans* does not appear to be a viable cancer model. However the germline does undergo division during adulthood. Germ cells at the distal end of the gonad undergo mitosis, before eventually undergoing meiosis as they move towards the proximal end. Therefore while the somatic tissue in *C. elegans* may not be a good model for the study of tumour development, the germline potentially is (Kyriakakis et al. 2016).

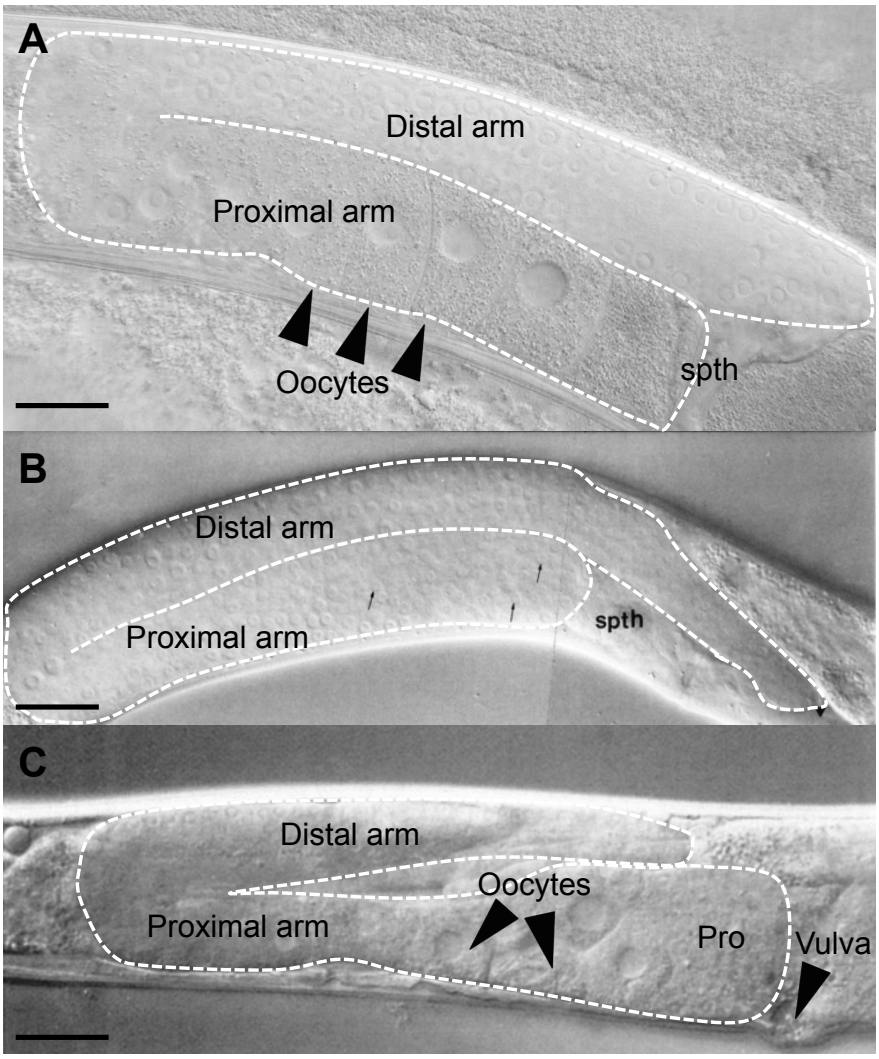

Figure 3.12. Germline tumours in *C. elegans* hermaphrodites. (A) Healthy gonad in a day 1 wild-type hermaphrodite. Oocytes develop along the entire proximal arm until they are fertilized in the spermatheca (spth). (Scale bar 20μM) **(B)** *gld-1(q268)* hermaphrodite with a germline tumour. Oocytes are not seen in the proximal arm, instead it fills entirely with mitotic germ cells (Francis et al. 1995). (Scale bar 10μM) **(C)** Wild-type hermaphrodite where certain cells of the somatic gonad were removed using laser ablation. This results in the formation of a proximal tumour (Pro) (Seydoux et al. 1990). (Scale bar 20μM).

There have been several studies detailing the generation of germline tumours in *C. elegans*. In certain *gld-1* mutants, germ cells exit meiosis and re-enter mitosis, resulting in a huge accumulation of germ cells (Francis et al. 1995). This generates a large tumour within the gonad (Figure 3.12B). The sheer volume of cells can result in cells bursting through the spermatheca and into the uterus. The increasing pressure can eventually cause protrusion of the vulva, which correlates with death. *daf-2* mutation reduced germ cell number and increased lifespan in a *gld-1* mutant background, suggesting these tumours may be lethal (Pinkston et al. 2006). In another study, the proximal gonad sheath was shown to be a latent tumour niche, as under normal circumstances it is not a niche but is capable of becoming one when it interacts with cells it would not usually come into contact with. In this case when mitotic germ cells interact with the proximal sheath, proximal tumours form in the gonad resulting in a Pro phenotype (McGovern et al. 2009). The Pro phenotype has also been observed in *lin-12* mutants and in wild-type hermaphrodites when certain cells in the somatic gonad were removed by laser ablation (Seydoux et al. 1990) (Figure 3.12C). These are some examples of studies that have been able to generate tumours in the *C. elegans* germline. Their formation was driven by mutation, much like the majority of malignant mammalian tumours, or by changes to morphology allowing improper cell interactions. Furthermore like mammalian tumours their growth is impelled by cell proliferation.

The uterine tumours we have focused on in this study directly correlate with the ageing process and form in all aged, wild-type hermaphrodites. Moreover they do not appear to be initiated by mutational changes nor is their growth due to cell division. Rather their expansion is caused by unfertilized oocytes entering the uterus and undergoing endoreduplication. In many ways these uterine tumours are different to most types of mammalian tumours: their growth is not due to cell proliferation; there is no evidence they invade nearby tissues and they cannot metastasise. Nevertheless these uterine tumours do seem

capable of affecting the activity of other tissues. For example, they can grow so large that they fill the entire body cavity of the worm, completely compressing the midsection of the intestine and potentially disrupting its function. This means uterine tumours more closely resemble benign tumours in humans. Firstly benign tumours do not invade nearby tissues, nor do they metastasise. Secondly like uterine tumours, large benign tumours can have a *mass effect* on nearby tissues. This is a term used to describe a tumour that squashes or moves nearby tissue to such an extent that the tissue's normal function is disrupted. Ovarian teratomas are benign tumours that develop in pre-menopausal women and potentially bear a striking resemblance to *C. elegans'* uterine tumours, particularly in that they are both derived from unfertilised, immature oocytes and both express genes usually associated with later embryonic growth (Wang et al. 2017, unpublished). This comparison will be explored in more detail in an upcoming publication from David Gems' group.

While *C. elegans* does not initially seem to be the most suitable cancer model, the convenience of maintaining worm populations makes them appealing to work with. They would be particular useful for drug screens. In this study we have demonstrated *C. elegans'* suitability for this because the cancer drug, FUDR, used to treat human tumours also reduces growth of *C. elegans'* uterine tumours. A major advantage of *C. elegans* is the ability to see tumour growth easily *in vivo* because the worms are transparent. We propose *C. elegans'* uterine tumours to be a useful model for some types of benign tumours found in humans, particularly those associated with ageing but not mutation accumulation. However the main goal of this project was to identify life-limiting pathology in wild-type *C. elegans* and we have shown uterine tumours are not associated with age-related mortality. Therefore we must now turn out attention to another organ in the worm that seems to be a likely source of a lethal pathology: the intestine.

3.5 Part 2: Altering apoptosis levels changes the rate of gonad disintegration in *C. elegans* hermaphrodites

3.6 Introduction to the structure of the *C. elegans* gonad

A focus of our group is to identify age-related pathologies in *C. elegans* and to determine whether they are the result of developmental run-on. Yila de la Guardia began studying a previously observed age-related phenomenon in the germline, the disintegration of the gonad (Hughes et al. 2011; Luo et al. 2010; Garigan et al. 2002). She analysed this pathology quantitatively during ageing and set out to determine whether it could be caused by a quasi-programme. Due to my previous interest in studying how developmental run-on could lead to uterine tumours in the germline, I decided to collaborate with her in this endeavour.

The *C. elegans* hermaphrodite gonad is made of two arched gonad arms, which converge on a central uterus (Figure 3.13A). During the L4 larval stage it generates sperm, which are stored in the spermatheca, but then shifts to making oocytes during adulthood. At the distal end of each arm is a distal tip cell (DTC), which preserves a stem cell population within the nearby germ cells (Lints & Hall 2009d). This means the distal end of the gonad contains proliferative germ cells and is known as the mitotic zone. As germ cells progress along the gonad, away from the influence of the DTC, they begin meiosis in the transition zone. They enter the pachytene stage, which continues around the bend of the gonad arm (Hirsch et al. 1976). During this stage the germ cells start to grow in volume. Within the distal arm, germ cells form a syncytium, where cells are not completely enclosed. Instead, a central cytoplasmic cylinder called a rachis connects them (Hirsch et al. 1976). Along the proximal arm, gametogenesis occurs and oocytes are formed. Oocytes progress along the proximal arm, continuing to grow in size and advance into diakinesis (Hirsch et al. 1976). They arrest in this state until they are ovulated into the spermatheca and fertilised.

Unlike the hermaphrodite, the male gonad consists of only one gonad arm that exclusively creates spermatids (Figure 3.13B). Similar to the hermaphrodite, the distal end is a mitotic zone and all germ cells are connected via a rachis. Germ cells enter meiosis in the transition zone before reaching the pachytene stage. In males, the pachytene stage continues around the loop of the gonad and along the proximal arm. Further down, spermatogenesis takes place and spermatids are formed, which accumulate within the somatic gonad to await ejaculation (Lints & Hall 2009b).

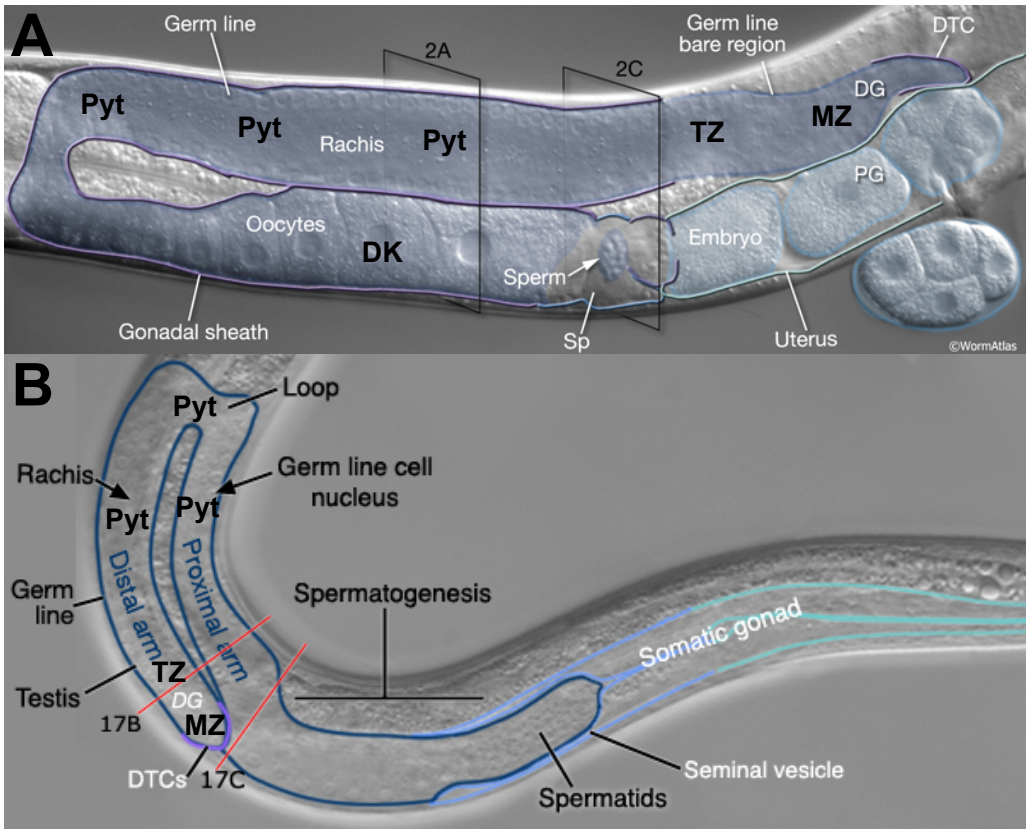

Figure 3.13. The structure of the *C. elegans'* gonad. (A) The hermaphrodite gonad (Lints & Hall 2009d). Germ cells proliferate in the mitotic zone (MZ), progress into meiosis in the transition zone (TZ) and then into pachytene (Pyt). They then form oocytes and arrest in diakinesis (DK) until fertilization in the spermatheca (Sp). **(B)** The male gonad (Lints & Hall 2009b). Germ cells proliferate in the mitotic zone (MZ), progress into meiosis in the transition zone (TZ) and then into pachytene (Pyt). Spermatogenesis then occurs and spermatids are formed. Distal arm (DG), proximal arm (PG), distal tip cell (DTC).

3.6.1 Apoptosis in *C. elegans* germline

During normal development in *C. elegans,* 131 of the somatic cells undergo programmed cell death via apoptosis (Sulston & Horvitz 1977). In adulthood, the somatic tissue is post-mitotic and no apoptosis occurs. However in the hermaphrodite germline, the only proliferative tissue in the adult, apoptosis does take place and occurs primarily in cells that are about to exit the pachytene region of the gonad (Gumienny et al. 1999; Gartner et al. 2000). Apoptotic cells are then quickly removed from the germline by the cells of the gonad sheath (Gumienny et al. 1999).

Two main forms of apoptosis can occur in the germline. The first form is known as stress-induced apoptosis (SIA) and happens as a reaction to DNA damage or environmental stresses such as UV exposure (Gartner et al. 2000). This allows for the removal of germ cells that may have accumulated harmful mutations that could be detrimental to the next generation. The second form is called physiological apoptosis (PA) and involves apparently healthy, viable germ cells undergoing apoptosis, despite the lack of any obvious external stresses (Gumienny et al. 1999). Therefore PA appears to function as a necessary programme for normal development within the germline.

Physiological apoptosis in the somatic tissue occurs via a tightly controlled apparatus. The core pathway contains CED-4 (cell death abnormal), the homologue of Apaf-1 (apoptotic peptidase activator 1) found in humans (Zou et al. 1997), and CED-3, the homologue of mammalian interleukin-1β- converting enzyme/caspase-1 that produces a cytokine (Yuan et al. 1993). CED-4 cleaves and activates CED-3, resulting in programmed cell death via apoptosis (Metzstein et al. 1998). CED-3 and CED-4 are essential for apoptosis because loss of them blocks apoptosis completely (Ellis & Horvitz 1986). CED-9, a homologue of the Bcl-2 protein that inhibits apoptosis in humans (Hengartner & Horvitz 1994a), operates in cells that are to be protected from apoptosis. It does this by binding to CED-4 and inactivating it (Chinnaiyan et al.

1997). The EGL-1 (egg-laying defective) protein possesses a region analogous to the BH3 domain (Bcl-2 homology region 3) that is found in mammalian Bcl-2 proteins that are activators of apoptosis (Condradt & Horivitz 1998). EGL-1 binds to CED-9 and sequesters it (Condradt & Horivitz 1998), allowing CED-4 to be free to initiate apoptosis.

Germline apoptosis is also dependent on the activity of CED-3 and CED-4, though in SIA and PA they are induced via different mechanisms. SIA can be initiated by CEP-1, a homolog to mammalian p53 that prevents tumour formation via apoptosis (Schumacher et al. 2001). CEP-1 acts in response to DNA damage to activate EGL-1 or CED-13 (Hofmann et al. 2002; Schumacher et al. 2005), which act upon CED-9 to allow apoptosis to be triggered (Gartner et al. 2000). In contrast, PA is *cep-1* independent (Schumacher et al. 2001); EGL-1 is not required for it to take place and over-activation of CED-9 does not prevent it (Gumienny et al. 1999). The upstream activators of PA continue to be a mystery (Figure 3.14).

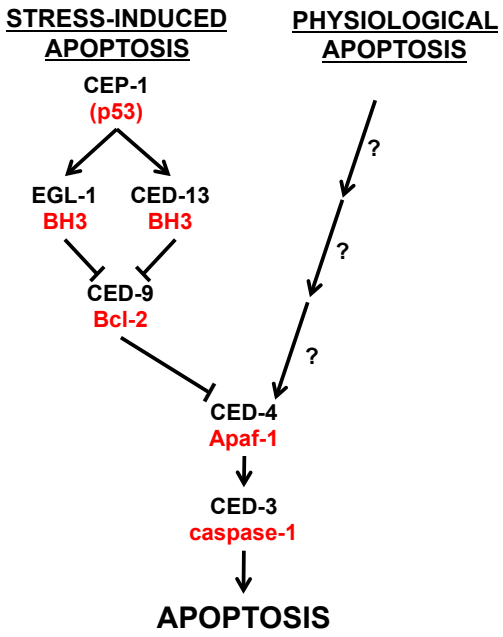

Figure 3.14. The apoptotic pathway in *C. elegans*. In stress-induced apoptosis, CEP-1 activates EGL-1 or CED-13 to inhibit CED-9. This allows CED-4 to activate CED-3 to initiate apoptosis. In physiological apoptosis, CED-4 and CED-4 are also required but the upstream activators are unknown. Mammalian homologs are in red.

Apoptosis of the germline is a hermaphrodite specific event. PA was never observed in the wild-type male germline (Gumienny et al. 1999). Even in the presence of stress, germ cells in wild-type males did not undergo SIA (Gartner et al. 2000).

3.6.2 The role of apoptosis in the germline of the *C. elegans* hermaphrodite

It was originally estimated that the destiny of approximately half of all germ cells in the hermaphrodite germline was to undergo apoptosis (Gumienny et al. 1999). A more recent study estimates this proportion to actually be greater than 90% (Jaramillo-Lambert et al. 2007). It is feasible these germ cells are removed because they have accumulated deleterious mutations. However it seems highly unlikely that this would be the case in such a high proportion of cells. In support of this, germs cells that would usually undergo apoptosis can develop into viable eggs, as seen in *ced-3* and *ced-4* mutants where apoptosis is blocked (Ellis & Horvitz 1986). Furthermore study of germ cells using electron microscopy did not reveal a substantial proportion to appear defective (Gumienny et al. 1999). Therefore an alternative theory about the purpose of PA has been proposed. It suggests PA contributes to reproductive fitness by sacrificing germ cells to act as nurse cells (Gumienny et al. 1999). In mammals, nurse cells provide growing oocytes with all the nutrients needed to form viable embryos upon fertilization. *C. elegans* do not have separate nurse cells, instead the nurse cell theory suggests other germ cells substitute for this role by undergoing apoptosis and donating their cytoplasm to the rachis. The rachis then uses this surplus cytoplasm to grow developing oocytes. In support of this idea, mature oocytes are very much larger than germ cells (Figure 3.13A). Oocytes will then be primed to form healthy embryos once they have been fertilised.

There is a large amount of evidence to support the nurse cell theory. For example, PA and oogenesis appear to be tightly linked. Germline

apoptosis occurs exclusively during hermaphrodite adulthood only once oogenesis has begun and is not seen during the larval stages (Gumienny et al. 1999). Germline apoptosis is also not seen in males (Gumienny et al. 1999). Presumably this is because there is no adaptive value for this to occur, as sperm are small and only require sufficient nutrients to complete fertilisation. The location of germline apoptosis, at the end of the pachytene region of the gonad, is also the location where germ cells start to swell (Gumienny et al. 1999). When apoptotic germ cells are removed from the syncytium by cells of the gonad sheath, the majority of their cytoplasm remains in the rachis (Gumienny et al. 1999). Cytoplasmic particles were also seen to flow along the rachis towards developing oocytes, presumably to provide them with a continuous supply of cytoplasm (Wolke et al. 2007). If the nurse cell theory were correct, this would mean PA is a programmed mechanism in young adulthood that improves the reproductive fitness of the *C. elegans* hermaphrodite.

3.6.3 Degeneration of the *C. elegans* gonad due to apoptotic run-on

The hermaphrodite gonad has been previously observed to undergo major degeneration during ageing, with the gonad shrivelling and eventually disintegrating (Garigan et al. 2002; Luo et al. 2010; Hughes et al. 2011). Work from de la Guardia explored the pattern of gonad degeneration in more detail (de la Guardia et al. 2016). A qualitative scoring system was created, inspired by a similar approach in a previous study (Garigan et al. 2002). Score 1 is a healthy gonad in a young adult while scores 2 and 3 indicate minor and major degeneration respectively. A score of 4 or above means disintegration has occurred (Figure 3.15). The purpose of this scoring system was to allow for the comparison of the dynamics of gonad pathology with those of other pathologies. It would also allow us to quantify the effects of various interventions on gonad pathology. The scoring system revealed that virtually all wild-type, hermaphrodite gonads disintegrated by day 12 (Figure 3.16A) (de la Guardia et al. 2016). I also showed that gonad disintegration continues

up until day 11, with no further increases seen after this age (Figure 3.16B).

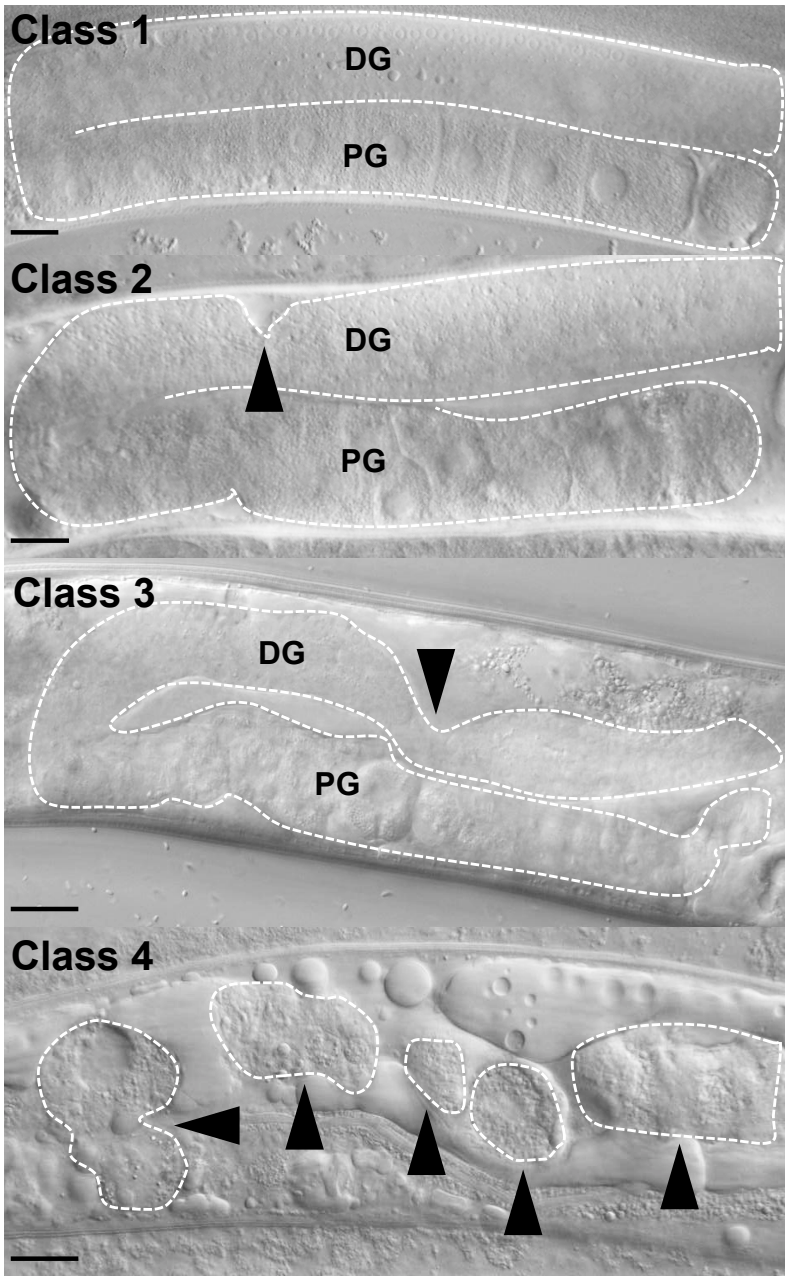

Figure 3.15. The *C. elegans* gonad scoring system. All images were taken at x400 magnification and are of wild-type hermaphrodites. Class 1 is a healthy gonad, where the distal gonad (DG) and proximal gonad (PG) fill the body cavity (Day 1, 25°C). Class 2 is where gonad degeneration begins and slight shrinkage is seen (black arrow) (day 6, 25°C). Class 3 is where major shrinkage is observed (black arrow) and disintegration is impending (day 12, 20°C). Class 4 is where the gonad has disintegrated into fragments (black arrows) (day 9, 25°C). Class 5 is where the gonad can no longer be identified. (Scale bar = 20µm).

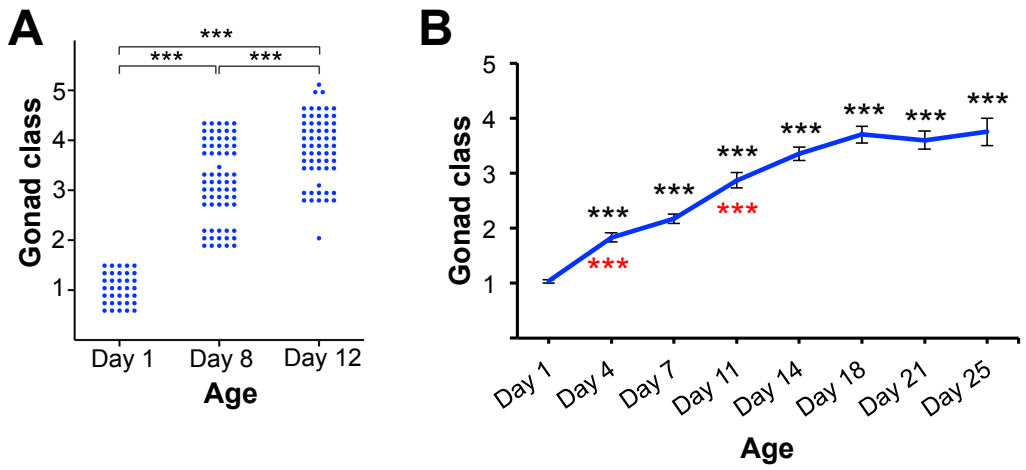

Figure 3.16. Gonad degeneration in ageing wild-type *C. elegans* hermaphrodites at 20°C. (A) Each dot represents a single worm. By day 12 virtually all gonads have undergone disintegration (Sample sizes day 1 n=35, day 8 n=66, day 12 n=60. Data from (de la Guardia et al. 2016). To adjust for multiple comparisons p<0.02 was was considered to be significant). **(B)** Gonad degeneration increases significantly up until day 14. Data mean±s.e.m, combined from three trials. (n=30 up until day 14, n=10 for remaining days) (*p*<0.001*** Wilcoxon-Mann-Whitney test; for **(B),** versus day 1 (black stars) or previous day (red stars) To adjust for multiple comparisons p<0.004 was considered to be significant).

A hypothesis for the cause of gonad atrophy was proposed. It was suggested that PA continued in post-reproductive worms, when it was no longer required (de la Guardia et al. 2016). This would fit with the hyperfunction theory of ageing, which was explained in more detail previously (Introduction section 1.2.3) (Blagosklonny 2008; Blagosklonny 2006). In young animals, PA contributes to reproductive fitness by nourishing developing oocytes (Gumienny et al. 1999). The gonad does not disintegrate because germ cell proliferation occurs at a high enough rate to ensure the total cell number remains stable. However once reproduction ceases there is no evolutionary pressure to terminate the apoptotic programme, so it continues to function when it is no longer needed and becomes a quasi-programme. PA is not operating incorrectly; it is simply not switched off at the appropriate time. As the germ cell mitotic population falls during ageing (Luo et al. 2010), run-on of

PA would lead to a decrease in total germ cell number, resulting in gonad atrophy.

Supporting this theory, de la Guardia showed that germline apoptosis continues until at least day 8, many days after self-reproduction ceases in hermaphrodites (de la Guardia et al. 2016). Furthermore blocking apoptosis using *ced-3* and *ced-4* mutants delayed gonad disintegration (de la Guardia et al. 2016). In the male germline, where no apoptosis occurs, gonad disintegration was not seen (de la Guardia et al. 2016). All these data so far agree with the hypothesis that run-on of PA is at least partly responsible for gonad atrophy. The aim of my work was to see how altering apoptosis levels in both the male and hermaphrodite germline affected the rate of gonad degeneration. In the following account, any work conducted by others is indicated as such (as in Figures 3.17A, 3.18A, 3.20). Some data and theories from this section are described in the paper by de la Guardia et al., 2016.

3.7 Results

3.7.1 Increasing apoptosis in hermaphrodites accelerates gonad disintegration

If run-on of apoptosis causes gonad atrophy in later life, then increasing germline apoptosis should accelerate gonad disintegration. GLD-1 (defective in germline development) is required for normal development of the germline. It is upregulated in the early stages of germline meiosis where it binds to various mRNA targets, including *cep-1* mRNA where it acts to block translation (Schumacher et al. 2005). By preventing synthesis of CEP-1, GLD-1 helps to prevent germline apoptosis at this stage of meiosis. In the final stages of pachytene, GLD-1 levels decrease, which permits germline apoptosis to proceed (Schumacher et al. 2005). In the *gld-1(op236)* mutant, *cep-1*-dependent apoptosis or SIA is increased and at 25°C PA is also increased (Schumacher et al. 2005). In

support of the apoptotic run-on theory for gonad degeneration, Y. de la Guardia showed that *gld-1(op236)* has accelerated gonad disintegration from early adulthood at 25°C (Figure 3.17A) (de la Guardia et al. 2016).

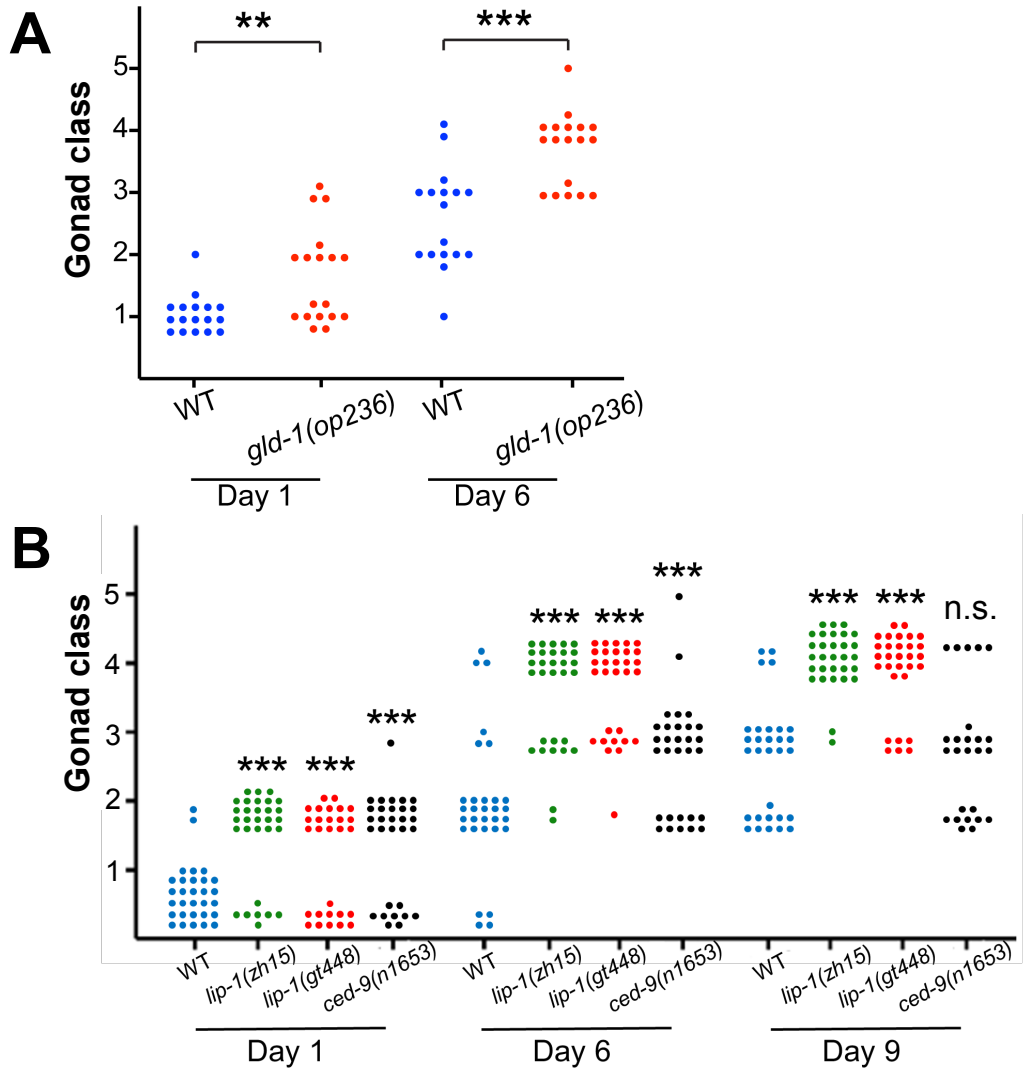

Figure 3.17. Accelerated gonad degeneration in *C. elegans* mutants with elevated apoptosis levels at 25°C. (A) *gld-1(op236)* accelerated gonad disintegration (n=17-18 per condition per timepoint). Data from (de la Guardia et al. 2016)) **(B)** *lip-1(zh15), lip-1(gt448)* and *ced-9(n1653)* all accelerated gonad degeneration. (p<0.01 **, p<0.001*** Wilcoxon-Mann-Whitney test vs wild-type hermaphrodites of the same age. To adjust for multiple comparisons p<0.017 was considered significant. n=30 per condition per time point). (All data can be seen in de la Guardia et al., 2016).

The LIP-1 (lateral-signal-induced phosphatase 1) protein in *C. elegans* is homologous to mitogen-activated protein kinase phosphatases (MPKs),

which supress Ras/mitogen-activated protein kinase (MAPK) (Berset et al. 2001). *lip-1* loss of function mutations cause an increase in Ras/MAPK signalling and also cause a rise in PA at 25°C (Rutkowski et al. 2011; Kritikou et al. 2006). How exactly increased Ras/MAPK signalling results in increased PA is unclear. It could initiate a signalling cascade that triggers apoptosis. On the other hand, Ras/MAPK signalling is required for cells to progress out of pachytene (Church et al. 1995). Apoptosis occurs to cells that are leaving the pachytene stage (Gumienny et al. 1999). Therefore increased Ras/MAPK signalling may simply push cells into a position where they are more vulnerable to apoptosis (Gumienny et al. 1999). I observed accelerated gonad disintegration in two loss of function alleles of *lip-1*, *lip-1(zh15)* and *lip-1(gt448),* at 25°C on all days examined, even in early adulthood (Figure 3.17B).

As previously described in this chapter, CED-9 protects cells from apoptosis by inhibiting CED-4 and thus preventing it from activating the caspase CED-3, which initiates apoptosis (Hengartner & Horvitz 1994b). The loss of function mutation *ced-9(n1653)* was shown to have increased levels of germline apoptosis (Gumienny et al. 1999). *ced-9(n1653)* did have increased gonad degeneration in early and mid life, but not in late life (Figure 3.17B).

These data demonstrate that increased germline apoptosis is associated with accelerated gonad degeneration. This provides further evidence that run on of PA in wild-type contributes to age-related gonad atrophy.

3.7.2 Decreasing physiological apoptosis reduces accelerated gonad disintegration

We wanted to confirm that the effect of *gld-1(op236)* on gonad disintegration was due to an increase in PA and not due to other effects of this mutation. Firstly we wanted to demonstrate that *gld-1(op236)* was increasing PA under our conditions. We stained day 1 hermaphrodites

with the vital dye SYTO 12, which specifically stains apoptotic cells (Gumienny et al. 1999). We then counted the number of fluorescent apoptotic cells in the germline of each worm and found *gld-1(op236)* had significantly more than wild-type (Figure 3.19A). Next I examined the *gld-1(op236);ced-3(n717)* double mutant, which has been previously shown to have no apoptosis (Schumacher et al. 2005). As expected *ced-3(n717)* was able to reduce gonad degeneration in the *gld-1(op236)* background (Figure 3.18). However gonad degeneration in the double mutant was still higher than in both *ced-3(n717)* and WT on day 6 (day 6 $p<0.01$ vs WT, $p<0.001$ vs *ced-3*). This implies that other additional factors in *gld-1(op236)* mutants can contribute to gonad degeneration, independent of apoptosis.

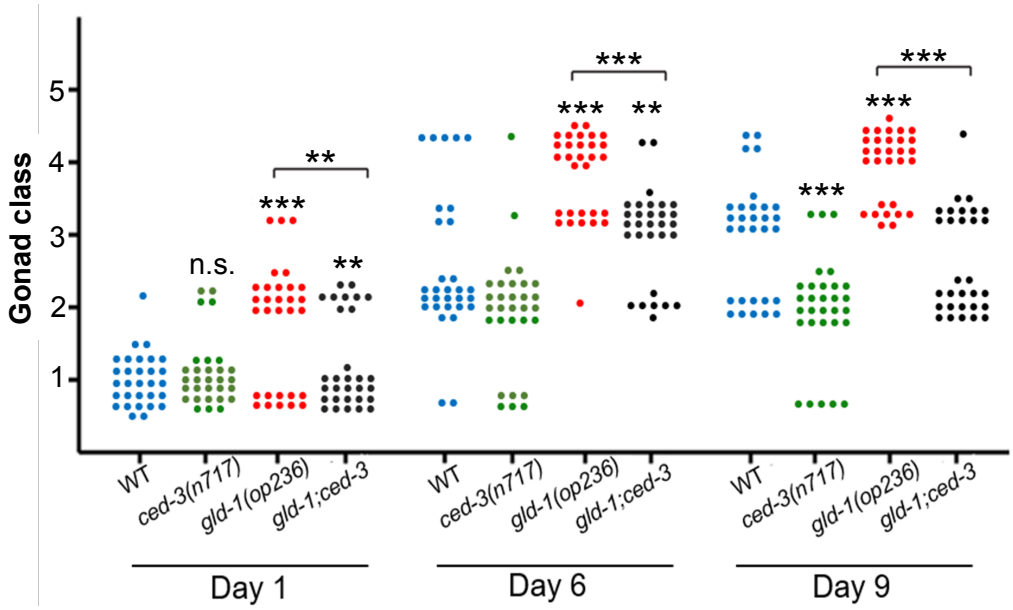

Figure 3.18. Suppression of accelerated gonad degeneration in *gld-1(op236)* mutants. *ced-3(n717)* can reduce gonad degeneration in a *gld-1(op236)* background. However it cannot entirely suppress it to the same extent as it can in a wild-type background (day 6 $p<0.01$ vs WT, $p<0.001$ vs *ced-3*). All trials performed at 25°C. ($p<0.01$ **, $p<0.001$*** Wilcoxon-Mann-Whitney test vs wild-type hermaphrodites of the same age. To adjust for multiple comparisons $p<0.01$ was considered significant. n=30 per condition per timepoint). (All data can be found in de la Guardia et al., 2016).

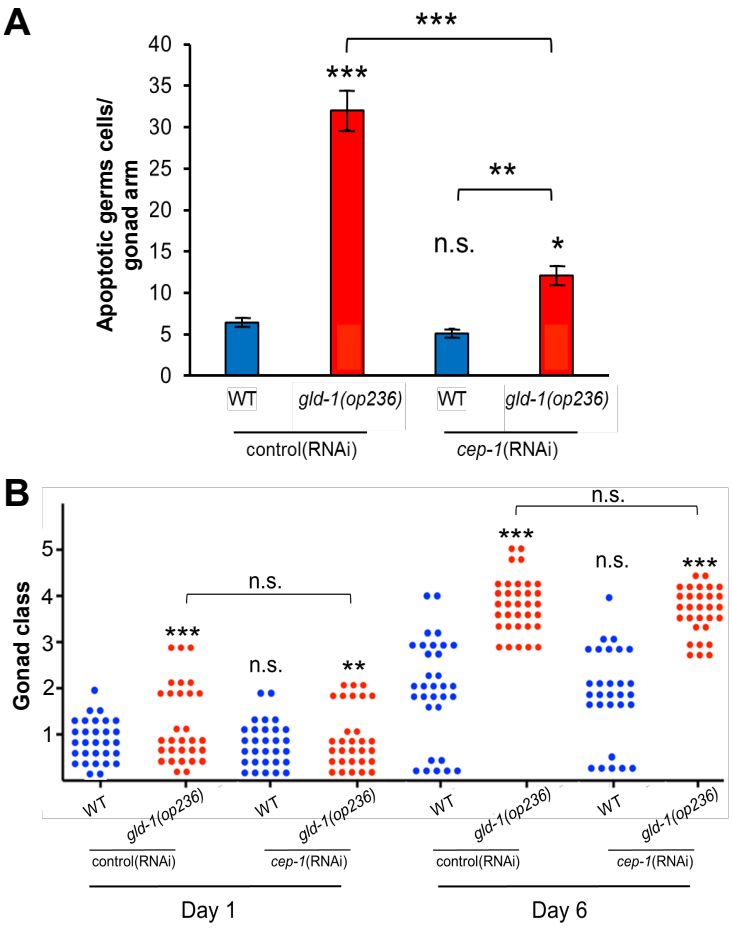

Figure 3.19. Accelerated gonad degeneration in *gld-1(op236)* does not require *cep-1*-dependent apoptosis. (A) *cep-1* RNAi can moderately reduce germline apoptosis in day 1 *gld-1(op236)* mutants. (p<0.05 *, p<0.01 **, p<0.001*** Tukey HSD test vs wild-type on control RNAi. n=29-33 per condition per time point) (1 trial performed by de la Guardia, 1 trial performed by Gilliat) **(B)** *cep-1* RNAi cannot reduce gonad degeneration in *gld-1(op236)*. All trials performed at 25°C. (p<0.01 **, p<0.001*** Wilcoxon-Mann-Whitney test vs wild-type on control RNAi. To adjust for multiple comparisons p<0.01 was considered to be significant. n=29-34 per condition per timepoint) (1 trial performed by de la Guardia, 1 trial performed by Gilliat. All data can be found in de la Guardia et al., 2016).

gld-1(op236) also increases SIA in the germline, which is *cep-1* dependent (Schumacher et al. 2005). We grew animals on *cep-1* RNAi from egg at 20°C and then shifted them to 25°C at the L4 stage. This is because at 25°C, PA is also increased in *glp-1(op236)* mutants (Schumacher et al. 2005). We then stained day 1 hermaphrodites with SYTO 12 to count apoptotic cells in the germline. A two-way ANOVA revealed a significant effect of both genotype and *cep-1* RNAi (comparison for genotype $F(1,119)=142.4$ $p<0.0001$, comparison for RNAi $F(1,119)=60.41$ $p<0.0001$). This is to be expected as apoptosis

levels are altered by both mutation of *gld-1* and *cep-1* RNAi. We then found *cep-1* RNAi had no effect on WT apoptotic levels (Figure 3.19A), as expected. In *gld-1(op236), cep-1* RNAi was able to significantly reduce the number of germline apoptotic cells (Figure 3.19A). However it was not able to bring apoptosis down to a wild-type level, consistent with prior work (Schumacher et al. 2005). This could be because the RNAi did not cause a complete knockdown of *cep-1* activity. However it could also imply that a proportion of the increased apoptosis seen in *gld-1(op236)* is *cep-1*-independent. Furthermore, despite *cep-1* RNAi dramatically reducing apoptosis in *gld-1(op236)*, it was not able to reduce gonad degeneration in this mutant (Figure 3.19B). This suggests that *cep-1*-independent apoptosis is the cause of the accelerated gonad degeneration in *gld-1(op236)*.

These data show the increase in PA, which is *cep-1*-independent, in *gld-1(op236)* mutants does augment age-related gonad decay. However *gld-1(op236)* can induce gonad degeneration in *ced-3(n717)* mutants, where apoptosis is completely blocked. This suggests *gld-1(op236)* can cause gonad degeneration through other mechanisms that are independent of apoptosis.

3.7.3 Inhibition of apoptosis in post-reproductive hermaphrodites suppresses gonad degeneration

The nurse cell theory proposes in young animals the apoptotic programme contributes to reproductive fitness by improving oocyte quality (Gumienny et al. 1999). However germline apoptosis continues to operate once reproduction has ended because there is no evolutionary pressure to switch it off (de la Guardia et al. 2016). We propose quasi-programmed apoptosis in post-reproductive hermaphrodites contributes to gonad degeneration. If this were true, switching off apoptosis only after reproduction has ceased should still prevent gonad degeneration.

To achieve this, I grew worms on control RNAi and *ced-3* RNAi from L4 at 20°C. On day 4 of adulthood, when reproduction is mostly complete, I transferred half of the worms from the control RNAi to *ced-3* RNAi and then examined the worms on day 8 and day 12. *ced-3* RNAi from L4 was able to significantly reduce gonad degeneration throughout (Figure 3.20A). Worms shifted onto *ced-3* RNAi on day 4 did not show a suppression of gonad degeneration on day 8 (Figure 3.20A). Perhaps this is due to a delay in the RNAi exerting its effect or because up to day 8 other factors, apart from apoptosis, cause minor gonad degeneration. However by day 12, *ced-3* RNAi from day 4 blocked any further gonad degeneration (Figure 3.20A) and completely prevented any gonad fragmentation (Figure 3.20B). This supports the idea that quasi-programmed apoptosis is the main driver of age-related gonad degeneration in wild-type hermaphrodites.

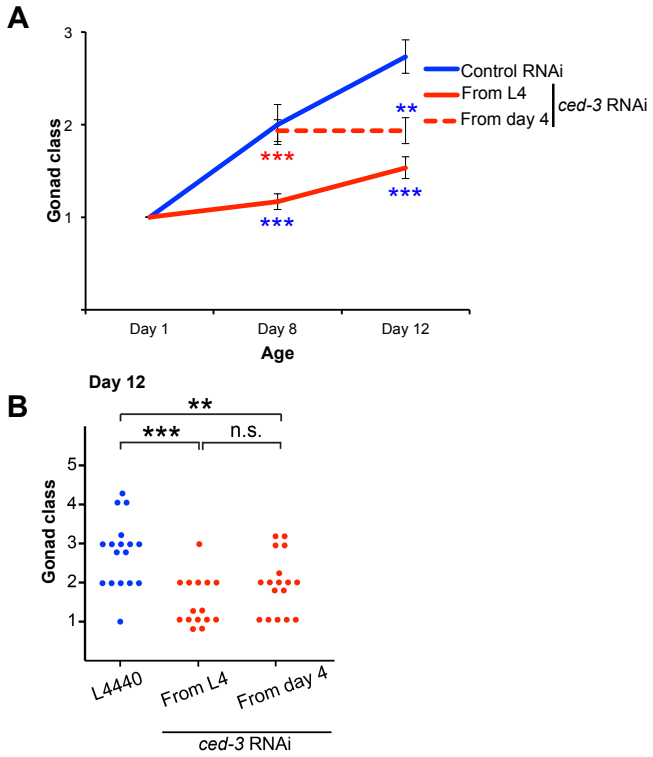

Figure 3.20. Blocking apoptosis in post-reproductive hermaphrodites prevents further gonad degeneration. (A) Exposure to *ced-3* RNAi on day 4 inhibits further gonad degeneration after day 8 in wild-type hermaphrodites. **(B)** By day 12, *ced-3* RNAi from both L4 larval stage and day 4 causes a significant reduction in gonad degeneration. All trials performed at 20°C. (p<0.01 **, p<0.001*** Wilcoxon-Mann-Whitney test; for **(A)** vs control RNAi at same age (blue stars); vs *ced-3* RNAi from L4 (red stars). To adjust for multiple comparisons p<0.017 was considered to be significant. n=10 per condition on day 1, n=15-17 per condition on day 8 and day 12) (Day 12 data can be found in de la Guardia et al., 2016).

3.7.4 Feminization does not induce gonad disintegration in males

The germ cells in male *C. elegans* never undergo apoptosis (Gumienny et al. 1999). While the male gonad does show slight atrophy during ageing, it was never seen to disintegrate (de la Guardia et al. 2016). We wanted to determine whether this was because of an absence of apoptosis or due to other protective mechanisms specific to the male. If germline apoptosis causes gonad disintegration, then switching it on in males should result in major degeneration of the male gonad.

FOG-1 (ferminization of germline) is required for spermatogenesis to occur in both males and hermaphrodites (Barton & Kimble 1990). In males, *fog-1* loss of function mutations result in a feminized germline while the somatic tissues remain male. Male *fog-1(q253)*/+ heterozygotes initially generate sperm but then switch to oocyte production, whereas the homozygotes always generate oocytes (Barton & Kimble 1990). The germline of the *fog-1(q253)* homozygous males has also been shown to have similar levels of apoptosis as the wild-type hermaphrodite (Gumienny et al. 1999). Therefore we set out to determine whether *fog-1(q253)* males exhibit gonad disintegration.

Firstly, given that male *fog-1(q253)*/+ can produce oocytes we decided to examine whether these worms have germline apoptosis. We generated *fog-1(q253)*/+ males by mating *fog-1(q253)* hermaphrodites with wild-type males at 20°C. I then collected L4 males and shifted them to 25°C due to the temperature sensitivity of the mutation. Males were kept in small groups because large groups of males have strongly reduced life spans (Gems & Riddle 2000). Day 1 *fog-1(q236)*/+ males were examined with Nomarski microscopy to confirm the presence of oocytes. I then stained day 1 wild-type hermaphrodites, wild-type males and *fog-1(q236)*/+ males with SYTO12 and counted fluorescent apoptotic cells in the germline. As expected we saw no apoptosis in the wild-type male germline (Figure

3.21A). However, *fog-1(q253)*/+ males had similar levels of apoptosis to wild-type hermaphrodites (Figure 3.21A). Despite this, *fog-1(q253)*/+ males did not show any age-related gonad disintegration, nor was there a significant increase in age-related gonad degeneration compared to wild-type males (Figure 3.21B). I then examined *fog-1(q253)* homozygotes and another germline feminized male, *gld-1(q126)* homozygotes, however due to severe abnormalities of the gonad in both cases quantitative analysis was not possible.

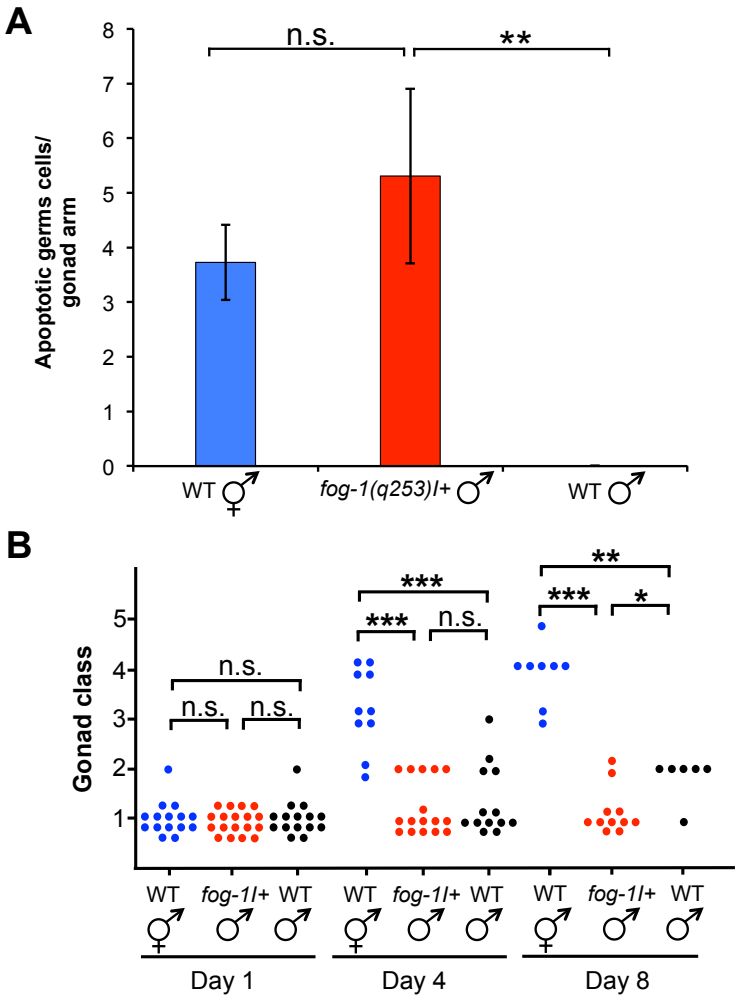

Figure 3.21. Partial feminization of males induces germline apoptosis but not gonad atrophy. (A) *fog-1(q253)*/+ males have germline apoptosis at similar levels to wild-type hermaphrodites. Data mean±s.e.m. (p<0.01 **, Student's t test. To adjust for multiple comparisons p<0.025 was considered significant. n=11-13 per genotype.). **(B)** *fog-1(q253)*/+ males do not undergo age-related gonad disintegration. All experiments performed at 25°C (p<0.017 *, p<0.01 **, p<0.001*** Wilcoxon-Mann-Whitney test. To adjust for multiple comparisons p<0.017 was considered to be significant. Day 1 WT hermaphrodite n=15, *fog-1/+* n=18, WT male n=15. Day 4 WT hermaphrodite n=10, *fog-1/+* n=16, WT male n=13. Day 8 WT hermaphrodite n=8, *fog-1/+* n=11, WT male n=6).

These data suggest germline apoptosis on its own cannot instigate gonad atrophy in feminized males. Other areas of the male, such as the somatic gonad sheath that engulfs apoptotic germ cells (Gumienny et al. 1999), may also need to be feminized. Alternatively as males generate large quantities of sperm, it may be that high levels of germ cell proliferation, even in older males, can offset the loss of germ cells via apoptosis (de la Guardia et al. 2016).

3.7.5 Endoreduplication contributes to oocyte hypertrophy

While studying age-related gonad degeneration, another phenomenon was observed by de la Guardia. In some aged worms the terminal oocyte, which is the oocyte closest to the spermatheca, had become enlarged (de la Guardia et al. 2016). While the rest of the gonad is decrepit, these oocytes are hypertrophic and healthy and appear robust. Hypertrophic oocytes were defined as those that are more than one standard deviation above the mean area of the terminal oocyte on day 1 (>945μm^2). Their occurrence was then confirmed to increase with age (de la Guardia et al. 2016).

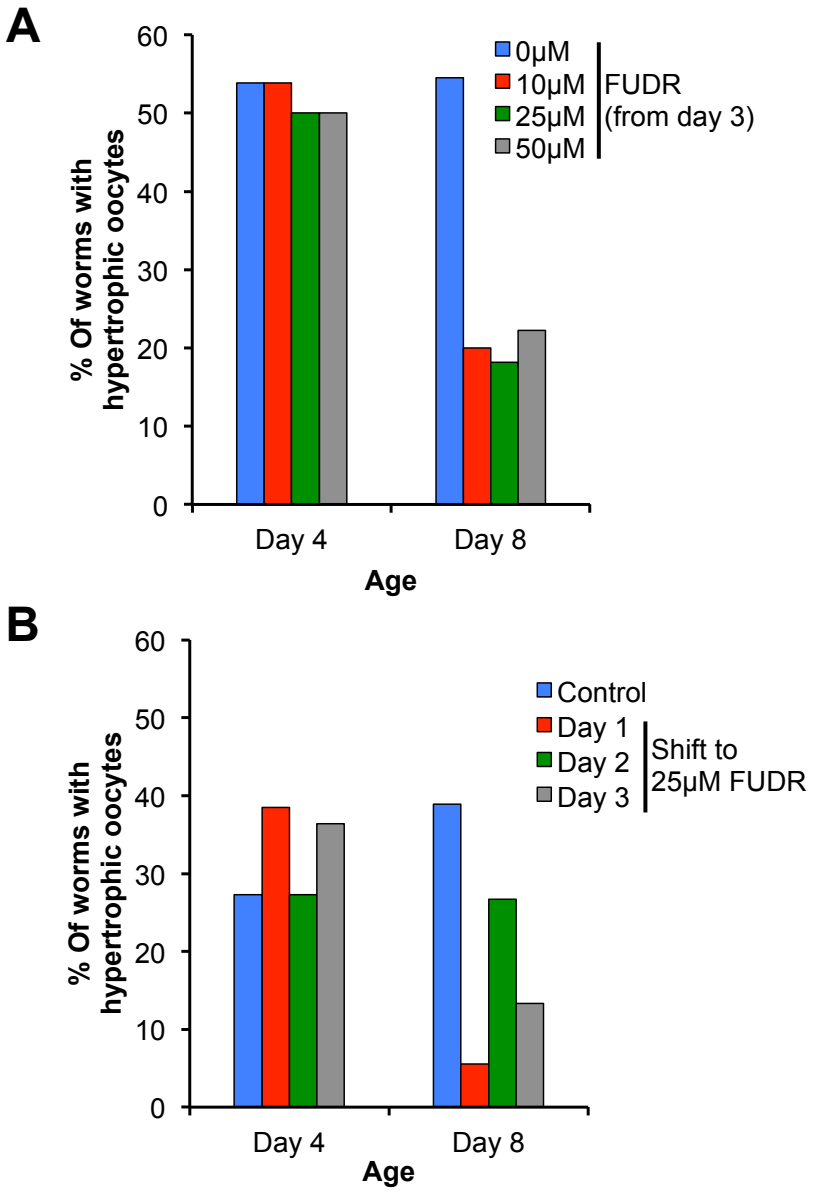

Figure 3.22. The effect of FUDR on percentage of hypertrophic oocytes. (A) Worms shifted onto 10-50μM FUDR on day 3 of adulthood had reduced prevalence of hypertrophic oocytes during ageing. (Sample sizes: Day 4 0μM 7/13, 10μM 7/13, 25μM 6/12, 50μM 5/10. Day 8 0μM 6/11, 10μM 2/10, 25μM 2/11, 50μM 2/9) **(B)** 25μM FUDR was most effective when worms were shifted on day 1 of adulthood. (Sample sizes: Day 4 control 3/11, day 1 shift 5/13, day 2 shift 3/11, day 3 shift 4/11. Day 8 control 7/18, day 1 shift 1/18, day 2 shift 4/15, day 3 shift 2/15) (Day 8 data can be found in de la Guardia et al., 2016).

One possibility as to why these cells grow so substantially is that, like unfertilised oocytes in the uterus, they are undergoing endoreduplication (McGee et al. 2012). Due to the previous success of using the DNA synthesis inhibitor FUDR to reduce tumour development (Riesen et al. 2014), I decided to test its effect on hypertrophic oocytes. Worms were

allowed to grow at 20°C without FUDR present until day 3 of adulthood. This was to allow full development of the germline. On day 3, worms were placed on 10μM, 25μM and 50μM FUDR and then imaged on day 4 and day 8. No effect was seen after only one day of exposure to FUDR, but by day 8 all three concentrations caused a major decrease in the percentage of hypertrophic oocytes (Figure 3.22A). To discover the optimum time that worms needed to be shifted onto FUDR, I shifted worms to 25μM FUDR on days 1, 2 and 3 of adulthood and then imaged them on day 4 and day 8. To have a strong reduction in the prevalence of hypertrophic oocytes, worms needed to be shifted onto 25μM FUDR on the first day of adulthood (Figure 3.22B).

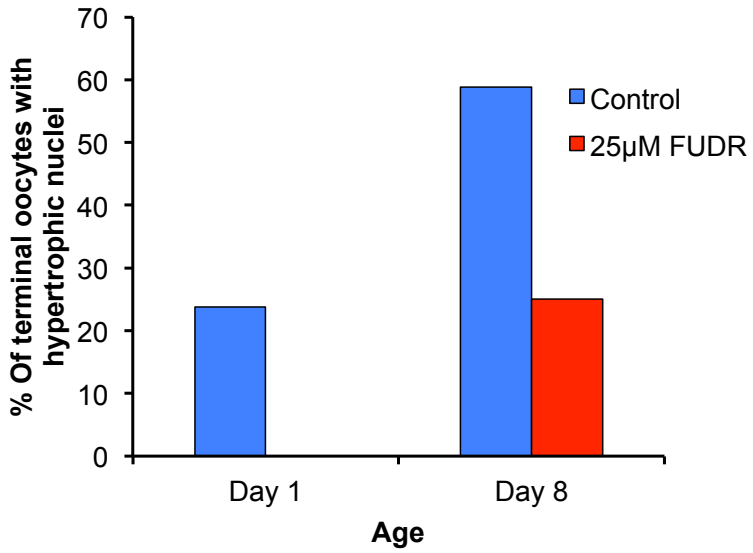

Figure 3.23. The effect of FUDR on percentage of hypertrophic nuclei in terminal oocytes. Surprisingly, hypertrophic nuclei were seen in terminal oocytes even on day 1. Worms were then shifted onto 25μM FUDR on day 1. This reduced the percentage of hypertrophic nuclei by day 8 (Sample sizes: Day 1 control 5/21. Day 8 control 10/17, 25μM 3/12).

Endoreduplicating oocytes in Emo mutants have enlarged nuclei (Iwasaki et al. 1996). To explore whether hypertrophic oocytes are endoreduplicating, I stained day 1 and day 8 worms with DAPI and then measured their nuclei area. I defined hypertrophic nuclei as being one standard deviation above the mean area of day 1 nuclei in terminal oocytes (>27.2 μm^2). This revealed that the percentage of terminal

oocytes with hypertrophic nuclei increased with age by 35% (Figure 3.23). Furthermore this increase was suppressed by exposure to 25μM FUDR from day 1 of adulthood (Figure 3.23). This suggests that continuous endoreduplication in the terminal oocytes promotes age-related hypertrophy, though other mechanisms, such as the uptake of yolk from the body cavity, may also contribute.

3.8 Discussion

3.8.1 Run-on of physiological apoptosis contributes to gonad disintegration

During ageing, the gonad of *C. elegans* hermaphrodites undergoes major atrophy. I have provided evidence that this atrophy is linked to the run-on of PA in post-reproductive animals. For example, gonad disintegration can be accelerated if PA levels are increased, such as in *gld-1(op236), lip-1(zh15)* and *lip-1(gt448)* mutants. When PA is blocked in a *ced-3(n717)* mutant background, the acceleration of gonad degeneration caused by *gld-1(op236)* was reduced.

Continued apoptosis in the post-reproductive germline does not seem to serve any purpose. The hyperfunction theory proposes PA becomes a quasi-programme at this point and continues to function simply because there is no evolutionary advantage to switching it off once reproduction has ceased. We artificially turned the apoptotic programme off at the "appropriate" time by exposing post-reproductive hermaphrodites to *ced-3* RNAi, which prevented gonad disintegration.

Apoptosis can also occur in the germline in response to DNA damage or other stresses (Gartner et al. 2000). This process is dependent on CEP-1. However we showed that *cep-1*-dependent apoptosis does not contribute significantly to the rate of gonad disintegration in

hermaphrodites. This argues against SIA having a major role in the development of this gonadal pathology.

This fits with the hyperfunction theory of ageing, as PA switches from being a programme contributing to reproductive fitness in young animals to a quasi-programme that promotes age-related pathology post-reproduction. Apoptosis may also have a role in the development of pathology in ageing mammalian tissues. For example, sarcopenia of mammalian muscle during ageing has also potentially been linked to apoptosis (Tower 2015). This shows that controlling apoptosis during ageing could have benefits to human health in later life.

3.8.2 The balance with germ cell proliferation

At the distal end of the gonad is the mitotic zone, where proliferation occurs to provide a continuous stream of germ cells. We propose that in a young animal this constant supply of germ cells replenishes the population within the gonad and counteracts the loss of cells via PA. Thus apoptosis does not cause gonad disintegration in young hermaphrodites. In older hermaphrodites, the number of germ cells in the mitotic region decreases, implying a loss of proliferative capacity (Luo et al. 2010). In these circumstances we suggest that even if apoptotic levels do not increase during ageing, there will be an overall loss of germ cell number that could eventually lead to gonad disintegration.

This model implies that mutants that are able to maintain or increase germ cell proliferation during ageing should be able to protect against gonad disintegration. For example, in feminized males, apoptosis is induced in the germline but no disintegration was observed (Figure 3.21). This could be due to males being able to better maintain germ cell proliferation rate during ageing and thus replenish any cells lost via apoptosis. To see disintegration in the feminized males could therefore require apoptosis levels to be increased dramatically to tip the balance

towards an overall decrease in germ cell population. Furthermore, *daf-2(m577)* can suppress age-related gonad disintegration without affecting PA (de la Guardia et al. 2016). It is possible it does this by protecting germ cell proliferation levels during ageing. In support of this it has been shown that *daf-2* mutants have a much smaller decline with age in the number of germ cells in the mitotic zone than wild-type (Luo et al. 2010). The *lip-1(zh15)* and *lip-1(gt448)* mutants used in this study are loss of function alleles. Previous work has shown that *lip-1(0)* mutants, in addition to their effect on PA, have reduced germ cell proliferation (Lee et al. 2006). Therefore both reducing germ cell proliferation and increasing PA concurrently may be the cause of the severe gonad atrophy that occurs in these mutants. To explore this further we wanted to study germ cell proliferation rate using 5-ethynyl-2'-deoxyuridine (EdU) labelling, which identifies the nuclei of S-phase cells (Michaelson et al. 2010). However attempts to use this method in our lab were unsuccessful (Marina Ezcurra, correspondence).

Therefore we hypothesise that while run-on of PA is required for gonad disintegration, it can only cause atrophy when its rate is higher than that of germ cell proliferation. One may view this system as being like a sink; the water from the tap (germ cell proliferation) fills the basin (germ cell population) but water is steadily lost via an open plughole (physiological apoptosis) (Figure 3.24). During ageing in wild-type hermaphrodites the tap is slowly closed causing the basin to gradually empty (gonad disintegration). In mutants such as *gld-1(op236),* the plughole is opened more and this causes the basin to empty faster (accelerated gonad disintegration). According to this model it is the balance between PA and germ cell proliferation that ultimately decides the rate of gonad disintegration.

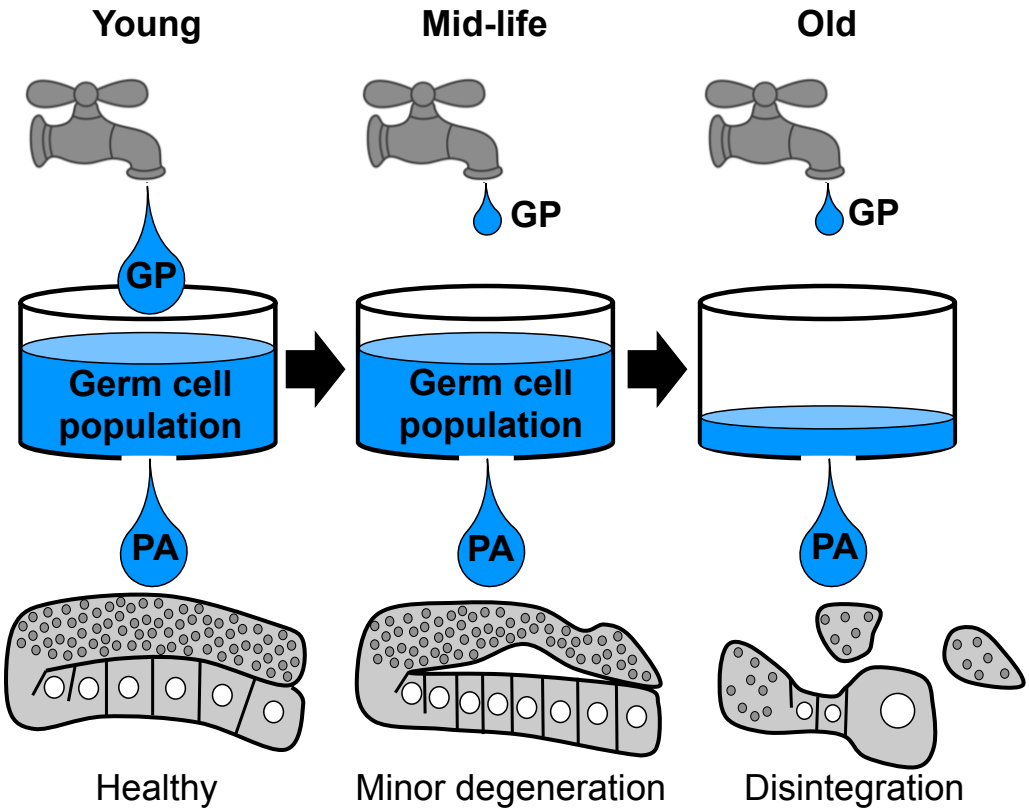

Figure 3.24. Quasi-programmed physiological apoptosis and declining germ cell proliferation lead to gonad disintegration. A faucet and sink model to explain how the balance of germ cell proliferation (GP) and physiological apoptosis (PA) during ageing results in gonad disintegration. In a young animal, GP and PA occur at the same rate so the germ cell population remains steady and the gonad remains healthy. In mid-life, GP rate starts to fall while PA levels are unchanged. Minor degeneration of the gonad begins. In old animals, the downturn in GP rate has caused the germ cell population (i.e the water in the sink) to fall as cells are lost via PA. This results in disintegration of the gonad. (Adapted from de la Guardia et al., 2016).

Chapter 4 Intestinal biomass conversion to yolk causes age-related intestinal atrophy in *C. elegans*

4.1 Introduction to the *C. elegans* intestine

Our hypothesis is that worm lifespan is restricted by life-limiting pathologies. Despite decades of work using *C. elegans* as a model organism for the study of ageing, their cause of death is still unclear. Previous work from David Gems' laboratory eliminated the germline as a possible site of life-limiting pathology in wild-type hermaphrodites (Riesen et al. 2014; de la Guardia et al. 2016). Therefore we focused on another candidate organ that could be the site of fatal pathology: the intestine.

The intestine is the major somatic organ in the worm. Unlike the mammalian intestine, it carries out many different functions beyond simply food digestion and absorption. It is the site of innate immune defence against external pathogens (Schulenburg et al. 2004). It can absorb and store important nutrients, such a lipids, which means it also functions as the adipose tissue (McGhee 2007). It is essential for reproductive fitness as it synthesises and exports yolk, a mixture of protein and associated lipids, which are eventually taken up by oocytes to provide nutrition for developing embryos (Kimble & Sharrock 1983). All of these functions are important and age-related degeneration of the intestine could conceivably impact any number of them, with lethal consequences.

4.1.1 The intestine as a site of life-limiting pathology

Our aim is to identify pathologies in the intestine and to understand how and why they develop. Specifically we wanted to see if any could be attributed to run-on of wild-type gene action or quasi-programmes, like pathologies in other tissues of the worm (Gems & de la Guardia 2013; de la Guardia et al. 2016). We also wanted to establish if any intestinal pathologies we identify could be life-limiting.

Aside from the intestine simply being the largest somatic organ in the worm there are several reasons we chose to study it. Firstly intestinal *daf-16* is partially responsible for *daf-2* mutant longevity (Libina et al. 2003), implying the importance of intestinal function in long-lived mutants. It has also been observed that the intestine does undergo age-related deterioration (Figure 4.1). The intestinal epithelium experiences significant age-related shrinkage or atrophy with intestinal cells appearing to lose a large proportion of their cytoplasmic mass (Herndon et al. 2002; Garigan et al. 2002; McGee et al. 2011). The intestinal lumen becomes variable in width, with both narrow and bloated regions (Garigan et al. 2002; McGee et al. 2011). The capacity for digestion also diminishes as undigested, potentially alive bacteria were observed in the lumen (Garigan et al. 2002; McGee et al. 2011). The microvilli also degrade, which could hamper effective nutrient absorption in later life (McGee et al. 2011). Intestinal nuclei also breakdown and sometimes completely vanish, which presumably prohibits the synthesis of new mRNA, which could impair control of cell metabolism (McGee et al. 2011). Importantly some of these age-related deteriorations are suppressed in long-lived mutants (McGee et al. 2011). Necrotic intestinal cells were also occasionally observed, potentially contributing to worm mortality (Herndon et al. 2002). Indeed, intestinal necrosis occurs during worm death (Coburn et al. 2013). The so-called smurf assay, first used in *Drosophila* (Rera et al. 2011) and recently shown to work in *C. elegans*

as well (Dambroise et al. 2016; Gelino et al. 2016), can test intestinal permeability. Here a dye is fed to animals, which permeates out of the intestine into the body cavity if there is a failure of intestinal barrier function, leading to the smurf (extensively coloured) state. Loss of such function could result in uncontrolled flow of material (e.g bacteria) into the pseudocoelom, likely with adverse effects. It was observed that with increasing chronological age there is a greater proportion of worm smurfs. Furthermore worm smurfs died sooner than non-smurfs (Dambroise et al. 2016).

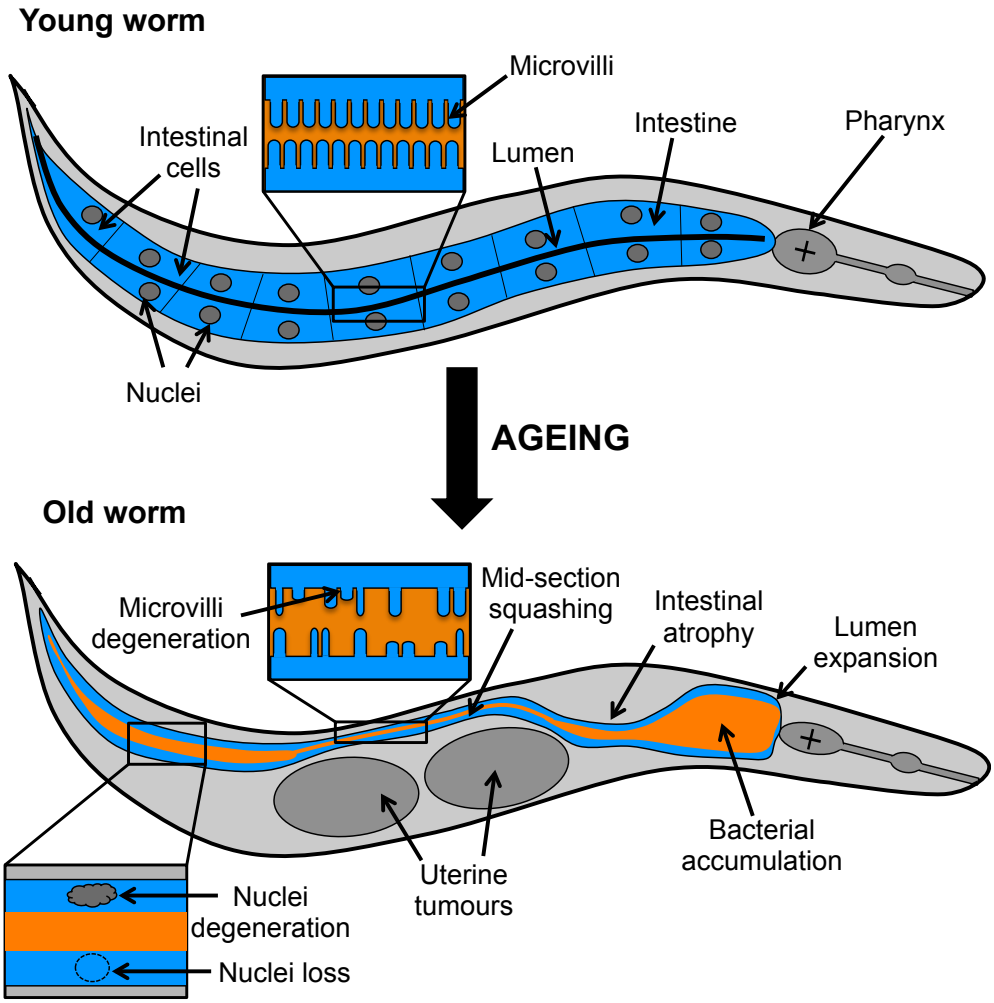

Figure 4.1. Age-related degeneration in the *C. elegans* intestine. The intestine of a young worm appears healthy: the lumen is narrow and regular in width; microvilli are in good condition; intestinal cells and nuclei can be identified and appear normal. After ageing the intestine undergoes many age-related changes. The lumen dilates in places and fills with bacteria (Garigan et al. 2002; McGee et al. 2011). The intestinal cells undergo atrophy (Garigan et al. 2002; Herndon et al. 2002; McGee et al. 2011). The mid-section of the intestine is squashed by uterine tumours (McGee et al. 2011). The microvilli degenerate, where many are shortened or lost (McGee et al. 2011). Finally, intestinal nuclei start to deteriorate or disappear entirely (McGee et al. 2011).

Intestinal atrophy is a striking age-related pathology and could be linked to loss of intestinal barrier function and necrosis, both of which are associated with death (Coburn et al. 2013; Dambroise et al. 2016). However such changes in intestinal size during ageing have not been analysed quantitatively, nor how intestinal atrophy is correlated with other pathologies. Therefore we set out to better characterise intestinal atrophy, to determine the cause of the atrophy and establish whether it contributes towards age-related mortality.

4.1.2 Obstacles to analysing intestinal atrophy

I decided to conduct a thorough description of intestinal atrophy, to try to understand its underlying causes. One reason quantitative analysis of intestinal atrophy has not yet been performed it that it is somewhat difficult to study the ageing intestine with Nomarski microscopy. The intestinal cytoplasm can often be difficult to identify when it has lost much of its mass and develops an irregular morphology. In older worms, the middle portion of the intestine can become squashed by uterine tumours, thus making it difficult to locate, though electron microscopy confirmed there are no breaks and that the intact intestine is still present in this section of the worm (McGee et al. 2011).

I initially attempted to circumvent some of these obstacles by blocking uterine tumour development and using various fluorescent reporters. Later I adopted a semi-quantitative method developed in our lab by Marina Ezcurra (Ezcurra et al., 2017, unpublished). This involved measuring the diameter of the intestine, lumen and body to create an intestinal score (Figure 4.2). This score revealed what percentage of the worm was occupied by intestinal cytoplasm at the point of measurement. Utilisation of all of these methods helped us to describe the atrophy of the intestine more accurately.

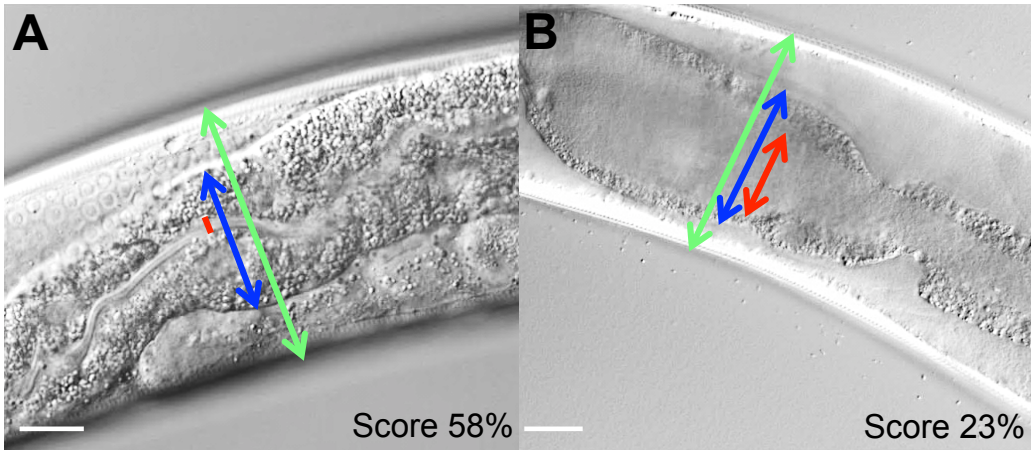

Figure 4.2. Scoring intestinal atrophy. (A) A young, healthy intestine from a day 1, wild-type hermaphrodite. **(B)** An old, atrophied intestine from a day 9, wild-type hermaphrodite. Body width (B) (green), intestinal width (I) (blue) and lumen (L) width (red) are all measured and used to generate an intestine (((I-L)/B)x100) or lumen score ((L/B)x100). A decreasing intestine score indicates atrophy has occurred. An increasing lumen score indicates dilation has occurred. (Scale bar = 20μm).

4.1.3 Bacterial proliferation as a possible cause of intestinal atrophy

In our search for a possible cause of intestinal atrophy one suspect was the worms' food source under standard laboratory conditions, *E. coli* OP50. There is evidence that OP50, though considered non-pathogenic, can cause infection and limit life in elderly worms (Garigan et al. 2002; Gems & Riddle 2000). Large quantities of *E. coli* accumulate in the intestine of ageing worms (McGee et al. 2011; Garigan et al. 2002). In young worms the pharyngeal grinder ensures all *E. coli* are macerated before entering the intestine. But during ageing, the grinder appears to lose efficiency as intact, live bacteria appear in the intestine (Garigan et al. 2002; Portal-Celhay et al. 2012). *E. coli* then proliferate and colonise the intestine. This could damage intestinal cells; indeed, degenerated microvilli are often associated with clusters of *E. coli* (McGee et al. 2011). Furthermore *E. coli* cells were occasionally observed within the intestinal tissue of aged worms (Herndon et al. 2002). This suggests *E. coli* is eventually harmful to the intestine. For example, the bacterial accumulation was described by one study as possibly causing

constipation of the intestine (Garigan et al. 2002). Constipation occurs when there is a blockage in the gastrointestinal tract resulting in a build up of material. Yet there is no evidence that the large bacterial load in the intestine actually impedes movement of material through the lumen. Therefore it remains to be determined to what extent the bacterial accumulation contributes to a decline in intestinal function.

In the wild, *C. elegans* feed on many different types of bacteria (Dirksen et al. 2016). When worms are grown on the soil microbe *B. subtilis*, their lifespan is extended (Garsin 2003). Furthermore if worms are fed on antibiotic-treated or UV-killed *E. coli* the accumulation of bacteria is largely prevented (Garigan et al. 2002), suggesting proliferating bacteria in the intestine is responsible for the build up. Notably, antibiotic and UV treatment of *E. coli* can also extend lifespan (Garigan et al. 2002; Gems & Riddle 2000). This all suggests *E. coli* is pathogenic in ageing *C. elegans*. Therefore it would be interesting to see how *E. coli* might contribute to intestinal atrophy.

4.2 Results

4.2.1 The *C. elegans* hermaphrodite intestine undergoes rapid atrophy during early ageing

To assess anecdotally for potentially interesting features of the ageing intestine that could warrant further study, the following simple screen was performed. I examined the ageing intestine of *glp-4(bn2)* worms. Worms were shifted to 25°C at L4 stage, to block uterine tumour growth without affecting lifespan. This was to ensure that the ageing of the intestine was not affected by any longevity mechanisms that could be switched on in *glp-4* mutants when they are long-lived when grown at 25°C from egg. Worms were also grown with or without the antibiotic carbenicillin. These two interventions allowed us to observe age-related changes in the intestine in the absence of *E. coli* accumulation and squashing by uterine tumours.

As previously observed, worms grown without antibiotics had *E. coli* accumulate in their intestine, especially in the most anterior portion (Figure 4.3A,B) (Garigan et al. 2002). Worms grown with antibiotics did appear to have a lower incidence of *E. coli* accumulation, as previously observed (Garigan et al. 2002). Nevertheless I noted that some still had a distended lumen, but that such lumens appeared to be devoid of densely packed bacteria (Figure 4.3E). This suggests that lumen dilation may occur independently of bacterial accumulation and instead happens due to intrinsic age-related mechanisms within the intestine. I also observed large fat droplets within *glp-4* intestinal cells (Figure 4.3C), something not usually seen in the ageing wild-type gut. As *glp-4* worms produce more yolk than wild-type (Riesen et al. 2014), these fat droplets may be due to ectopic deposition of lipid. Atrophy of the intestine occurred along its entire length and in the absence or presence of antibiotic. Extensive atrophy still occurred in the mid-section of the worm, despite the absence of uterine tumours (Figure 4.3A). Therefore while uterine tumours could slightly worsen atrophy, they are not its primary

cause. I also noted marked irregularity in the extent of atrophy along the intestine, with some regions more atrophy than others, in an apparently random fashion (Figure 4.3D).

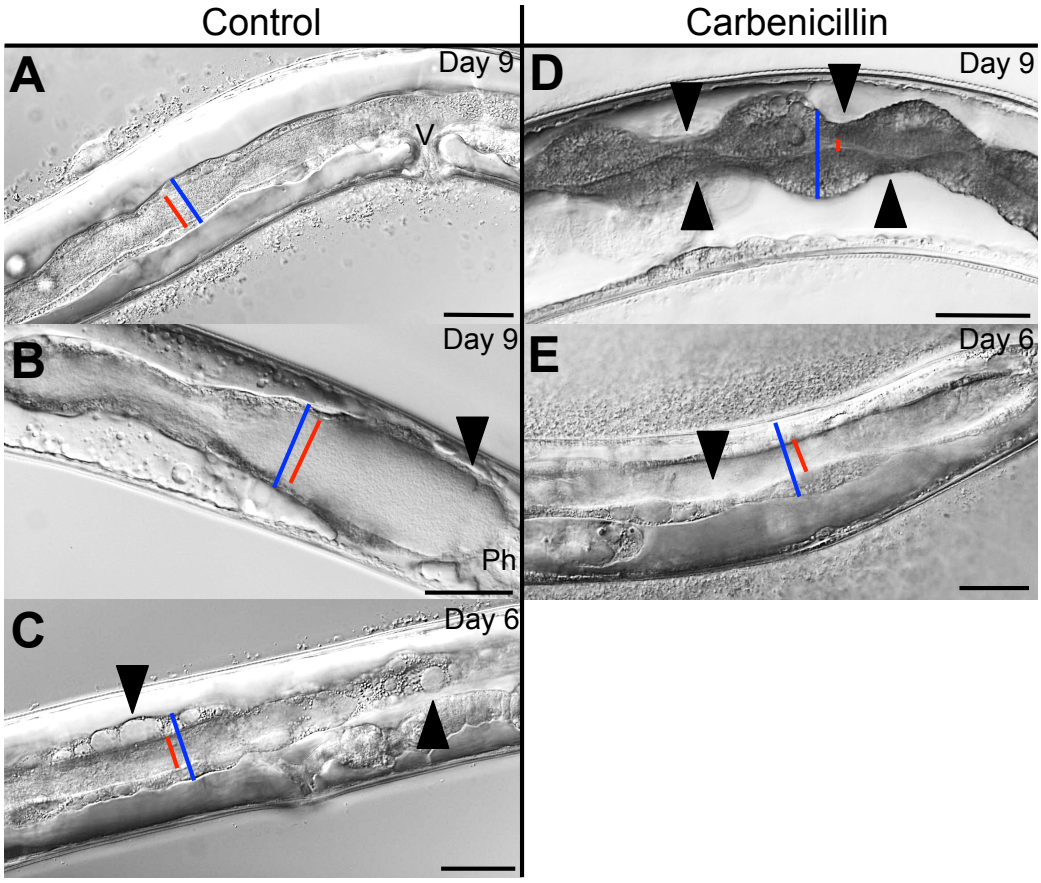

Figure 4.3. Age-related changes to the *C. elegans* intestine in *glp-4* mutants. All images were captured at x400 magnification. **A-C** were grown on proliferating *E. coli*. **D,E** were grown on carbenicillin-treated *E. coli*. The intestine (blue line) and the lumen (red line) are indicated. **(A)** The intestinal lumen is filled with *E. coli* and intestinal cells undergo severe atrophy. Vulva (V). **(B)** *E. coli* accumulation (arrow) is usually most severe in the most anterior portion of the intestine near the pharynx (Ph). **(C)** Fat droplets (arrows) appear in the cytoplasm of atrophied intestinal cells. These were also seen in worms grown with carbenicillin. **(D)** Certain points of the intestine show more atrophy (arrows), resulting in irregularity in intestinal width. **(E)** Worms grown on carbenicillin sometimes had a distended lumen that appeared devoid of *E. coli* (arrow). Atrophy of the intestinal cells was still observed on carbenicillin. In all panels, oily yolk pools can also be seen to be filling the body cavity (Scale bars = 40µm).

This preliminary study of the ageing intestine emphasised to us that intestinal atrophy is a severe age-related pathology and warrants further study, as outlined in the rest of this chapter. It also implied that uterine tumours and proliferating *E. coli* are not significant contributors to the development of this pathology, given that atrophy still occurred when both are removed. Furthermore, the lumen still distended in the absence of

proliferative bacteria, which suggests that bacteria accumulate within the intestine, not because of constipation, but merely to fill the space made available by age-related changes to the intestine. Therefore I set out to examine intestinal atrophy using quantitative analysis of this pathology.

To quantify overall intestinal atrophy, I measured the cross-sectional area of the intestine during ageing. To investigate lumenal dilation, I measured lumenal cross-sectional area at the same time. To view the entire length of the worm intestine in a single image, images were taken at x100 magnification. Given that this resulted in a lower resolution image, I employed a number of markers to assist with the identification of the intestine. The intestinal cytoplasm emits blue autofluorescence, which was used to help identify the intestinal biomass. A strain bearing *oxIs144*[INX-16::GFP, *lin-15*+] was used to mark the intestinal cell boundaries with GFP. INX-16 is a transmembrane protein found at gap junctions that connect the intestinal cells together (Peters et al. 2007). Finally I also grew worms on *E. coli* OP50 expressing a RFP protein (OP50-RFP) to help to visualise the lumen and gain a greater understanding of the pattern of *E. coli* accumulation in the intestine. The bacteria were also grown either with or without the antibiotic carbenicillin present to help to determine how proliferating bacteria might affect intestinal atrophy.

Worms were imaged on days 1, 4, 8 and 11 (20°C). To calculate the cross-sectional area of the intestinal biomass, lumenal area was subtracted from the total intestinal area. In some worms, especially on day 1 of adulthood, the lumen was too narrow to measure accurately so it was estimated as 1% of the total intestinal area. A two-way ANOVA indicated there was a significant effect of age on intestinal area ($F(2,52)=15.5$), $p<0.0001$). Intestinal area significantly decreased between day 4 and day 8 (Figure 4.4). In worms on antibiotic-treated bacteria, intestinal area also declined between days 4 and 8. Furthermore the two-way ANOVA revealed there is no overall significant effect of carbenicillin on intestinal atrophy ($F(1, 52)=0.64$, $p=0.43$). Therefore while

proliferating bacteria may contribute to atrophy, as growth on UV-treated bacteria could delay it (Marina Ezcurra, unpublished), this pathology is at least partly independent of *E. coli* accumulation.

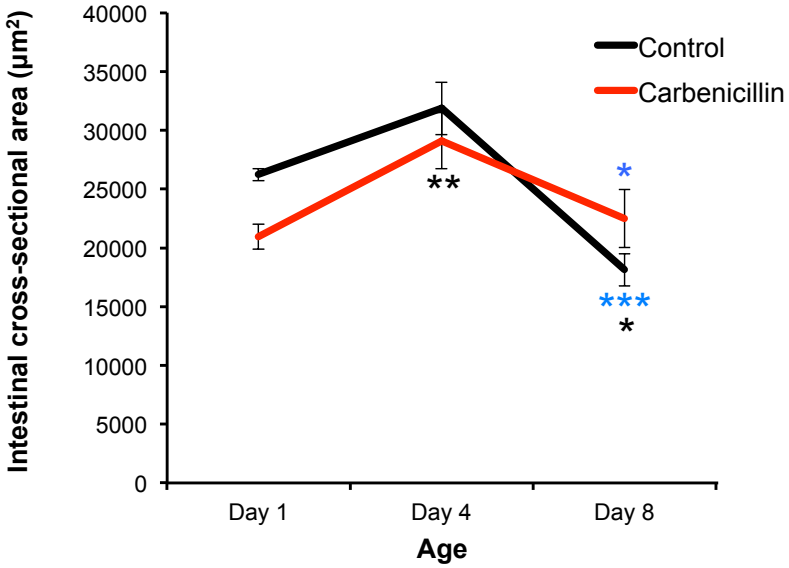

Figure 4.4. Intestinal atrophy in *oxIs144*[INX-16::GFP, *lin-15*+] *C. elegans*. (A) Age-related changes in intestinal cross-sectional area in worms grown with and without carbenicillin. Intestinal atrophy occurs in both conditions between day 4 and day 8. Data±s.e.m (n=10 per time point, per condition except day 8 control n=8). (Black stars vs day 1 of same condition, blue stars vs previous day. $p<0.05$ *, $p<0.01$ **, $p<0.001$ *** Sidak's test)

A two-way ANOVA revealed the mean luminal area does change significantly with age ($F(2,52)=17.87$, $p<0.0001$) and carbenicillin also has a significant effect on lumen size ($F(1,52)=8.09$, $p=0.0064$). The mean lumenal area increased dramatically on proliferative bacteria between day 1 and day 4, from 265µm^2 to 7,931µm^2, a 30-fold increase (Figure 4.5). On antibiotic-treated bacteria there was also an increase in the mean lumenal area between day 1 and day 4, from 211µm^2 to 4,013µm^2. However in both cases lumen size appeared to plateau after day 4 (Figure 4.5). This supports a previous study that showed the bacterial load in the *C. elegans'* intestine increases until day 4 and then remains constant until day 14 (Portal-Celhay et al. 2012). This suggests dilation may be partly due to proliferating bacteria but other mechanisms also appear to contribute to this phenomenon. Collectively these data show

that endogenous changes in the intestine could cause both lumenal dilation and intestinal atrophy.

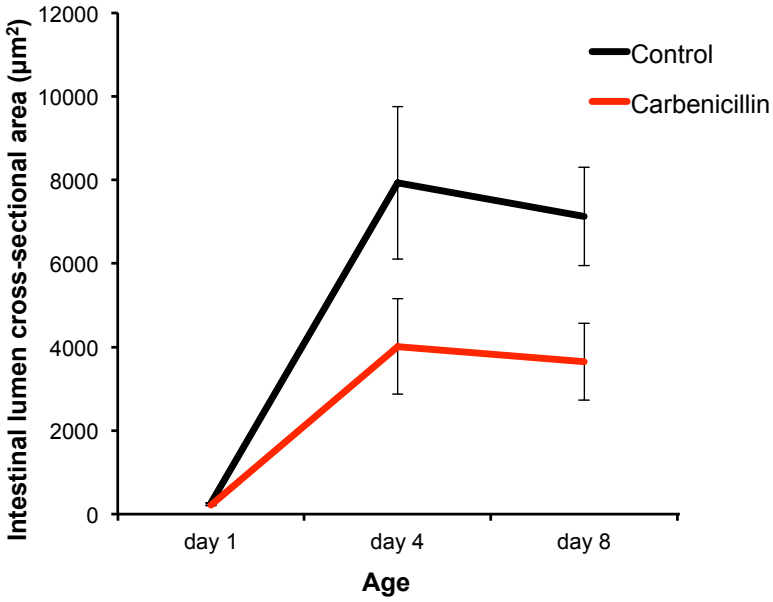

Figure 4.5. Intestinal lumen distension in *oxIs144*[INX-16::GFP, *lin-15*+]. Age-related changes in intestinal lumen cross-sectional area in worms grown with and without carbenicillin. Lumen dilation shows a trend for being reduced on carbenicillin. Data±s.e.m (n=10 per time point, per condition except day 8 control n=8).

The INX-16::GFP marker revealed another characteristic of intestinal atrophy, that it is greater at the cell boundaries (Figure 4.6). This explains the variable diameter I previously observed in the ageing intestine. This could be due to a loosening of the connections between the intestinal cells or because atrophy occurs more rapidly at the transverse cell membranes. In contrast this could be due to mislocalisation of gap junctions and therefore a defect specific to gap junctions rather than the plasma membrane as a whole.

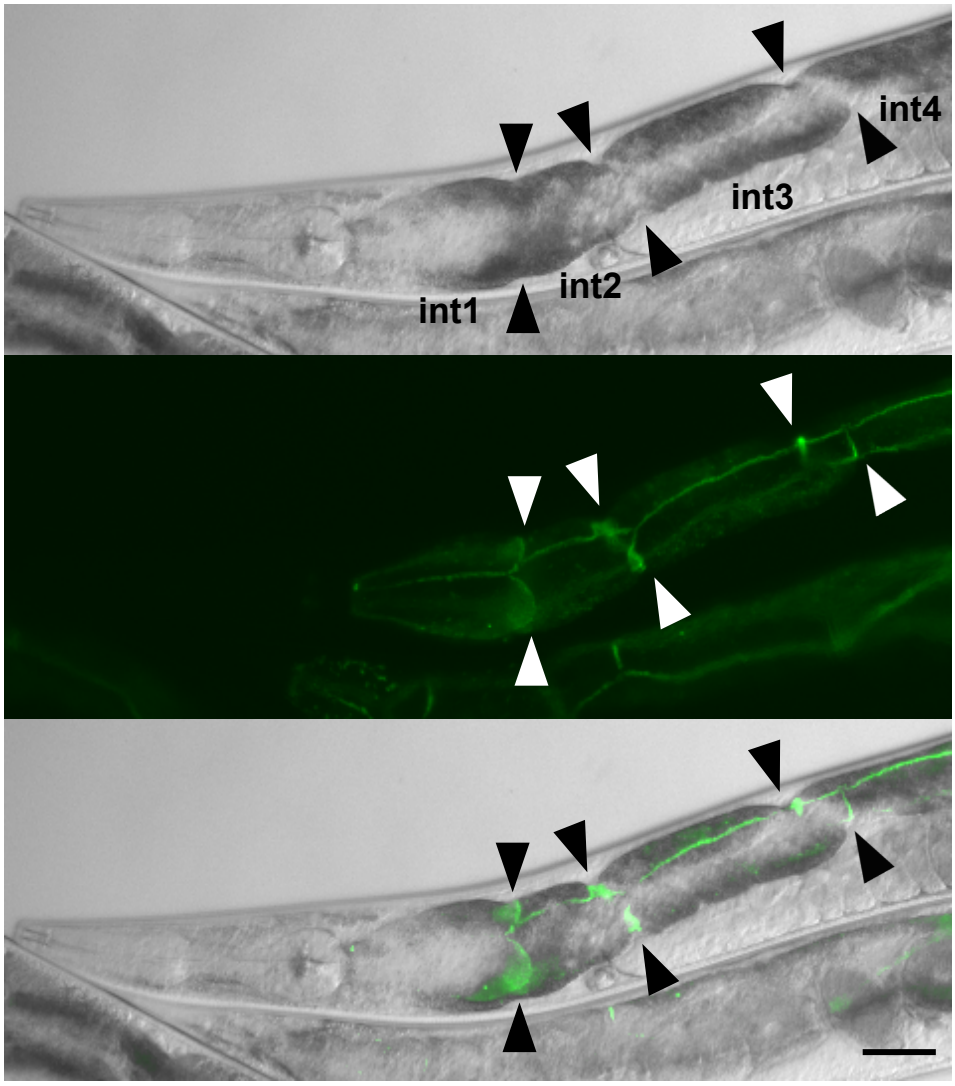

Figure 4.6. Accelerated atrophy at intestinal cell boundaries. Images were taken at x100 magnification and are of a day 4 worm. Cell boundaries in *oxIs144*[INX-16:GFP, *lin-15*+] have been tagged with GFP (arrows). A pinching at the boundaries can be observed indicating more atrophy at these points. (Scale bar = 40μm).

Another observation was that OP50-RFP fluorescence was absent from the lumen of some of the older worms, even though the lumen appeared to be full of densely packed bacteria (Figure 4.7). Moreover, the intestine's red autofluorescence increased in older worms, as had been observed previously (Coburn et al. 2013), making it difficult to distinguish the intestinal cytoplasm from the fluorescent bacteria in the lumen. This was especially a problem in areas of the intestine where the lumen was narrower. This is why I was unable to obtain data for day 11 worms on carbenicillin-treated plates because a combination of background

fluorescence from the intestine and the small amount of red fluorescence in the lumen made it difficult to measure lumenal area. Furthermore, close inspection of the images taken of worms grown on OP50-RFP showed that sometimes only OP50-RFP in the centre of the lumen was fluorescing (Figure 4.7). This was seen in some worms as early as day 4. Perhaps this is a transitional stage before all OP50-RFP in the lumen stops fluorescing. It could be that the bacteria closest to the intestinal cells are exposed to something that stops them fluorescing first. It could also imply an intermediate stage of *E. coli* accumulation, where bacteria line the gut and there is a lime scale-type effect (e.g as occurs in water pipes) as a biofilm is produced. Biofilms are created when bacteria adhere to both a surface and to each other. They then produce an extracellular polymeric matrix to enclose themselves. Biofilms are resistant to various biocides including acid exposure and antibiotics (Hall-Stoodley et al. 2004), so may protect the bacteria in the acidic environment of the *C. elegans* intestine (Allman et al. 2009).

Together these results demonstrate that the hermaphrodite intestine undergoes rapid atrophy during ageing, particular at the cell boundaries, along with lumenal dilation. While both of these appear to be partly dependent on proliferating bacteria, it appears that other endogenous mechanisms contribute to their formation. Therefore we set out to discover what these mechanisms could be.

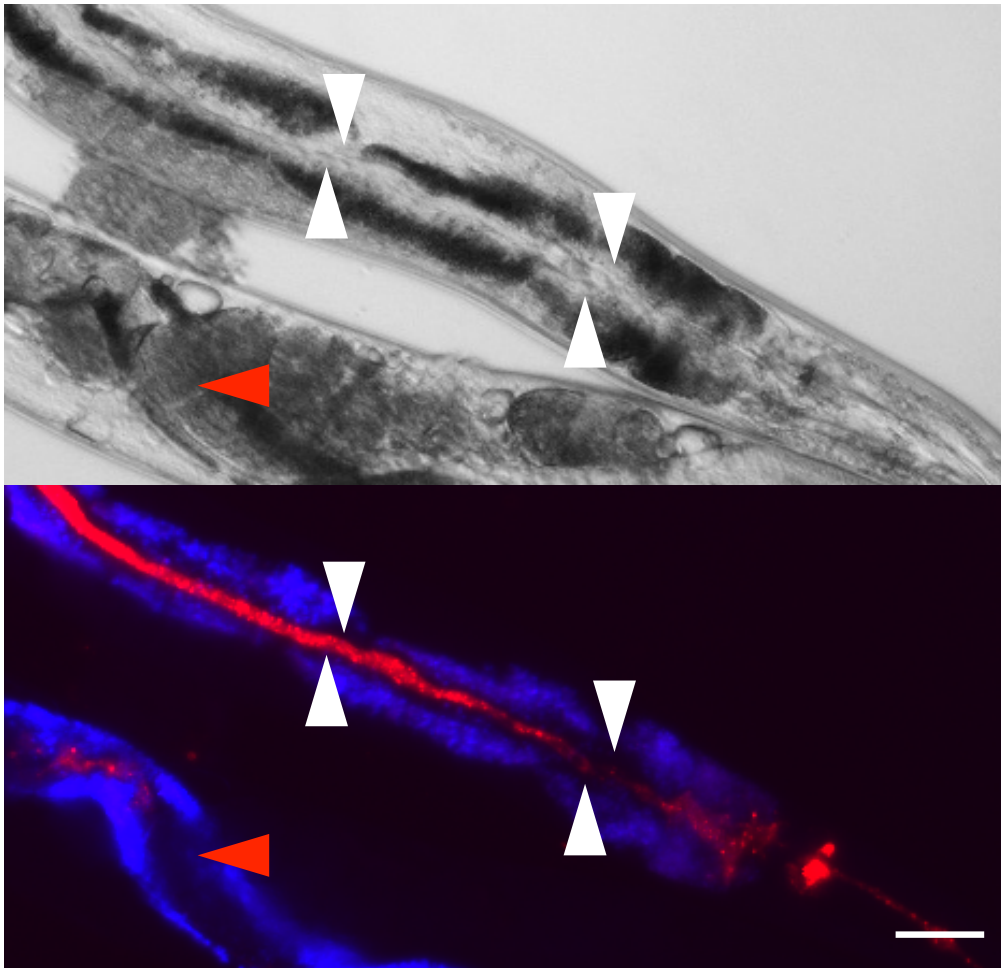

Figure 4.7. Loss of fluorescence of *E. coli* OP50-RFP in the intestinal lumen during ageing. Images were taken at x100 magnification and are of a day 4 worm. The blue autofluorescence is from the intestinal cytoplasm while the red fluorescence marks OP50-RFP in the lumen. At certain points OP50-RFP has either stopped fluorescing at the outer edges of the lumen (white arrows) or throughout (red arrows). (Scale bar = 40μm).

4.2.2 The biomass conversion theory

As there is only partial suppression of intestinal atrophy in the presence of antibiotics, atrophy is at least partly independent of proliferating *E. coli*. We hypothesised that the remaining atrophy could be the result of a quasi-programme. One quasi-programme that could be linked to intestinal atrophy is yolk production in ageing *C. elegans*.

Yolk is made up of protein, produced in *C. elegans* by the *vit* genes, and lipid (Sharrock et al. 1990). As viewed on protein gels, the three yolk

proteins of *C. elegans* are YP170, YP115 and YP88 and all are synthesised in the intestine (Kimble & Sharrock 1983). Yolk is then transported out of the intestine into the body cavity where, during the reproductive period, it is taken up by maturing oocytes. However once reproduction has ceased at around day 4, the body cavity starts to fill with yolk, suggesting the worm is incapable of switching off yolk production when it is no longer required (DePina et al. 2011; Garigan et al. 2002; Herndon et al. 2002; McGee et al. 2011). In fact yolk proteins continue to be synthesised until around day 14 of adulthood, with YP170 reaching 7 times the levels seen in early adulthood (Ezcurra at el., 2017, unpublished). Therefore post-reproductive yolk production appears to be a quasi-programme, as it does not result from any sort of malfunction during ageing, but rather that it is simply not switched off.

In young worms, the pharynx pumps at a high rate to ingest the resources sufficient to fuel yolk production. Therefore in early adulthood, the bacterial food source is the primary nutrient supplier for vitellogenesis. However in older worms the pharyngeal pumping rate declines until pumping completely ceases (Chow et al. 2006; Huang et al. 2004). One possibility is that in the absence of an alternative nutrient supply, continued yolk production requires the intestine to consume its own biomass. Alternatively, as most intestinal atrophy occurs between days 4 and 8, when pharyngeal pumping is still relatively high, demand for yolk production might always outweigh what can be supplied through the bacterial food source. Therefore putative intestinal biomass conversion to yolk might be required earlier to promote fitness. If this mechanism was maintained (i.e runs on) during ageing, it could result in extensive intestinal atrophy.

This theory was developed during various discussions in our laboratory and was dubbed the biomass conversion hypothesis. Other members of David Gems' group have provided evidence to support this hypothesis. Firstly, intestinal atrophy and yolk accumulation occur at similar times, mostly between days 3 and 7, though of course this does not prove

causation (Figure 4.8) (Ezcurra at el., 2017, unpublished). Various interventions that extend lifespan, such as dietary restriction and *daf-2* mutations, all decrease both yolk accumulation and intestinal atrophy (Ezcurra at el., 2017, unpublished). Furthermore total protein content in worms does not change between days 5 and 7, yet the percentage that is yolk protein continues to rise (Ezcurra at el., 2017, unpublished). I decided to determine whether there was any sexual dimorphism in this pathology, given we had seen this with another pathology we had examined previously: gonad atrophy (de la Guardia et al. 2016). Some of the work from this section will be published in an upcoming paper from our laboratory, Ezcurra at el., 2017.

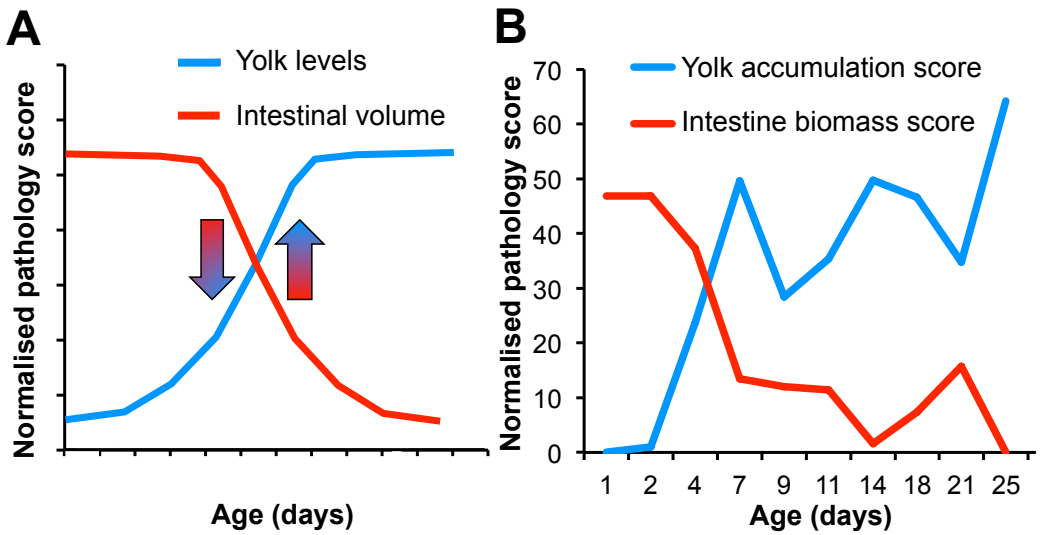

Figure 4.8. The biomass conversion theory. (A) A theoretical graph of how yolk levels and intestinal volume might change during ageing in *C. elegans.* **(B)** Actual yolky pool and intestinal biomass scores from wild-type worms aged at 20°C, showing yolk accumulation and intestinal atrophy occur at similar times, mostly between days 3 and 7, data from Marina Ezcurra (Ezcurra et al., 2017, unpublished).

4.2.3 Males do not accumulate lipid pools during ageing

In hermaphrodites, run-on of yolk production results in large, shiny fat pools or 'yolky' pools that contain yolk protein and other constituents including lipids (Garigan et al. 2002; Ezcurra et al., 2017 unpublised). The male intestine does not synthesise vitellogenin (Kimble & Sharrock 1983), therefore males would not be expected to accumulate yolky pools in the

body cavity. Upon examination of young males we did observe what appeared to be small fat pools, generally in the posterior portion of the worm, apparently within the vas deferens (Figure 4.9). These are putative lipid pools, as we cannot be certain of their components, though their appearance strongly suggests they contain lipids. For simplicity, they shall henceforth be designated simply as lipid pools. I set out to examine how lipid pools changed during ageing in males. A lipid pool score was obtained using a method developed by Marina Ezcurra by calculating the percentage of the body cavity area occupied by these pools in one field of view (Figure 4.10) (Ezcurra et al., 2017 unpublished).

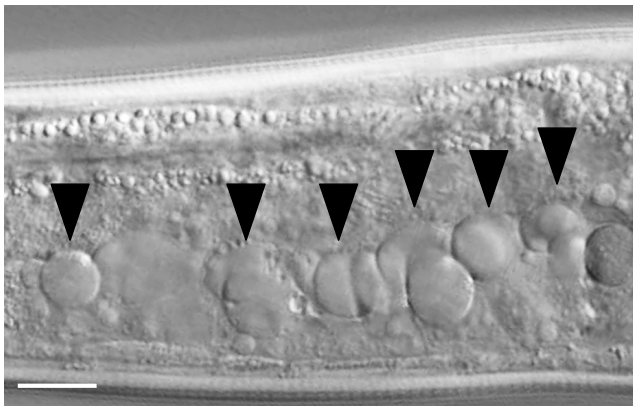

Figure 4.9. Lipid pools in wild-type male *C. elegans*. Image was taken at x630 magnification and is of a day 1 wild-type male. Lipid pools are found in the posterior portion of the worm (black arrows). (Scale bar = 10μm).

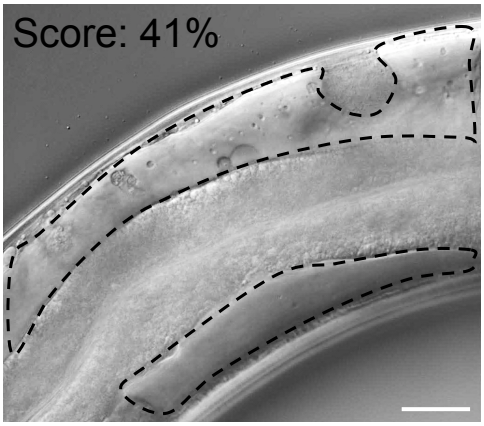

Figure 4.10. Measuring yolky/lipid pools in *C. elegans*. Yolky pools (Y) in a day 7 wild-type hermaphrodite are outlined (black). A score is generated by measuring the percentage of the body cavity area (B) occupied by the yolky pools ((Y/B)x100)). An increasing score indicates yolk accumulation has taken place. (Scale bar = 20μm).

When ageing *C. elegans* in the laboratory, worms are typically kept in large groups on NGM plates and such grouping has no impact on hermaphrodite lifespan (Gems & Riddle 2000). However males cultured in groups are much shorter lived than individually cultured males, with group size negatively correlating with lifespan (Gems & Riddle 2000). This could be because males form mating clumps, which could result in them physically damaging each other (Gems & Riddle 2000). On the other hand, it could be because males secrete compounds that have been shown to reduce hermaphrodite lifespan (Maures et al. 2014). Therefore to study ageing in *C. elegans* males, it is ideal to study them individually on plates. However individual males often crawl off NGM plates and die from desiccation on the sides of the plates. To solve this problem a method was developed to culture males individually in liquid culture in 96-well plates. The surface tension of the liquid prevents the males from escaping (McCulloch & Gems 2003). Therefore I decided to adopt this method to study age-related changes to lipid pools in males. However as liquid culture is quite different from culturing on NGM plates, the culturing method used in the majority of experiments for this project, I decided to examine males kept in small groups on plates (5 per plate). This would allow me to see if the two conditions produced very different results and determine which was more convenient for future experiments.

Wild-type males and hermaphrodites were kept individually in liquid culture at 20°C from L4 stage and imaged on days 1, 7, 11, 14 and 18. A two-way ANOVA revealed that there was a significant difference with age and between the two sexes ($F(4,58)=5.744$, $p=0.0006$ and $F(1,58)=62.75$), $p<0.0001$ respectively). I observed that, as expected, hermaphrodites had a dramatic accumulation of yolk pools between days 1 and 7, though levels did not rise further after day 7 (Figure 4.11A). This demonstrates that run-on of yolk synthesis still occurs in hermaphrodites grown in liquid culture. However in males, lipid pools did not increase above the levels seen on day 1 and were significantly smaller than

hermaphrodite yolky pools on days 7, 11, 14 and 18 (Figure 4.11A). On NGM plates worms were also grown at 20°C and imaged on days 1, 4, 7, 11 and 14. Again a two-way ANOVA revealed that there was a significant difference with age and between the two sexes ($F(4,160)=46.40$, $p<0.0001$ and $F(1,160)=196.2$), $p<0.001$ respectively). The hermaphrodites accumulated large yolk pools, which continually increased until day 11 (Figure 4.11B). The lipid pools did not increase during ageing in males on plates and were always significantly smaller than hermaphrodite yolky pools (Figure 4.11B). Therefore males grown in small groups on NGM plates and individually in liquid culture appear very similar in terms of this pathology.

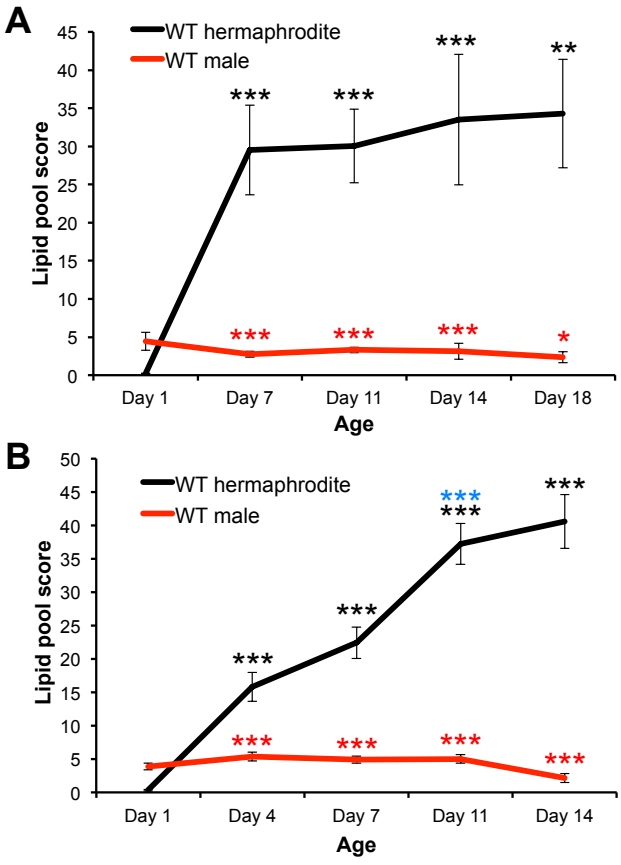

Figure 4.11. Lipid pool scores in ageing wild-type male and hermaphrodite *C. elegans* (A) Worms were grown individually in liquid culture. While yolk accumulates in ageing hermaphrodites, lipid pools do not increase in males. (n=8 per condition per timepoint until day 18 where n=2 for hermaphrodites and n=5 for males) **(B)** Worms were grown on plates, with males kept in small groups (5 per plate). While yolk accumulates in ageing hermaphrodites, lipid pools do not increase in males. Data±s.e.m. (n=18-20 per condition per time point, until day 14 where n=3 for males and n=10 for hermaphrodites) (Black stars vs day 1 of same gender; red stars vs hermaphrodite of same age; blue stars vs previous day. Tukey HSD $p<0.05$ *, $p<0.01$ **, $p<0.001$ ***).

4.2.4 The male intestine does not undergo atrophy

If intestinal atrophy is caused by intestinal biomass conversion to yolk then intestinal atrophy should not happen in males because males do not make yolk (Barton & Kimble 1990) nor do they accumulate lipid pools during ageing. I therefore examined the male intestine during ageing, measuring atrophy and lumen dilation. For this experiment and all ones henceforth where I investigate intestinal atrophy, I adopted a method developed by Marina Ezcurra to measure intestinal atrophy and lumen dilation by generating a score for each using measurements from high magnification (x630) Nomarski images (Figure 4.2) (Ezcurra et al., 2017, unpublished). A high intestinal score indicates a large intestinal volume, while a decrease in score indicates a decrease in intestinal volume, indicating intestinal atrophy has taken place. Here we are assuming that a decrease in volume also correlates with a decrease in biomass (i.e weight of intestine). For this to be correct a decrease in intestinal volume should not result in an increase in density. To support this it has been demonstrated that during ageing the *C. elegans* hermaphrodite intestine does have a reduced lipid density, (Ezcurra et al., unpublished) suggesting a decrease in intestinal volume may be associated with a decrease in intestinal biomass. An increase in lumen score demonstrates lumen dilation has occurred. I switched to this method due to the previous problems I had encountered when measuring whole cross-sectional area of the intestine, particularly the issue of the declining fluorescence of lumenal OP50-RFP during ageing. The DIC images taken at higher magnification made it much easier to distinguish between the lumen and the intestinal cytoplasm. The posterior intestine was selected for measurement, since atrophy in the anterior intestine is highly variable, and the middle of the intestine gets squashed by uterine tumours.

In individual liquid culture, wild-type males and hermaphrodites were imaged on days 1, 7, 11, 14 and 18. It was noted that males have a smaller intestine than hermaphrodites in early adulthood, which could

theoretically mean they are unable to lose similar proportions of intestinal biomass as hermaphrodites. This would mean any small changes to intestinal size in the ageing male could be harder to detect. As usual, the hermaphrodite intestine appeared to atrophy during ageing (two-way ANOVA, comparison for age $F(4,58)=3.029$ $p<0.0245$), and there was no evidence of intestinal atrophy in the males (Figure 4.12A). A two-way ANOVA showed the lumen appeared to dilate in both sexes with increasing age ($F(4,58)=8.026$, $p<0.0001$), however there was no significant difference between the two sexes ($F(1,58)=0.9894$, $p=0.3240$) (Figure 4.12B). It is important to note that there was a small sample size in this trial, particularly on later days. This was because it was difficult to maintain a large ageing population using the more labour intensive individual liquid culture method. On plates, intestinal atrophy did occur in hermaphrodites (two-way ANOVA, comparison for age $F(4,160)=10.73$, $p<0.0001$), with the intestine continuously losing volume up until day 11 (Figure 4.13A). Furthermore I again saw no evidence of intestinal atrophy in males (Figure 4.13A). The lumen seems to alter its width with age (two-way ANOVA, comparison for age $F(4,160)=7.723$, $p<0.0001$), first increasing and decreasing in both sexes (Figure 4.13B). Additionally there appears to be a difference between the two sexes (two-way ANOVA, comparison for sex $F(1,160)=7.955$ $p=0.005$), which demonstrates that males are able to maintain a narrower lumen during ageing.

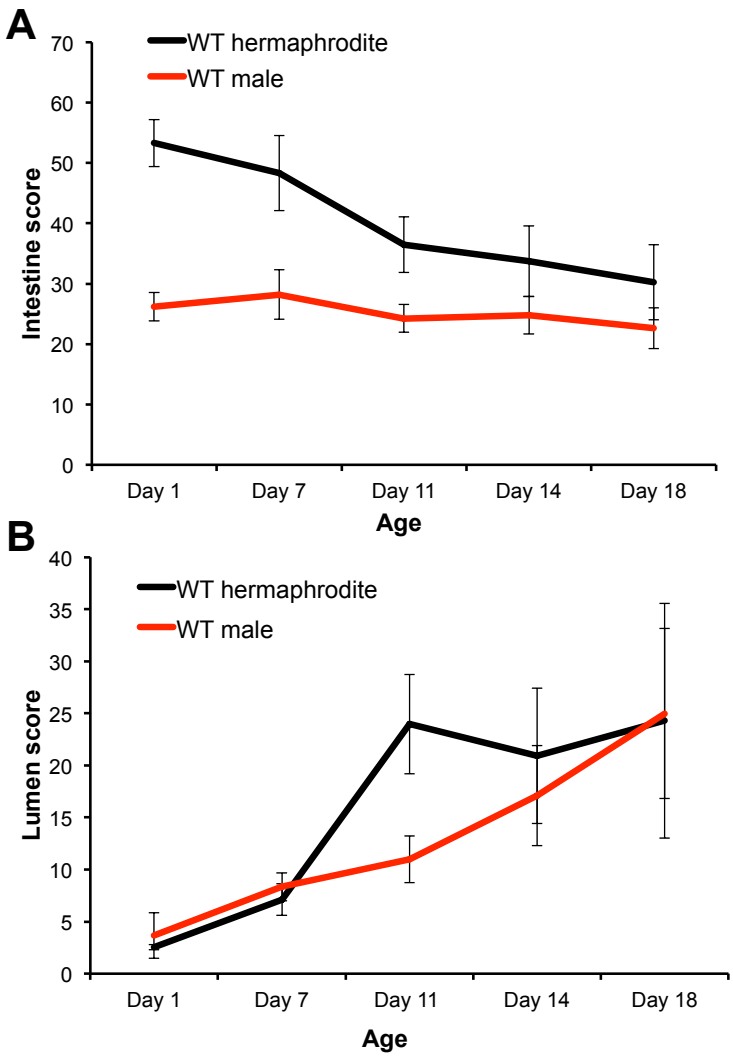

Figure 4.12. Intestinal atrophy and lumen dilation in ageing wild-type hermaphrodites and males in liquid culture. (A) Males show no intestinal atrophy, while hermaphrodites show a trend for intestinal atrophy. **(B)** Males and hermaphrodites show an increase in lumen dilation but there is no significant difference between the two sexes. Data±s.e.m. (n=8 per condition per timepoint until day 18 where n=2 for hermaphrodites and n=5 for males).

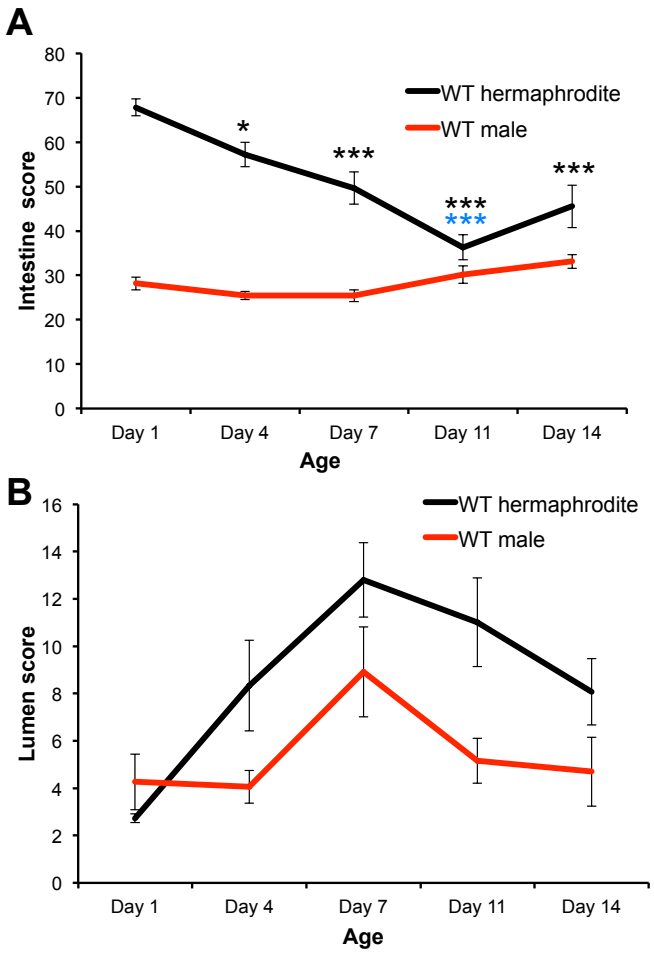

Figure 4.13. Intestinal atrophy and lumen dilation in ageing wild-type hermaphrodites and males on plates. (A) Males show no intestinal atrophy, while hermaphrodites undergo significant intestinal atrophy. (Black stars vs day 1 of same gender, Tukey HSD $p<0.05$ *, $p<0.01$ **, $p<0.001$ ***) **(B)** Lumen size varies throughout age, first increasing and peaking on day 7 before then decreasing. Additionally males appear to be able to maintain a narrower lumen throughout life. (n=18-20 per condition per time point, until day 14 where n=3 for males and n=10 for hermaphrodites) Data±s.e.m.

Thus these data show that on both plates in small groups and in individual liquid culture, the male intestine does not undergo atrophy during ageing. This is consistent with the biomass conversion hypothesis. Given the similarity between the results from the two culturing conditions, I opted to perform future experiments with males on plates at low population density.

4.2.5 Feminised males undergo intestinal atrophy

To test the biomass conversion hypothesis further, I decided to see whether turning on yolk production in the male intestine could induce intestinal atrophy. The MAB-3 transcription factor acts downstream of TRA-1, which controls many pathways involved in sex determination in *C. elegans* (Shen & Hodgkin 1988; Yi et al. 2000; Hodgkin 1987). *mab-3(-)* mutant males were identified in a screen for mutations that caused an impairment of male mating behaviour due to the defects in their tails (Hodgkin 1983). MAB-3 acts in the intestine of wild-type males to prevent transcription of the vitellogenin genes (Shen & Hodgkin 1988). Therefore *mab-3* mutant males have a feminized intestine, which produces yolk as indicated by the presence of yolk protein bands on protein gels and the appearance of yolky pools in the body cavity (Shen & Hodgkin 1988). MAB-3 appears to exert its effects in the male only, as *mab-3* mutant hermaphrodites appear normal (Shen & Hodgkin 1988). If the biomass conversion theory were true, it would be expected that *mab-3* mutant males would undergo intestinal atrophy.

I examined *mab-3(mu15)* males, which are maintained in a *him-5(e1490)* background to give a high incidence of males. I first tested whether *mab-3* males accumulate yolky pools during ageing, and this proved to be so (Figure 4.17). Yolky pools increased up until day 7 in *mab-3* males where they appeared to reach a threshold (Figure 4.14). Furthermore on day 7, *mab-3* males had significantly larger yolky pool levels than their hermaphrodite counterpart (day 7 $p<0.0001$ vs *mab-3* hermaphrodite, Student's *t* test). This may be because *mab-3* males do not produce oocytes, which would normally take up yolk from the body cavity, and reduce yolk accumulation. Immunofluorescent staining of yolk proteins also revealed that the yolk *mab-3* mutant males produce does not enter the gonad (Shen & Hodgkin 1988). As before, lipid pools did not accumulate in wild-type or *him-5* males (Figure 4.14). I also examined

another *mab-3* allele, *mab-3(e1240)* and, again, these males accumulated yolky pools in the body cavity (Figure 4.16A). These data provide further evidence the yolky pools are the result of vitellogenic run-on.

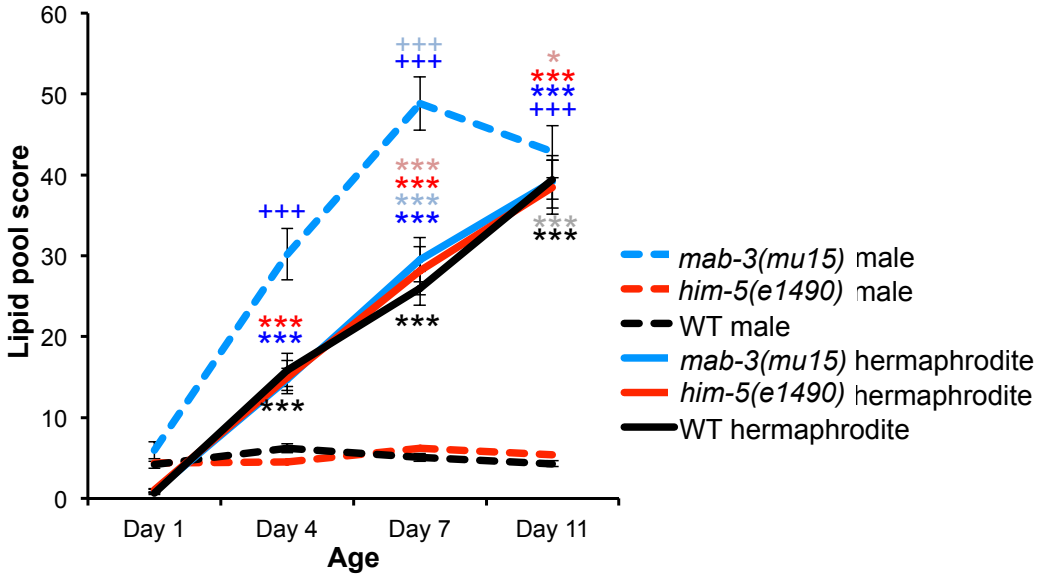

Figure 4.14. Lipid pool accumulation in feminized *mab-3(mu15)* males. Experiment was performed on plates. *mab-3(mu15)* males accumulate yolky pools during ageing at an even greater rate than hermaphrodites. Data±s.e.m. (n=20 per timepoint per condition) (+ for males, * for hermaphrodite. Colours match the line. Dark colours vs day 1, light colours vs previous day. Tukey HSD $p<0.05$ */+, $p<0.001$ ***/+++)

I next asked whether loss of MAB-3 activity could induce age-related intestinal atrophy in males. The intestine of *mab-3(mu15)* males was larger on day 1 than the intestine of wild-type males. This is consistent with feminisation of the intestine as the intestine of the wild-type hermaphrodite is greater in size relative to the wild-type male intestine. As before, the intestines of all the hermaphrodite strains underwent atrophy by day 7 (Figure 4.15A) and the intestine of wild-type males and *him-5* mutant males did not undergo atrophy (Figure 4.15A). However the *mab-3* mutant male intestine underwent continuous atrophy until day 7, like the hermaphrodites (Figure 4.15A, Figure 4.17). Furthermore, the intestinal atrophy was more severe, with *mab-3* males losing a greater percentage of their intestinal biomass than any of the hermaphrodite strains (Figure 4.15B). Similar atrophy was seen in the intestine of *mab-*

3(e1240) mutant males, where most atrophy occurred by day 4 (Figure 4.16B).

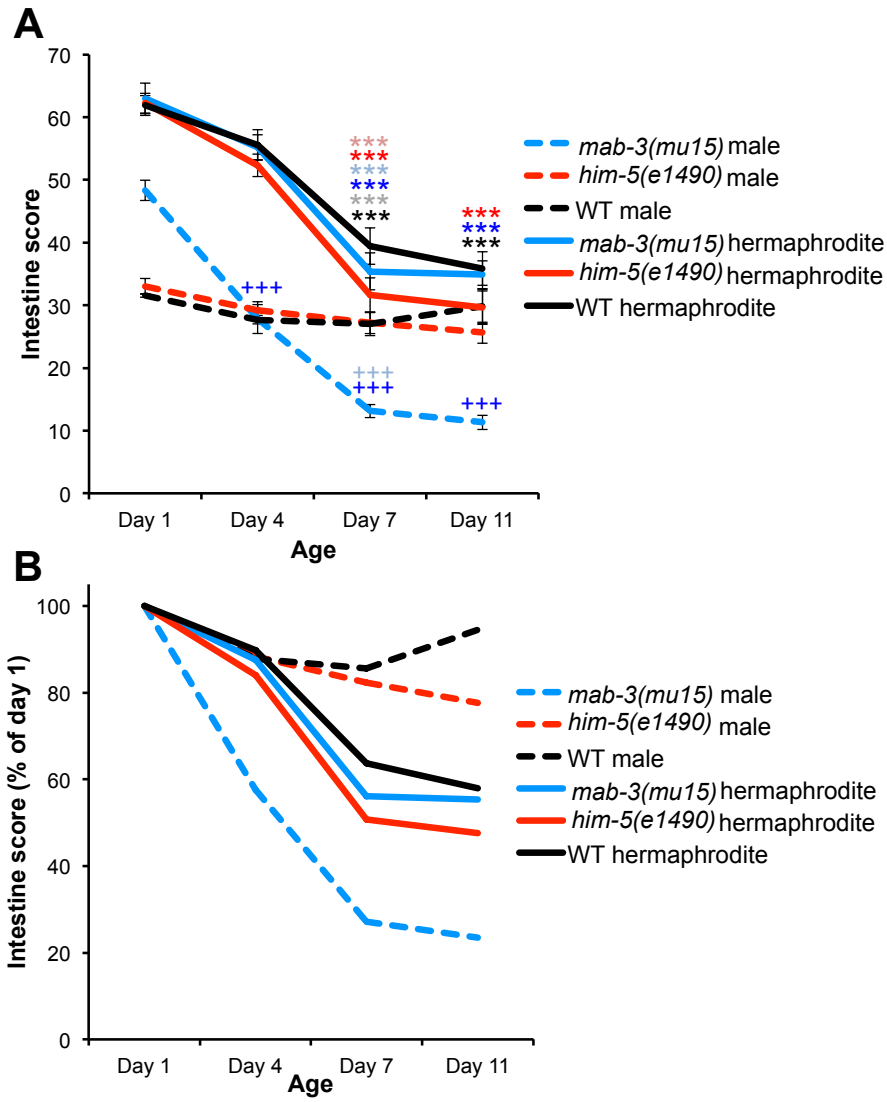

Figure 4.15. Intestinal atrophy in feminized *mab-3(mu15)* males. Experiment was performed on plates. **(A)** *mab-3(mu15)* males undergo intestinal atrophy during ageing. Data±s.e.m. (n=20 per timepoint per condition) (+ for males, * for herm. Colours match the line. Dark colours vs day 1, light colours vs previous day. Tukey HSD $p<0.001$ ***/+++). **(B)** *mab-3(mu15)* males undergo atrophy at a greater rate than hermaphrodites and lose a greater percentage of their original biomass.

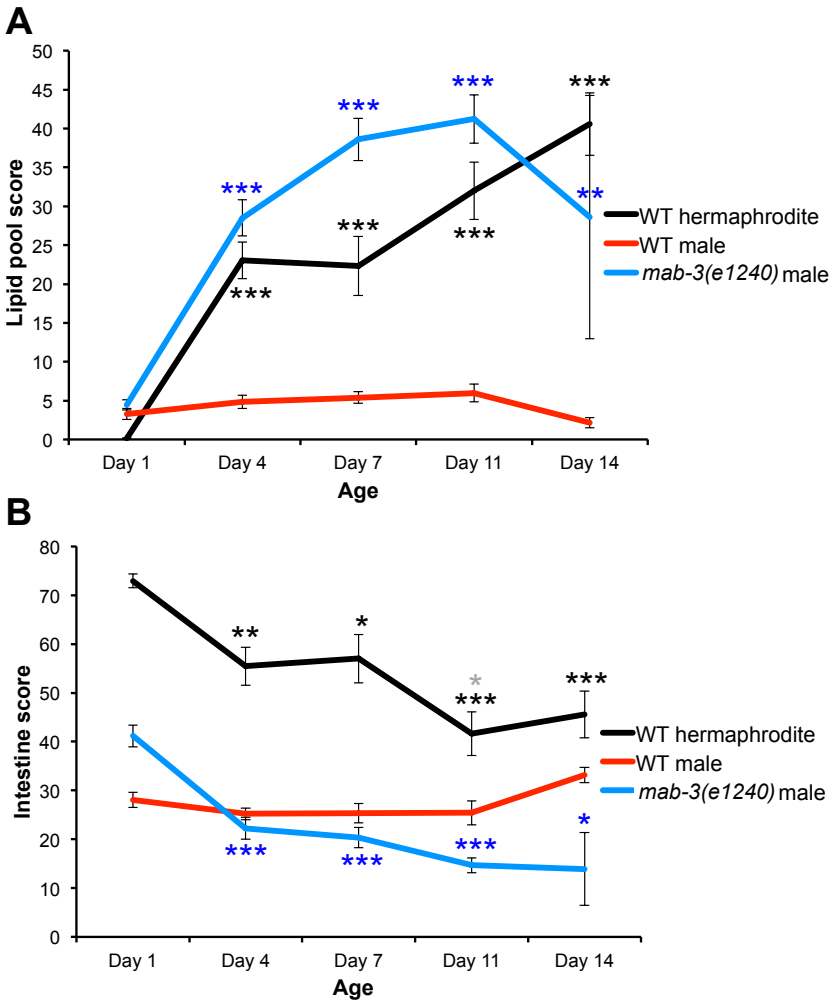

Figure 4.16. Lipid pool accumulation and intestinal atrophy in *mab-3(e1240)* males. (A) *mab-3(e1240)* males accumulate yolky pools during ageing. **(B)** *mab-3(e1240)* males undergo intestinal atrophy during ageing. Data±s.e.m. (n=8-11 per timepoint per condition, except on day 14 where WT hermaphrodite n=10, WT male n=3, *mab-3* male n=2) (Colours match the line. Dark colours vs day 1, light colours vs previous day. Tukey HSD $p<0.05$ *, $p<0.01$ **, $p<0.001$ ***).

These results provide further evidence to support the biomass conversion theory. It appears that induction of vitellogenin synthesis in the feminised male intestine results in intestinal atrophy because of the conversion of intestinal biomass into yolk. However it is also possible that the feminised intestine undergoes atrophy due to other mechanisms unrelated to yolk synthesis that do not usually occur in a wild-type male intestine. One such mechanism could be aberrant *E. coli* accumulation in the intestine.

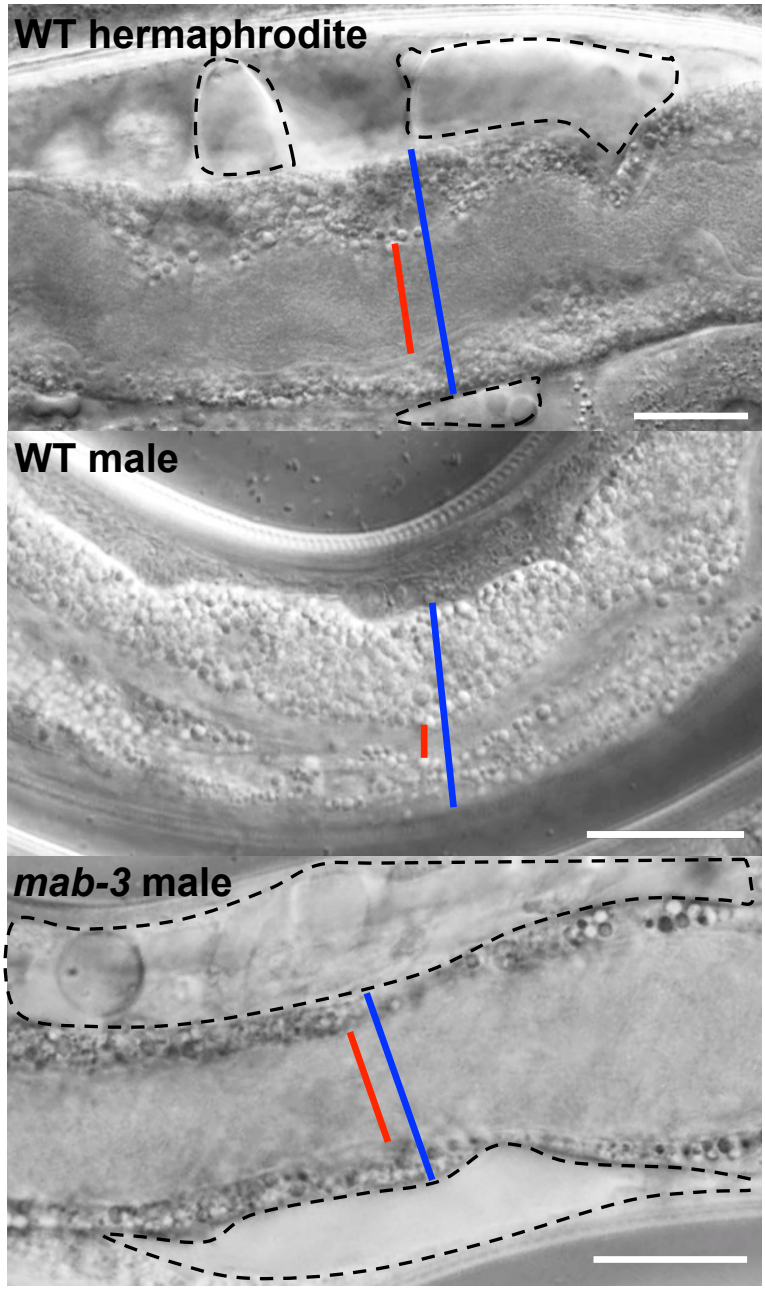

Figure 4.17. Intestinal atrophy and lumen dilation in *mab-3(e1240)* males. Images at x630 magnification of day 7 worms at 20°C. Intestinal width (blue), lumenal width (red) and yolky pools (black) are indicated. (Scale bar = 20μm).

4.2.6 Intestinal atrophy in feminised males is not due to proliferative *E. coli*

While examining the *mab-3* mutant males, I noticed the intestinal lumen became greatly distended and filled with bacteria during ageing (Figure 4.17). In fact, by day 11 the *mab-3(mu15)* male lumen score was significantly higher than all the other groups tested (two-way ANOVA, comparison of mutants $F(2,114)=19.30$, $p<0.0001$ and comparison of sex $F(1,114)=12.09$, $p=0.0007$. $p<0.0001$ for *mab-3* male vs each other group (Tukey HSD)) (Figure 4.18). Given that *E. coli* accumulation has been suggested to cause lumen dilation (putative constipation) (Garigan et al. 2002), I wondered whether abnormally profuse *E. coli* proliferation in the intestine of *mab-3* mutant males might contribute to the marked intestinal atrophy.

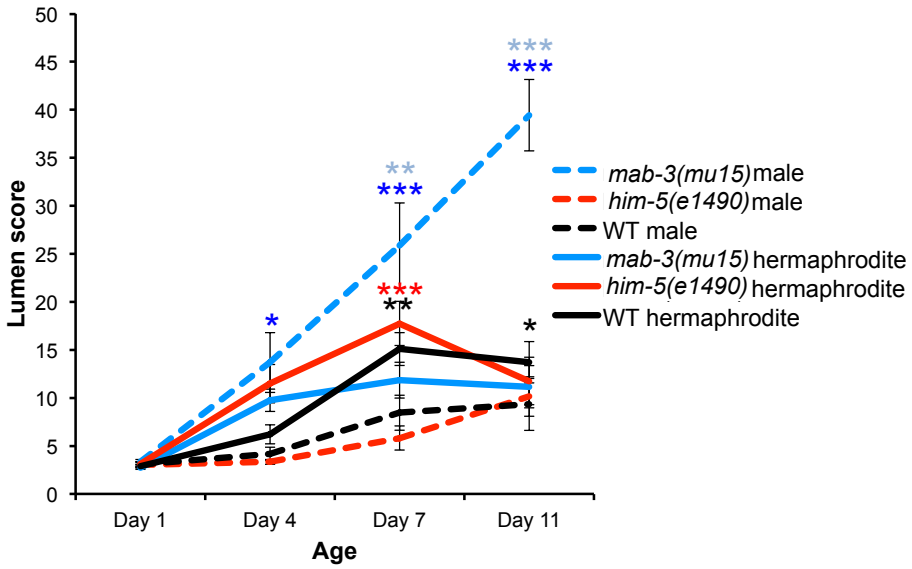

Figure 4.18. Lumen dilation in *mab-3(mu15)* males during ageing. The male *mab-3(mu15)* intestinal lumen undergoes a dramatic distension during ageing, that is significantly higher than all other strains by day 11 ($p<0.0001$ vs all strains). Data±s.e.m (n=20 per timepoint per condition) (Colours match the line. Dark colours vs day 1, light colours vs previous day. Tukey HSD $p<0.05$ *, $p<0.01$ **, $p<0.001$ ***).

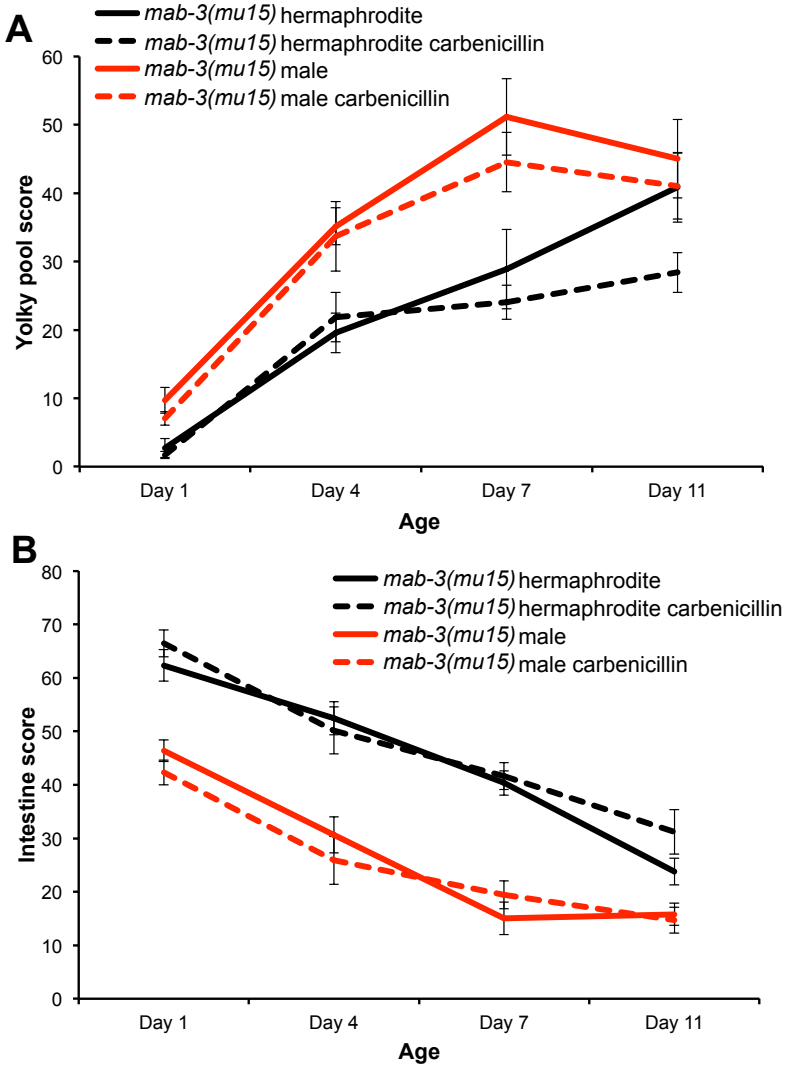

Figure 4.19. Yolky pool accumulation and intestinal atrophy is not affected by antibiotic treatment in *mab-3(mu15)* mutant males. (A) *mab-3(mu15)* mutant males accumulate yolky pools to the same extent on carbenicillin-treated bacteria. **(B)** Intestinal atrophy is unchanged in *mab-3(mu15)* mutant males that are grown on carbenicillin-treated bacteria. Data±s.e.m (n=10 per timepoint, per condition).

To block *E. coli* proliferation, bacterial plates were treated with carbenicillin as previously described (Garigan et al. 2002). Both *mab-3* males and hermaphrodites were then aged on these plates. Yolk accumulation still occurred in both males and hermaphrodites on antibiotic-treated plates (Two-way ANOVA, comparison for age in males $F(3,72)=34.34$, $p<0.0001$. Comparison for age in hermaphrodites $F(3,72)=31.00$, $p<0.0001$) (Figure 4.19A). However the extent of yolk accumulation was unchanged by antibiotic exposure (Two-way ANOVA, comparison for carbenicillin in males $F(1,72)=1.507$, $p=0.2235$.

Comparison for carbenicillin in hermaphrodites F(1,72)=2.633, p=0.1091). The intestine also underwent extensive intestinal atrophy on antibiotic-treated plates in both genders (Two-way ANOVA, comparison for age in males F(3,72)=42.05, p<0.0001. Comparison for age in hermaphrodites F(3,72)=49.67, p<0.0001) and, again, the degree of atrophy was unaffected by antibiotic treatment (Two-way ANOVA, comparison for carbenicillin in males F(1,72)=0.4545, p=0.5024. Comparison for carbenicillin in hermaphrodites F(1,72)=1.415, p=0.2381) (Figure 4.19B, Figure 4.20). Additionally lumen dilation was unaffected by antibiotic treatment (Two-way ANOVA, comparison for carbenicillin in males F(1,72)=0.026, p=0.8720. Comparison for carbenicillin in hermaphrodites F(1,72)=0.1078, p=0.7436). Thus, intestinal pathology in *mab-3* males appears to be independent of the presence of proliferating *E. coli* in the intestine and certainly not a consequence of constipation.

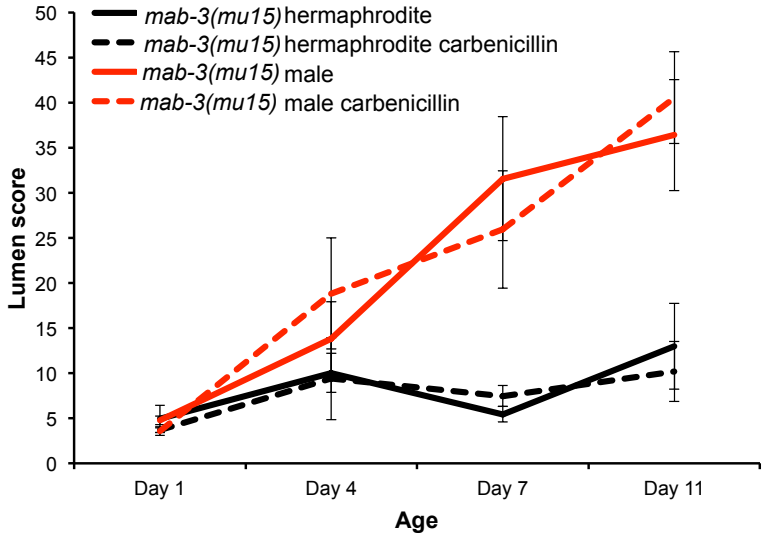

Figure 4.20. Antibiotic treatment does not prevent lumen dilation in *mab-3(mu15)* mutants males. Treatment with carbenicillin had no effect on lumen dilation in either *mab-3(mu15)* mutant males or hermaphrodites. Data±s.e.m (n=10 per time point, per condition).

4.2.7 Blocking yolk production does not reduce intestinal atrophy in feminised males

Does yolk production in *mab-3* males cause intestinal atrophy? To test this, I prevented yolk production by using RNAi against the *vit* genes, which produce the protein portion of yolk. Earlier work in our lab showed that double RNAi using *vit-5,6* RNAi completely blocked accumulation of all three yolk protein bands until at least day 11 of adulthood in wild-type hermaphrodites (Ezcurra et al. 2017, unpublished). Additionally *vit-5,6* RNAi from egg both reduced yolky pool accumulation and intestinal atrophy in hermaphrodites grown at 25°C (Ezcurra et al. 2017, unpublished). Therefore I set out to determine whether under those conditions, *vit-5,6* RNAi had a similar effect on *mab-3(mu15)* males.

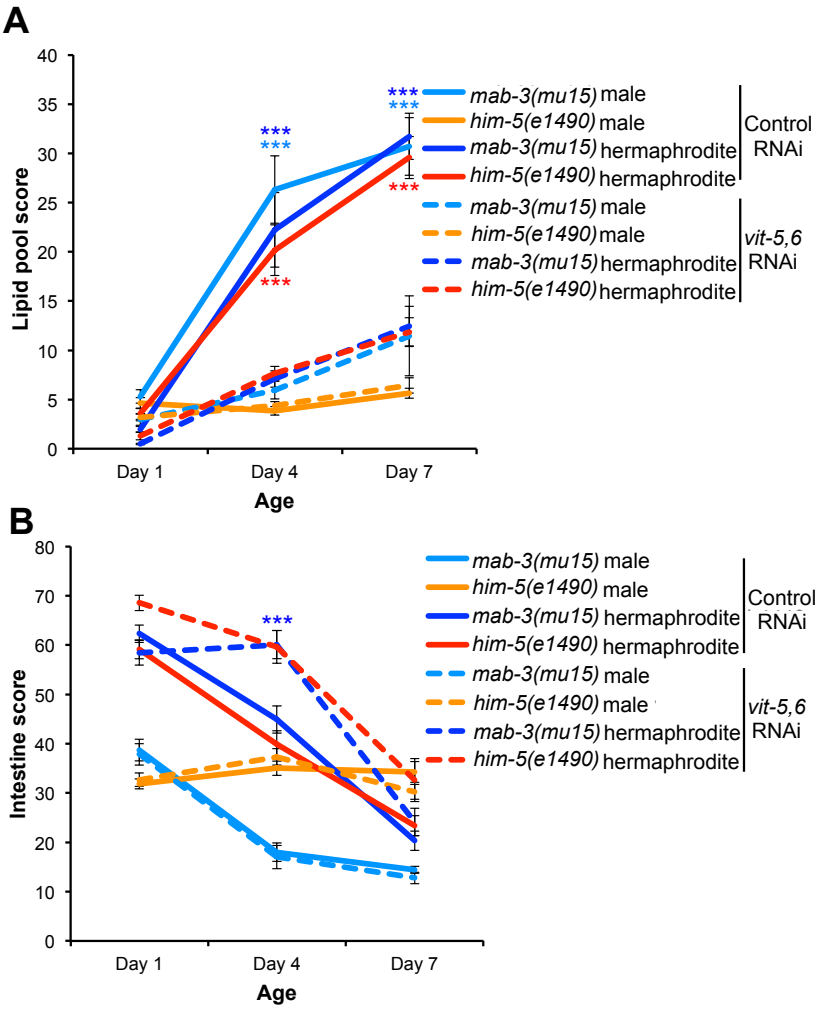

Figure 4.21. The effect of *vit-5,6* RNAi on yolk accumulation and intestinal atrophy in *mab-3(mu15)* males. Worms were exposed to RNAi from egg and grown at 25°C **(A)** *vit-5,6* RNAi reduces yolk accumulation in hermaphrodites and in *mab-3(mu15)* males **(B)** *vit-5,6* RNAi reduces intestinal atrophy in *mab-3* hermaphrodites but not in *mab-3(mu15)* males. Data±s.e.m (Colours match the line, vs *vit-5,6* RNAi at the same timepoint. Sidak's test $p<0.001$ ***. n=20 per time point per condition.).

I mixed together equal parts of each clone to create the *E. coli* HT115 culture used for *vit-5,6* RNAi. This was used to inoculated NGM plates that contained IPTG. Worms were then bleached to remove *E. coli* OP50 and to create a synchronised population. Bleached eggs were pipetted onto IPTG plates containing either the control or *vit-5,6* clones and allowed to grow until the L4 stage. Worms were then selected for experiments and grown at 25°C before being imaged on days 1, 4 and 7. As previously observed, *vit-5,6* RNAi greatly reduced yolky pool accumulation in hermaphrodites (Ezcurra et al., 2017, unpublished). It

also dramatically reduced the accumulation in *mab-3* males (Figure 4.21A) (See table A.7 for two-way ANOVA statistics). Thus *vit-5,6* RNAi had the expected impact on yolk accumulation. Intestinal atrophy was significantly reduced in day 4 *mab-3* hermaphrodites by *vit-5,6* RNAi. However, surprisingly it had no effect on intestinal atrophy in *mab-3* males (Figure 4.21B) (See table A.8 for two-way ANOVA statistics).

This result could argue against the biomass conversion theory by demonstrating that it is possible for yolk accumulation and intestinal atrophy to be uncoupled. However, another possibility is that while vitellogenesis is switched on in *mab-3* males, other mechanisms that regulate yolk production in hermaphrodites remain switched off. For example, in hermaphrodites presumably there are upstream mechanisms that regulate the breakdown of the intestinal biomass for yolk synthesis. If yolk production is turned off via RNAi, the hermaphrodites may be able to respond to this by generating a signal that results in the inhibition of the upstream biomass conversion mechanism. *mab-3* males may not have the ability to initiate this signal, thus when yolk production is reduced, catabolism of the intestine continues. Where the intestinal biomass goes in these males is unclear, but perhaps it is used to generate alternative proteins that, like yolk proteins, are ultimately exported from the intestine. In short: in *mab-3* males, intestinal biomass conversion and yolk production may not be as tightly coupled as in hermaphrodites. To block intestinal atrophy in these males, one would need to inhibit the upstream mechanism that directly causes the breakdown of the intestine biomass.

4.2.8 Autophagy promotes intestinal biomass conversion to yolk

A possible element of the upstream intestinal biomass conversion mechanism is autophagy, which involves the recycling of large quantities of cytoplasm. During autophagy, double-membrane structures called autophagosomes form, engulfing an area of cytoplasm. These then fuse to lysosomes, forming autophagolysosomes, within which enzymes break

down cytosolic components allowing them to be reused by the cell (Melendez & Levine 2009; Klionsky 2007). If autophagy facilitates intestinal biomass conversion to yolk, then blocking it should prevent intestinal atrophy. One way of inhibiting autophagy is to use *atg-13* RNAi. ATG-13 acts upstream during autophagy (Tian et al. 2009). To induce autophagy, ATG-13 is dephosphorylated causing it to be free to bind to ATG-1. This association allows ATG-1 to initiate autophagy (Reggiori et al. 2004).

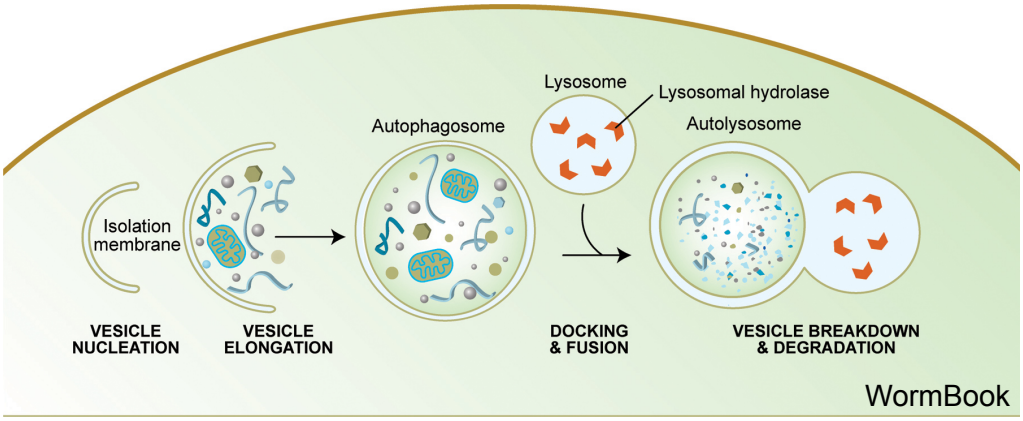

Figure 4.22. The process of autophagy. A double membrane vesicle called an autophagosome is formed, which encloses a variety of cytosolic components, including organelles. This then binds and fuses with a lysosome. The enzymes from the lysosome breakdown the cytosolic components, allowing them to be recycled within the cell. (image from (Melendez & Levine 2009)).

In wild-type hermaphrodites *atg-13* RNAi was able to reduce both yolk accumulation and intestinal atrophy (Ezcurra et al., 2017, unpublished). Moreover, adult and intestine specific *atg-13* RNAi was sufficient to induce this effect (Ezcurra et al., 2017, unpublished). Therefore its effect on these two pathologies in *mab-3(mu15)* males was tested by Alexandre Benedetto. He confirmed *atg-13* RNAi had a similar effect in these males, in that it reduced both yolk accumulation and intestinal atrophy (Ezcurra et al. 2017, unpublished). These results suggest that autophagy functions in the intestine to recycle intestinal biomass into other components, including yolk. Thus, autophagy promotes development of pathology in the ageing *C. elegans* intestine.

4.2.9 Later yolk production increases reproductive fitness

Under standard laboratory conditions continued yolk synthesis in ageing hermaphrodites appears to be a quasi-programme, as it seems to serve no function. However it is possible under certain conditions it could provide a benefit for reproductive fitness. Self-reproduction in hermaphrodites ceases around day 4 of adulthood due to sperm depletion. However mated hermaphrodites reproduce for much longer (Hughes et al. 2007), therefore in such animals continued yolk synthesis may enhance production of offspring. Possibly mating is relatively common in wild populations, where more stressful conditions might boost the number of males. Therefore mated hermaphrodites may sacrifice their own health by breaking down their intestine to fuel later reproductive output. In this way, *C. elegans* hermaphrodites could be viewed as undergoing reproductive death because they funnel all their resources into a short, highly productive period of reproduction before expiring. This is similar to other species such as the marsupial mouse *Antechinus stuartii*, which have a short, frantic mating period that results in the sudden death of the entire adult male population (Naylor et al. 2008).

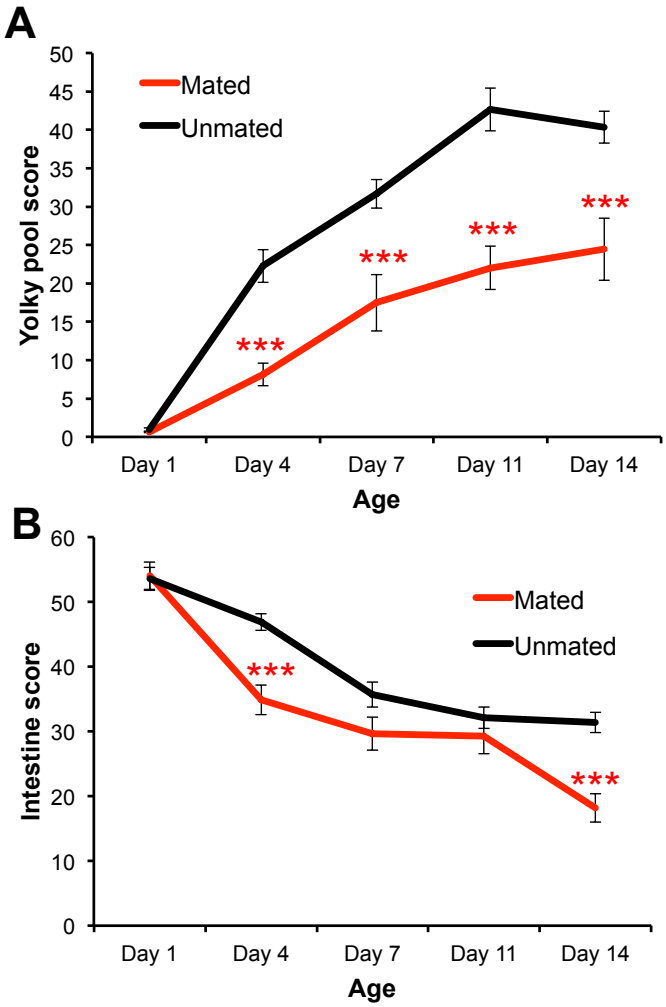

Figure 4.23. The effects of mating on yolk accumulation and intestinal atrophy in wild-type hermaphrodites. Worms were exposed to males from L4 stage to day 4 of adulthood at 20°C **(A)** Yolk accumulation is reduced by mating. **(B)** Intestinal atrophy is worsened by mating. Data±s.e.m. (n=20 per time point per condition) (vs unmated at same timepoint. Sidak's $p<0.001$ ***).

To prove this, I tested whether intestinal atrophy is enhanced in mated hermaphrodites. Mated hermaphrodites were generated as previously described in chapter 3.1 of this thesis. In brief, hermaphrodites were cultured with males between the L4 stage and day 4 of adulthood and then kept in hermaphrodite-only groups for the remainder of the experiment. As expected, given the extended egg-laying period, mating caused a significant reduction in yolk accumulation up until at least day 14, well beyond the last mating event (Figure 4.23A) (Two-way ANOVA comparison for mating $F(1,199)=71.49$, $p<0.0001$). This supports a

previous study that demonstrated mating caused hermaphrodites to lose approximately half of their total fat content (Shi & Murphy 2014). Interestingly, intestinal atrophy was exacerbated in mated hermaphrodites (Figure 4.23B) (Two-way ANOVA comparison for mating $F(1,199)=26.81$, $p<0.0001$). This could imply that the presence of males, or of mating triggers a signal in hermaphrodites that causes an upregulation of intestinal biomass conversion. A previous study showed functional sperm from males was required to induce shrinkage in mated hermaphrodites (Shi & Murphy 2014). While they did not look in detail at the condition of the internal organs, it is possible this phenomenon reflects an increase in biomass conversion and loss of yolk biomass through egg laying.

This all suggests that mating causes hermaphrodites to make more yolk to provide nutrients for a greater number of embryos, thereby improving reproductive fitness. However this seems to be to the detriment of hermaphrodite viability, as mated worms appear less healthy and have much shorter lifespans than their unmated counterparts (Gems & Riddle 1996; Shi & Murphy 2014). Whether this is solely due to increased intestinal atrophy or because of other detrimental effects from mating such as cuticle damage is unclear (Woodruff et al. 2014). Therefore further study into reproductive death in *C. elegans* is warranted.

4.3 Discussion

4.3.1 Autophagy-dependent biomass conversion causes intestinal atrophy

The intestine had been previously observed to undergo atrophy, with proliferation of bacteria within it suggested to cause constipation, which was hypothesised to be a major contributor to the development of this pathology (McGee et al. 2011; Garigan et al. 2002). However prior to this study, intestinal atrophy had not been studied quantitatively, nor had the role of proliferating bacteria in its development been formally tested. We confirmed intestinal atrophy does occur in worms, with the greatest loss in intestinal biomass occurring between days 3 and 7 (Figure 4.8) (Ezcurra et al., 2017, unpublished). However, although blocking bacterial proliferation did reduce intestinal atrophy to an extent, major atrophy still occurred (Figure 4.4). Therefore while proliferating bacteria likely contribute to intestinal atrophy, they appear not to be the main cause. Furthermore, as intestinal lumen dilation can occur in the absence of proliferating bacteria, it appears expansion of the lumen is not a consequence of constipation; rather bacteria simply fill the lumen as other age-related changes cause it to distend. Thus the previous hypothesis that bacterial constipation is the main driver of both intestinal atrophy and lumen expansion seems to be invalid.

I have presented evidence from work by myself and also from colleagues that run-on of yolk production results in intestinal atrophy in hermaphrodites. Yolk production continues well into old age (Ezcurra et al., 2017, unpublished), confirming as previously suggested that yolk production is not switched off once reproduction has ceased when it is no longer required (Herndon et al. 2002). Blocking yolk production using *vit-5,6* RNAi in hermaphrodites also reduced intestinal atrophy (Ezcurra et al., 2017, unpublished). In *C. elegans* fatty acids and protein can be

obtained from the bacterial food source. However the age decline in pharyngeal pumping rate implies that availability of food for yolk production declines with age (Huang et al. 2004; Chow et al. 2006). Therefore the worm intestine may have to start to perform *de novo* fatty acid synthesis and breakdown of intestinal proteins into the amino acids used to synthesise vitellogenins. However given that intestinal atrophy starts around day 3 when worms still pump relatively fast, one might assume that worms are still consuming an adequate food supply to fuel yolk production. One possibility is that yolk production occurs at such a high rate that worms can never consume enough food to support its synthesis. Therefore even from a young age, intestine biomass conversion must take place to optimise reproductive fitness.

Males, which do not make yolk, do not undergo intestinal atrophy (Figure 4.13A). However feminization of the male intestine resulted in yolk accumulating in the body cavity, at a higher rate even than in hermaphrodites (Figure 4.14). Perhaps this is due to males not producing oocytes to act as a yolk sink. Alternatively it could be due to yolk production in feminized males being completely uncontrolled as regulatory mechanisms that operate in hermaphrodites may not be switched on. This could result in the high levels of yolk accumulation I observed. The feminized male intestine also underwent extensive intestinal atrophy, losing a greater percentage of its biomass than the hermaphrodite intestine (Figure 4.15). While *vit-5,6* RNAi reduced yolk accumulation in feminized males, it did not reduce intestinal atrophy (Figure 4.21). This could be because there is a lack of coordination between intestinal biomass conversion and vitellogenin production in these males, perhaps due to the absence of regulatory mechanisms. By contrast, in the hermaphrodite these two processes appear coupled, such that if vitellogenin production is blocked, intestinal biomass conversion is also inhibited.

To perform biomass conversion, the *C. elegans* intestine must be able to breakdown and recycle cytosolic components to allow them to be reused

for yolk synthesis. This process seems to be performed by autophagy, which can break down various components of the cytosol, including proteins and organelles. In support of autophagy-dependent intestinal biomass conversion, inhibiting autophagy using *atg-13* RNAi reduced yolk accumulation and intestinal atrophy in both hermaphrodites and feminized males (Ezcurra et al, 2017, unpublished). This would mean during adulthood in *C. elegans*, intestinal autophagy is a promoter of senescent pathology. Autophagy has long been considered to be a beneficial process during ageing. The molecular damage accumulation theory of ageing suggests a build up of damaged molecules throughout life results in a loss of normal cellular function, eventually causing organ failure and subsequent death. Autophagy has been proposed to protect against this by breaking down damaged components of cells and releasing them to be reused (Gelino & Hansen 2012). If this were true, continued activity of autophagy should protect against age-related pathology and increase lifespan. Indeed some studies suggest that autophagy is required for the longevity in *daf-2* mutants (Hars et al. 2007; Meléndez et al. 2003), and in *eat-2* mutants (Hansen et al. 2008), which have a reduced pumping rate that may result in dietary restriction (see chapter 5) (Raizen et al. 1995). Further work showed that autophagy activity specifically in the *eat-2* intestine is required for the lifespan extension (Gelino et al. 2016). Compared to wild-type, *eat-2* mutants better maintain their intestinal barrier function during ageing and this was also dependent on intestinal autophagy activity (Gelino et al. 2016).

On the other hand, autophagy may be detrimental to health in certain conditions. For example, in mammals it could help to support the growth of advanced tumours by recycling cellular components where nutrients may have started to become limited (Shintani & Klionsky 2004; Kang & Avery 2008). Furthermore, in senescent cells autophagy promotes the senescence-associated secretory phenotype (SASP), which can promote cancer development (Narita et al. 2011). In *C. elegans gbp-2* mutants, which are sensitive to starvation, high levels of autophagy during

starvation resulted in deterioration of the pharyngeal muscle causing a decline in function (Kang et al. 2007).

The role of autophagy in wild-type *C. elegans* longevity and pathology development has previously been less clear. Inhibition of autophagy often caused a very minor or no reduction to wild-type lifespan (Hars et al. 2007; Gelino et al. 2016). Furthermore, one study found that inhibition of some autophagy genes via RNAi after worm development actually extended lifespan, suggesting autophagy during adulthood could be detrimental (Hashimoto et al. 2009). Our group also showed that *atg-13* RNAi extends lifespan consistently at 25°C, but not at 20°C (Ezcurra et al., 2017, unpublished). A possible explanation for this is that while autophagy promotes the progression of some pathologies, it inhibits the development of others. Therefore the effect on lifespan of reducing autophagy will depend on which pathologies are life limiting and this could vary in different wild-type backgrounds or under different conditions. Nevertheless I have presented evidence that during adulthood, autophagy in the wild-type *C. elegans* intestine promotes biomass conversion into yolk. This results in the development of two age-related pathologies: yolk accumulation and intestinal atrophy.

4.3.2 Intestinal atrophy as a life-limiting pathology in *C. elegans*

A question that remains is whether intestinal atrophy actually limits life in *C. elegans*. The intestine accounts for approximately one third of the somatic mass and performs multiple functions beyond just nutrient absorption (McGhee 2007). It also acts as an essential barrier against the external environment, including potentially harmful pathogens. Therefore one would assume extensive atrophy of the intestine during ageing could conceivably be lethal.

There is now a sizeable amount of evidence that suggests the aged intestine is indeed the site of life-limiting pathology. RNAi of the *vit* genes,

which reduced intestinal atrophy, also extended lifespan (Murphy et al. 2003; Ezcurra et al., 2017, unpublished). Intestinal atrophy is also reduced in *daf-2* mutants, which have a greatly extended lifespan (Ezcurra et al., 2017, unpublished). Furthermore, restoring *daf-16* activity specifically in the intestine of *daf-16;daf-2* double mutants increased lifespan and to a greater extent than when *daf-16* expression was re-established in the neurons or muscle (Libina et al. 2003). SKN-1, another transcription factor required for longevity in *daf-2* mutants, translocates to the nuclei of the intestinal cells in *daf-2* mutants to activate transcription (Tullet et al. 2008). Perhaps most convincingly, the level of intestinal atrophy on day 7 can be used to forecast the eventual lifespan of an individual worm (Ezcurra et al., 2017, unpublished). Moreover, progressive necrosis along the intestine, often initiated from the most anterior intestinal cells, occurs concurrently with organismal death in *C. elegans* (Coburn et al. 2013). Together these results imply the maintenance of the intestine during ageing is essential for continued viability. We propose that autophagy-dependent intestinal biomass conversion to yolk causes intestinal atrophy, a senescent pathology that is life limiting in *C. elegans*.

However while *atg-13* RNAi reduced intestinal biomass conversion, it only extended lifespan at 25°C; no consistent longevity effect was seen at 20°C by our group. This is despite it preventing intestinal atrophy at both temperatures (Ezcurra et al., 2017, unpublished). As previously suggested, this implies that the pathologies that limit life vary under different conditions. For example, at 25°C, autophagy-dependent intestinal biomass conversion causes intestinal atrophy that is the primary cause of death. At 20°C, this biomass conversion still occurs, but another pathology could reach a lethal threshold first. As in humans, it seems that there are multiple causes of death in *C. elegans* (Figure 4.24).

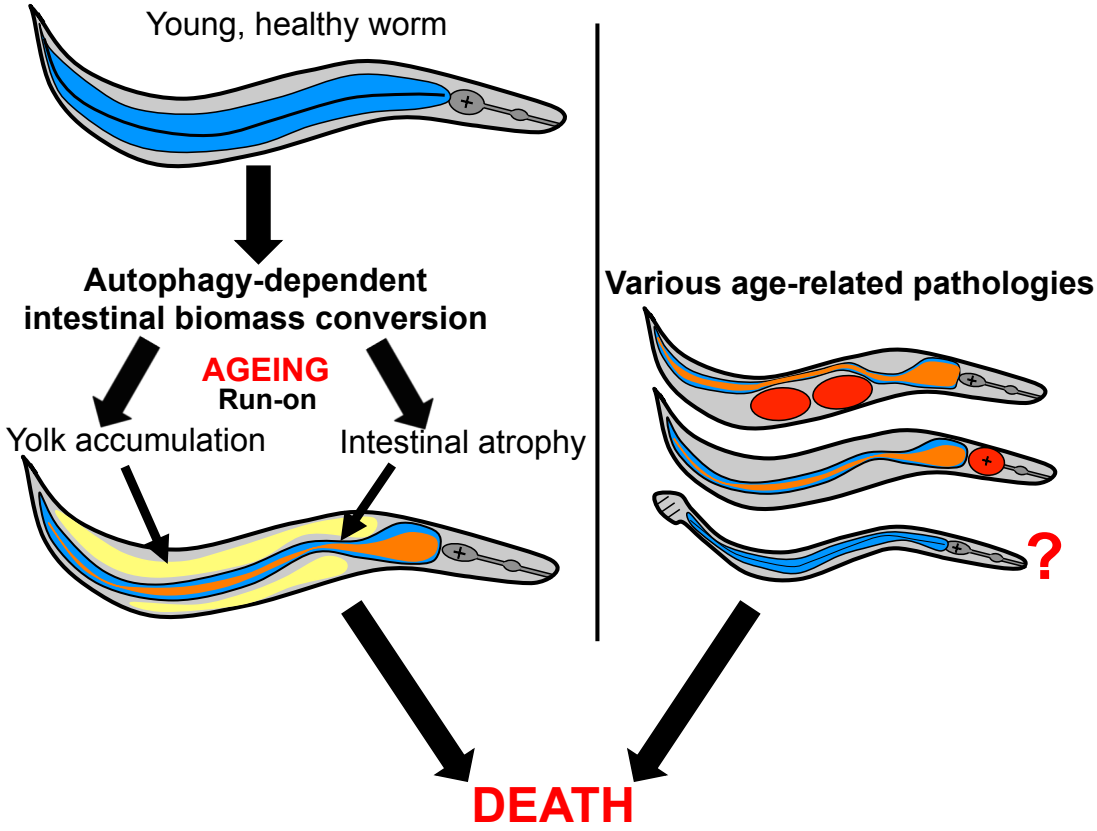

Figure 4.24. Intestinal atrophy as a cause of death in ageing *C. elegans*. Autophagy-dependent intestinal biomass conversion results in the generation of two age-related pathologies, yolk accumulation and intestinal atrophy. We propose that intestinal atrophy is a life limiting pathology. However presumably other pathologies can also limit lifespan depending on the conditions. For example, bacterial infection of the uterine tumours or of the pharynx could both potentially be lethal pathologies (Zhao et al., 2017). Additionally, we currently do not know what age-related pathology could be causing death in males.

Chapter 5 Pharyngeal infection is a life-limiting pathology in ageing *C. elegans*

5.1 Introduction to the *C. elegans* pharynx

In addition to the intestine, another part of the alimentary canal shows both a decline in function and extensive tissue degeneration during ageing: the pharynx (Herndon et al. 2002; Garigan et al. 2002; Chow et al. 2006; Huang et al. 2004). The pharynx is primarily made up of muscle, though also contains other cell types including marginal cells, which provide structural strength, and gland cells, which secrete digestive enzymes into the pharyngeal lumen through long cellular protrusions (Altun & Hall 2009b) (Figure 1.6). In response to food, serotonin is released, which stimulates the pharyngeal muscle to pump continuously in the young adult. This action draws bacteria from the environment into the posterior bulb of the pharynx, where the grinder is (Horvitz et al. 1982) (Figure 5.1). Muscular contractions push the 'teeth' of the grinder against one another to cause complete maceration of the bacteria before it enters the intestine. In this way, when the pharynx operates correctly, it prevents intact and potentially pathogenic bacteria from entering the worm and also ensures that there is a continuous supply of fresh nutrients.

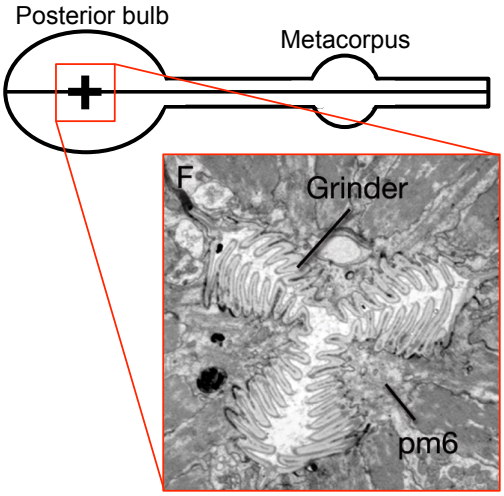

Figure 5.1. The grinder of the *C. elegans* pharynx. The posterior bulb of the pharynx contains the grinder. The grinder 'teeth' engage with one another to completely macerate bacteria in the lumen. pm6, pharyngeal muscle segment 6. (TEM image from (Altun & Hall 2009b)).

5.1.1 Age-related functional decline and tissue degeneration in the pharynx

Studies have shown that there is age-related tissue degeneration of the pharynx (Herndon et al. 2002; Garigan et al. 2002), particularly in the muscle (Chow et al. 2006). Initial studies noted that during ageing the structure of the pharynx becomes more irregular. The posterior bulb seems to be particularly affected and loses its even, circular shape (Herndon et al. 2002; Garigan et al. 2002). The internal structures also became harder to distinguish, with the muscle fibres appearing to vanish (Herndon et al. 2002). Furthermore bacteria were seen to accumulate in the pharyngeal lumen, much like it does in the ageing intestine (Garigan et al. 2002). TEM revealed that bacteria were also capable of invading the pharyngeal tissue of aged worms (McGee et al. 2011). This suggests bacteria may contribute towards pharyngeal decline. The pharyngeal muscle also appears to undergo sarcopenia, like human muscle, during ageing (Chow et al. 2006). This could be driven by the high pumping rate in young adulthood because *eat-2* mutants, which have a lower pharyngeal pumping rate throughout life (Raizen et al. 1995), had a slower rate of pharyngeal muscle deterioration (Chow et al. 2006). The

authors propose several mechanisms by which high pumping rate in early life could cause decay of the pharynx (Chow et al. 2006). They suggest pharyngeal pumping may deteriorate muscle that has already been weakened by other age-related processes. Alternatively, a high pumping rate would presumably require high levels of respiration. This would generate large amounts of ROS that could damage cellular components. Finally they propose high levels of activity could also cause mechanical damage to the pharynx.

An advantage of studying age-related decline in the pharynx is that pharyngeal contractions or pumps are reasonably easy to count, even at a low magnification. Therefore pumping rate can give a convenient read out of pharyngeal function during ageing. The pharynx pumps at a fairly constant and fast rate in young animals, with pumping rate peaking on day 2 of adulthood (Huang et al. 2004). From day 3 onwards the pumping rate declines dramatically and virtually ceases by day 9 (Huang et al. 2004). Intriguingly, worms that maintained a higher pumping rate for longer, typically also lived longer as well. Thus mid-life pumping rate is a predictor of lifespan (Huang et al. 2004). Antibiotic treatment reduced the age-related decline in pharyngeal pumping rate, but did not completely prevent it (Chow et al. 2006), suggesting that bacteria contribute to impairment of pharyngeal function. Notably, the pumping rate exhibited may not reflect the full functional capacity of the pharynx. Between days 2 – 12, serotonin exposure in the absence of food could noticeably increase pumping rate compared to untreated worms feeding on a bacterial lawn (Chow et al. 2006). This implies other factors that could be independent of tissue degeneration, such as a decline in endogenous levels of serotonin, may contribute to the decline in pumping rate.

Overall these data raise the possibility that the ageing pharynx harbours a life-limiting pathology that also results in a decline in function as it develops. A high pumping rate in early adulthood may be essential for robust growth and reproductive fitness. The caveat is this may cause the pharynx to deteriorate and become virtually inoperative in later life (Chow

et al. 2006). Given the relationship between pharyngeal function and lifespan (Huang et al. 2004), and the fact the pharynx undergoes noticeable age-related degeneration (Herndon et al. 2002; Garigan et al. 2002; Chow et al. 2006), high pumping rate in young adults could lead to the development of a life limiting pathology in ageing *C. elegans*. This suggests the existence of a trade off between the early life benefits of high pumping rate, and resulting late life pathology. By this view the effects of wild-type alleles, such as that of *eat-2*, exemplify antagonistic pleiotropy.

5.1.2 Studying age-related pharyngeal pathology

Previous studies of pharyngeal pathology have used either Nomarski microscopy or electron microscopy (Chow et al. 2006; Herndon et al. 2002; Garigan et al. 2002; McGee et al. 2011). To determine the level of tissue degeneration, qualitative scoring has also been used (Chow et al. 2006; Garigan et al. 2002), similar to the classification systems we used previously to study uterine tumours and gonad atrophy (Riesen et al. 2014; de la Guardia et al. 2016). Marina Ezcurra developed a more detailed pharyngeal pathology scoring system, inspired by the previous work, where the pharynx was rated from class 1 – 5 depending on the level of degeneration (Ezcurra et al., unpublished) (Figure 5.2).

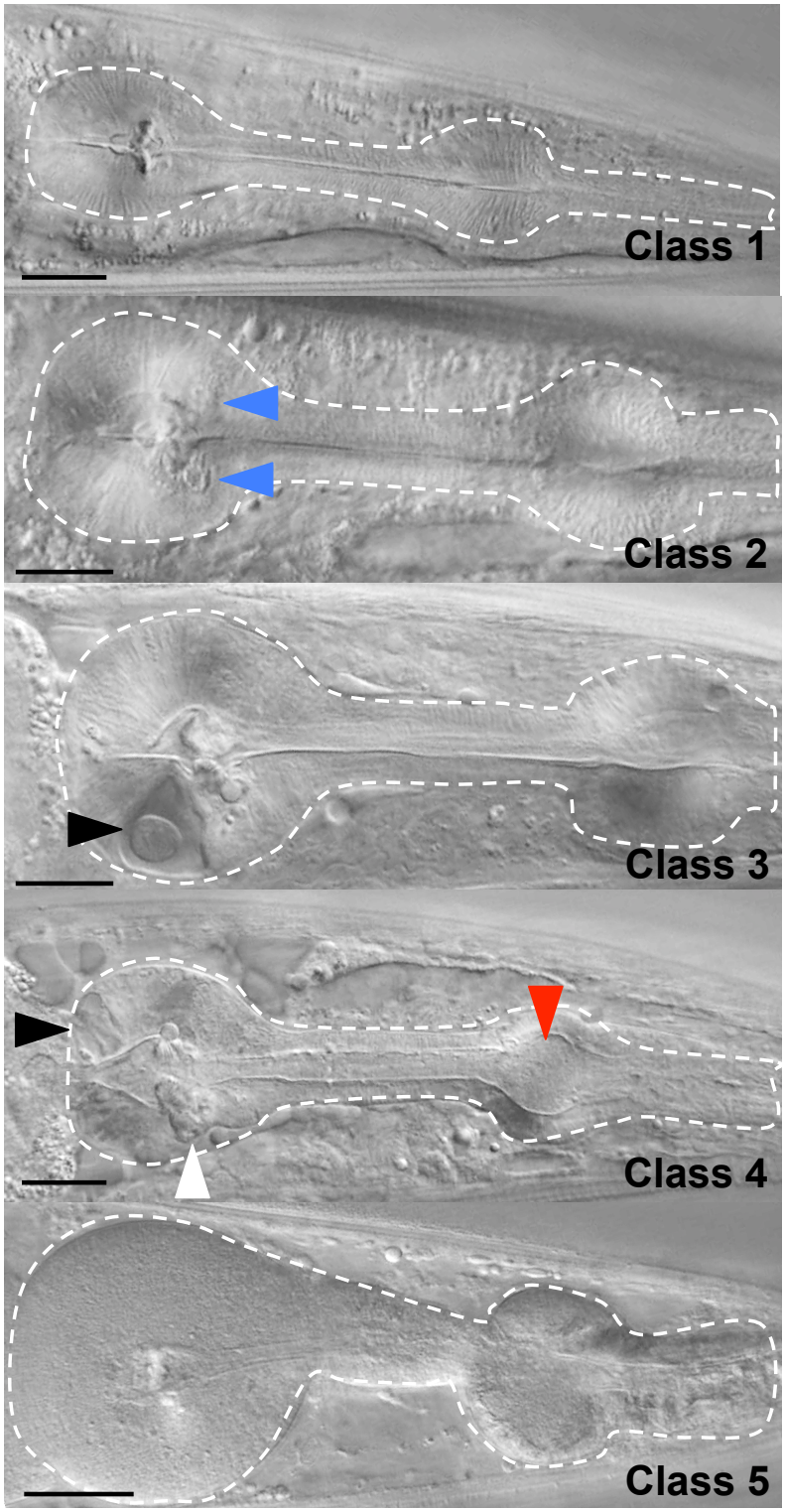

Figure 5.2. The pharynx pathology scoring system. All pharynxes are outlined in white. Class 1 is a young, healthy pharynx. Class 2 shows early stages of deterioration, such as small, dense inclusions (blue arrows), small blister-liked vacuoles or fading muscle striations. Class 3 pharynxes have one of the following major age-related traits: bacteria accumulated in the lumen (red arrow); muscle striations no longer visible; large blisters (black arrows) or dense inclusions (white arrow). Class 4 pharynxes possess two or more of these age-related traits. Class 5 pharynxes have deteriorated to such an extent that structures within the posterior bulb of the pharynx can no longer be identified (Scale bars = 20μm).

In humans, when the cause of death is unclear, one option is to perform an autopsy. This involves dissection and the careful examination of the internal organs to determine the likely cause of death. Yuan Zhao implemented this idea in worms and performed necropsies on them. This involved the examination of worms that had died from old age using Nomarski microscopy. Conveniently, as worms are transparent, there is no need to dissect them to examine the internal organs. The majority of corpses retained a surprisingly high degree of structural integrity, with different tissue types still easily distinguishable. Initial observations suggested that there is a difference between worms that died at a relatively young age (between days 8 – 14) and those that died at older ages (day 15 onwards). Young corpses showed a highly degenerated pharynx with a morbidly swollen posterior bulb. Older corpses did not display this pathology; instead the pharynx appeared to have undergone age-related atrophy (Figure 5.3). These initial findings suggested the interesting possibility that there are at least two distinct causes of death in *C. elegans*, with earlier deaths being caused by pharyngeal pathology. Using both the qualitative scoring and necropsy methodology, I set out to investigate this possibility, since a key objective of my PhD work was to identify pathologies of ageing that cause death in *C. elegans*.

This study has been a truly cooperative exploration and I would like to thank Yuan Zhao, Marina Ezcurra, Matthias Ziehm, Hongyuan Wang, Mark Turmaine and Chenhao Yang for contributing work to this chapter. When others have conducted work or data was gathered in collaboration, it will be indicated as such (as in Figures 5.5, 5.6C, 5.7, 5.8A, 5.9, 5.10A,B, 5.15 5.20, 5.22A). I would also like to extend a special thank you to Yuan Zhao who I have worked with jointly on this project. She has not only contributed work to this chapter but has also helped extensively with discussions and ideas. She and I are joint first authors on a recent publication (Zhao et al. 2017), which includes much of the work presented in this chapter.

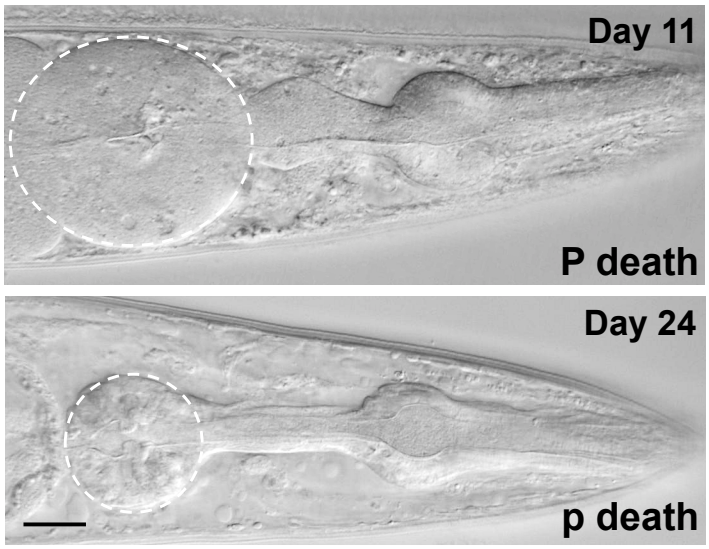

Figure 5.3. Pharyngeal pathology in *C. elegans* corpses. Early deaths in *C. elegans* are associated with swollen pharynxes ('big P death'), while later deaths are associated with smaller pharynxes ('small p death'). (Scale bar = 20μm). (Observation by Yuan Zhao, images from Ann Gilliat.)

5.2 Results

5.2.1 Pharyngeal pathology increases with age and correlates with lifespan

First I decided to examine the dynamics of pharyngeal pathology in an ageing *C. elegans* population by quantifying tissue degeneration and measuring changes to pharyngeal size. A group of worms were removed from the population and their pharynxes imaged at regular time points from day 1 onwards. The cross-sectional area of the posterior bulb of the pharynx (henceforth pharynx size) was measured and then each pharynx was given a qualitative score based on the degree of tissue deterioration. The pharynx pathology score increased during ageing, consistent with prior work (Figure 5.4A) (Chow et al. 2006; Garigan et al. 2002). The largest increase occurred between days 4 and 7, after which no further significant increase was observed (Figure 5.4A). This suggests that the majority of pharyngeal deterioration occurs within this small timeframe, relatively early in life. The pharyngeal size also increased steadily during ageing and was observed to have grown significantly by day 9 (Figure 5.4B). Presumably, a proportion of this size increase is due to normal

development, as worm body length continues to increase up until day 4 (Shi & Murphy 2014). However a fraction of the increase could be due to the aberrant pharyngeal swelling observed by Y. Zhao in worms that expired early in survival assays.

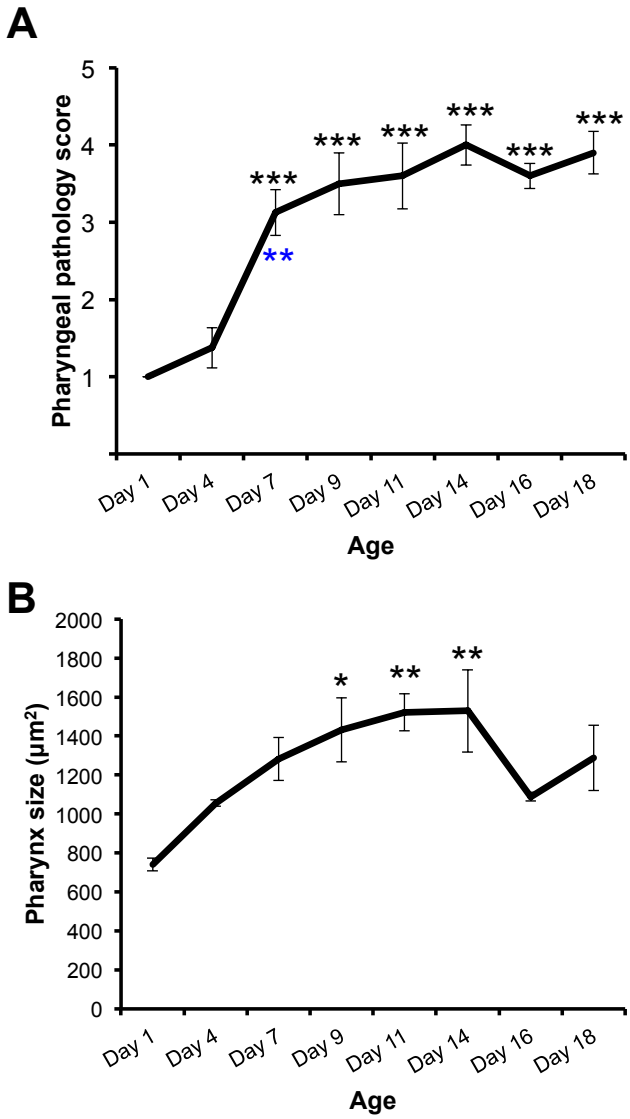

Figure 5.4. Age-related changes to the *C. elegans* pharynx in wild-type hermaphrodites. (A) The pharyngeal pathology score increases significantly during ageing, indicating deterioration of the pharynx. Data mean±s.e.m. (Black vs day 1, blue vs previous day; $p<0.004$ **, $p<0.001$ *** Wilcoxon-Mann-Whitney test. To adjust for multiple comparisons, $p<0.004$ was considered to be significant.) **(B)** The cross-sectional area of the posterior pharyngeal bulb also increases significantly during ageing. Data mean±s.e.m. (Black vs day 1; $p<0.05$ *, $p<0.01$ ** Tukey HSD test). (For both **A** and **B** days 1-9 n=8, days 11-18 n=10)

To determine what pathologies may be life limiting in *C. elegans*, M. Ezcurra monitored a number of pathologies, including pharyngeal deterioration, in individually cultured worms. Worms were removed from their plates and carefully placed on microscopy slides. Using low light conditions, worms were imaged on a cooled microscopy stage, which reduced worm movement. Once imaging was completed, worms were returned to their plates (Figure 5.5A). This was repeated at several time points, up until day 18. The lifespan of each worm was recorded and then compared to its pathology state earlier in life. Importantly, continuous imaging using this technique did not affect lifespan (Figure 5.5B). M. Ezcurra found that, out of all the pathologies tested, only two correlated with lifespan at more than one of the timepoints examined (Table 5.1). One was intestinal atrophy, which showed correlations with lifespan on days 4 and 11. This was unsurprising given the results from chapter 4. The other was pharyngeal deterioration, which showed correlations with lifespan on days 7 and 11 (Figure 5.5C,D). This demonstrates that the level of pharyngeal function and tissue deterioration in mid-life can be a predictor of lifespan (Huang et al. 2004). This provides further evidence that the pharynx could be harbouring a lethal age-related pathology.

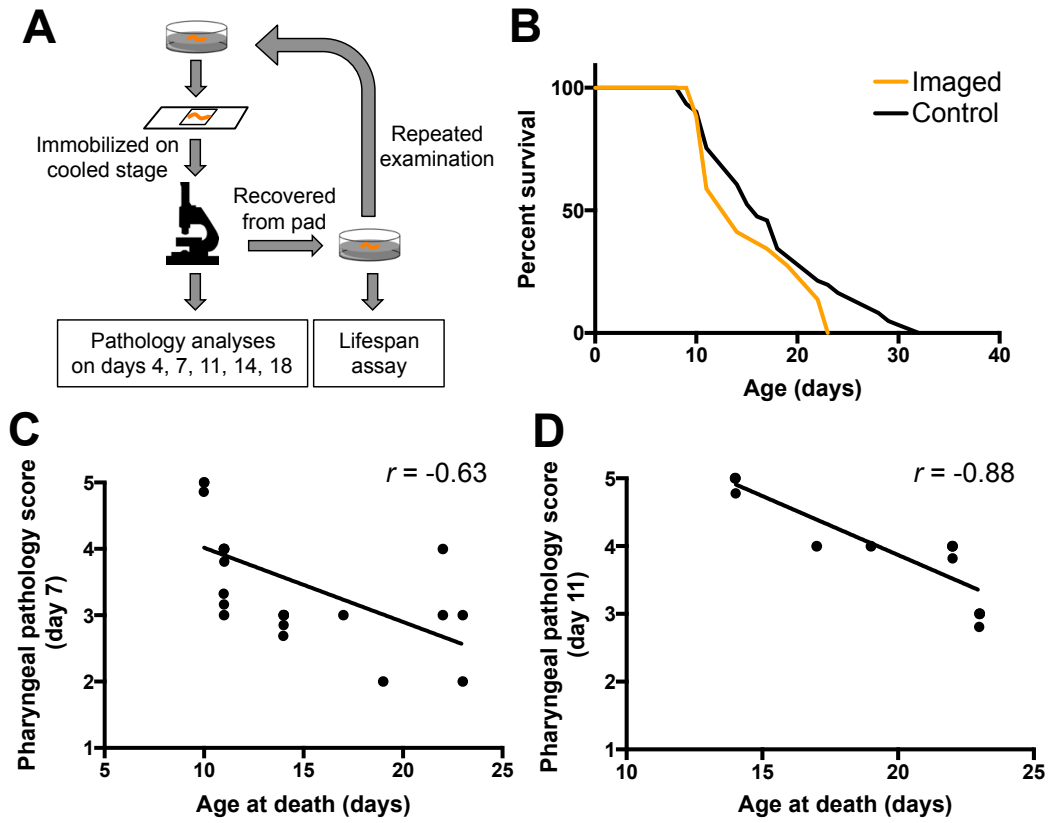

Figure 5.5. Tracking development of age-related pathologies in individual worms. **(A)** Worms were kept on individual plates and repeatedly imaged, on a slide, under a microscope at various time points. After imaging, worms were recovered to allow for a survival assay to be performed. **(B)** This imaging protocol did not affect life span (p=0.16, log rank, control vs imaged. Imaged n=16, control n=61). **(C**) On day 7, a significant correlation was seen between life span and pharyngeal pathology (n=16). **(D)** On day 11, a significant correlation was seen between life span and pharyngeal pathology (n=8). (Method in **A** developed by Marina Ezcurra (Ezcurra et al., 2017, unpublished). Data in **B,C** and **D** collected by Marina Ezcurra).

	Day 4		Day 7		Day 11		Day 14	
	R square	*p* value	R square	*p* value	R square	*p* value	R square	*p* value
Pharyngeal deterioration	0.0019	0.8723	0.3963	0.0090	0.7826	0.0035	0.2667	0.2943
Gonadal atrophy	0.0108	0.7130	0.4122	0.0099	0.3706	0.1468	0.1938	0.5598
Intestinal atrophy	0.4443	0.0067	0.0013	0.9003	0.5584	0.0331	0.4396	0.2226
Yolk pool accumulation	0.1781	0.1171	0.2411	0.0631	0.3031	0.2003	0.1003	0.6035
Uterine tumor size	0.1837	0.0977	0.5185	0.0017	0.0014	0.9298	0.0741	0.6578

Table 5.1. Correlations between life span and pathology severity. Data was collected as described in **Figure 5.5**A and significant correlations (green) were sought using linear regression. (Day 4 n=16, day 7 n=16, day 11 n=8, day 14 n=4) (Data collected by Marina Ezcurra and analysed by Yuan Zhao).

5.2.2 Early deaths are associated with pharyngeal swelling

We decided to determine whether pharyngeal swelling was in fact closely associated with early mortality in *C. elegans*. A necropsy analysis was performed on a large population (n=585), where corpses from worms that had died during survival assays were imaged using Nomarski microscopy and their pharynxes measured. To establish a value beyond which a pharynx can be defined as swollen, we measured the size of pharynxes from healthy day 7 and 10 animals and calculated the mean area. Healthy animals were defined as being class A, which are fast moving worms or worms that move quickly when prodded with a worm pick. We then added one S.D. to the mean area of these pharynxes, giving us a value of 1833μm^2. Any pharynxes with an area larger than this were defined as swollen. One S.D. below this mean is 1480μm^2 and pharynxes below this value were defined as atrophied.

The necropsy profile revealed that 38% of worms died with swollen pharynxes (Figure 5.6A). The bulk of these worms also died prior to day 15. The rest of the population died with pharynxes that appeared to have undergone atrophy. Therefore *C. elegans* possesses at least two clear categories of death, in terms of pharyngeal pathology. We decided to name deaths with a swollen pharynx as P deaths (‘big’ P death) and those with an atrophied pharynx as p deaths (‘small’ p death). In regards to lifespan, as anticipated worms that underwent P death died decidedly earlier (median lifespan = 11 days) than those that experienced p death (median lifespan = 21 days) (Figure 5.6B).

To analyse the development of pharyngeal pathology in P and p death during life, Y. Zhao monitored pharyngeal size in individual worms until death. Worms were imaged at x200 magnification on plates, which were cooled on ice prior to imaging to inhibit movement. This revealed pharyngeal swelling did occur before death, which meant that the swelling

was not caused by the decomposition of the corpses. Furthermore the swelling only started to occur a few days before death, before plateauing a day or so prior to the death of the worm (Figure 5.6C). This is emphasised by an anomalous worm, which underwent P death much later in life on day 33, yet swelling only started to happen after day 28 (Figure 5.6C). On the other hand, the pharynxes of worms that underwent p death start to atrophy after day 10 and then continuously decreased in size until death. Together these results show that early mortality is closely connected to a potentially lethal, pharyngeal pathology in *C. elegans*.

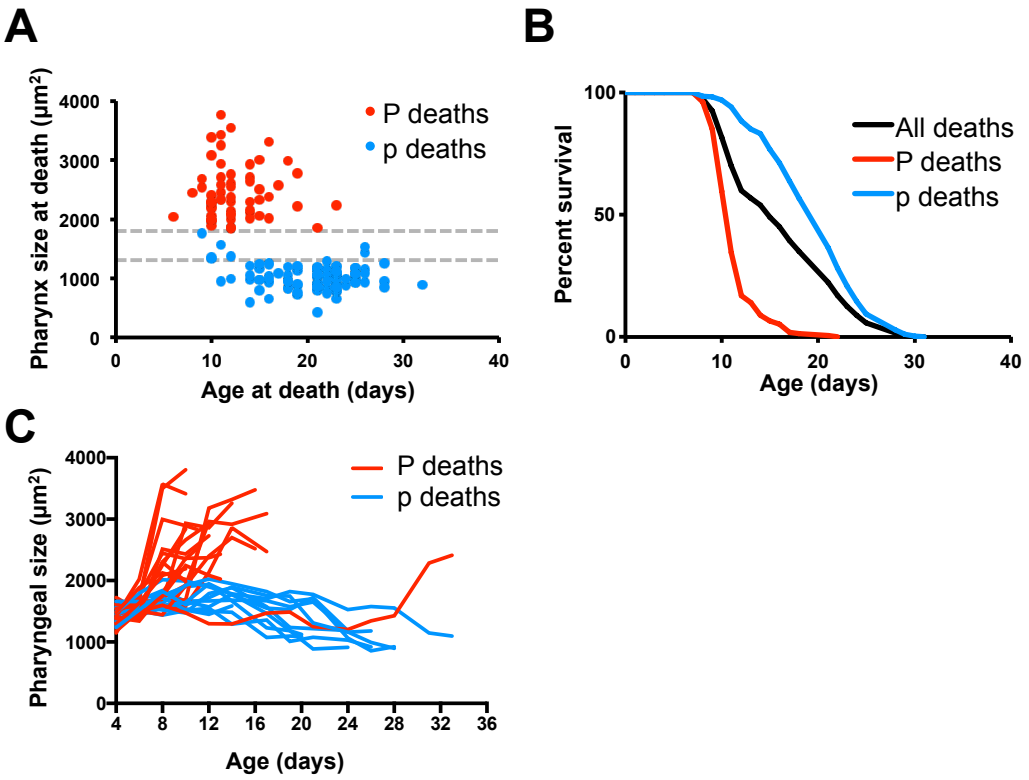

Figure 5.6. Early death in *C. elegans* is associated with pharyngeal swelling and reduced lifespan (P death). (A) The majority of P deaths occurred before day 15 and were associated with a large pharynx size, whereas p deaths were associated with a smaller pharynx size. For comparison the size range of a healthy pharynx is indicated (grey dotted lines represent the mean area of healthy day 7 and 10 pharynxes ± S.D.). (n=157) **(B)** P deaths have a much lower lifespan than p deaths with median lifespans of 11 days and 21 days respectively (n=585). **(C)** Pharyngeal swelling in P deaths happened only just before death. In p deaths, the pharynx size continued to decrease up until death (n=29). (Data in **C** collected by Yuan Zhao).

5.2.3 Two forms of death explain mortality deceleration in ageing *C. elegans* populations

C. elegans' mortality rate rises with age, however a significant decrease in the mortality rate acceleration is often observed in mid life, around days 8-12 (Figure 5.7A) (Vaupel et al. 1994; Brooks et al. 1994; Johnson et al. 2001). This means a two stage Gompertz model is more appropriate for ageing *C. elegans* populations (Johnson et al. 2001). The mortality rate deceleration was proposed to be due to population heterogeneity, which exists despite the population being genetically identical (Johnson et al. 2001). Such heterogeneity must be expressed relatively early in life to result in subpopulations with different mortality rates. Given that P death mostly occurs in early to mid life, we decided to determine whether P and p deaths had different mortality rates and if this could explain the long observed mortality rate deceleration in *C. elegans* populations.

Firstly Y. Zhao, with assistance from M. Ziehm, confirmed that the populations she had subjected to necropsy analysis also showed a mortality rate deceleration, with a significant slope change seen on day 11 (Figure 5.7B). Next they analysed the mortality rates of P and p death. They discovered the mortality rate of P death accelerates much faster than p death, causing a spike in mortality around day 11 (Figure 5.7C). Therefore P death represents a vulnerable subset of worms that die earlier. Thus, the mortality rate deceleration in *C. elegans* populations is due to two distinct subpopulations with different mortality rates.

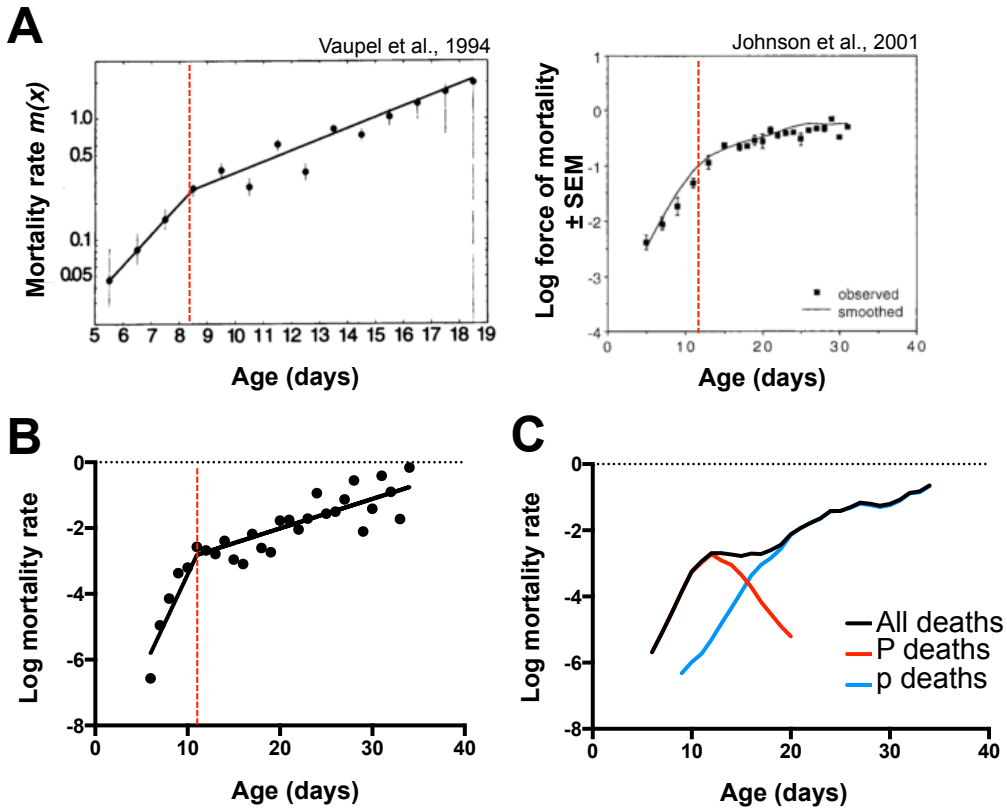

Figure 5.7. Mortality rate deceleration in ageing *C. elegans* populations. (A) Mortality rate deceleration has been previously observed in ageing *C. elegans* hermaphrodite populations (Vaupel et al. 1994; Brooks et al. 1994; Johnson et al. 2001). The deceleration is observed relatively early in the life span. For example, in these data it was observed at around ~8.3 days and ~12 days respectively (red line). **(B)** *C. elegans* populations that underwent necropsy analysis also showed a mortality rate deceleration occurring around day 11 (red line), with a statistically significant slope change at this point (p=2.81x10^{-9}, slope test). **(C)** Examining the mortality rates of the P and p death subpopulations revealed the deceleration is due to population heterogeneity, caused by a subset of worms with pharyngeal infection dying faster and earlier. (n=622) (Data in **B** and **C** collected by Yuan Zhao and analyzed by Matthias Ziehm and Yuan Zhao).

5.2.4 Bacterial infection is the primary cause of pharyngeal swelling

Next we wanted to establish what was causing the morbid swelling of the pharynx in P death. Examination of swollen pharynxes under high magnification revealed they had a grainy appearance that appeared similar to the densely packed *E. coli* that I had previously seen in the intestinal lumen and uterine tumours. Furthermore, previous work had shown that the pharynxes of worms with an impaired immune system were particularly vulnerable to infection by the pathogenic bacteria

Salmonella typhimurium and *Salmonella enterica* (Tenor & Aballay 2008; Haskins et al. 2008). A small number of *E. coli* were also seen within the pharyngeal tissue of an aged worm, indicating the invasive capabilities of this species (McGee et al. 2011). Finally, proliferative *E. coli* has also been shown to be detrimental to *C. elegans* longevity (Gems & Riddle 2000; Garigan et al. 2002). Therefore we set out to determine whether bacterial infection of the pharynx by *E. coli* OP50 was the primary cause of pharyngeal swelling in P death.

To try and identify any live bacteria that had invaded the pharynx, I stained both day 1 and day 8 worms with the vital dye, SYTO13. This is a nucleic acid dye that has been previously used to stain live bacteria associated with a rectal infection in *C. elegans* (Nicholas & Hodgkin 2004). Worms on day 1 took up the dye efficiently and as expected there was no evidence of bacteria within the pharyngeal tissue. On day 8, uptake of the dye appeared to be much less, perhaps due to the age-related decrease of pharyngeal pumping rate (Huang et al. 2004). Out of approximately 20 worms examined on day 8, only one showed possible staining within the pharyngeal tissue. However it was difficult to be certain whether this staining was due to bacteria (data not shown). Thus, it may be difficult to stain the pharynxes of older worms when the method is dependent on efficient uptake of the dye by a functioning pharynx.

We continued to seek evidence of live bacteria within the pharyngeal tissue. C. Yang categorised live day 10 or 11 worms into two groups: those with either swollen or unswollen pharynxes. He then dissected out the posterior bulb of the pharynx before washing and then pulverizing the tissue. The subsequent solution was then spread onto plates to allow the colony forming units (CFUs) to be counted. This revealed swollen pharynxes had a bacterial load that was 42 fold larger than unswollen pharynxes (Figure 5.8A).

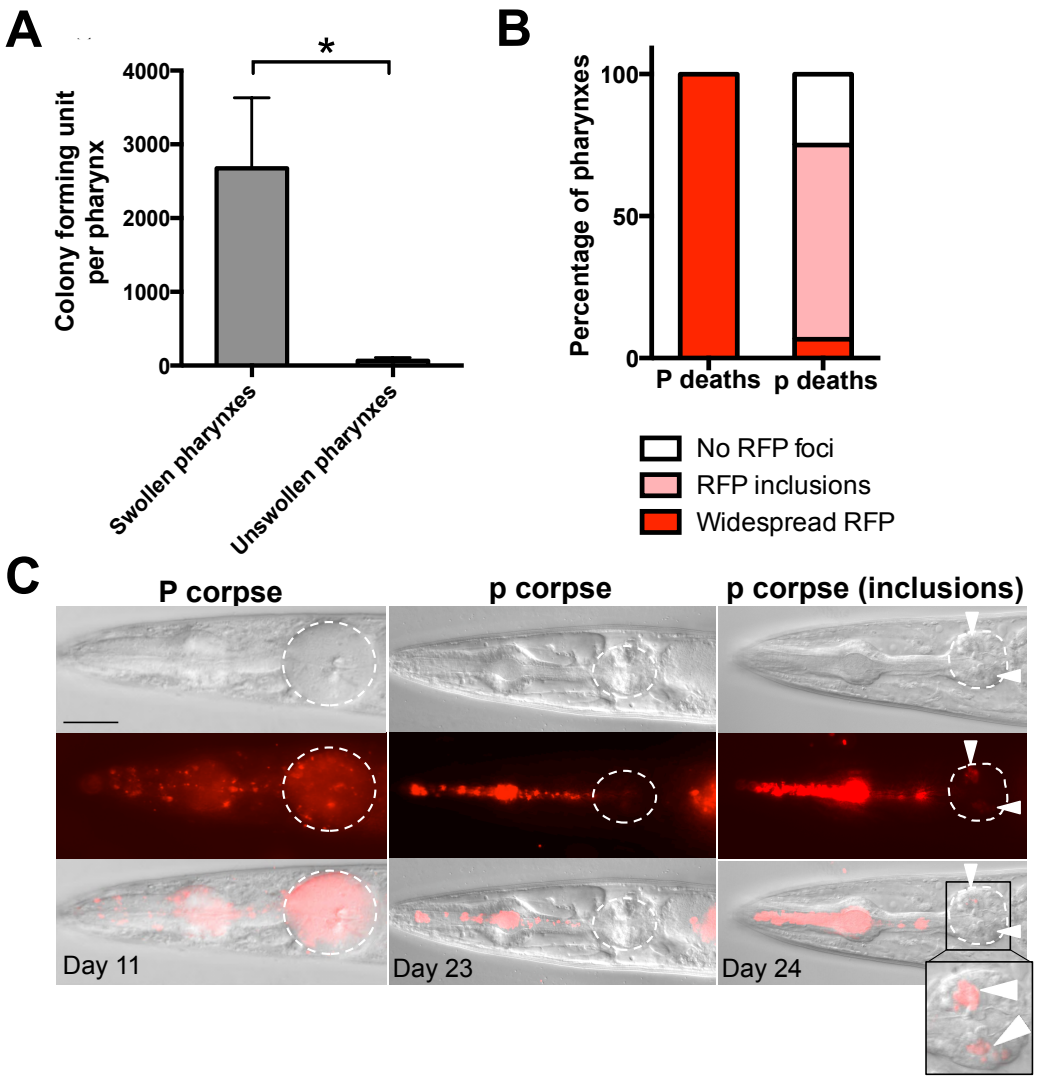

Figure 5.8. Bacterial infection causes pharyngeal swelling. (A) Swollen pharynxes from day 10 and 11 live, wild-type worms have significantly higher CFUs than unswollen pharynxes. Data mean±s.e.m. (p<0.05 * Student's t test. Swollen n=8, unswollen n=10). **(B)** Comparison of the distribution of red fluorescence in the corpses of wild-type worms grown on OP50-RFP that underwent either P or p death. All worms that undergo P death have widespread red fluorescence in the pharynx, whereas the vast majority that undergo p death do not. (P death n=70, p death n=75) **(C)** Corpses from wild-type worms fed on OP50-RFP, with the posterior bulb highlighted in white. P corpses had widespread red fluorescence throughout the pharynx. p corpses either had no red fluorescence in the pharyngeal tissue or had small inclusions of red fluorescence (white arrows), often near the grinder (Scale bar = 40μm). (Data in **A** collected by Chenhao Yang).

Next I performed a necropsy analysis on worms grown on OP50-RFP to observe the pattern of any bacterial invasion within the pharyngeal tissue. OP50-RFP was prepared as described in chapter 2. In brief, bacteria were grown in the presence of tetracycline to select for the plasmid

possessing the RFP gene, before being resuspended in broth containing no antibiotic. This was to ensure bacterial pathogenicity was not reduced by the presence of antibiotic. A fluorescent and brightfield image of the pharynx from each corpse was collected. From this, I observed three patterns of RFP distribution within the pharyngeal tissue: no RFP present; small RFP inclusions and widespread RFP. P deaths worms all had widespread RFP that completely filled the pharyngeal tissue (Figure 5.8B,C). Interestingly in p death, the vast majority had small RFP foci present in the pharyngeal tissue (68%), while only a relatively small proportion had no RFP present in the pharynx (24%) (Figure 5.8B,C). This suggests that many p death worms do experience minor bacterial invasion of the pharynx, but are able to contain it.

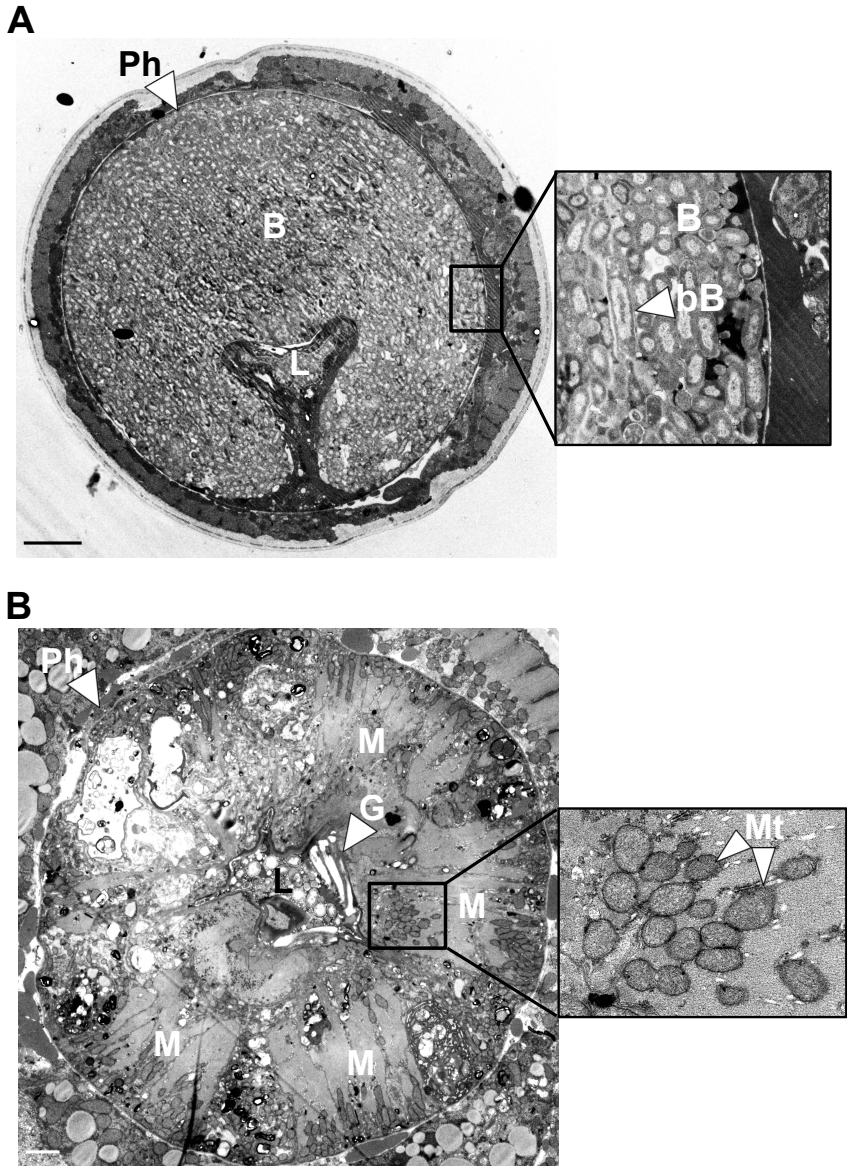

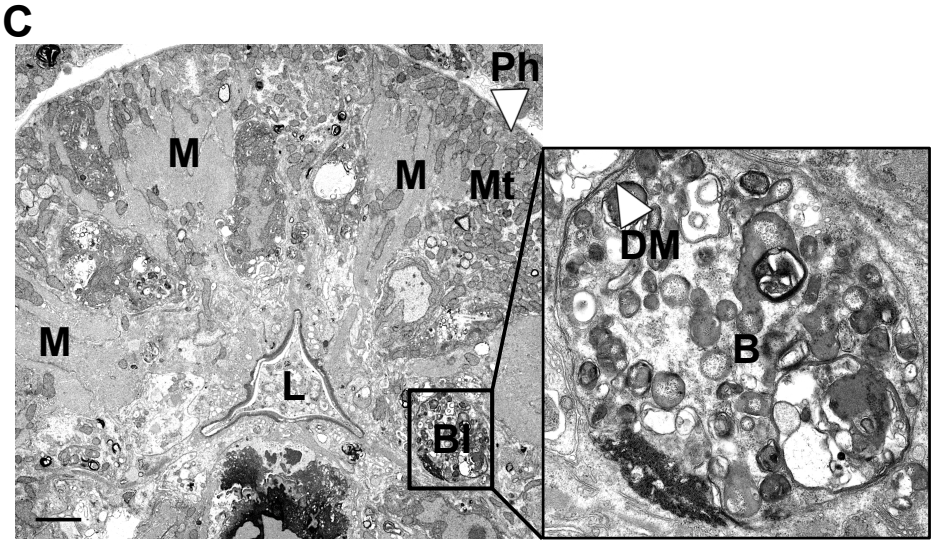

Figure 5.9. Evidence from electron microscopy of bacterial invasion of the pharynx. Images are from day 8 live adults. **(A)** A swollen pharynx (Ph) is completely invaded with bacteria (B), with evidence of bacteria dividing in the tissue (dB). (Scale bar = 5μm). (3 swollen pharynxes were imaged). **(B)** In this unswollen pharynx, bacteria are only seen in the lumen (L). The muscle (M), mitochondria (Mt) and grinder (G) are all clearly visible (Scale bar = 2μm). **(C)** In this unswollen pharynx, bacteria can be seen within a small bacterial inclusion (BI) within the pharyngeal tissue, where the bacteria is surrounded by a double membrane (DM) (Scale bar = 2μm). (2 unswollen pharynxes were imaged). (Images collected jointly by Ann Gilliat and Yuan Zhao, with technical assistance from Mark Turmaine).

To confirm definitively that bacteria are present within the tissue of swollen pharynxes, Y. Zhao and I performed TEM on worms with technical assistance from M. Turmaine. We aged worms on OP50-RFP until day 8 and then noted if the pharynx was swollen or not before dividing them into two groups based on whether or not RFP was present within the pharynx. Those with no RFP were assumed to have not developed infection while those with widespread RFP were assumed to have advanced infection. These worms were then prepared and imaged using TEM. In the three worms we imaged that had widespread RFP, all the pharynxes were swollen and entirely invaded by bacteria (Figure 5.9A). Additionally, some bacteria within the pharynx had a lengthened appearance, indicating bacterial proliferation may be occurring (Figure 5.9A). In contrast we did not see such extensive invasion in the two pharynxes we imaged from worms that had had no RFP within the pharyngeal tissue. In one, no invasive bacteria were observed (Figure

5.9B), while in the other a small number of bacteria were identified (Figure 5.9C). However these bacteria were sequestered within a double membrane structure (Figure 5.9C), suggesting containment of the infection.

Finally we wanted to confirm that proliferative bacteria were required for the development of pharyngeal swelling. Y. Zhao blocked bacterial division using carbenicillin while I killed bacteria via exposure to UV light. Both treatments have been previously shown to extend lifespan (Gems & Riddle 2000; Garigan et al. 2002), and we were able to replicate this finding (Figure 5.10B,D). Furthermore both treatments abolished P death (Figure 5.10A,C). This confirms live and proliferative bacteria are required for the occurrence of this pathology.

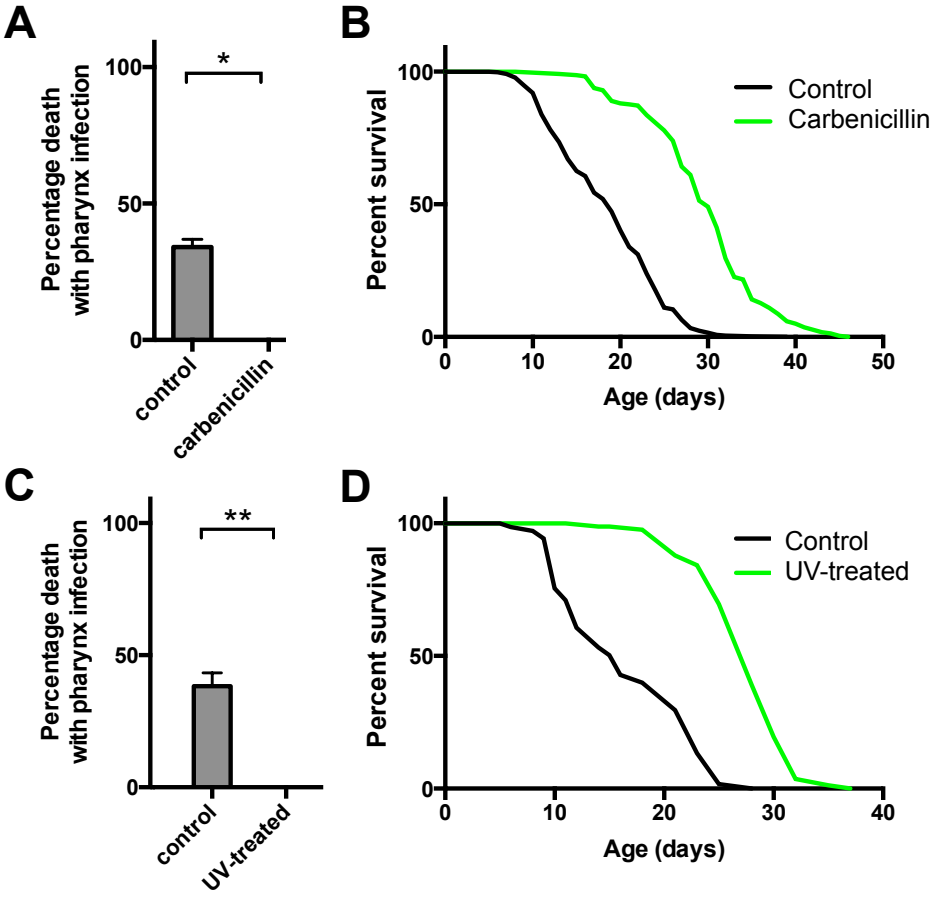

Figure 5.10. Blocking bacterial proliferation prevented P death and extended lifespan. (A) Treating plates with carbenicillin to prevent bacterial proliferation completely prevented P death. **(B)** Carbenicillin treatment extended lifespan. **(C)** Exposing plates to UV light killed bacteria and completely prevented P death. **(D)** UV treatment extended lifespan. (**A, C** Data mean±s.e.m, $p<0.05$ *, $p<0.01$ **, Student's *t* test. **B, D** see appendix, Table A.2 for survival statistics table and sample sizes). (Data in **A** and **B** collected by Yuan Zhao).

5.2.5 Pharyngeal infection is associated with a sudden decline in function

As stated in the introduction to this chapter, the pharynx undergoes a major age-related decline in function (Huang et al. 2004). This decline occurs primarily between days 4 and 10, which is a similar timeframe to when pharyngeal infection seems to develop. TEM revealed extensive deterioration of the pharyngeal tissue in swollen pharynxes, with the muscle fibres virtually absent (Figure 5.9A). Therefore it is logical to assume that progression of this pathology should impair pharyngeal function and eventually inhibit it entirely, contributing to the age-related decline in pharyngeal pumping rate (Huang et al. 2004). To explore this idea, I monitored the pumping rate in individual worms throughout their lifespan and performed necropsy analysis once they had expired. This revealed that in most worms that eventually underwent p death, pharyngeal pumping rate decreased gradually throughout life, up until death (Figure 5.11A). However in worms that ultimately experienced P death, there was often a sudden and dramatic decrease in pumping rate, not long before death (Figure 5.11A). Indeed this sudden decline in function occurred just prior to the start of pharyngeal swelling (Figure 5.11B). Soon thereafter, pharyngeal pumping ceased entirely (Figure 5.11B). Therefore the previously observed correlation between the period of pharyngeal function and lifespan is likely to be partially explained by the development of this pathology (Huang et al. 2004). Thus, early mortality with pharyngeal infection is closely associated with a loss of pharyngeal function.

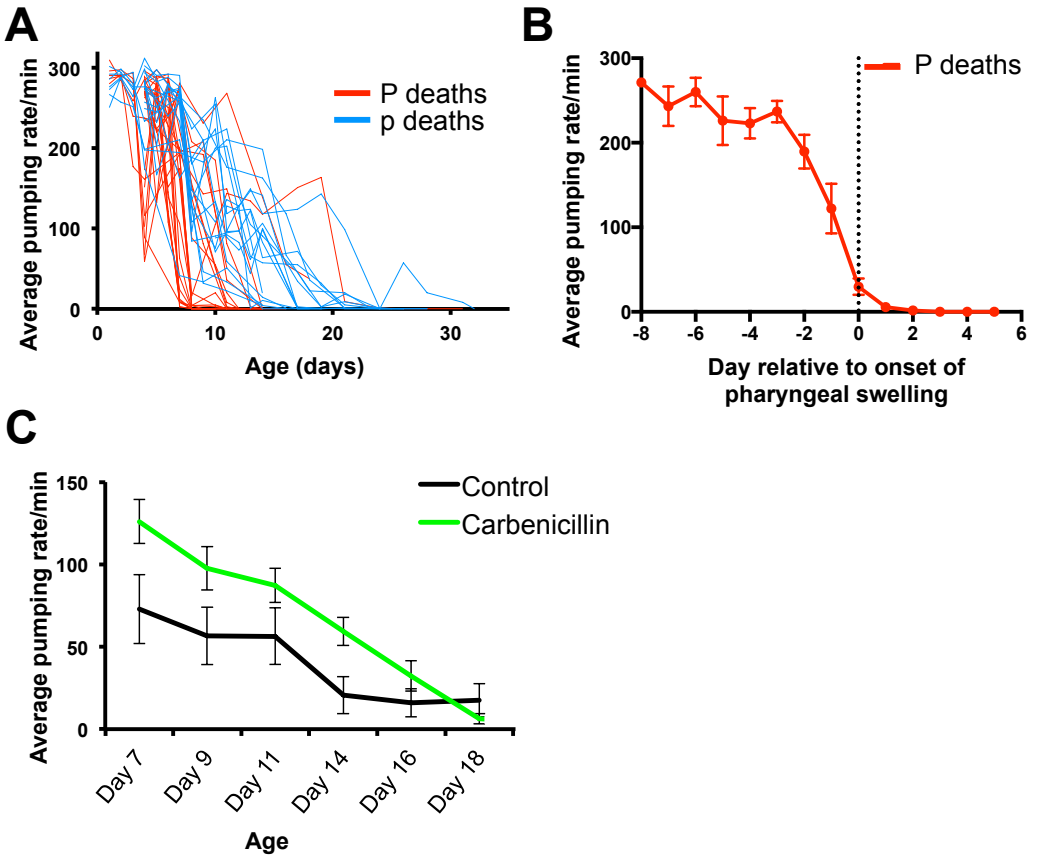

Figure 5.11. Bacterial infection is associated with a sudden decline in pharyngeal function. (A) Pumping rate throughout the life of individual worms that eventually died from either P or p death (n=43). **(B)** A few days before pharyngeal swelling is first observed in P deaths (day 0), there is a major decline in pharyngeal function. Data mean±s.e.m (n=17). (Pharyngeal swelling monitored by Y. Zhao) **(C)** Carbenicillin treatment is able to slow the age-related decline in pharyngeal pumping rate. Data mean±s.e.m (n=10 per time point per condition, except on day 1 n=8 per condition).

Prior work did reveal a potential link between proliferative bacteria and a decline in pharyngeal function. Treatment with the antibiotic ampicillin was shown to slightly reduce the age-related decline in pharyngeal function (Chow et al. 2006). I was able to replicate this result using the antibiotic carbenicillin (two-way ANOVA comparison for carbenicillin $F(1,104)=15.21$ $p=0.0002$) (Figure 5.11C). If the occurrence of P death is the primary cause of the correlation between pharyngeal pumping span and lifespan then complete suppression of pharyngeal infection should remove or reduce this correlation. Carbenicillin was not able to significantly reduce the correlation between both pharyngeal pumping span and fast pharyngeal pumping span with lifespan (Figure 5.12A,B). This suggests other pharyngeal pathologies that are independent of

infection, such as perhaps sarcopenia (Chow et al. 2006), contribute towards the decline in function and associated mortality (Huang et al. 2004).

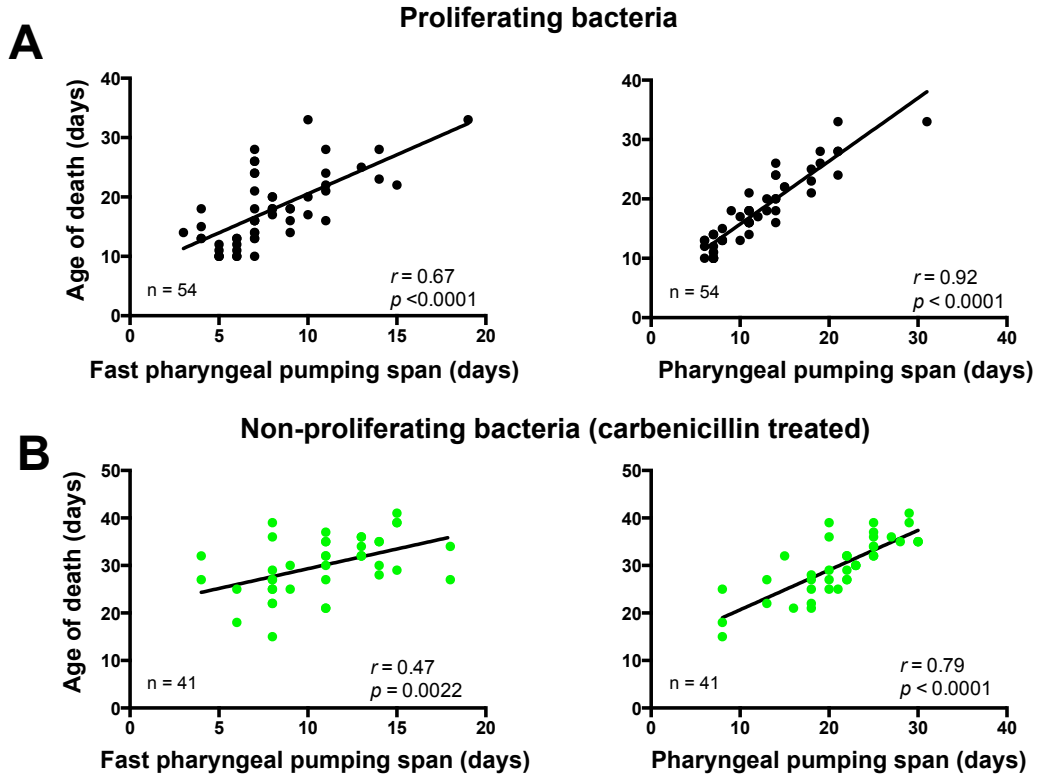

Figure 5.12. The effect of carbenicillin treatment on the correlation between pharyngeal function and lifespan. (A) As previously shown (Huang et al. 2004), there is a correlation between fast pharyngeal pumping span (days at >149 pumps/min) and pharyngeal pumping span (days at 6-149 pumps/min) with life span. (n=54). **(B)** These correlations were reduced on carbenicillin. (n=41). (Linear model comparison between proliferating and non-proliferating bacteria. Pharyngeal pumping span p=0.056, fast pharyngeal pumping span p=0.13).

5.2.6 Mechanical damage may promote pharyngeal infection

Pharyngeal infection could be due to a systematic age-related decline in immune function across the entire worm. Alternatively, it could be due to a more localised defect, which occurs specifically in the pharynx. To explore this, I decided to determine whether worms with pharyngeal infection are more likely to experience bacterial infection elsewhere. Worms were grown on OP50-RFP and then scored on days 10 and 14 for the presence of RFP within the pharynx and uterine tumours. Those with

extensive RFP in the region of interest were defined as infected. This revealed on both days 10 and 14 that worms with infected pharynxes were not more likely than other members of the population to have infected uterine tumours (Figure 5.13A,B). This suggests there is not a systematic loss of immune function in worms that undergo P death. Rather this implies there is an age-related defect that promotes bacterial infection, which is restricted to the pharynx.

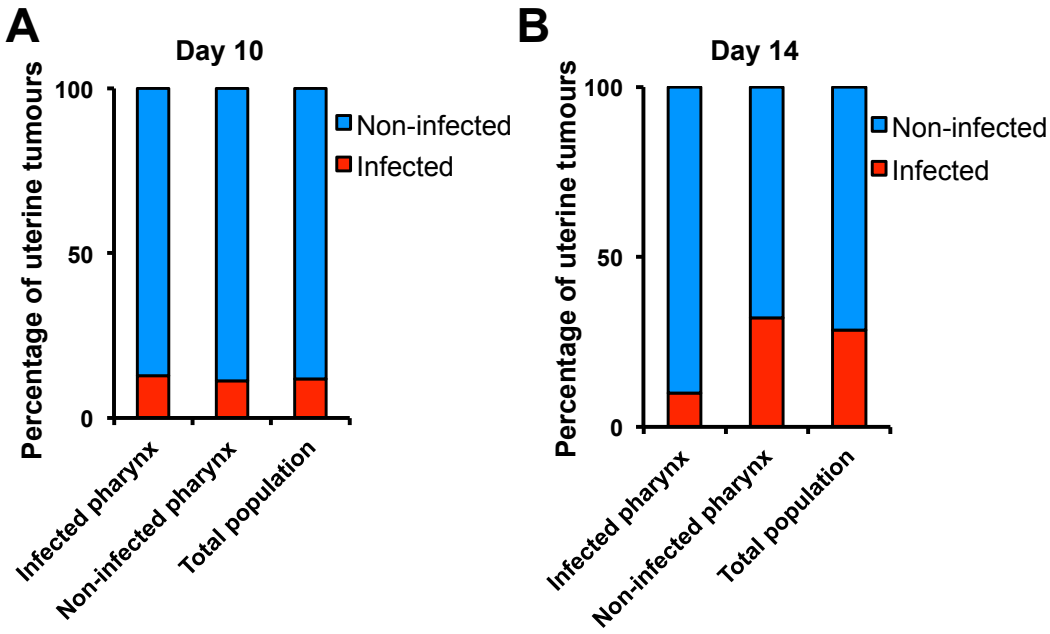

Figure 5.13. Uterine tumour infection in worms with infected pharynxes. Wild-type hermaphrodites were grown on OP50-RFP at 20°C. **(A)** On day 10, those with pharyngeal infection were no more likely to have infected uterine tumours than other members of the population. (101 worms examined) **(B)** On day 14, those with pharyngeal infection were no more likely to have infected uterine tumours than other members of the population. (63 worms examined).

To determine where bacterial infection starts and therefore gain insights into the main route of invasion into the pharynx, worms with early infection were examined. These worms were grown on OP50-RFP and inspected on days 8, 9 or 10. Those with low levels of RFP were assumed to be in the initial stages of infection and were selected for confocal microscopy. Worms where three different pharyngeal cells types (either muscle, marginal or g1 gland cells) had been tagged with GFP were used for this study. This was to establish if infection preferentially starts in a particular cell type. After imaging, worms were divided into three categories: those where RFP was seen in both GFP+ and GFP-

cells, those where RFP was only seen in the GFP+ cells and those where no RFP was seen in the GFP+ cells. When RFP was only seen in the GFP+ cells, this suggested that infection had begun within this cell type. Infection was observed in all three cell types (Figure 5.14A), however infection never began in marginal cells and rarely in g1 gland cells (Figure 5.14B). In fact, infection mostly started within muscle cells and frequently in close proximity to the grinder (Figure 5.14A,B). To explore this further, TEM was performed on worms that had early infection on day 8 and confirmed that initial bacterial invasion was often observed near the pharyngeal grinder (Figure 5.15A,B).

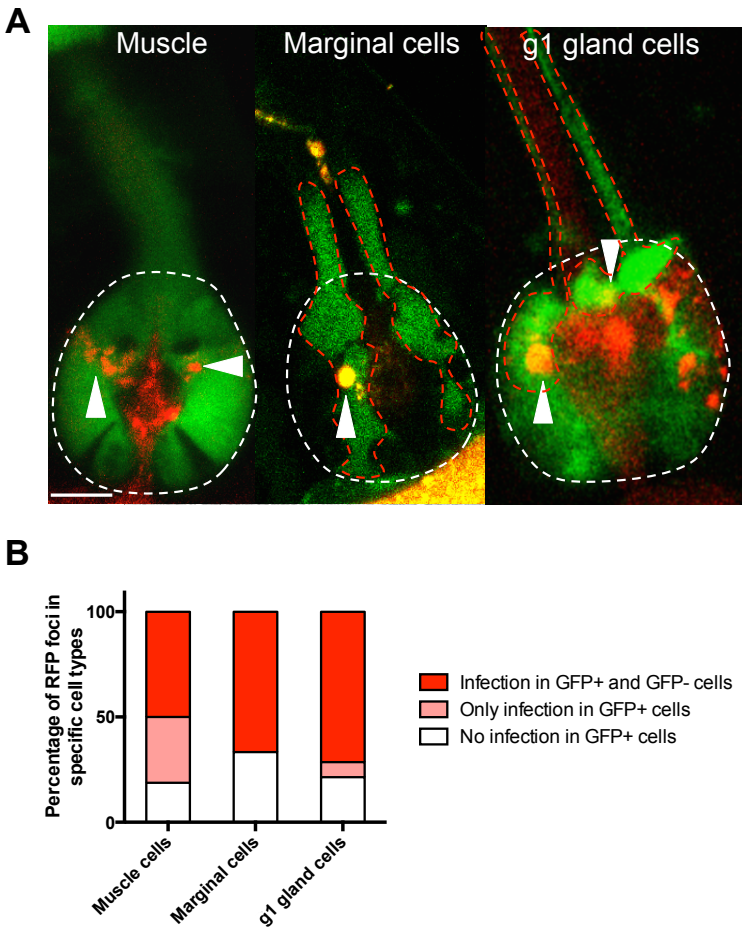

Figure 5.14. Bacterial infection in different cell types within the pharynx. (A) The posterior pharyngeal bulb is indicated (outlined in white) with either the muscle, marginal or g1 gland cells (outlined in red) tagged with GFP. Colonies can be seen within GFP positive cells, often near the grinder (white arrows). **(B)** Out of the three cell types examined, bacterial infection appears to mostly begin within muscle (pharyngeal muscle n=14, marginal cells n=12, g1 gland cells n=16).

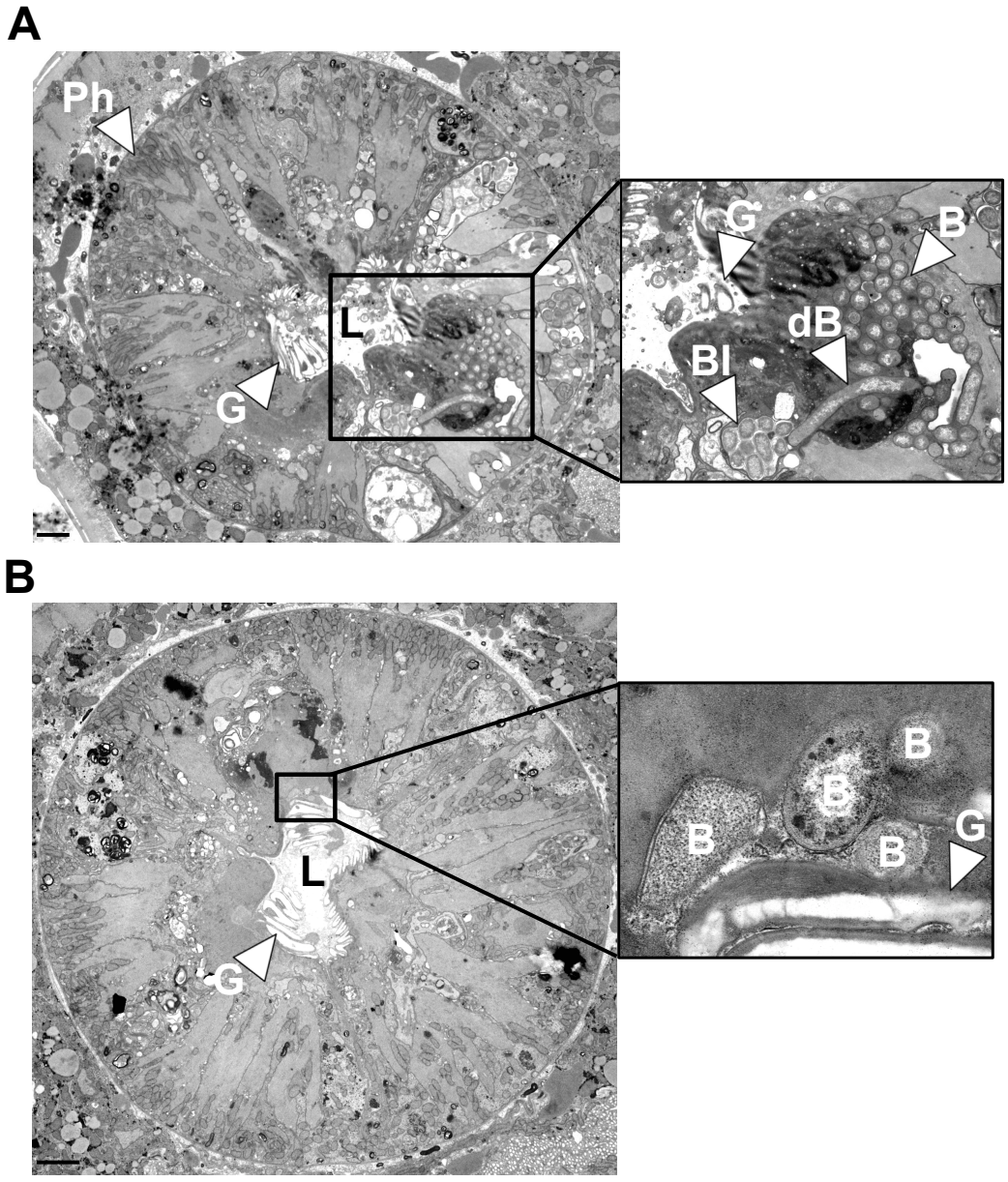

Figure 5.15. Evidence from electron microscopy that bacterial infection starts near the grinder. Images are from day 8 live adults with early infection. **(A)** A relatively large number of bacteria (B) can be seen near the grinder (G) of the pharynx (Ph). There is also evidence of proliferation (dB) within the tissue. A small bacterial inclusion (BI) can be seen, where bacteria are contained within a double membrane structure. **(B)** In very early infection, a small number of bacteria (B) can be seen near the grinder (G). L, lumen. (Scale bars = 2μm). (3 pharynxes with early infection were imaged) (Images collected jointly by Ann Gilliat and Yuan Zhao, with technical assistance from Mark Turmaine).

Next we wanted to explore whether a subpopulation worms (~40%) were predisposed from early in life to develop pharyngeal infection and undergo subsequent P death. To test this worms were raised on antibiotic-treated bacteria from egg and then shifted to proliferative

bacteria at various time points throughout adulthood. If 40% of worms had acquired a predisposition to pharyngeal infection early in life then exposure to proliferative bacteria, even later in life, should expose this vulnerability and cause those 40% of worms to undergo P death. Unexpectedly, shifting worms onto proliferative bacteria from day 4 onwards resulted in a gradual decrease in the proportion of P death (Figure 5.16A). Shifts from day 6 onwards also caused increases in lifespan (Figure 5.16B). To confirm this result was not due to the residual effects of ingested carbenicillin, the experiment was repeated using UV-killed bacteria, which produced similar results (Figure 5.16C,D). These data suggest that there is a short period during early adulthood where worms must be exposed to proliferative bacteria for P death to occur.

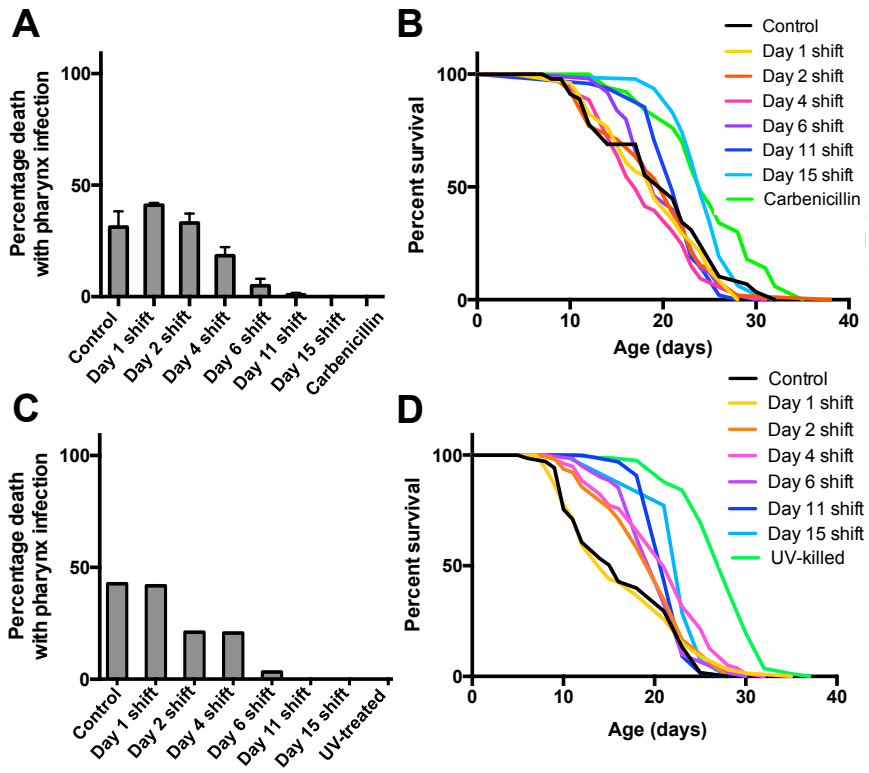

Figure 5.16. The effect on lifespan and the occurrence of P death of initially growing worms on non-proliferating bacteria. (A) Worms grown on carbenicillin-treated plates until day 1 of adulthood had normal levels of P death. Transfer to proliferating bacteria later in life resulted in decreases in P death frequency. Data mean±s.e.m. **(B)** Transfer to proliferating bacteria later in life (from day 6 shift onwards) caused significant increases in lifespan. (See appendix, Table A.3 for survival statistics table and sample sizes). **(C)** Worms grown with UV-killed bacteria until day 1 of adulthood had normal levels of P death. Transfer to proliferating bacteria later in life resulted in decreases in P death frequency. **(D)** Transfer to proliferating bacteria, even early in life (from day 2 shift onwards), caused significant increases in lifespan. (See appendix, Table A.3 for survival statistics table and sample sizes).

Taking all these results together we hypothesised that high pharyngeal activity in early life causes mechanical damage to the pharyngeal cuticle near the grinder. This could result in fissures in the cuticle, providing a route for bacterial invasion. As this damage would occur in young worms, it might also explain why pharyngeal infection starts to develop relatively early in life, resulting in the early wave of P death. The shift experiments also imply that to develop P death, worms must be exposed to proliferative bacteria in early life, at the same time that the pharyngeal cuticle is being damaged.

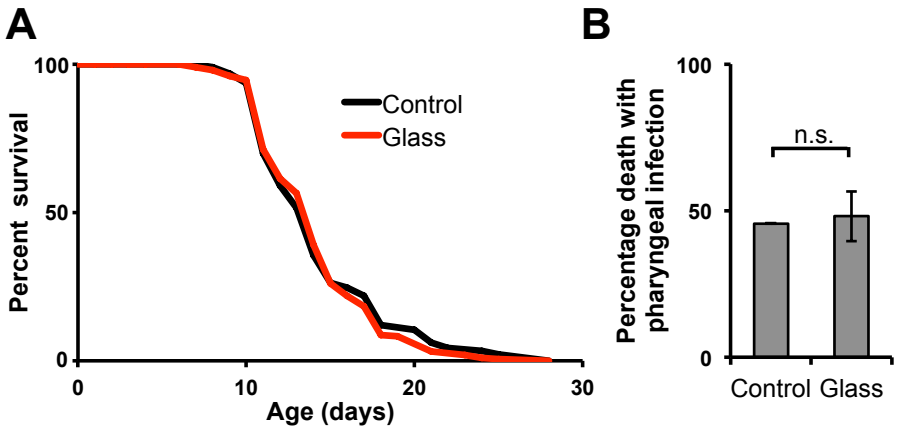

Figure 5.17. The effect of feeding powdered glass on *C. elegans* longevity and pharyngeal infection. Worms were fed powdered glass from L4 larval stage until day 4, before being transferred onto untreated plates. **(A)** Feeding on ground glass had no effect on lifespan. (See appendix, Table A.4 for survival statistics table and sample sizes). **(B)** Feeding on ground glass did not alter the level of P death. Data mean±s.e.m. (Student's *t* test).

If this theory were correct, then increasing the damage inflicted to the pharyngeal cuticle should increase P death. In an attempt to do this, worms were shifted at the L4 stage to plates where the surface was covered in microscopic glass particles that, upon examination under high magnification, appeared similar in size to bacteria (data not shown). As the glass particles had a jagged shape, it was hoped ingestion of them could exacerbate mechanical damage to the pharyngeal cuticle. Worms remained on the glass plates until day 4, as this is the period when the pharynx is pumping fastest (Huang et al. 2004). Exposure to glass had no effect on either lifespan or the levels of P death (Figure 5.17A,B). However no glass particles were observed within the intestine of these

worms, even under high magnification, making this result difficult to interpret.

In another attempt to increase pharyngeal damage, worms were maintained in the presence of exogenous serotonin. Serotonin stimulates pharyngeal pumping and has been previously shown to increase pumping rate in the absence of bacteria, where pumping rate is much lower (Horvitz et al. 1982; Chow et al. 2006). However to study bacterial infection and P death, worms must be exposed to serotonin in the presence of bacteria. Serotonin (dissolved in HCl) or HCl alone was added topically to plates and worms were grown on these plates from the L4 larval stage until day 8. A two-way ANOVA revealed an overall significant effect of the bacterial lawn and serotonin on both days 4 and 7 (day 4 comparison of bacterial lawn $F(1,36)=199.6$ $p<0.0001$, comparison for serotonin $F(1,36)=228.3$ $p<0.0001$. Day 7 comparison of bacterial lawn $F(1,36)=60.08$ $p<0.0001$, comparison for serotonin $F(1,36)=76.48$ $p<0.0001$). This is to be expected as both the bacterial lawn and serotonin stimulate pharyngeal pumping. On day 4, serotonin did dramatically increase pumping rate in worms that were located away from the bacterial lawn (Figure 5.18C), as previously shown (Chow et al. 2006). However it only slightly increased pumping rate in worms on the bacterial lawn (Figure 5.18C). On day 7, again serotonin increased pumping rate in worms away from the bacterial lawn, however it did not have an effect while worms were on the lawn (Figure 5.18D). Given these results, it was not surprising that serotonin had no significant effect on lifespan or the levels of P death (Figure 5.18A,B). In fact in both conditions, P death was lower than expected (~20%), suggesting HCl may reduce bacterial pathogenicity. Furthermore, long-term exposure to serotonin seemed to have various deleterious and pleiotropic effects, resulting in an increased proportion of animals being censored during the experiment. In a bid to reduce these effects and allow worms to become fully grown adults before treatment, the exposure time was reduced. This time worms were only grown on serotonin plates from day 4 to 8. However similar results were obtained (Figure 5.19) (Two way ANOVA.

Day 4 comparison for bacterial lawn $F(1.36)=364.0$ $p<0.0001$, comparison for serotonin $F(1,36)=172.8$ $p<0.0001$. Day 7 comparison for bacterial lawn $F(1,36)=157.4$ $p<0.0001$, comparison for serotonin $F(1,36)=66.83$ $p<0.0001$).

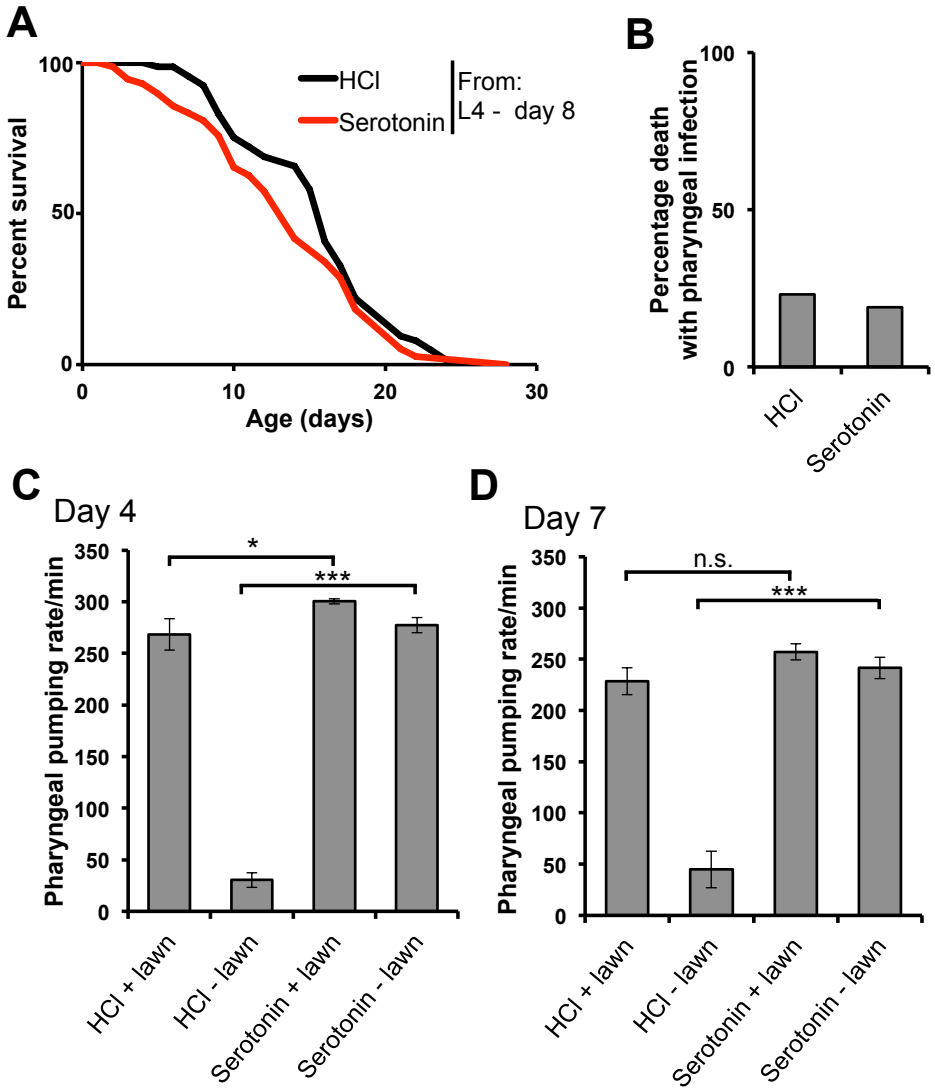

Figure 5.18. The effects of serotonin exposure until mid-life on longevity, pharyngeal infection and pharyngeal pumping rate. Worms were exposed to 12mM serotonin (dissolved in HCl) or 1mM HCl from L4 larval stage until day 8, before being transferred onto untreated plates. **(A)** Serotonin had no effect on lifespan. (See appendix, Table A.5 for survival statistics table and sample sizes) **(B)** Serotonin had no effect on the percentage death with pharyngeal infection. **(C)** On day 4, serotonin can dramatically increase pharyngeal pumping rate when worms are off bacteria, but only has a small effect when worms are on bacteria. (n=10 per condition) **(D)** On day 7, serotonin can increase pharyngeal pumping rate when worms are off bacteria, but not when worms are on the bacterial lawn (n=10 per condition). Data mean±s.e.m. ($p<0.05$ *, $p<0.01$** $p<0.001$ *** Sidak's test).

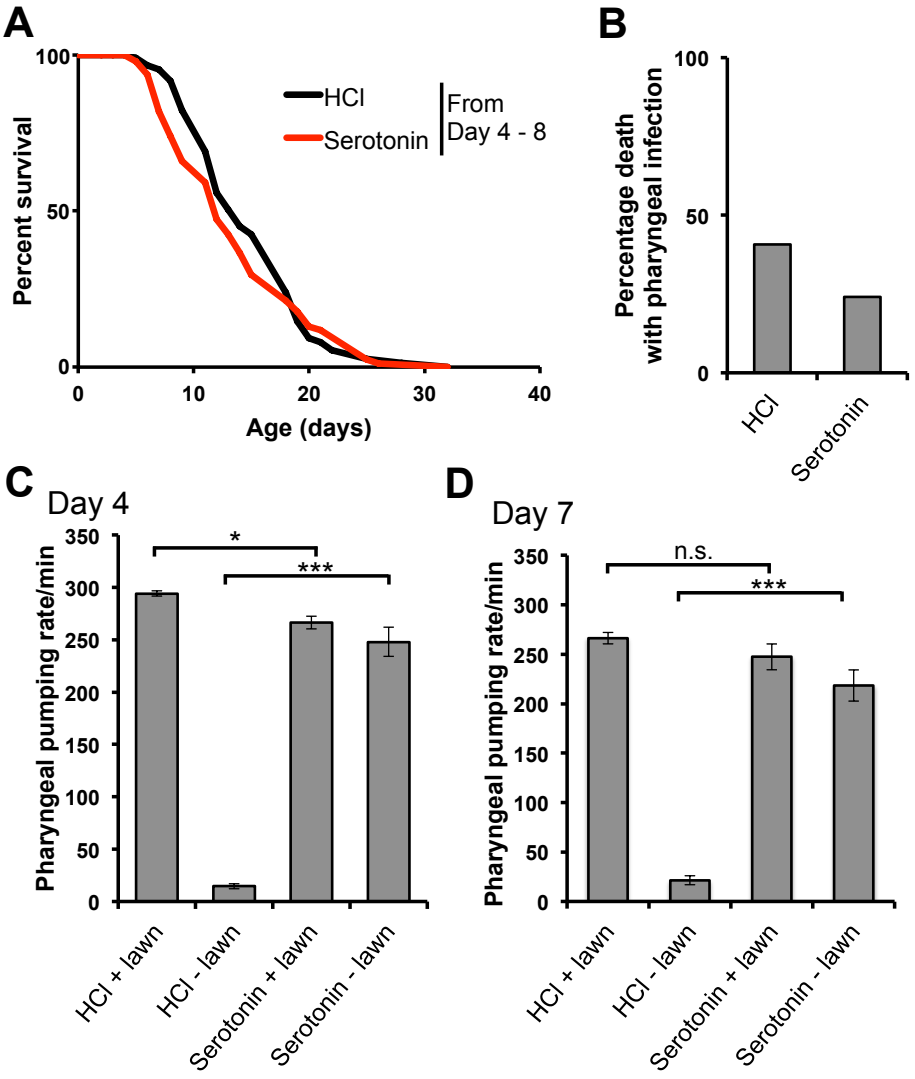

Figure 5.19. The effects of serotonin exposure, only in mid-life, on longevity, pharyngeal infection and pharyngeal pumping rate. Worms were exposed to 12mM serotonin (dissolved in HCl) or 1mM HCl from day 4 until day 8 before being transferred onto untreated plates. **(A)** Serotonin had no effect on lifespan. (See appendix, Table A.5 for survival statistics table and sample sizes) **(B)** Serotonin showed a trend for reducing the percentage death with pharyngeal infection. **(C)** On day 4, serotonin can increase pharyngeal pumping rate when worms are off bacteria, but slightly decreases pumping rate of worms on the lawn. (n=10 per condition) **(D)** On day 7, serotonin can increase pharyngeal pumping rate when worms are off bacteria, but not when worms are on the bacterial lawn. Data mean±s.e.m. (n=10 per condition) (p<0.05 *, p<0.01** p<0.001 *** Sidak's test).

Finally Y. Zhao and H. Wang tried the reverse experiment by exploring a situation where pharyngeal damage may be reduced. They looked at the levels of P death in various mutants, including *eat-2(ad1116)*, where the pharyngeal pumping rate is lower than wild-type levels (Raizen et al. 1995). In most cases these mutations caused a reduction in frequency of P death (Figure 5.20A). It has been previously shown that *eat-2* mutants

have an extended lifespan and this was presumed to be due to DR, which was proposed to be caused by this mutation reducing food intake (Lakowski & Hekimi 1998). However by analysing the survival curves of both P and p death in *eat-2*, Y. Zhao and H. Wang showed that the timing of both P and p death was not altered in this mutant (Figure 5.20B). This suggests that the lifespan extension in *eat-2* is mostly due to amelioration of pharyngeal infection rather than DR. Nevertheless it remains possible that, in certain conditions, the DR effect caused by mutation of *eat-2* does have a larger contribution toward the longevity of this mutant.

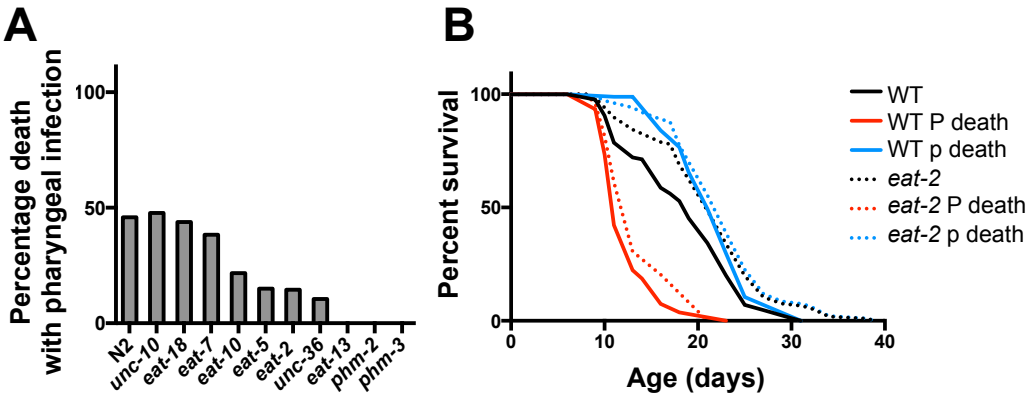

Figure 5.20. Lowering pharyngeal pumping rate reduces the level of P death. (A) The prevalence of P death is reduced in the majority of mutants that have a reduced pharyngeal pumping rate. (N2 n=47, *eat-5* n=48, *eat-13* n=39, *unc-10* n=48, *phm-2* n=32, *eat-10* n=10, *eat-18* n=50, *eat-2* n=55, *unc-36* n=19, *eat-7* n=39, *phm-3* n=18) **(B)** The timing of both P and p death is unaffected in *eat-2(ad1116)* mutants. Data collected by Yuan Zhao and Hongyuan Wang (See appendix, Table A.6 for survival statistics and sample sizes).

Overall these results provide evidence that the high pharyngeal pumping rate in early adulthood promotes mechanical senescence. When this occurs in the presence of proliferative bacteria early in life, it can cause pharyngeal infection later in life and subsequent P death.

5.2.7 Evidence of wound healing in the pharyngeal cuticle as defence against bacterial infection

We considered why only a fraction of an ageing *C. elegans* population experience P death. Conceivably, it could be due variations in pharyngeal

pumping rate early in life. Those that pump faster may accumulate more damage to the pharyngeal cuticle and thus be more vulnerable to bacterial invasion. The pumping rate of individual worms was recorded on day 1 and then necropsy analysis was performed upon their death. This revealed that there was no significant difference in the pumping rate on day 1 of adulthood between P and p death (Figure 5.21). Therefore variation in pumping rate in early adulthood does not explain the development of the two subpopulations.

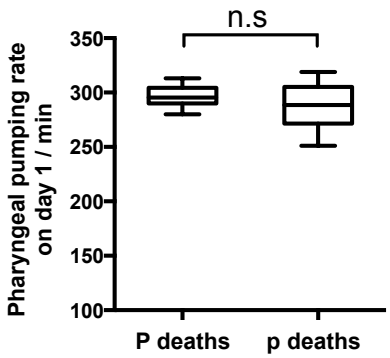

Figure 5.21. Pharyngeal pumping rate on day 1 of adulthood of P and p death worms. Worms that died from P death did not have a higher pumping rate on day 1 than worms that eventually died from p death. (P death n=14, p death n=10) (Student's *t* test).

As development of P death required exposure to proliferative bacteria early in life (Figure 5.16A,C), we hypothesised that in early adulthood the pharyngeal cuticle is able to initiate a wound healing response upon injury. We supposed the high pumping rate in early adulthood results in injury in the majority of worms, or perhaps in all of them. However, if efficient wound healing occurs, the resulting perforations could be sealed. Nonetheless, due to the stochastic nature of this damage, a proportion of worms may sustain higher levels of injury. In such worms, wound healing might not be rapid enough to repair all the injuries before extensive bacterial invasion has taken place. Therefore these worms will become the subpopulation that ultimately undergoes P death. Additionally, the presence of proliferating bacteria within or near the injuries could impede wound healing. This might explain why worms maintained for longer on

non-proliferating bacteria had lower levels of P death when subsequently exposed to proliferating bacteria (Figure 5.16A,C).

Previous work showed that injuries caused to the *C. elegans* body wall cuticle, either using a needle or a laser beam, can heal resulting in the formation of scar tissue (Figure 5.22B) (Pujol et al. 2008). This demonstrates that *C. elegans* is capable of mounting a wound-healing response when damage occurs. Therefore to determine whether the pharyngeal cuticle can generate a wound healing response as well, we set out to find evidence of scar tissue within the pharynx. Worms expressing either PQN-2 or ABU-1 tagged with GFP were kindly sent to us by David Raizen's group. These two proteins are found within the pharyngeal cuticle (David Raizen, correspondence). If either of these proteins were assimilated into any scar tissue, this should result in small puncta of GFP in the pharyngeal cuticle, particularly near the grinder. These worms were examined on days 1, 2, 3, 4 and 8 using epifluorescence microscopy and on day 9 using confocal microscopy. However no GFP puncta were detected in either strain (data not shown), suggesting either the absence of scars, or that if scars did form, they did not contain either PQN-2 or ABU-1.

Next TEM images of day 8 worms were examined for any evidence of scar tissue, particularly near the pharyngeal grinder. This revealed electron dense material close to the grinder, analogous to the scars previously seen in the body wall cuticle (Figure 5.22A,B) (Pujol et al. 2008). These images were sent to N. Pujol for an opinion and she also believed the pharyngeal cuticle to contain scar tissue. This implies that while the pharyngeal cuticle does become injured relatively early in life, it is able to launch a wound healing response. This results in the repair of any breaches to the external environment and therefore protects against bacterial invasion.

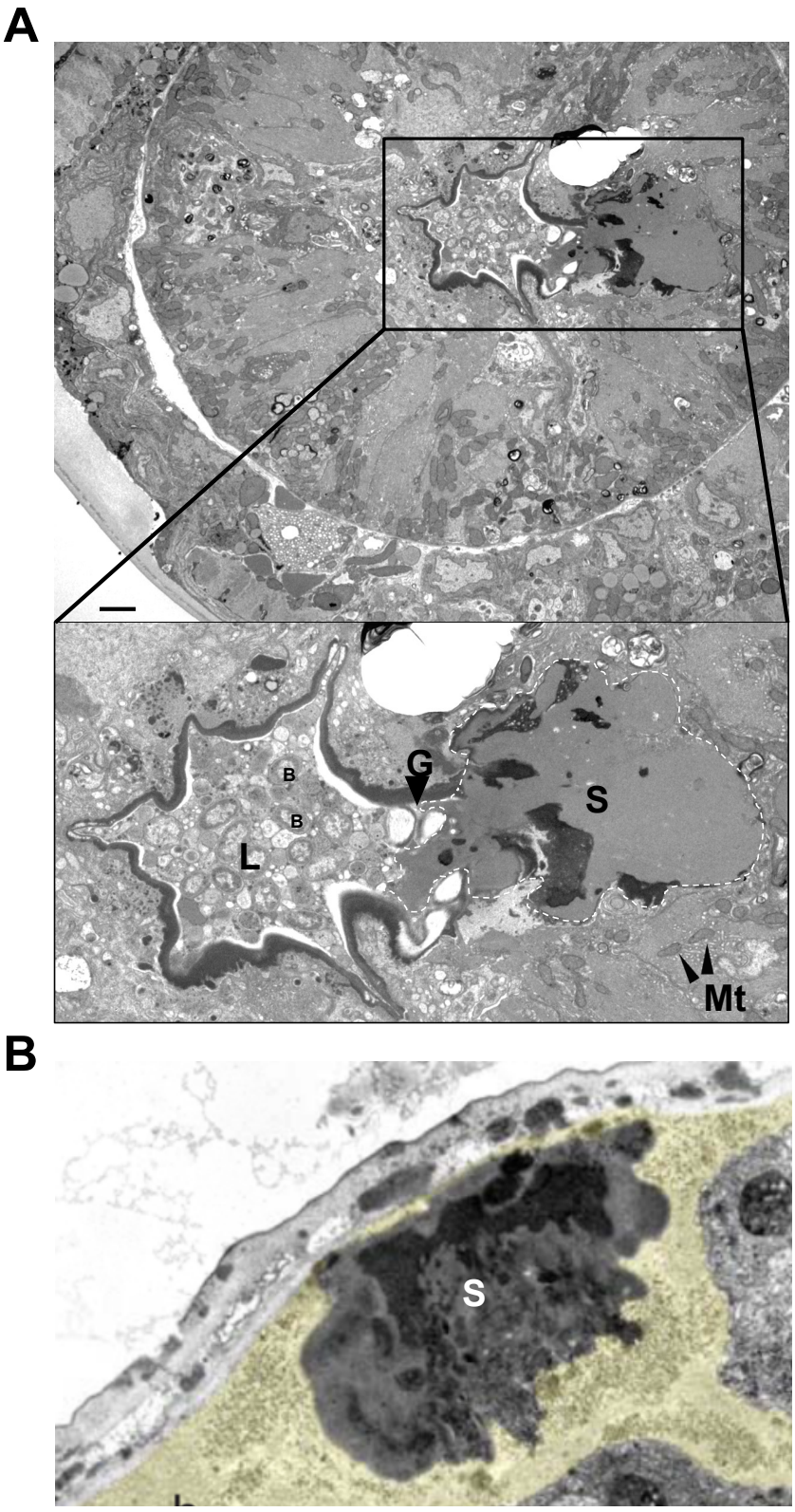

Figure 5.22. Evidence of scarring in the *C. elegans* pharynx. (A) Image is from a day 8 live adult. A large mass of material can be seen near the grinder (G). This appears to be caused by injury and subsequent wound healing, resulting in a scar (S). B, bacteria; L, lumen; Mt, mitochondria. (Scale bar = 2μm). (Images collected jointly by Ann Gilliat and Yuan Zhao, with technical assistance from Mark Turmaine). **(B)** Further evidence these masses are scars comes from their similarity to scars (S) that form in the epidermis of *C. elegans* after wound healing (Image from (Pujol et al. 2008)).

5.3 Discussion

5.3.1 Latent infection may lead to P death in ageing *C. elegans*

The results from this chapter demonstrate that a subpopulation of worms is subject to bacterial infection of the pharynx, which is associated with pharyngeal swelling and an early demise. This infection requires both exposure to proliferative bacteria, and wild-type pharyngeal function in early adulthood. The high pharyngeal pumping rate in early life is presumably beneficial to worms, as it allows for the rapid ingestion of food to fuel both the growth and huge reproductive output that occurs during this period. However, the evidence in this chapter suggests that high pharyngeal activity causes mechanical senescence. This promotes initial bacterial invasion and, in a subset of worms, subsequent death with pharyngeal infection, which we designated as P death.

What remains unknown is the complete mechanism by which pharyngeal infection develops and ultimately results in P death. Furthermore it is unclear how worms that undergo p death are able to escape this fate. We propose the following model as an explanation to these queries (Figure 5.23). As previously explained, in young worms the pharynx is healthy and functioning at full capacity. This high pumping rate causes injuries to the pharyngeal cuticle near the grinder. This is because the cuticle in this area experiences a high level of mechanical strain due to the force the grinder must exert to fully break down bacteria at high speed. Live bacteria in the pharyngeal lumen take advantage of the wounds in the cuticle and use them as route through which to invade the pharyngeal tissue. A wound healing response then occurs at the injury site, resulting in the formation of a scar. This closes the wound and should prevent further invasion. Two scenarios are then possible. Firstly, the bacteria that successfully invaded into the pharyngeal tissue, before wound healing occurred, continue to proliferate throughout the pharynx. This increase in bacterial load causes tissue degeneration, pharyngeal swelling and ultimately P death. Alternatively the bacteria from the initial

invasion could be contained, possibly within the double membrane structures seen in the TEM images (Figure 5.9C). Their proliferation could also be suppressed by action of the immune system. In some of these worms, these contained invasions remain latent until age-related deterioration occurs, e.g of the anti-bacterial responses. This could lead to the bacteria being free to resume proliferation throughout the pharynx and subsequently cause P death. This particular scenario proposes that the development of P death occurs in two distinct steps. Firstly, initial bacterial invasion, which ensues after mechanical injury. Then further escalation of the infection, which is promoted by age-related decline. In this model, the pharyngeal pathology associated with P death cannot simply be viewed as a result of infection and therefore something that should be ignored or eliminated for the purposes of ageing studies. Rather it is a pathology whose development requires the ageing process. Furthermore, it is a potential model for the study of damage or infections that remain latent until late life, when they become detrimental or virulent once again, due to the age-related decline of protective mechanisms.

Examples of this can also be seen in humans. Contact sports, such as rugby, often cause significant knee or hip injuries to participants. These may eventually heal, yet ex-international rugby players are more likely to develop osteoarthritis in their hips and knees in later life than the rest of the general population (Davies et al. 2016). Another example of this phenomenon is the *Varicella zoster* virus, which causes chicken pox in young children. Once the individual has recovered, the virus is not cleared from the body but remains in a latent state within nerve cells. In old age, it can reactivate and cause shingles, a disease much more severe than chicken pox (Herpes Zoster and Functional Decline Consortium 2015). Perhaps the example most relevant to the work presented here is latent tuberculosis (Campion et al. 2015). *Mycobacterium tuberculosis* can invade the lungs but then be enclosed within granulomas, similar to how initial *E. coli* invasion of the pharynx is sometimes also contained. These individuals have no symptoms and can carry the latent infection for many years. However in 5-15% of cases, the

bacteria are able to escape suppression, resulting in full progression of the disease. This demonstrates the importance of understanding the age-related mechanisms that can lead to the resurgence, in late life, of infections or injuries obtained early in life.

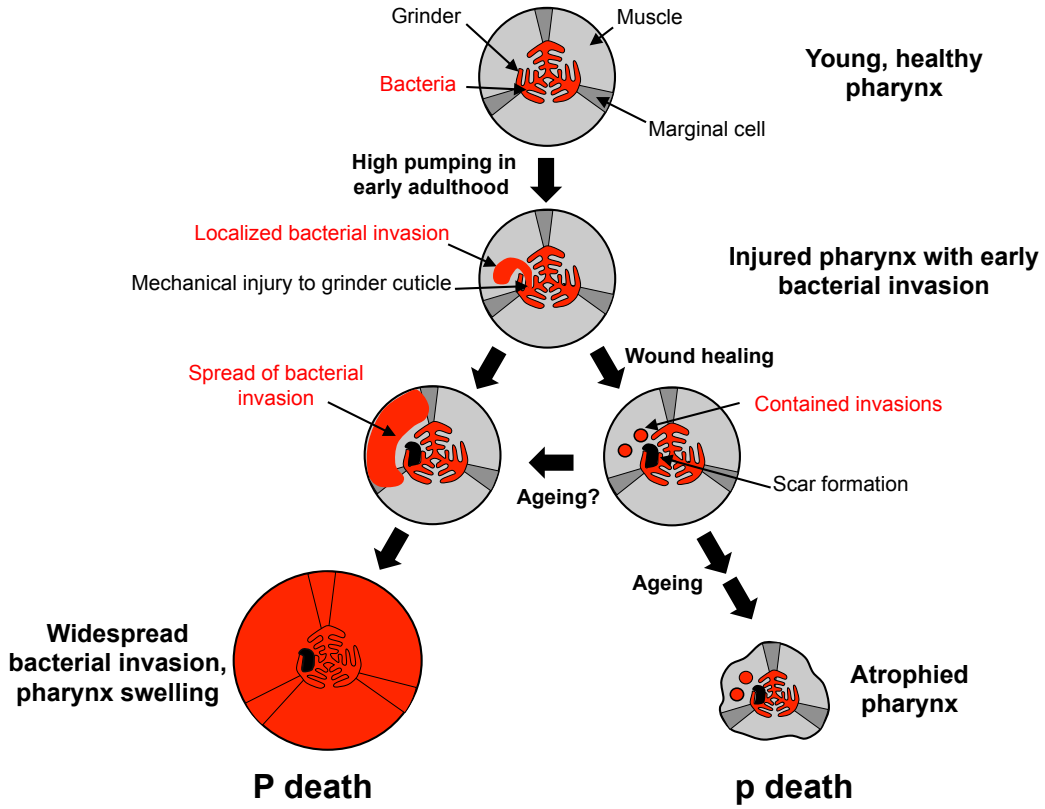

Figure 5.23. A proposed mechanism for the development of P death. High pumping rate during adulthood causes a localized injury to the pharyngeal cuticle near the grinder. This creates a route through which bacteria can invade into the pharyngeal tissue. Wound healing occurs at the injury site, resulting in the formation of a scar. In some worms the infection immediately starts to progress; in others it is slightly delayed as invasions are initially contained, before age-related deterioration results in the infection starting to spread. In these worms the bacteria proliferates throughout the pharynx causing it to swell. This results in a lethal pathology and subsequent P death. In p deaths, presumably if initial invasions do occur, the worm is able to keep them contained throughout life. The age-related pathology that kills worms that undergo p death is still not clear.

In worms that eventually undergo p death, either the mechanisms that inhibit the advancement of pharyngeal infection remain active throughout life, or other pathological changes that promote re-emergence of infection do not occur. Therefore the initial bacterial invasion remains contained, which could result in the OP50-RFP foci seen within the pharynxes of corpses from worms that underwent p death (Figure 5.8B,C). The lethal pathology in p death is currently unknown, though previous work from chapter 4 and M. Ezcurra et al. suggests that it could be intestinal atrophy.

5.3.2 Deconvolving mortality to solve the mysteries of ageing

Nearly 25 years ago, Cynthia Kenyon made the remarkable discovery that mutation of *daf-2* caused huge increases in lifespan in *C. elegans* (Kenyon et al. 1993). Since then many studies have shown that various other genes can also extend lifespan across a wide range of species, from yeast to mice (Kenyon 2010). Yet despite all these years of research, the biological mechanisms that drive the ageing process are still unknown. Why is this? The majority of work in the ageing field has focused mostly on searching for genes and pathways that have effects on lifespan. However it is difficult to establish a link between the biochemical activity of a gene product and a numerical parameter such as lifespan and mortality rate. For example, if mutation of a gene extends lifespan, while this result is interesting, a survival assay does not provide details on how pathologies are affected in these mutants. Without this information, it is very difficult, even impossible, to determine whether or how this gene contributes to the ageing process.

To solve this longstanding problem, we propose that future work on ageing can be helped by a more pathology centred approach, including a method we termed ‘mortality deconvolution’. This involves the investigation of both mortality and necropsy data. This should help us to understand how various mutations or treatments actually extend lifespan,

in terms of how they affect different senescent pathologies. If a pathology is lethal in a proportion of the population, extending lifespan must suppress or postpone its development. Given there are a large number of lethal age-related pathologies in humans and at least two forms of death in ageing *C. elegans*, different interventions that extend lifespan may achieve this by affecting different pathologies. If mortality deconvolution is performed, these differential effects on pathology may be revealed. For example, in this work, by deconvolving *eat-2(ad1116)* mutant mortality, Y. Zhao and H. Wang were able to demonstrate the longevity caused by mutation of *eat-2* is mostly due to a suppression of P death, rather than because of DR, as previously thought (Lakowski & Hekimi 1998). Furthermore, later work from Y. Zhao showed that the lifespan extension seen in *glp-1(e2141)* mutants was due to a delay in the occurrence of p death, with no effect seen on P death (Zhao et al., 2017). With such new approaches we can begin to be understand how the activity of certain genes contributes towards the biology of the ageing process. Thus lethal, senescent pathologies can be identified and their development inferred, paving the way for the discovery of treatments that could promote longevity.

Chapter 6 Conclusions

Here we have examined the development and underlying causes of a number of age-related pathologies across a range of different tissues in *C. elegans*. A central aim of my PhD was to determine what causes mortality in ageing *C. elegans*. To achieve this we set out to identify the tissue in the worm that develops life-limiting senescent pathology. Throughout this study we examined both previously described pathologies, such as uterine tumours, and novel ones that were discovered during this work, such as pharyngeal and tumour infection (Table 6.1). The *C. elegans* germline does undergo age-related deterioration, however work presented here in chapter 3 and elsewhere suggests that this is not lethal (Riesen et al. 2014; de la Guardia et al. 2016). On the other hand, we have demonstrated in chapter 5 that pharyngeal infection is almost certainly a cause of age-related mortality. We propose that this initial bacterial invasion is promoted by cuticular injury, caused by high pharyngeal activity in early life. This work has been supported by a recent publication that revealed that wild-type *C. elegans* dies prematurely due to bacterial infection (Podshivalova et al. 2017). In chapter 4, we also succeeded in gathering morphometric data on the ageing intestine, which allowed the dynamics of intestinal atrophy to be scrutinised, revealing that the majority of intestinal biomass is lost relatively early in adult life. Furthermore yolk accumulation and intestinal atrophy occur at similar times in the hermaphrodite (Ezcurra et al., unpublished). This suggests these two pathologies are related. We propose that intestine biomass conversion to yolk drives intestinal atrophy. Additionally, M. Ezcurra and A. Benedetto have shown that various interventions that extend lifespan also suppress intestinal atrophy, implying that this pathology could also be lethal (Ezcurra et al., unpublished).

In many cases we have provided evidence that quasi-programmes may be the main cause of the development of some of these pathologies, along with other contributory factors such as mechanical damage to the pharyngeal cuticle. For example, quasi-programmed apoptosis in the germline and run-on of yolk production in the intestine both appear to contribute to the development of age-related pathology in their respective tissues. This provides support for the hyperfunction theory of ageing. However degeneration of these tissues might not solely be due to quasi-programmes. Firstly, when apoptosis is blocked the hermaphrodite gonad still degenerates (de la Guardia et al. 2016). Secondly, even when intestinal biomass conversion is reduced by inhibiting autophagy, intestinal atrophy still occurs (Ezcurra et al, unpublished). Finally, it is unclear what age-related deteriorations result in widespread proliferation of bacteria within pharyngeal tissue. For example, damage to anti-bacterial proteins could lead to advanced pharyngeal infection. Therefore in these situations it is possible molecular damage could be driving the development of pathology.

Thus while this thesis have provided further evidence that hyperfunction promotes age-related pathology in *C. elegans*, it cannot be ruled out that molecular damage could also be a major contributory factor to the ageing process. Additionally, as emphasised in section 1.5, it is likely that in humans many different mechanisms will interact to promote age-related pathology.

We have also revealed sexual dimorphism in ageing *C. elegans,* as the male gonad and intestine seems to be largely protected from the pathologies seen in the hermaphrodite. Perhaps this is because males have a very different reproductive state to hermaphrodites, thus protecting them from pathologies that are driven by the large reproductive output of the hermaphrodite.

Hopefully future work will identify more life-limiting pathologies in both male and hermaphrodite *C. elegans*. For example, it is unknown what

kills worms that undergo p death. One possibility is intestinal atrophy, but it is likely there are still many other causes of death that have yet to be identified. The study of non-lethal pathology is also warranted as these pathologies are still related to ageing and can provide information about mechanisms that drive pathology, such as in the case of germline pathology in *C. elegans*. Furthermore even if they do not affect lifespan they may affect health span, such as reproductive ageing in humans. Thus by unravelling the complex mechanisms that drive age-related pathology, we hope future researches will gain fascinating insights into the ageing process.

Pathology	Possible causes
Uterine tumours (Golden et al. 2007)	Endoreduplicating unfertilised oocytes (McGee et al. 2012) Bacterial invasion
Intestinal atrophy (Herndon et al. 2002; McGee et al. 2011) (primarily between days 3 – 7)	Constipation (Garigan et al. 2002) Intestinal biomass conversion
Irregular intestinal atrophy	Contraction or atrophy of intestinal cell boundaries
Intestinal lumen dilation (Garigan et al. 2002)	Constipation (Garigan et al. 2002) Intestinal atrophy caused by intestinal biomass conversion
Yolk accumulation (Herndon et al. 2002; Garigan et al. 2002; DePina et al. 2011; McGee et al. 2011)	Continued synthesis post-reproduction (DePina et al., 2011; Garigan et al., 2002; Herndon et al., 2002) Intestinal biomass conversion
Pharyngeal swelling	Bacterial invasion (McGee et al. 2011)
Pharyngeal atrophy	Sarcopenia (Chow et al. 2006) Other bacterial effects

Table 6.1. The possible causes of pathologies examined in this study. Pathologies and possible causes in black have been previously described. Those in red have been discovered or proposed during this project.

Appendix 1. Statistics

Strain/condition	Number of deaths/ censors	Mean [median] life span (days)	% change vs. WT (no FUDR)	*p* vs. WT (no FUDR) (log rank)	% change vs. no FUDR	*p* vs. no FUDR (log rank)
N2 (wild-type)	**[C] 87/33** [1] 46/14 [2] 41/19	**17.0 [16]** 17.5 [16] 16.8 [14]				
mdl-1(tm311)	**[C] 98/22** [1] 49/11 [2] 49/11	**12.9 [14]** 12.4 [14] 13.3 [11]	**-24.1 [-12.5]** -29.1 [-12.5] -20.8 [-21.4]	**<0.0001** <0.0001 0.0027		
N2 (wildtype) 50μM FUDR	**[C] 112/8** [1] 55/5 [2] 57/3	**16.0 [16]** 17.3 [16] 14.6 [14]	**-5.9 [0]** -1.1 [0] -13.1 [0]	**0.0323** 0.5571 0.0227	**-5.9 [0]** -1.1 [0] -13.1 [0]	**0.0323** 0.5571 0.0227
mdl-1(tm311) 50μM FUDR	**[C] 103/17** [1] 54/6 [2] 49/11	**12.2 [11]** 12.7 [11] 11.6 [11]	**-28.2 [-31.3]** -27.4 [-31.3] -31.0 [-21.4]	**<0.0001** <0.0001 <0.0001	**-5.4 [-21.4]** +2.4 [-21.4] -12.8 [0]	**0.1854** 0.8005 0.0320

Table A.1. Survival statistics for wild-type and *mdl-1* treated with FUDR from L4.
[n] trial number, [C] combined data from all trials.

Strain/condition	Number of deaths/censored	Mean [median] life span (days)	% change vs. control	*p* vs. control (log rank)
N2 (control)	**[C] 157/42** [1] 67/18 [2] 90/24	**17.6 [18]** 16.6 [16] 18.3 [19]		
N2 (UV-killed)	**[C] 157/44** [1] 83/18 [2] 74/26	**26.6 [28]** 27.7 [28] 25.5 [25]	**+51.1 [+56]** +66.9 [+75] +39.3 [+32]	**<0.0001** <0.0001 <0.0001
N2 (control)	**[C] 419/75** [1] 42/8 [2] 277/51 [3] 59/6 [4] 41/10	**17.7 [17]** 17.9 [17] 18.8 [20] 17.2 [15] 18.7 [18]		
N2 (carbenicillin)	**[C] 225/13** [1] 50/0 [2] 68/1 [3] 67/9 [4] 40/3	**29.4 [30]** 30.4 [32] 30.5 [30] 29.7 [29] 27.1 [27]	**+66.1 [+76]** +69.8 [+88] +62.0 [+50] +73.0 [+93] +45.2 [+50]	**<0.0001** <0.0001 <0.0001 <0.0001 <0.0001

Table A.2 Survival statistics for growing wild-type worms on non-dividing bacteria. [n] trial number, [C] combined data from all trials.

Strain/condition	Number of deaths/censored	Mean [median] life span (days)	% change vs. control	*p* vs. control (log rank)
N2 (control)	**[C] 95/33** [1] 37/19 [2] 58/14	**19.1 [18]** 19.5 [21] 18.8 [18]		
N2 (day 1 shift off carbenicillin)	**[C] 110/15** [1] 50/7 [2] 60/8	**19.0 [19]** 19.0 [19] 19.1 [18]	**-0.5 [+5.6]** -2.6 [-9.5] +1.6 [0.0]	**0.9469** 0.4215 0.4972
N2 (day 2 shift off carbenicillin)	**[C] 111/14** [1] 52/5 [2] 59/9	**18.9 [21]** 19.2 [21] 18.6 [21]	**-1.0 [+16.7]** -1.5 [0.0] -1.1 [+16.7]	**0.8428** 0.6741 0.6125
N2 (day 4 shift off carbenicillin)	**[C] 109/9** [1] 54/1 [2] 55/8	**19.1 [18]** 18.1 [17] 20.0 [21]	**0.0 [0.0]** -7.2 [-19.0] +6.4 [+16.7]	**0.9957** 0.1169 0.1600
N2 (day 6 shift off carbenicillin)	**[C] 107/8** [1] 50/4 [2] 57/4	**20.7 [21]** 20.0 [19] 21.2 [21]	**+8.4 [+16.7]** +2.6 [-9.5] +12.8 [+16.7]	**0.1291** 0.7477 0.0115
N2 (day 11 shift off carbenicillin)	**[C] 107/1** [1] 48/0 [2] 59/1	**21.3 [21]** 21.1 [21] 21.5 [21]	**+11.5 [+16.7]** +8.2 [0.0] +14.4 [+16.7]	**0.0598** 0.9389 0.0092
N2 (day 15 shift off carbenicillin)	**[C] 101/1** [1] 47/0 [2] 54/1	**23.5 [24]** 24.3 [24] 22.8 [23]	**+23.0 [+33.3]** +24.6 [+14.3] +21.3 [+27.8]	**<0.0001** 0.0037 <0.0001
N2 (carbenicillin)	**[C] 116/13** [1] 50/8 [2] 66/5	**27.2 [28]** 24.8 [24] 29.0 [30]	**+42.4 [+55.6]** +27.2 [+14.3] +54.3 [+66.7]	**<0.0001** 0.0002 <0.0001
N2 (control)	[1] 67/18	16.6 [16]		
N2 (day 1 shift off UV-killed)	[1] 66/9	16.6 [14]	0.0 [-12.5]	0.7922
N2 (day 2 shift off UV-killed)	[1] 61/14	19.6 [21]	+18.1 [+31.25]	0.0233
N2 (day 4 shift off UV-killed)	[1] 62/13	19.2 [21]	+15.7 [+31.25]	0.0979
N2 (day 6 shift off UV-killed)	[1] 61/14	20.3 [21]	+22.3 [+31.25]	0.0201
N2 (day 11 shift off UV-killed)	[1] 65/10	21.7 [21]	+30.7 [+31.25]	0.0010
N2 (day 15 shift off UV-killed)	[1] 64/11	22.6 [23]	+36.1 [+43.8]	<0.0001
N2 (UV-killed)	[1] 83/18	27.7 [28]	+66.9 [+75.0]	<0.0001

Table A.3. Survival statistics for maintaining wild-type worms on non-dividing bacteria, until various time points in adulthood. [n] trial number, [C] combined data from all trials.

Strain/condition	Number of deaths/ censors	Mean [median] life span (days)	% change vs. control	*p* vs. control (log rank)
Control	**[C] 184/31** [1] 94/12 [2] 90/19	**14.4 [14]** 13.1 [12] 15.7 [15]		
Glass (from L4 stage to day 4)	**[C] 200/18** [1] 99/8 [2] 101/10	**14.2 [14]** 12.9 [12] 15.5 [15]	**-1.4 [0]** -1.5 [0] -1.3 [0]	**0.6269** 0.4393 0.4403

Table A.4. Survival statistics for worms fed ground glass. [n] trial number, [C] combined data from all trials.

Strain/condition	Number of deaths/ censors	Mean [median] life span (days)	% change vs. HCl control	*p* vs. HCl control (log rank)
1 mM HCl (from L4 stage to day 8)	[1] 64/19	15.4 [16]		
12mM serotonin (from L4 stage to day 8)	[1] 42/41	13.7 [14]	-11.0 [-12.5]	0.2078
1 mM HCl (from day 4 to day 8)	[1] 76/34	14.8 [14]		
12mM serotonin (from day 4 to day 8)	[1] 87/30	13.6 [12]	-8.1 [-14.3]	0.4341

Table A.5. Survival statistics for worms treated with serotonin.

Strain/ condition	Number of deaths/ censored	Mean [median] lifespan (days)	% change vs. N2 control	*p* vs. control (log rank)
N2 (control)	**[C] 109/31** [1] 46/24 [2] 63/7	**18.6 [19]** 18.8 [18] 18.4 [19]		
eat-2(ad1116)	**[C] 109/23** [1] 55/15 [2] 54/8	**21.4 [21]** 21.2 [21] 21.6 [23]	**+15.1 [+10.5]** +12.8 [+16.7] +17.4 [+21.1]	**0.0009** 0.0440 0.0039

Table A.6. Survival statistics for the *eat-2* mutant. [n] trial number, [C] combined data from all trials.

Genotype	Comparison	F	Df	P	Significance
mab-3 male	Interaction	8.008	2 ,114	0.0006	***
	Age	23.78	2, 114	<0.0001	****
	vit-5,6	45.91	1, 114	<0.0001	****
mab-3 herm	Interaction	10.47	2, 114	<0.0001	****
	Age	54.10	2, 114	<0.0001	****
	vit-5,6	51.90	1, 114	<0.0001	****
him-5 male	Interaction	2.721	2, 114	0.0701	n.s
	Age	9.904	2, 114	0.0001	***
	vit-5,6	0.0095	1, 114	0.9225	n.s
him-5 herm	Interaction	12.91	2, 114	<0.0001	****
	Age	71.09	2, 114	<0.0001	****
	vit-5,6	73.31	1, 114	<0.0001	****

Table A.7 Two-way ANOVA statistics for the effect of *vit-5,6* RNAi on lipid pool scores during ageing in *mab-3(mu15)* and *him-5(e1490)* males and hermaphrodites.

Genotype	Comparison	F	Df	P	Significance
mab-3 male	Interaction	0.0247	2, 114	0.9756	n.s
	Age	101.9	2, 114	<0.0001	****
	vit-5,6	0.5983	1, 114	0.4408	n.s
mab-3 herm	Interaction	7.431	2, 114	0.0009	***
	Age	131.9	2, 114	<0.0001	****
	vit-5,6	6.175	1, 114	0.0144	*
him-5 male	Interaction	2.273	2, 114	0.1077	n.s
	Age	4.165	2, 114	0.0180	*
	vit-5,6	0.0572	1, 114	0.8113	n.s
him-5 herm	Interaction	2.262	2, 114	0.1088	n.s
	Age	81.55	2, 114	<0.0001	****
	vit-5,6	30.88	1, 114	<0.0001	****

Table A.8 Two-way ANOVA statistics for the effect of *vit-5,6* RNAi on intestinal atrophy during ageing in *mab-3(mu15)* and *him-5(e1490)* males and hermaphrodites.

Appendix 2. Publications

Riesen, M., Feyst, I., Rattanavirotkul, N., Ezcurra, M., Tullet, J., Papatheodorou, I., Ziehm, M., Au, C., **Gilliat, A**., Hellberg, J., Thornton, J. and Gems, D., 2014. MDL-1, a growth- and tumor-suppressor, slows aging and prevents germline hyperplasia and hypertrophy in *C. elegans*. Aging. 6, 98-117.

de la Guardia, Y., **Gilliat, A. F**., Hellberg, J., Rennert, P., Cabreiro, F. and Gems, D., 2016. Run-on of germline apoptosis promotes gonad senescence in *C. elegans*. Oncotarget. 7, 39082-39096

Zhao, Y.*, **Gilliat, A. F**.*, Ziehm, M., Turmaine, M., Wang H., Ezcurra, M., Yang C., Phillips, G., McBay, D., Zhang W. B., Partridge, L., Pincus Zachary and Gems, D., 2017. Two forms of death in ageing *Caenorhabditis elegans*. Nature Comm.

*Authors contributed equally

www.impactaging.com AGING, February 2014, Vol. 6, No 2

Research Paper

MDL-1, a growth- and tumor-suppressor, slows aging and prevents germline hyperplasia and hypertrophy in *C. elegans*

Michèle Riesen[1], Inna Feyst[1], Nattaphong Rattanavirotkul[1], Marina Ezcurra[1], Jennifer M.A. Tullet[1], Irene Papatheodorou[2], Matthias Ziehm[2], Catherine Au[1], Ann F. Gilliat[1], Josephine Hellberg[1], Janet M. Thornton[2], and David Gems[1]

[1]*Institute of Healthy Ageing, and Research Department of Genetics, Evolution and Environment, University College London, London, United Kingdom;*
[2]*European Molecular Biology Laboratory, European Bioinformatics Institute, Wellcome Trust Genome Campus, Hinxton, Cambridge, United Kingdom*

Key words: *aging, C. elegans, FoxO, germline, hyperplasia, hypertrophy, Mad transcription factor*
Received: *12/22/13; Accepted: 2/14/14; Published: 2/16/14*
Correspondence to: *David Gems, PhD;* ***E-mail:*** *david.gems@ucl.ac.uk*

Copyright: *© Riesen et al. This is an open-access article distributed under the terms of the Creative Commons Attribution License, which permits unrestricted use, distribution, and reproduction in any medium, provided the original author and source are credited*

Abstract: In *C. elegans*, increased lifespan in *daf-2* insulin/IGF-1 receptor mutants is accompanied by up-regulation of the MDL-1 Mad basic helix-loop-helix leucine zipper transcription factor. Here we describe the role of *mdl-1* in *C. elegans* germline proliferation and aging. The deletion allele *mdl-1(tm311)* shortened lifespan, and did so significantly more so in long-lived *daf-2* mutants implying that *mdl-1(+)* contributes to effects of *daf-2* on lifespan. *mdl-1* mutant hermaphrodites also lay increased numbers of unfertilized oocytes. During aging, unfertilized oocytes in the uterus develop into tumors, whose development was accelerated by *mdl-1(tm311)*. Opposite phenotypes were seen in *daf-2* mutants, i.e. *mdl-1* and *daf-2* mutant germlines are hyperplastic and hypoplastic, respectively. Thus, MDL-1, like its mammalian orthologs, is an inhibitor of cell proliferation and growth that slows progression of an age-related pathology in *C. elegans* (uterine tumors). In addition, intestine-limited rescue of *mdl-1* increased lifespan but not to wild type levels. Thus, *mdl-1* likely acts both in the intestine and the germline to influence age-related mortality.

INTRODUCTION

In most animals, advancing age is accompanied by the deteriorative process of aging (senescence). Aging is the main cause of severe illness and death in humans, but the proximate biological mechanisms that cause it have proved difficult to identify. One approach to understand aging is to study simple model organisms [1], such as the nematode *Caenorhabditis elegans* which is particularly suitable for this purpose given e.g. its sequenced genome and very short lifespan (2-3 weeks).

The identification from the 1980s onwards of many *C. elegans* mutants with altered aging rate [1] led to optimism that discovery of gene products of aging control genes would reveal the mechanisms of aging in this organism. Yet although many signaling pathways and processes affecting aging rate have been identified, the nature of aging itself has remained obscure. For example, mutation of the *daf-2* insulin/IGF-1 receptor gene can more than double adult lifespan [2]. This increase requires the presence of the DAF-16 FoxO transcription factor [2-4], suggesting that transcriptional targets of DAF-16 encode proximal biochemical determinants of aging. But these target genes have proved to be very numerous [5, 6], 2,274 by one estimate [7], complicating the search for DAF-16 target genes that control aging. Understanding DAF-16/FoxO action is important, particularly because the role of insulin/IGF-1 signaling and FoxO in the control of aging shows evolutionary conservation, e.g. in the fruitfly Drosophila [8], and perhaps even in humans,

where age changes in allele frequency e.g. of the IGF-1 receptor and FoxO3A genes have been detected [1].

One approach to understand DAF-16 action is to map the gene regulatory network in which it acts. Previously we used a genome-wide approach to identify genes to which DAF-16 both binds and causes a change in gene expression [9]. This identified a mere 65 high confidence DAF-16 direct targets, which were enriched for genes encoding proteins involved in signaling and gene regulation, and transcription factors. Among the latter class was *mdl-1* (Mad-like 1), which encodes a basic helix-loop-helix (bHLH) TF homologous to mammalian Mad transcription factors [10] (Figure 1A). In mammals, Mad TFs act as heterodimers with Max bHLH TFs. Mad competes with Myc bHLH TFs to dimerize with Max, and bind to target genes containing E-box sequences (5'-CANNTG-3') [11]. Myc/Max dimers mainly activate gene expression, and are a major activator of cell proliferation of growth. By contrast, Mad/Max dimers mainly inhibit gene expression, antagonizing Myc/Max, and suppressing cell division and growth [11]. Inhibition of gene expression by Mad/Max is facilitated by recruitment of the Sin3 histone deacetylase (HDAC) corepressor complex. Myc TFs are potent oncogenes, while Mad TFs show some properties of tumor suppressors [11].

Our attention was drawn to *mdl-1* for several reasons. First, many genes that promote growth also promote aging [12]. Thus, growth suppressors activated by DAF-16 are candidates for downstream effectors slowing aging, and MDL-1, as a Mad TF, is a potential growth suppressor and, in fact, can suppress activated cMyc/Ras-induced cell transformation in mammalian cells [10]. Second, four mammalian Mad TFs, *mad1, mxi1, mad3* and *mad4*, are up-regulated by FoxO3a in a human colorectal adenocarcinoma cell line [13]. Thus, regulatory interactions between FoxO and Mad show at least some evolutionarily conservation between nematodes and mammals. Consistent with this, in *C. elegans mdl-1* is an activator of intestinal expression of *ftn-1* (H ferritin, an iron storage protein) [14], while in mammals, Myc can repress H ferritin expression, which contributes to cell proliferation [15].

C. elegans possesses several Max-like (*mxl*) genes, including *mxl-1* which can form heterodimers with MDL-1 but, surprisingly, lacks Myc [10, 16, 17]. Previous RNAi screens have not detected major effects of expression knockdown of *mdl-1* or *mxl-1* (Wormbase.org). However, *mdl-1* exerts some influence upon the germline, as follows. Loss of *daf-2* inhibits lethal, *gld-1*-induced distal germline tumors via decreased cell division and increased DAF-16/p53-dependent apoptosis [18], and *mdl-1* is a mediator of this inhibition [19]. Moreover, RNAi of *mdl-1* can reduce *daf-2* mutant longevity, but has little effect on lifespan in *daf-2*(+) worms [6].

In this study, we explore the possible role of *mdl-1* as a downstream effector of DAF-16 in the control of aging. In particular, we detail the phenotypic effects of mutation of *mdl-1*. We report that *mdl-1* acts as a repressor of germline hyperplasia and hypertrophy which otherwise contributes to age-related pathology in the germline.

RESULTS

mdl-1(tm311) increases production of unfertilized oocytes

To investigate *mdl-1* gene function, we studied the *mdl-1(tm311)* mutant allele, which contains a 471 bp base pair deletion that removes exon 2 of the gene (Figure 1A). This results in a frame shift after 51/281 amino acid residues and loss of the entire bHLH domain, implying that this is a null allele. The mutation was first backcrossed 6x into the *Caenorhabditis* Genetics Center wild type male stock to remove possible second site mutations, and ensure a wild type background [20].
Previous work on *mdl-1* and the function of Mad TFs in mammals led to several expectations about the possible effects of *mdl-1(0)*. First, since it is a DAF-16-activated gene, it might suppress *daf-2* mutant traits, e.g. constitutive dauer larva formation (Daf-c), stress resistance and increased longevity (Age). Second, since Mad TFs inhibit cell division and growth, *mdl-1(0)* might increase either somatic growth or germline proliferation.

We first examined effects of *mdl-1(0)* on somatic development and growth in wild type and *daf-2* mutant backgrounds. *mdl-1(0)* had no detectable effect on larval or adult growth (Figure 1B), but caused a slight reduction in constitutive dauer formation in *daf-2(m577)* mutants (Figure 1C). Next we probed the effects of *mdl-1* on the germline, first by looking at levels of fertility. The number of progeny produced by self-fertilized hermaphrodites was not affected by *mdl-1(0)*, either in terms of overall brood size or reproductive schedule (Figure 1D,E). As self sperm becomes depleted, N2 hermaphrodites start laying unfertilized oocytes [21]. Notably, *mdl-1(0)* caused a marked increase in the number of unfertilized oocytes laid, from 121 ± 15 to 219 ± 30, an 81% increase (Figure 1D). *mdl-1*(RNAi) applied to RNAi-sensitive *rrf-3(pk1426)* mutants also increased unfertilized oocyte number (data not shown).

In *daf-2(m577)* mutants, progeny number was also not different to N2, but the number of unfertilized oocytes laid was significantly reduced (Figure 1D,E), consistent with previous findings [22]. For convenience, to describe this mutant phenotype we introduce the term Uno (abnormal in unfertilized oocyte production), and Uno-o, to describe mutants that are unfertilized oocyte over-producers (e.g. *mdl-1*), and Uno-d, to describe mutants that are unfertilized oocyte deficient (e.g. *daf-2*).

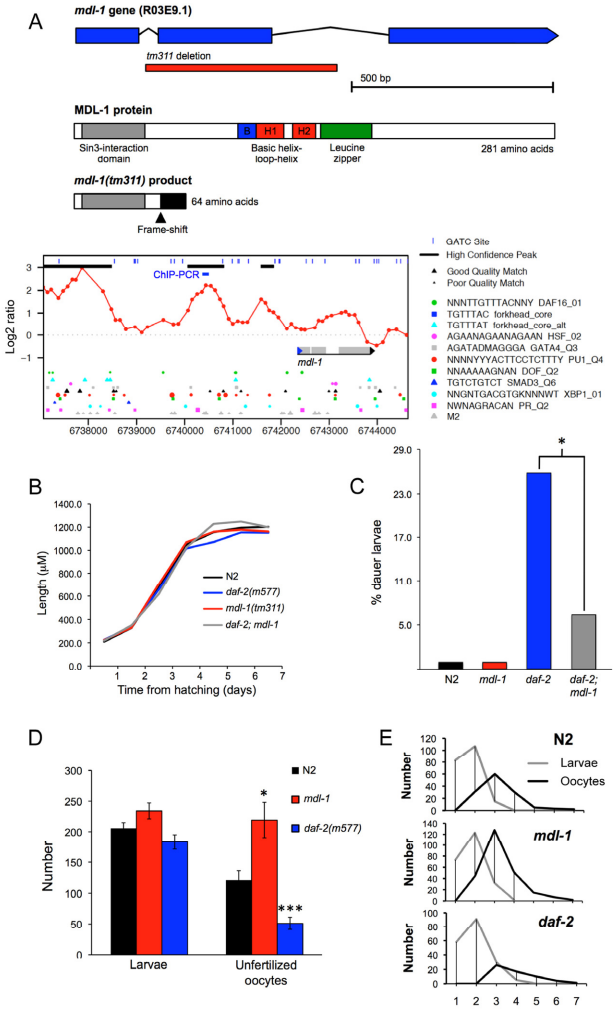

Figure 1. Phenotypic analysis of *mdl-1(tm311)* mutant. (A) *mdl-1* gene and protein description, including *tm311* deletion and effects on protein, DAF-16 binding sites (chromatin profile [DamID] data and DBEs) and site of ChIP analysis. For chromatin profile, y axis represents log2 ratio of DAF-16 binding relative to control, and peaks correspond to potential DAF-16 binding sites [9]. **(B –F)**. Phenotypic effects of *mdl-1(0)*. **(B)** Little effect on larval and adult growth. Samples sizes ranged from 23-39. **(C)** *mdl-1(0)* slightly reduces *daf-2(m577)* Daf-c, measured at 22.9˚C. * $0.01 < p < 0.05$ (Student's *t* test). 4 trials conducted, in which *mdl-1(0)* reduced dauer formation in 3. **(D, E)** Effect of *mdl-1* and *daf-2* on fertility. Number of broods scored: N2, 19; *daf-2*, 20; *mdl-1*, 17. **(D)** Mean total progeny and unfertilized oocytes. * $0.01 < p < 0.05$, *** $p < 0.001$ (Student's *t* test). **(E)** Mean daily progeny and unfertilized oocyte numbers.

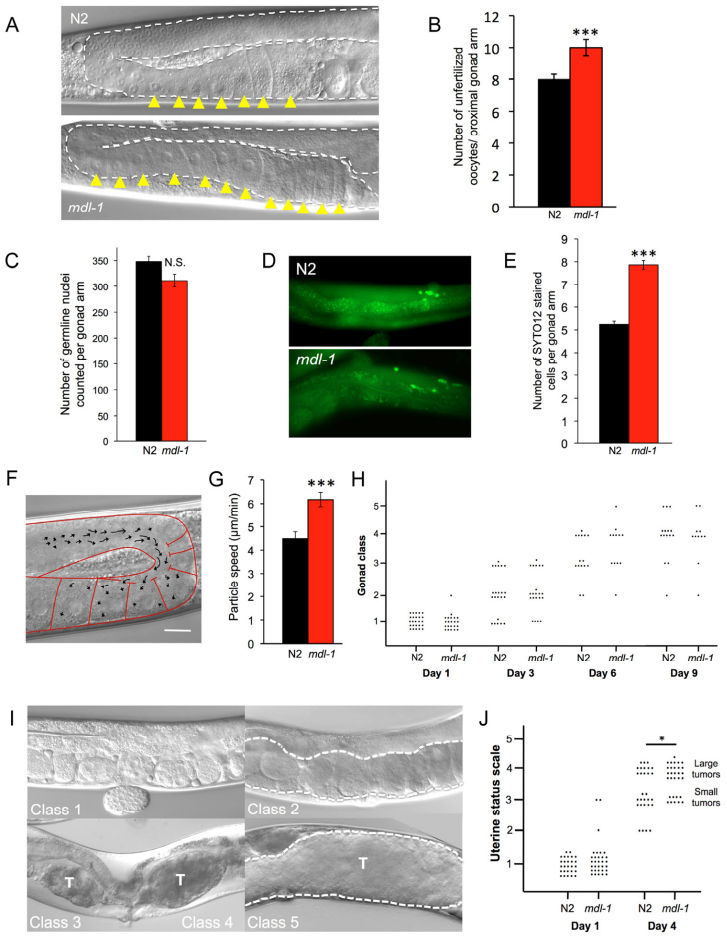

Figure 2. *mdl-1* causes hyperplasia and hypertrophy. (A, B) *mdl-1(0)* causes oocyte stacking in 1 day old worms. **(A)** Nomarski images. **(B)** Quantitation of stacking. Sample sizes: N2, 23; *mdl-1*, 17. *** $p < 0.001$ (Student's *t* test). **(C)** No effect of *mdl-1* on number of germline nuclei. $p > 0.05$ (Student's *t* test). **(D, E)** *mdl-1* increases levels of germline apoptosis. **(D)** Epifluorescence images of SYTO12 stained cells in young adult hermaphrodite germline. **(E)** Quantitated data. Number of gonads scored: N2, 153; *mdl-1*, 132. *** $p < 0.001$ (Student's *t* test). **(F, G)** *mdl-1* increases cytoplasmic streaming in the proximal gonad. **(F)** Single image obtained from a time-lapse recording. Arrows represent DIC-particle tracks. DIC-particles were tracked over a period of 1 minute. Scale bar: 20 µm. **(G)** Cytoplasmic streaming rate (mean particle speed ± standard error). 30 particle speed measurements performed for each genotype. Number of worms examined: N2, 4; *mdl-1*, 3. *** $p < 0.001$ (Student's *t* test). **(H)** Absence of effect of *mdl-1(0)* on gonad disintegration (25˚C). $p > 0.05$ for all comparisons of N2 *vs.* *mdl-1* of the same age (Wilcoxon Mann test). **(I)** Uterine status scale for quantitation of uterine tumor formation rate (5 classes). Class 1, normal uterus containing eggs (day 1 adult). Class 2, slightly abnormal uterine contents, but no tumor visible. Class 3, small tumor. Class 4, medium sized tumor. Class 5, large tumor, filling body cavity and squashing the intestine. Dotted line, outline of uterus. T, tumor. **(J)** *mdl-1(0)* increases uterine tumor formation (25˚C), data summed from 3 trials. * $0.01 < p < 0.05$ (Wilcoxon Mann test).

mdl-1(tm311) causes germline hyperplasia and hypertrophy

The *mdl-1* Uno-o phenotype suggests increased cell production in the germline distal to the spermatheca. To test this we compared proximal gonad contents in wild type and *mdl-1* animals on day 1 of adulthood. This revealed increased oocyte density, or stacking [23, 24], in *mdl-1* (Figure 2A,B), implying increased oocyte synthesis. This in turn suggests increased germ cell proliferation in the distal gonad. To probe this, we examined germ cell number by staining nuclei with the fluorescent DNA-binding dye 4',6-diamidino-2-phenylindole (DAPI), but no effect of *mdl-1* was detected (Figure 2C). However, an increase in the overall rate of germline cell turnover in *mdl-1* mutants could leave cell number unaffected.

If the distal proliferative zone is the source of germ cell nuclei, then the major sink is germline apoptosis. At least 50% [25] and as many as 97% [26] of germ cells undergo p53-independent, "physiological" apoptosis, their cytoplasm supplying expanding oocytes near the gonad bend. Using the SYTO 12 dye to detect apoptotic cell corpses, we found that *mdl-1* mutants showed a significant increase in apoptotic cell number in the germline in 3 out of 4 trials (Figure 2D, E).

The transfer of cytoplasm released by germ cells to nascent oocytes occurs by a process of cytoplasmic streaming (Figure 2F) [27]. We examined the effect of *mdl-1(0)* on the rate of cytoplasmic streaming in the mid-late pachytene region of the distal gonad, on day 1 of adulthood. Cytoplasmic streaming rate in *mdl-1* worms was significantly greater than in wild type (Figure 2G). Taken together, these results suggest that an increase in production of germ cells is matched by an increase in apoptosis, resulting in little change in overall germ cell number in the distal arm. Overall, this suggests that the increase in oocyte production is driven by a hyperplastic state in the distal gonad.

Next we studied the effect of *mdl-1* on pathologies of aging in the germline. The aging hermaphrodite gonad undergoes dramatic pathological changes. The distal gonad shrivels and eventually disintegrates [28, 29], while in the uterus large, amorphous masses (tumors) with very high DNA content develop [24, 29-31]. These tumors form from unfertilized oocytes which undergo multiple rounds of endoreduplication, and can grow to fill the entire body cavity in the mid-body. Continued germline apoptosis in late life contributes to gonad disintegration, and increased apoptosis rate is sufficient to increase gonad disintegration rate (Y. de la Guardia and D. Gems, unpublished). However, despite their increased apoptosis rate (Figure 2D,E) gonad disintegration rate was not detectably altered in *mdl-1* mutants (Figure 2H).

Casual observation of *mdl-1* hermaphrodites under Nomarski microscopy suggested an increase in uterine tumors in these mutants. To verify this, we used a semi-quantitative approach [28] with a uterine status scale. According to the appearance of the uterus, worms were scored from 1 (healthy, no tumors) to 5 (large tumors) (Figure 2I) (see Materials and Methods). Using this scale to compare N2 and *mdl-1* mutants confirmed that uterine tumors grow significantly faster in *mdl-1* worms (Figure 2J).

mdl-1 does not mediate effects of daf-2 on germline proliferative status

We next investigated whether MDL-1, like DAF-16, is an effector of *daf-2* mutant phenotypes. We first verified that DAF-16 acts directly on *mdl-1* to increase its expression, as predicted by mRNA and chromatin profiling studies [9]. Quantitative RT-PCR confirmed that *mdl-1* mRNA levels are higher in *daf-2* than in *daf-16; daf-2* strains (Figure 3A). Chromatin immuno-precipitation and PCR (ChIP-PCR) confirmed that DAF-16 binds to the *mdl-1* promoter (Figure 3B). This implies that *mdl-1* expression is activated by DAF-16 binding to its promoter.

mdl-1 mutants are Uno-o while *daf-2* mutants are Uno-d (Figure 1D,E) [22], and DAF-16 activates *mdl-1* expression (Figure 3A,B) [9]. This could imply that increased *mdl-1* activity in *daf-2* mutants reduces oocyte production. To test this we asked whether *mdl-1(tm311)* would suppress *daf-2* Uno-d, but it did not. Instead, *daf-2(m577); mdl-1* worms were Uno-d (Figure 3C), i.e. *daf-2* is epistatic to *mdl-1*. *daf-2(m577)* also suppressed *mdl-1* effects on oocyte stacking and uterine tumor formation (data not shown). These results negate our hypothesis that *daf-2* Uno-d is caused by *mdl-1* over-activity. A different model was suggested by additional epistasis data as follows. In a *daf-2*(+) background, *daf-16* suppressed *mdl-1* Uno-o, consistent with the observation that *daf-16* over-expression in a *daf-2*(+) background can cause germline hyperplasia [32]. Thus, DAF-16 promotes oocyte production in a *daf-2*(+) background but inhibits it in a *daf-2(m577)* background (Figure 3D). Moreover, mutation of *daf-16* in a *daf-2; mdl-1* mutant did not restore MDL-1 Uno-o (Figure 3C). This suggests that MDL-1 suppresses the effect of DAF-16 on oocyte production in *daf-2*(+) worms, but plays no role in *daf-2* mutants (Figure 3D).

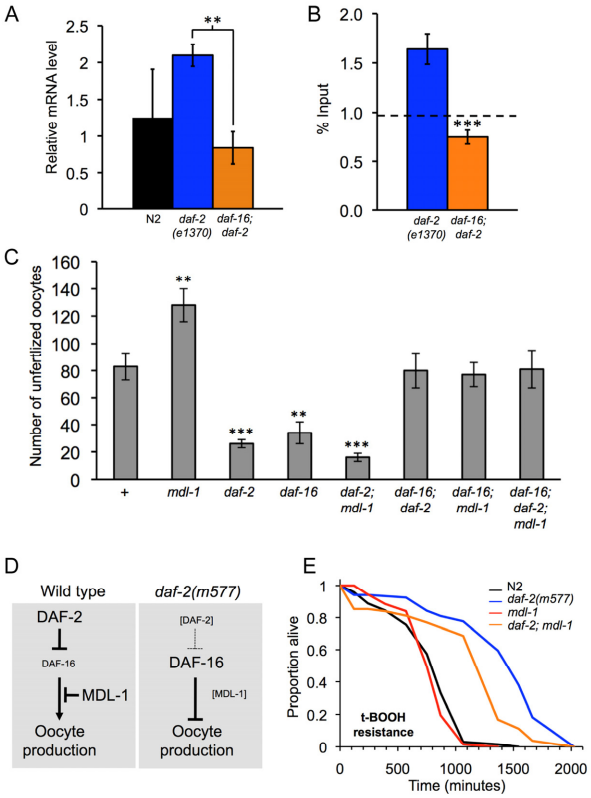

Figure 3. Distinct epistatic relationships between *daf-2* and *mdl-1* in hyperplasia and hypertrophy. (A, B). *mdl-1* is a direct transcriptional target of DAF-16. **(A)**. *mdl-1* mRNA levels are increased in *daf-2* relative to *daf-2; daf-16* (Q-PCR data). ** $0.001 < p < 0.01$. **(B)** DAF-16 binds to the *mdl-1* promoter (ChIP-PCR data). One experiment is shown which contained 3 immuno-precipitation replicates from the same chromatin preparation (error bars show the standard deviation between them). The dotted line shows the average inputs from 3 genes/genomic regions that do not show enrichment for DAF-16 binding in *daf-2 vs daf-16; daf-2* in this particular trial, i.e. it reflects background DAF-16 binding levels. Significant DAF-16 binding was detected one of two additional trials. The position of the DAF-16 binding site detected is shown in Figure 1A. **(C)** *mdl-1*, *daf-2* and *daf-16* epistasis analysis with respect to unfertilized oocytes production (Uno). Total unfertilized oocyte production per worm was measured at 25˚C. Means of 12 broods assessed; error bars, standard error. ** $0.001 < p < 0.01$; *** $p < 0.001$ (Student's *t* test). **(D)** Model for interactions between DAF-2, DAF-16 and MDL-1, deduced from interactions between mutations. DAF-16 promotes oocyte production in *daf-2*(+) worms, but inhibits it in *daf-2(m577)* worms. MDL-1 acts via DAF-16 to inhibit oocyte formation in *daf-2*(+) worms, but does not influence oocyte production in *daf-2(m577)* worms. **(E)** Resistance to 7.5 mM *tert*-butylhydroperoxide (*t*-BOOH). Sample sizes (censored values): N2, 67 (7); *daf-2(m577)*, 61 (8); *mdl-1,* 67 (8); *daf-2; mdl-1,* 70 (12). Probability of being the same: N2 *vs. mdl-1*, $p = 0.24$; *daf-2 vs. daf-2; mdl-1*, $p < 0.001$ (log rank test).

daf-2 mutants exhibit various forms of stress resistance, including oxidative stress resistance (Oxr) [33]. We tested whether MDL-1 contributes to *daf-2* Oxr, specifically to *tert*-butylhydroperoxide (*t*-BOOH). In a wild-type background, *mdl-1(0)* did not affect Oxr, while *daf-2(m577)* markedly increased Oxr (Figure 3E). Notably, in a *daf-2(m577)* background, *mdl-1(0)* significantly decreased Oxr. This implies that MDL-1 contributes to *daf-2* Oxr.

MDL-1 contributes to *daf-2* mutant longevity by reducing baseline hazard

Next, we examined the effect of *mdl-1* on aging. First we compared effects of *mdl-1*(RNAi) on lifespan in *rrf-3* and *rrf-3; daf-2(e1368)* strains (25˚C), and detected a reduction in lifespan only in the latter strain (data not shown), consistent with previous observations [6]. We then assessed the effect of *mdl-1(tm311)* on lifespan in wild-type or *daf-2(m577)* mutant backgrounds. *mdl-1* decreased lifespan in both wild-type and *daf-2* backgrounds, but the decrease was proportionally greater in the latter (Figure 4A, Table S1). This corresponded to a significantly greater *mdl-1*-induced increase in mortality in a *daf-2* background (4.5-fold vs 1.8-fold; significant interaction term, $p < 10^{-15}$, Cox proportional hazard analysis), suggesting that *mdl-1* activity contributes to the *daf-2* longevity increase.

To further characterize the effect of *mdl-1* on aging, we examined its effect on the pattern of age-specific mortality in wild-type and *daf-2(m577)* backgrounds. Aging animal populations typically show exponential increases in mortality rate, and in *C. elegans* this occurs in two stages, with an initial faster exponential increase and a subsequent slower exponential increase [34, 35]. We fitted mortality data to a logistic model, which contains 3 components: a baseline hazard (initial mortality rate, parameter *a*), a mortality increase rate (parameter *b*) and a late-life mortality deceleration (parameter *s*).

In this analysis we wanted to probe whether *mdl-1(tm311)* shortens lifespan by accelerating aging or whether it could act by a life-shortening effect unrelated to aging. An effect of *mdl-1* on parameters *b* and *s* would imply an effect on aging, whereas an effect on parameter *a* could imply a non-aging related deleterious effect. In fact, *mdl-1* increased baseline hazard (*a*) without affecting the mortality increase rate (*b*) (Figure 4B-D). By contrast, relative to wild type, *daf-2(m577)* markedly decreased parameters *b* and *s*, while also slightly increasing parameter *a*. Reducing insulin/IGF-1 signaling has long been known to slow the age-related mortality rate increase [36]. In a *daf-2* background, *mdl-1(0)* again increased baseline hazard, and had no significant effect on parameters *b* and *s* ($p > 0.05$) (Figure 4C,D). In summary, this analysis confirms that *daf-2* increases lifespan by slowing demographic aging, while *mdl-1* shortens lifespan mainly by increasing baseline hazard. That *mdl-1* shortens lifespan more in a *daf-2* background could imply that MDL-1 contributes to *daf-2* longevity by reducing baseline hazard (see Discussion).

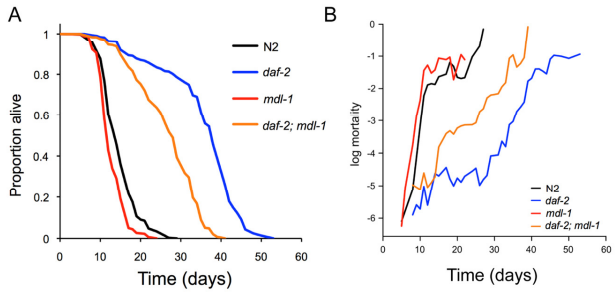

C

	a	*b*	*s*
N2	0.00051	0.500	1.679
daf-2(m577)	0.00069	0.133	0.032
mdl-1(tm311)	0.00094	0.500	1.023
daf-2; mdl-1	0.00155	0.152	$2.5*10^{-07}$

D

	a	*b*	*s*
N2 - *daf-2*	$7.8*10^{-03}$	$2.2*10^{-46}$	$2.0*10^{-26}$
N2 - *mdl-1*	$8.2*10^{-07}$	0.984	$9.6*10^{-06}$
daf-2 - *daf-2; mdl-1*	$4.0*10^{-03}$	0.065	0.582
mdl-1 - *daf-2; mdl-1*	$5.1*10^{-06}$	$2.7*10^{-46}$	$1.2*10^{-12}$

Figure 4. Effects of *mdl-1* on aging. (A) Effects of *mdl-1(tm311)* on lifespan (for statistics, see Table S1, combined data). **(B)** Effect of *mdl-1* on age-specific mortality profiles. **(C, D)** Mortality analysis using logistic model. **(C)** Estimated values of logistic model parameters. **(D)** Probability, *p*, of parameters in compared genotypes being the same, holding other parameters constant.

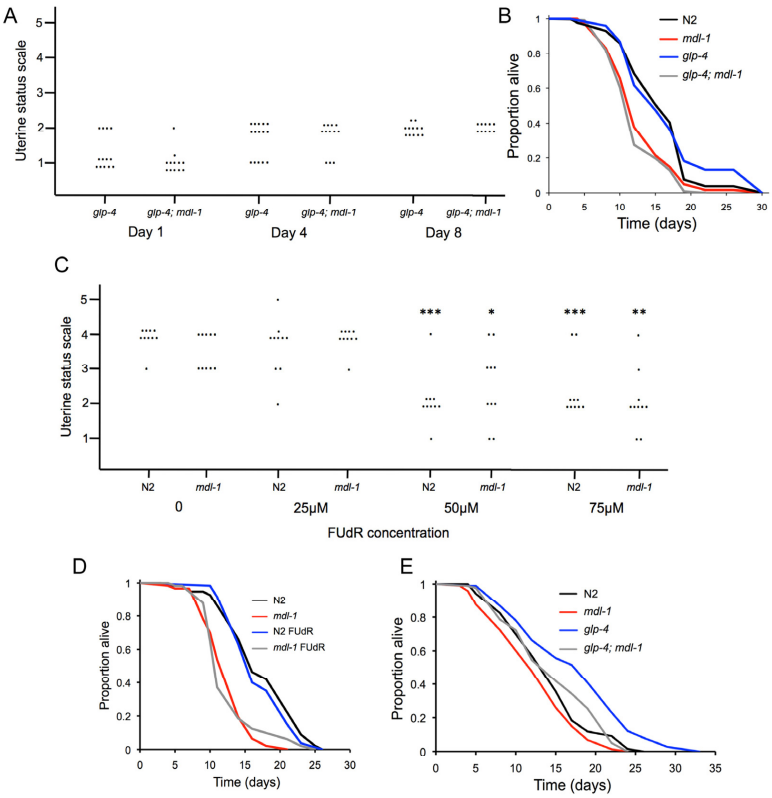

Figure 5. **No effect of uterine tumors on lifespan. (A)** Uterine tumors are not seen in *glp-4(bn2)* mutants (raised at 15˚C to L4 then shifted to 25˚C). Uterine classes 2-5 indicate presence of tumors. Each dot corresponds to a uterine status measurement. **(B)** *glp-4* does not suppress *mdl-1* effects on lifespan (for statistics, see Table S2, trial 1). **(C)** FUdR suppresses formation of uterine tumors at 50µM or greater. Stars represent a significant difference to worms of the same genotype in the absence of FUdR. No significant difference in tumor levels between N2 and *mdl-1* were detected at this age at any FUdR concentration. * $0.01 < p < 0.05$; ** $0.001 < p < 0.01$; *** $p < 0.001$ (Wilcoxon Mann test). **(D)** 50µM FUdR does not suppress *mdl-1* shortevity or increase N2 lifespan (for statistics, see Table S2, trial 1). **(E)** Effect of *mdl-1* on *glp-4* longevity (for statistics, see Table S2, trial 2).

Uterine tumors do not limit lifespan

mdl-1(0) accelerates formation of uterine tumors, which frequently grow very large, filling the body cavity in the mid-body region and squashing the intestine [31]. One possibility is that uterine tumors can contribute to mortality and that increased tumor formation in *mdl-1(0)* mutants causes a shortened lifespan. To test this, we examined the effect of *mdl-1* on lifespan in the absence of uterine tumors. *glp-4(bn2)* mutants have a temperature-sensitive germline proliferation defect; if raised at 15˚C to L4 and then switched to 25˚C, oocyte production is blocked but longevity is not increased [7]. We first confirmed that *glp-4* blocks formation of uterine tumors (Figure 5A). We then compared lifespan in *glp-4*, *mdl-1* and *glp-4; mdl-1* worms. *glp-4* worms were normal-lived, but both *mdl-1* strains were similarly short lived (Figure 5B; Table S2).

We also blocked uterine tumor formation using the inhibitor of DNA replication 5-fluoro-deoxyuridine (FUdR), which is also commonly used to treat colorectal cancer. Application of FUdR at low concentrations (e.g. 10-25μM) from L4 stage is a convenient means to block progeny production, and has little effect on lifespan [37]. 50μM FUdR, but not lower FUdR concentrations, was sufficient to block formation of uterine tumors (Figure 5C). We then compared effects of 50μM FUdR on lifespan in wild type and *mdl-1* worms, and saw no effect on lifespan in either case (Figure 5D; Table S2). These results show that accelerated formation of uterine tumors do not cause the shorter lifespan of *mdl-1* worms. They also demonstrate that uterine tumors do not limit lifespan in wild type worms under standard culture conditions. This contrasts with the case of *daf-16* over-expression, where life shortening is suppressed by blocking germline hyperplasia either with *glp-1* or FUdR [32].

A number of interventions that remove the hermaphrodite germline cause increased lifespan, including raising *glp-4(bn2)* mutants at 25˚C, and this effect is *daf-16* dependent [38, 39]. Notably, *mdl-1(0)* also reduced the longevity of *glp-4* mutants raised at 25˚C (Figure 5E, Table S2). *mdl-1* shortened lifespan more in a *glp-4* background than in a wild-type background (Table S2). This suggests that *mdl-1(+)* contributes to *glp-4* longevity as well as *daf-2* longevity.

Evidence that *mdl-1* can act in the intestine to promote longevity

The intestine plays an important role in *daf-2* mutant longevity [40], and is a site of *mdl-1* expression [10]. One possibility is that *mdl-1* affects intestinal protein synthesis. Mutation of *daf-2* causes a global reduction in protein synthesis, which may contribute to longevity [41, 42]. In aging hermaphrodites, yolk proteins (vitellogenins) become very abundant indeed [43, 44], and this accumulation is suppressed *daf-2*, apparently by inhibition of protein translation in the intestine [45] where yolk is synthesized [46]. Thus, vitellogenin accumulation rate gives some indication of intestinal protein synthesis rate. However, *mdl-1(0)* did not alter vitellogenin accumulation, either in wild type or *daf-2* mutant backgrounds (Figure 6A,B). One possibility is that *mdl-1* mutants do synthesize more vitellogenin, but due to increased laying of unfertilized oocytes, this does not result in increased vitellogenin accumulation. To check this we compared sterile *glp-4* and *glp-4; mdl-1* worms (shifted at L4 to 25˚C), but again no effect of *mdl-1* was seen (Figure 6A,B).

Next, we asked whether intestine-limited rescue of *mdl-1* using the *ges-1* promoter [47] would rescue *mdl-1* shortevity. A transgene array from which *mdl-1* was expressed using its own promoter was able to restore wild-type lifespan to *mdl-1(tm311)* mutants (Figure 6C; Table S3). Notably, *pges-1::mdl-1* too increased lifespan in *mdl-1* mutants, though the effect was smaller such that lifespan was not restored to wild type. This suggests short lifespan in *mdl-1* mutants is caused by loss of *mdl-1* from several sites, including the intestine. Possibly, a second site of action of *mdl-1* on lifespan is the germline, given its impact on that tissue.

The extent of loss of Myc among nematodes

One puzzle relating to *mdl-1* function is the absence of Myc in *C. elegans*. In mammals, the Mad/Max/Myc system works in concert with the Tor pathways to control growth [48]. *C. elegans* also lacks key components of the Tor pathway, including the Tsc1/Tsc2 complex [49], and 4E-BP [50] (Figure 7A). To try to understand the significance of the absence of Myc in the broader context of nematode gene loss, we tested for the presence of Myc, Tsc1, Tsc2 and 4E-BP throughout the Nematoda. It was previously noted that Myc orthologs are absent not only from *C. elegans* and *C. briggsae*, but also the filarial parasite *Brugia malayi* (nematode order Spirurida), and even the bilharzia parasite *Schistosoma mansoni* (phylum Platyhelminth) [51]. Searching the genomes of 13 nematode species, including representatives of the major nematode orders, no Myc orthologs were detected (Figure 7B). Myc was also absent from all 5 platyhelminth species examined. This implies that Myc evolved in the common ancestor of arthropods and chordates after divergence from the common ancestor of nematodes and platyhelminths, as previously suggested [51]. Thus, the Myc-less Mad-Max circuit in *C. elegans* appears to represent a more ancient regulatory system.

By contrast, both Tsc1/Tsc2 and 4E-BP were found in several nematode groups but were absent from many others, in a pattern indicating that each gene has been lost several times during nematode evolution. For Tsc1 and Tsc2, gene loss was correlated, i.e. both genes were either present or absent. There was no correlation between loss of Tsc/Tsc2 and 4E-BP: nematode species exist with Tsc1/Tsc2 but lacking 4E-BP and vice versa. The distribution of Tsc1/Tsc2 is surprising in that most nematode and all platyhelminth groups lack this complex, apart from spirurid nematodes, and two rhabditid species. Sequence comparisons of Tsc1 and Tsc2 protein sequences from nematodes and other animal groups is consistent with multiple instances of gene loss (rather than horizontal gene transfer) (Figure 7C).

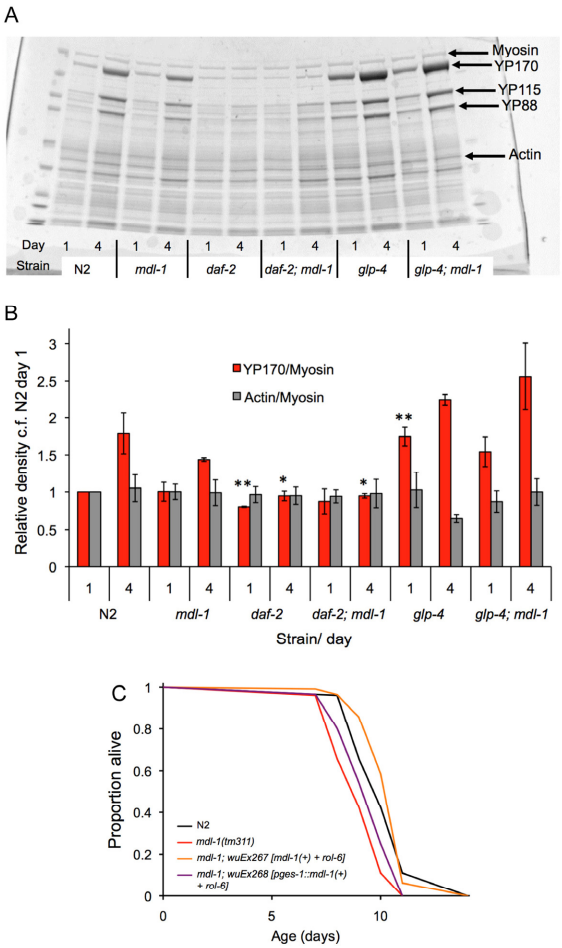

Figure 6. Tests for action of *mdl-1* in the intestine. (A,B) Effect of *mdl-1* on yolk accumulation. **(A)** Example of Coomassie stained gel with *C. elegans* protein extracts. **(B)** Bar graph data is derived from densitometric measurement of protein on gels (means of 3 biological replicates; error bars, standard error). It shows levels of the major yolk protein YP170 normalized to myosin levels (which are not expected to change), and again to levels in N2 on day 1. Actin/myosin ratio gives an indication of the reliability of myosin as a standard. * $0.01 < p < 0.05$; ** $0.001 < p < 0.01$, compared to N2 of the same age. **(C)** Effects on lifespan of *pges-1::mdl-1(+)* rescue of *mdl-1(0)* (for statistics, see Table S3, trial 2).

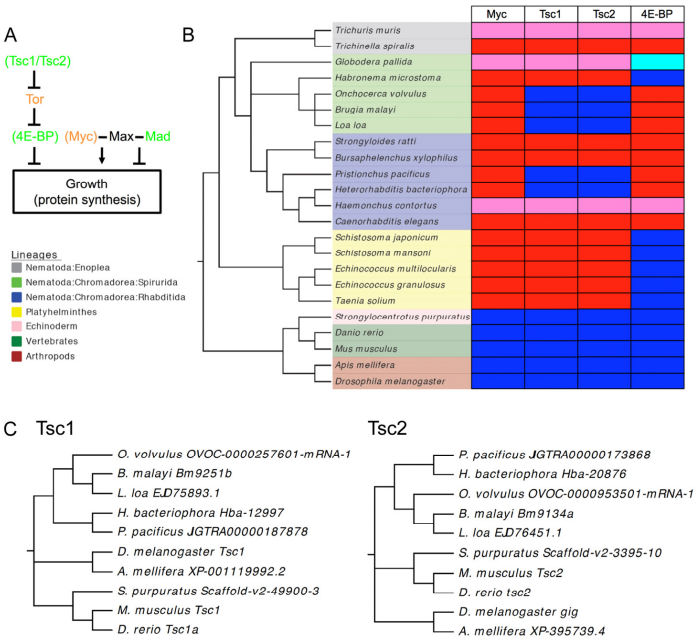

Figure 7. Extent of loss of Myc, Tsc1/Tsc2 and 4E-BP among the Nematoda. (A) Outline of missing elements of Tor and Myc/Max/Mad pathways in *C. elegans*. Green, tumor-suppressor/anti-aging; orange, oncogene/pro-aging. In brackets, proteins missing from *C. elegans*. **(B)** Presence and absence of Myc, Tsc1, Tsc2 and 4E-BP among nematodes and platyhelminths. Red, absent; dark blue, present; pink, not found; pale blue, putative but somewhat divergent 4E-BP. Not found: a caveat to this analysis may be the incompleteness of the genomic sequences of some of these species with draft assemblies being available for *G. pallida* and *H. contortus* and only contigs available for *T. muris*. **(C)** Phylodendrograms of Tsc1 and Tsc2 sequences for nematodes and other animal groups. Note that species and sequence phylogenies correspond.

DISCUSSION

In this study we have shown that MDL-1 acts as an inhibitor of germline proliferation, and of oocyte hypertrophy, thereby inhibiting a salient aging-related pathology (uterine tumors). These properties of *mdl-1* mutants recapitulate effects of Mad TFs in mammals, e.g. mice lacking the Mad TF Mxi1 show hyperplasia in a number of tissues (e.g. prostatic epithelium), and are tumor prone [52]. We also confirm that MDL-1 inhibits aging, consistent with the observed association between tumor suppressors and inhibition of aging [53, 54].

Does mdl-1 act downstream of daf-16?

Our initial hypothesis was that activation of *mdl-1* expression by DAF-16 contributes to *daf-2* longevity. The results of analysis of *mdl-1* expression (Figure 3A,B) and the effects on lifespan of *mdl-1(tm311)* (Figure 4A) are consistent with this hypothesis. We also noted that *mdl-1* and *daf-2* have opposing effects on the germline: *mdl-1(0)* causes Uno-o, increased oocyte stacking and increased uterine tumors (this study), while mutation of *daf-2* has opposite effects [22, 29]. This suggested that the effects of *daf-2* on the germline

might be mediated by *mdl-1*. However, epistasis analysis shows that this is not the case for oocyte production (Figure 3C). Instead *mdl-1* appears to have no effect on the germline in *daf-2* mutants, but to inhibit promotion of germline proliferation by DAF-16 in *daf-2*(+) worms (Figure 3D).

Does mdl-1 affect aging?

The life-shortening effect of *mdl-1(0)* is mainly the result of increased base-line hazard (Figure 4B-D). This could imply that *mdl-1(0)* does not affect aging but, rather, shortens lifespan by causing a pathology that is distinct from aging. In similar fashion, a comparison of mortality in two groups of people during the 1940s, either in Australia or interned by the Japanese, showed increased base-line hazard but not increased demographic aging in the latter [55]. It is interesting to consider whether this necessarily means that the effect of *mdl-1* on lifespan does not involve an effect on aging. The impact of *mdl-1(0)* on lifespan is greater in a *daf-2* background, suggesting that MDL-1 does contribute to *daf-2* longevity, i.e. that *mdl-1* does affect aging. Arguably, the critical point here is that something that affects demographic aging necessarily affects biological aging, while something that affects base-line hazard may or may not affect biological aging. In other words, the biological process of aging is not always the same thing as demographic aging.

One working definition of biological aging is the set of endogenously generated pathologies that increase in later life [56]. In principle, interventions that reduce one or more age-related pathology (i.e. part or all of aging) could increase lifespan by reducing base-line hazard, demographic aging, or both. One possibility is that the wider the spectrum of age-related pathologies that an intervention suppresses, the more likely will a reduction in demographic aging be seen. In conclusion, *mdl-1(0)* may or may not affect aging. Its greater effect on *daf-2* could imply that it does; however, an alternative possibility is that *mdl-1(0)* causes a pathology that is distinct from those seen during aging, and that *daf-2(-)* slightly increases the severity of this pathology, or increases its effect on mortality.

Where and how does *mdl-1* act to impact lifespan?

The phenotype of *mdl-1(tm311)* mutants demonstrates that MDL-1 acts as a repressor of growth and proliferation in the germline. This is consistent with the role of Mad TFs as repressors of growth and proliferation in mammals [11]. A long-standing hypothesis about aging is that it is caused by molecular damage, but more recently it has been suggested that aging is caused by the run on of developmental and reproductive processes in late life, leading e.g. to pathological hyperplasia, hypertrophy and atrophy [57-59]. The action of MDL-1 as a DAF-16-activated suppressor of growth is broadly consistent with this model.

The *mdl-1* mutant phenotype also suggests that this gene may affect lifespan through its effects on the germline. One possibility is that over-production of oocytes or increased formation of uterine tumors *per se* cause a decrease in lifespan. However, our findings argue against this: suppression of these effects in *mdl-1* mutants using *glp-4* or FUdR does not suppress the life-shortening effects of *mdl-1(0)* (Figure 5B,D). A second possibility is that *mdl-1(0)* affects signaling from the germline; removal of the germline can extend lifespan, and this effect is *daf-16* dependent [39]. Consistent with this possibility, *mdl-1(0)* shortens lifespan somewhat more in long-lived germlineless *glp-4* mutants than in otherwise wild-type worms (Figure 5E).

Another possible site of *mdl-1* action on lifespan is the intestine, which plays a significant role in the control of aging [40], and where *mdl-1* is expressed [10]. Notably, intestine-limited rescue of *mdl-1(+)* in otherwise *mdl-1(0)* worms was sufficient to modestly increase lifespan. However, how *mdl-1* acts in the intestine remains unclear. Mutation of *daf-2* increases intestinal expression of *ftn-1*, which encodes the iron storage protein ferritin. This increase is wholly *daf-16* dependent and partially *mdl-1* dependent [14]. Free iron is required for growth (e.g. ferroprotein synthesis) but also generates oxidative stress. Thus, increased activity of MDL-1 in *daf-2* mutants might retard intestinal aging as part of a program of suppression of protein biosynthesis. However, we did not detect an effect of *mdl-1* on accumulation of the most abundant protein class in *C. elegans* hermaphrodites, the vitellogenins (Figure 6A,B), which are synthesized in the intestine [46]. However, it remains possible that other aspects of protein synthesis are reduced by *mdl-1*.

Alternatively, mutation of *mdl-1* might increase levels of free iron in the intestine, perhaps accelerating aging by increasing oxidative damage, as suggested by the free radical theory. Consistent with this, *mdl-1(0)* partially suppress *daf-2* Oxr (Figure 3E), suggesting that MDL-1 promotes Oxr in *daf-2* mutants. However, *mdl-1(0)* alone did not affect Oxr; moreover, free iron levels appear to have little effect on aging under standard culture conditions [60]. More broadly, a range of studies suggest that oxidative damage is not a central determinant of aging, particularly in *C. elegans* [61, 62]. Together, these findings suggest that the intestine is one of several sites of action of *mdl-1* on lifespan.

The significance of uterine tumors in *C. elegans*

The oocyte-derived growths in the *C. elegans* uterus have been noted in previous studies and referred to as *'tumor-like' growths* [30], *masses* [24] and *oocyte clusters* [29]. Dictionary definitions of the word *tumor* vary, but in the common understanding of *tumor*, as in "a growth — a mass of tissue — that has no function" [63], these entities are tumors, hence our use of the term in this study. Arguably, *C. elegans* uterine tumors are both different and similar to mammalian cancer. It seems likely that *C. elegans* uterine tumors result from aging-associated overgrowth rather than mutations in oncogenes or tumor suppressor genes. But much of mammalian cancer, like worm uterine tumors, is part of the aging process. While it is clear that aging and cancer are associated, the relationship between the two remains unclear. One possibility is that aging results in changes in tissue microenvironment, e.g. due to senescent cell accumulation, that create more permissive conditions for cancer growth [64]. Aging-related tumors can occur even in the absence of transforming mutation, as in benign prostatic hyperplasia (BPH). We postulate that *C. elegans* uterine tumors, like BPH, exemplify the non-mutationally driven component of aging-associated cancer.

The regulatory network within which *mdl-1* might function

In mammals, Mad TFs act antagonistically to Myc TFs, which promote the cell cycle, growth and apoptosis, and reduce H ferritin expression [11, 15]. Consistent with this, MDL-1 inhibits germline growth and apoptosis (this study), and activates *ftn-1* expression [14]. Moreover, in mammals over-expression of Myc can induce endomitosis and cause increased ploidy [65], often seen in tumors, and also in senescent cells [66, 67], while MDL-1 antagonizes growth of uterine tumors formed from endomitotic oocytes (this study). Thus, MDL-1 in *C. elegans* behaves as one would expect of an antagonist of Myc – which is perhaps surprising given that *C. elegans* does not possess Myc. Indeed, Myc appears to be absent from the entire Nematode phylum (this study) [51].

In mammals, the Tor pathway and Myc TFs work in concert to control protein synthesis. Myc TFs activate expression of translational machinery genes, including eIF4E, eIF4A and eIF4G, which are components of the eIF4F complex that promotes translational initiation [48]. *C. elegans* lacks many genes that are present in other animal phyla [68], which can limit its usefulness as a model organism. Besides Myc, this also affects the worm Tor pathway, which lacks several key proteins, notably Tsc1/Tsc2 and 4E-BP. Thus, *C. elegans* possesses what appears to be a different version of the IIS/Tor/Mad network of higher animals. To fully understand the worm network requires understanding these differences.

Several interpretations have been made of the absence of Myc in *C. elegans*. First, that it reflects the relatively restricted *C. elegans* cell proliferation program [10]. Second, that in *C. elegans* the Myc role is played by a different bHLH TF, for example MML-1 (Myc and Mondo-like 1) [16]. However, arguing against this interpretation, MML-1 resembles Mondo rather than Myc, it dimerizes with MXL-2 while MDL-1 dimerizes with MXL-1, and deletion of *mxl-2* has only minor phenotypic effects (abnormal migration of ray 1 precursor cells in the male tail), and does not affect e.g. growth or lifespan [16].

Another possibility is that the Myc-less Mad-Max circuit ensures rapid growth, i.e. the nematode machinery for protein translation is, in the absence of DAF-16 and MDL-1, constitutively active. Consistent with this, Tsc1/Tsc2 and 4E-BP, which both antagonize growth, are absent from *C. elegans*, and most other nematodes (Figure 7B). Notably, in *Drosophila*, inhibition of growth resulting from reduced Tor kinase activity (e.g. by over-expression of Tsc1 and Tsc2) can be rescued by overexpression of dMyc [69]. An intriguing detail is the presence of Tsc1/Tsc2 in several spirurid nematodes (Figure 7B, Table S4); notably this group includes the longest lived nematode species known, e.g. the maximum lifespan of adult *Loa loa* is at least 20 years [70]. Another possibility is that the growth inhibitory functions of Tsc1/Tsc2 and 4E-BP have been taken over by DAF-16/FoxO, which is a major regulator of protein synthesis in *C. elegans* [41, 42, 45]. Thus, perhaps DAF-16 suppresses growth in soma and germline, while MDL-1 suppresses growth in the germline alone.

Conclusions

These results confirm that the Mad TF MDL-1 contributes to the *daf-2* longevity phenotype, and reveal a major role in inhibition of germline growth and reduction of uterine tumor development. They also suggest a role for intestinal MDL-1 in longevity assurance. The action of *mdl-1* as a DAF-16 activated gene that inhibits growth is broadly consistent with the possibility that the effects of insulin/IGF-1 signaling and DAF-16 on aging are a function of their effects on growth.

EXPERIMENTAL PROCEDURES

C. elegans culture and strains. Worms were cultured as previously described [71], at 20˚C unless otherwise stated. Nematode strains used include N2 (wild type),

DR1567 *daf-2(m577)III*, SS104 *glp-4(bn2)I*, GA1200 *mdl-1(tm311)X* (6X out-crossed), GA91 *daf-16(mgDf50)I; daf-2(m577),* GA1204 *daf-2(m577); mdl-1(tm311),* GA1208 *daf-16(mgDf50); daf-2(m577); mdl-1(tm311)*, GA1226 *daf-16(mgDf50); mdl-1(tm311)*, GA1230 *glp-4(bn2); mdl-1(tm311)*, GA1604 *mdl-1(tm311); wuEx267[mdl-1 + rol-6(su1006)]*, GA1605 *mdl-1(tm311); wuEx268[pges-1::mdl-1 + rol-6(su1006)]*. Primers to identify *mdl-1(tm311)* were atggaacagcaactcaaccttgg and ttaaacttggaggttgattggcaag, and heterozygotes aatgatgtgatctcgggctcg. Primers to genotype *daf-16(mgDf50)* were as described [72].

Strain construction. Multiple mutant strains were generated using standard genetic and molecular methodologies. Strains carrying mutations on the X chromosome (e.g. *mdl-1(tm311)*) were crossed with N2 males to generate hemizygous mutant males which were mated with L4 hermaphrodites of the strain carrying the second mutation of interest. F1 offspring were picked, and allowed to self-fertilise and 80 F2 were picked, allowed to lay eggs overnight, lysed and stored at -20˚C. Genomic deletions were identified using PCR. In the presence of the temperature sensitive *daf-2(m577)* allele, F1 animals were shifted to 25˚C to select for dauer formation in the F2, dauers were picked and left to recover at 15˚C to lay eggs, the F2 were lysed and tested for deletions. The *daf-16(mgDf50); daf-2(m577); mdl-1(tm311)* triple mutant was constructed by mating *daf-16; daf-2* males with *daf-2; mdl-1* hermaphrodites. The F2 generation was cloned, lysed and offspring raised at 25˚C. *daf-16(mgDf50)* homozygotes in the F3 were initially identified as non-dauer formers, and *mdl-1(tm311)* homozygotes identified by PCR.

mdl-1 transgenic lines were created by microinjection using PCR products and PCR fusion [73]. Primers used to make GA1604 were aaattgcacatgcagagacg and gaaagatacggaaggtgtgc. Primers used to make GA1605 were ttgtctattggtatggctgc; ggttgagttgctgttccattacaaggaa tatccgcatctg; gcgctaccaataaggctaag; aatggaacagcaactc aacc; gaaagatacggaaggtgtgc; and tttacaacacgatccacacg.

Staining protocols. To quantify germ cell number, nuclei were stained using DNA-binding dye 4',6-diamidino-2-phenylindole (DAPI). Animals were fixed in methanol, washed with M9 buffer and incubated in the dark in a 500ng/µl DAPI solution for 30 min. Thereafter they were washed again in M9 buffer. To quantify the number of apoptotic cells in living animals, nematodes were stained with SYTO 12 Green Fluorescent Nucleic Acid Stain (Molecular Probes). The animals were incubated in the dark in a 33µM SYTO 12 solution for 4 hr, and then placed on an OP50 lawn for 1 hr.

Quantitative RT-PCR and chromatin immuno-precipitation PCR (ChIP-PCR). RT-PCR and ChIP-PCR were performed largely as previously described [9, 74]. Primers for RT-PCR amplification from *mdl-1* mRNA were cccgtttgcgtgtcattgt and atggattgtgagagtgttgagaat. Primers for ChIP-PCR of an *mdl-1* promoter region (Figure 1A) were ccccctcgttttctccatgt and gccgctcgctccaatg.

Microscopy. Freshly prepared agar pads were created by dropping 35µl of 2% agarose onto a glass slide. Worms were anaesthesised using 5µl 0.2% levamisole. Nomarski microscopy was performed on a Zeiss Axioskop2 plus microscope with a Hamamatsu ORCA-ER digital camera C4742-95. Images were acquired using Volocity 5.5 software, with 10x eyepieces and a 40x objective lens. For body size measurements, worms were synchronized and hatched overnight in M9 buffer. The next day, ~30 worms per strain were imaged, and the remainder cultured on OP50 and thereafter imaged consecutively for 6 days. Volocity 5.5 was used to quantify the length of the worm from head to tail and the width across the pharyngeal-intestinal valve region.

Uterine tumor scoring system. Uterine status was scored from 1 to 5, where scores of 3-5 indicates the presence of a tumor. Class 1 denotes a normal, youthful uterus containing fertilized eggs and/or unfertilized oocytes of normal appearance. Class 2 denotes a uterus whose contents appear somewhat abnormal, but without a clear increase in size. Class 3 denotes a uterus containing a small tumor. Class 4 denotes a uterus containing a medium sized tumor, that does not fill the body cavity in the mid-body region. Class 5 denotes a uterus where the tumor is large, and fill the entire body cavity in the mid-body region, and even causes distension of the body wall. For the scoring, the tumor images was randomised, and the scoring was performed blinded by 3 different scorers. The non-parametric Wilcoxon test was used to compare tumor classes between worm strains and within the same strain on day 1 and day 4. The analysis was performed using the statistical programme JMP 9 (SAS Institute Inc.)

Fertility measurements. Brood sizes were assayed as previously described [22]. Briefly, 10-12 L4 hermaphrodites, raised at 20˚C were cloned on individual plates, shifted to 25˚C and transferred daily for 7 days. Plates were incubated at 20˚C for 24 hr to allow offspring to hatch and then larvae, unfertilized oocytes and dead eggs were scored.

Yolk level measurements. For each test sample, 50 hermaphrodites at day 1 and 4 of adulthood were transferred into an Eppendorf tube filled with 1 ml M9

buffer. Worms were spun at 800 rpm for 2 min and supernatant removed, leaving 25 µl. Then 25 µl of 2x Laemmli buffer (Sigma) was added, and samples incubated at 70˚C for 15 min, vortexed every other minute and then shifted to 95˚C for 5 min. Lysates were centrifuged at 13,000 rpm at 4˚C for 15 min. 20 µl of each sample was loaded onto a Criterion XT Tris-Acetate gel. The gel was run at 200V in SDS-PAGE chamber with 1x 3-(N-morpholino) propanesulfonic acid (MOPS) buffer for 45 min. The gel was fixed in methanol, acetic acid and ultrapure water in ratio of 50:10:40 for 30 min. The fixing solution was then discarded and replaced with Coomassie fixation solution (50:3:40:10 methanol: Coomassie stock solution: ultrapure water: acetic acid). 12.0 g of Brilliant Blue R-250, 300 ml methanol and 60ml acetic acid were used to prepare Coomassie stock solution. The gel was incubated overnight in destaining solution (45:10:45 methanol: acetic acid: ultrapure water). Protein bands on the gel were visualised by a Image Quant GE Healthcare scanner system connected to a computer, and analysed by ImageQuant software with which densitometry was performed. Each experiment was done in triplicate.

Lifespan measurements**.** These were conducted as previously described [22]. Briefly, 5 plates per condition were seeded with OP50 2 days before the start of the experiment. 10 µM FUdR was topically applied before beginning the trial. Animals were raised at 20˚C, or for assays including *glp-4(bn2)* mutants, animals were raised at 15˚C and switched to 25˚C at L4 stage. All animals were transferred to fresh plates on day 5 and 10. Deaths were scored and losses due to causes other than death were censored. Lifespan data were deposited in SurvCurv [75] <IDs filled in proof>.

Dauer formation measurement. Dauer formation was assessed at 22.9˚C as previously described [22]. Briefly, 12 L4s were picked and raised to adulthood at 20˚C for 2 days. These gravid adults were then placed on 35mm plates to lay eggs for 6 hrs at the test temperature, after which the adults were removed and the larvae were allowed to develop at the test temperature. Dauers and normal larvae were scored 72 hr after the midpoint of the egg lay and the percentage dauer formation was calculated by dividing the number of dauer larvae by the total number of offspring.

Oxidative stress resistance. 1 day old adults were tested for resistance to 7.5 mM *tert*-butylhydroperoxide (*t*-BOOH) as previously described [33]. Briefly, L4 animals were picked from mixed stage plates raised at 20˚C, then shifted to 25˚C overnight. NGM agar was supplemented with 7.5 mM *t*-BOOH and the plates were left to dry overnight. The next day, each plate was supplemented with a blob of densely grown OP50, and 15 young adults were added per plate. The trial was conducted at 25˚C and animals were scored every 2 to 3 hr until the last animal had perished.

Bioinformatics. Myc, Tsc1, Tsc2 and 4E-BP orthologs were sought by local alignment searches of the 4 protein sequences to the gene models in *Mus musculus* using BLASTP searches. Since not all genomes were available in WormBase, orthologs for the parasitic helminths (*B. xylophilus*, *E. granulosus, E. multilocularis, T. solium, H. microstoma*, *S. mansoni* and *S. japonicum*) were derived from GeneDB. Orthologs for *G. pallida, H. contortus, O. volvulus, S. ratti and T. muris* were sought using the data available on the Sanger Institute Resources. Orthologs to *T. muris* were sought by local alignment searches of the 4 genes to contigs, using a "protein versus translated DNA" a TBLASTN search. Finally, orthologs of *P. pacificus* were sought among the gene predictions available from www.pristionchus.org. Multiple sequence alignments of the Tsc1/2 protein sequences were done using MUSCLE [76]. All trees were constructed and visualised as previously described [74].

Statistical analysis. Lifespans were analysed using the Cox Proportional Hazard method with the Efron approximation for ties of the survival package in R. The logistic mortality models were fitted to the lifespan data and parameter difference tested using the Survomatic R package. The body sizes were analysed using a linear regression model taking into account the trial as random factor in R. The Wilcoxon Mann test was used for tumors and the brood sizes were compared using a standard Student's t Test.

ACKNOWLEDGEMENTS

We wish to thank Mikhail Nikiforov for useful discussion, and Filipe Cabreiro for comments on the manuscript. Some nematode strains used in this work were provided by the Caenorhabditis Genetics Center, which is funded by the National Institutes of Health National Center for Research Resources and the National Bioresource Project of Japan. This work was supported by the Wellcome Trust (Strategic Award), EMBL and the European Union (IDEAL).

Conflicts of Interest Statement

The authors of this manuscript have no conflict of interest to declare.

REFERENCES

1. Kenyon C. The genetics of ageing. Nature. 2010; 464:504-512.

2. Kenyon C, Chang J, Gensch E, Rudener A and Tabtiang R. A *C. elegans* mutant that lives twice as long as wild type. Nature. 1993; 366:461-464.

3. Lin K, Dorman JB, Rodan A and Kenyon C. *daf-16*: An HNF-3/forkhead family member that can function to double the life-span of *Caenorhabditis elegans*. Science. 1997; 278:1319-1322.

4. Ogg S, Paradis S, Gottlieb S, Patterson GI, Lee L, Tissenbaum HA and Ruvkun G. The Fork head transcription factor DAF-16 transduces insulin-like metabolic and longevity signals in *C. elegans*. Nature. 1997; 389:994-999.

5. McElwee J, Bubb K and Thomas J. Transcriptional outputs of the Caenorhabditis elegans forkhead protein DAF-16. Aging Cell. 2003; 2:111-121.

6. Murphy CT, McCarroll SA, Bargmann CI, Fraser A, Kamath RS, Ahringer J, Li H and Kenyon CJ. Genes that act downstream of DAF-16 to influence the lifespan of *C. elegans*. Nature. 2003; 424:277-284.

7. McElwee JJ, Schuster E, Blanc E, Thomas JH and Gems D. Shared transcriptional signature in *C. elegans* dauer larvae and long-lived *daf-2* mutants implicates detoxification system in longevity assurance. J Biol Chem. 2004; 279:44533-44543.

8. Partridge L, Alic N, Bjedov I and Piper MD. Ageing in Drosophila: the role of the insulin/Igf and TOR signalling network. Exp Gerontol. 2011; 46:376-381.

9. Schuster E, McElwee JJ, Tullet JMA, Doonan R, Matthijssens F, Reece-Hoyes JS, Hope IA, Vanfleteren JR, Thornton J and Gems D. DamID in *C. elegans* reveals longevity-associated targets of DAF-16/FoxO. Mol Syst Biol. 2010; 6:399.

10. Yuan J, Tirabassi RS, Bush AB and Cole MD. The C. elegans MDL-1 and MXL-1 proteins can functionally substitute for vertebrate MAD and MAX. Oncogene. 1998; 17:1109-1118.

11. Grandori C, Cowley SM, James LP and Eisenman RN. The Myc/Max/Mad network and the transcriptional control of cell behavior. Ann Rev Cell Dev. 2000; 16:653-699.

12. Gems D and Partridge L. Genetics of longevity in model organisms: Debates and paradigm shifts. Annual Review of Physiology. 2013; 75:621-644.

13. Delpuech O, Griffiths B, East P, Essafi A, Lam EW, Burgering B, Downward J and Schulze A. Induction of Mxi1-SR alpha by FOXO3a contributes to repression of Myc-dependent gene expression. Mol Cell Biol. 2007; 27:4917-4930.

14. Ackerman D and Gems D. Insulin/IGF-1 and hypoxia signaling act in concert to regulate iron homeostasis in C. elegans. PLoS Genet. 2012; 8:e1002498.

15. Le N and Richardson D. The role of iron in cell cycle progression and the proliferation of neoplastic cells. Biochim Biophys Acta. 2002; 1603:31–46.

16. Pickett CL, Breen KT and Ayer DE. A C. elegans Myc-like networks cooperates with semaphorin and Wnt signaling pathways to control cell migration. Dev Biol. 2007; 310:226-239.

17. Grove CA, De Masi F, Barrasa MI, Newburger DE, Alkema MJ, Bulyk ML and Walhout AJ. A multiparameter network reveals extensive divergence between C. elegans bHLH transcription factors. Cell. 2009; 138:314-327.

18. Pinkston JM, Garigan D, Hansen M and Kenyon C. Mutations that increase the life span of C. elegans inhibit tumor growth. Science. 2006; 313:971-975.

19. Pinkston-Gosse J and Kenyon C. DAF-16/FOXO targets genes that regulate tumor growth in Caenorhabditis elegans. Nat Genet. 2007; 39:1403-1409.

20. Gems D and Riddle DL. Defining wild-type life span in *Caenorhabditis elegans*. J Gerontol A Biol Sci Med Sci. 2000; 55:B215-B219.

21. Ward S and Carrel JS. Fertilization and sperm competition in the nematode *Caenorhabditis elegans*. Dev Biol. 1979; 73:304-321.

22. Gems D, Sutton AJ, Sundermeyer ML, Larson PL, Albert PS, King KV, Edgley M and Riddle DL. Two pleiotropic classes of *daf-2* mutation affect larval arrest, adult behavior, reproduction and longevity in *Caenorhabditis elegans*. Genetics. 1998; 150:129-155.

23. Jud M, Razelun J, Bickel J, Czerwinski M and Schisa JA. Conservation of large foci formation in arrested oocytes of Caenorhabditis nematodes. Dev Genes Evol. 2007; 217:221-226.

24. Hughes SE, Huang C and Kornfeld K. Identification of mutations that delay somatic or reproductive aging of Caenorhabditis elegans. Genetics. 2011; 189:341-356.

25. Gumienny TL, Lambie E, Hartwieg E, Horvitz HR and Hengartner MO. Genetic control of programmed cell death in the Caenorhabditis elegans hermaphrodite germline. Development. 1999; 126:1011-1022.

26. Jaramillo-Lambert A, Ellefson M, Villeneuve AM and Engebrecht J. Differential timing of S phases, X chromosome replication, and meiotic prophase in the C. elegans germ line. Dev Biol. 2007; 308:206-221.

27. Wolke U, Jezuit EA and Priess JR. Actin-dependent cytoplasmic streaming in C. elegans oogenesis. Development. 2007; 134:2227-2236.

28. Garigan D, Hsu A, Fraser A, Kamath R, Ahringer J and Kenyon C. Genetic analysis of tissue aging in *Caenorhabditis elegans*: a role for heat-shock factor and bacterial proliferation. Genetics. 2002; 161:1101-1112.

29. Luo S, Kleemann GA, Ashraf JM, Shaw WM and Murphy CT. TGF-beta and insulin signaling regulate reproductive aging via oocyte and germline quality maintenance. Cell. 2010; 143:299-312.

30. Golden T, Beckman K, Lee A, Dudek N, Hubbard A, Samper E and Melov S. Dramatic age-related changes in nuclear and genome copy number in the nematode Caenorhabditis elegans. Aging Cell. 2007; 6:179-188.

31. McGee MD, Day N, Graham J and Melov S. cep-1/p53-dependent dysplastic pathology of the aging C. elegans gonad. Aging. 2012; 4:256-269.

32. Qi W, Huang X, Neumann-Haefelin E, Schulze E and Baumeister R. Cell-nonautonomous signaling of FOXO/DAF-16 to the stem cells of Caenorhabditis elegans. PLoS Genet. 2012; 8:e1002836.

33. Tullet JM, Hertweck M, An JH, Baker J, Hwang JY, Liu S, Oliveira RP, Baumeister R and Blackwell TK. Direct inhibition of the longevity-promoting factor SKN-1 by insulin-like signaling in C. elegans. Cell. 2008; 132:1025-1038.

34. Johnson T, Wu D, Tedesco P, Dames S and Vaupel J. Age-specific demographic profiles of longevity mutants in *Caenorhabditis elegans* show segmental effects. J Gerontol A Biol Sci Med Sci. 2001; 56:B331-B339.

35. Vanfleteren JR, De Vreese A and Braeckman BP. Two-parameter logistic and Weibull equations provide better fits to survival data from isogenic populations of *Caenorhabditis*

elegans in axenic culture than does the Gompertz model. J Gerontol A Biol Sci Med Sci. 1998; 53:B393-B403.
36. Johnson TE. The increased lifespan of *age-1* mutants of *Caenorhabditis elegans* results from a lowering of the Gompertz rate of aging. Science. 1990; 249:908-912.
37. Gandhi S, Santelli J, Mitchell DG, Stiles JW and Raosanadi D. A simple method for maintaining large, aging populations of *Caenorhabditis elegans*. Mech Ageing Dev. 1980; 12:137-150.
38. Arantes-Oliveira N, Apfeld J, Dillin A and Kenyon C. Regulation of life-span by germ-line stem cells in *Caenorhabditis elegans*. Science. 2002; 295:502-505.
39. Hsin H and Kenyon C. Signals from the reproductive system regulate the lifespan of *C. elegans*. Nature. 1999; 399:362-366.
40. Libina N, Berman J and Kenyon C. Tissue-specific activities of *C. elegans* DAF-16 in the regulation of lifespan. Cell. 2003; 115:489-502.
41. Depuydt G, Xie F, Petyuk VA, Shanmugam N, Smolders A, Dhondt I, Brewer HM, Camp DG, Smith RD and Braeckman BP. Reduced insulin/IGF-1 signaling and dietary restriction inhibit translation but preserve muscle mass in Caenorhabditis elegans. Mol Cell Proteomics. 2013.
42. Stout GJ, Stigter EC, Essers PB, Mulder KW, Kolkman A, Snijders DS, van den Broek NJ, Betist MC, Korswagen HC, Macinnes AW and Brenkman AB. Insulin/IGF-1-mediated longevity is marked by reduced protein metabolism. Mol Syst Biol. 2013; 9:679.
43. McGee MD, Weber D, Day N, Vitelli C, Crippen D, Herndon LA, Hall DH and Melov S. Loss of intestinal nuclei and intestinal integrity in aging C. elegans. Aging Cell. 2011; 10:699-710.
44. Herndon L, Schmeissner P, Dudaronek J, Brown P, Listner K, Sakano Y, Paupard M, Hall D and Driscoll M. Stochastic and genetic factors influence tissue-specific decline in ageing *C. elegans*. Nature. 2002; 419:808-814.
45. Depina A, Iser W, Park S, Maudsley S, Wilson M and Wolkow C. Regulation of Caenorhabditis elegans vitellogenesis by DAF-2/IIS through separable transcriptional and posttranscriptional mechanisms. BMC Physiol. 2011; 11:11.
46. Kimble J, Sharrock, WJ. Tissue-specific synthesis of yolk proteins in *Caenorhabditis elegans*. Dev Biol. 1983; 96:189-196.
47. Aamodt EJ, Chung MA and McGhee JD. Spatial control of gut-specific gene expression during Caenorhabditis elegans development. Science. 1991; 252:579-582.
48. Lin C-J, Malina A and Pelletier J. c-Myc and eIF4F consistute a feedforward loop that regulates cell growth: implications for anticancer therapy. Cancer Res. 2009; 69:7491-7494.
49. Kapahi P, Chen D, Rogers AN, Katewa SD, Li PW, Thomas EL and Kockel L. With TOR, less is more: a key role for the conserved nutrient-sensing TOR pathway in aging. Cell Metab. 2010; 11:453-465.
50. Syntichaki P, Troulinaki K and Tavernarakis N. eIF4E function in somatic cells modulates ageing in Caenorhabditis elegans. Nature. 2007; 445:922-926.
51. McFerrin LG and Atchley W. Evolution of the Max and Mlx networks in animals. Genome Biol Evol. 2011; 3:915–937.
52. Schreiber-Agus N, Meng Y, Hoang T, Hou H, Jr., Chen K, Greenberg R, Cordon-Cardo C, Lee HW and DePinho RA. Role of Mxi1 in ageing organ systems and the regulation of normal and neoplastic growth. Nature. 1998; 393:483-487.
53. Blagosklonny MV. Cell cycle arrest is not yet senescence, which is not just cell cycle arrest: terminology for TOR-driven aging. Aging. 2012; 4:159-165.
54. Budovsky A, Tacutu R, Yanai H, Abramovich A, Wolfson M and Fraifeld V. Common gene signature of cancer and longevity. Mech Ageing Dev. 2009; 130:33-39.
55. Finch CE, Pike MC and Witten M. Slow mortality rate accelerations during aging in some animals approximate that of humans. Science. 1990; 249:902-905.
56. Gems D. What is an anti-aging treatment? Exp Gerontol. 2014 (In press).
57. Blagosklonny MV. Aging and immortality: quasi-programmed senescence and its pharmacologic inhibition. Cell Cycle. 2006; 5:2087-2102.
58. Blagosklonny MV. Paradoxes of aging. Cell Cycle. 2007; 6:2997-3003.
59. Gems D and de la Guardia Y. Alternative perspectives on aging in C. elegans: reactive oxygen species or hyperfunction? Antioxid Redox Signal. 2013; 19:321-329.
60. Valentini S, Cabreiro F, Ackerman D, Alam MM, Kunze MBA, Kay CWM and Gems D. Manipulation of *in vivo* iron levels can alter resistance to oxidative stress without affecting ageing in the nematode *C. elegans*. Mech Ageing Dev. 2012; 133:282-290.
61. Van Raamsdonk JM and Hekimi S. Reactive oxygen species and aging in Caenorhabditis elegans: causal or casual relationship? Antioxid Redox Signal. 2010; 13:1911-1953.
62. Gems D and Doonan R. Antioxidant defense and aging in C. elegans: is the oxidative damage theory of aging wrong? Cell Cycle. 2009; 8:1681-1687.
63. Vocabulary.com. (2013). tumor.
64. Campisi J. Senescent cells, tumor suppression, and organismal aging: good citizens, bad neighbors. Cell. 2005; 120:513-522.
65. Yin XY, Grove L, Datta NS, Long MW and Prochownik EV. C-myc overexpression and p53 loss cooperate to promote genomic instability. Oncogene. 1999; 18:1177-1184.
66. Smogorzewska A and de Lange T. Different telomere damage signaling pathways in human and mouse cells. EMBO J. 2002; 21:4338-4348.
67. Wagner M, Hampel B, Bernhard D, Hala M, Zwerschke W and Jansen-Durr P. Replicative senescence of human endothelial cells in vitro involves G1 arrest, polyploidization and senescence-associated apoptosis. Exp Gerontol. 2001; 36:1327-1347.
68. Coghlan A. (2005). Nematode genome evolution. In: Community TCeR, ed. WormBook.
69. Gallant P. Myc/Max/Mad in invertebrates: the evolution of the Max network. Curr Top Microbiol Immunol 2006; 302:235-253.
70. Gems D. Longevity and ageing in parasitic and free-living nematodes. Biogerontology. 2000; 1:289-307.
71. Brenner S. The genetics of *Caenorhabditis elegans*. Genetics. 1974; 77:71-94.
72. Love D, Ghosh S, Mondoux M, Fukushige T, Wang P, Wilson M, Iser W, Wolkow C, Krause M and Hanover J. Dynamic O-GlcNAc cycling at promoters of Caenorhabditis elegans genes regulating longevity, stress, and immunity. Proc Natl Acad Sci U S A. 2010; 107:7413-7418.
73. Hobert O. PCR fusion-based approach to create reporter gene constructs for expression analysis in transgenic C. elegans. Biotechniques. 2002; 32(4):728-730.
74. Tullet JMA, Araiz C, Sanders MJ, Au C, Benedetto A, Papatheodorou I, Clark E, Schmeisser K, Jones D, Schuster EF, Thornton JM and Gems D. DAF-16/FoxO directly regulates an atypical AMP-activated protein kinase gamma isoform to

ARTICLE

Received 4 Jul 2016 | Accepted 31 Mar 2017 | Published 23 May 2017

DOI: 10.1038/ncomms15458 OPEN

Two forms of death in ageing *Caenorhabditis elegans*

Yuan Zhao[1,*], Ann F. Gilliat[1,*], Matthias Ziehm[1,2], Mark Turmaine[3], Hongyuan Wang[1], Marina Ezcurra[1], Chenhao Yang[1], George Phillips[1], David McBay[1], William B. Zhang[4], Linda Partridge[1,5], Zachary Pincus[4] & David Gems[1]

Ageing generates senescent pathologies, some of which cause death. Interventions that delay or prevent lethal pathologies will extend lifespan. Here we identify life-limiting pathologies in *Caenorhabditis elegans* with a necropsy analysis of worms that have died of old age. Our results imply the presence of multiple causes of death. Specifically, we identify two classes of corpse: early deaths with a swollen pharynx (which we call 'P deaths'), and later deaths with an atrophied pharynx (termed 'p deaths'). The effects of interventions on lifespan can be broken down into changes in the frequency and/or timing of either form of death. For example, *glp-1* mutation only delays p death, while *eat-2* mutation reduces P death. Combining pathology and mortality analysis allows mortality profiles to be deconvolved, providing biological meaning to complex survival and mortality profiles.

[1] Institute of Healthy Ageing, Department of Genetics, Evolution and Environment, University College London, London WC1E 6BT, UK. [2] European Molecular Biology Laboratory, European Bioinformatics Institute (EMBL-EBI), Wellcome Trust Genome Campus, Hinxton, Cambridge CB10 1SD, UK. [3] Department of Cell and Developmental Biology, University College London, London WC1E 6BT, UK. [4] Department of Genetics, Washington University in St Louis, St. Louis, Missouri 63110, USA. [5] Max Planck Institute for Biology of Ageing, Köln D-50931, Germany. * These authors contributed equally to this work. Correspondence and requests for materials should be addressed to D.G. (email: david.gems@ucl.ac.uk.).

The nematode *Caenorhabditis elegans* is an excellent model organism for investigating the biology of ageing. Although much progress has been made in terms of identifying genes and pathways that affect lifespan[1,2], the underlying mechanisms of ageing remain poorly defined. One obstacle has been the difficulty of relating gene function to lifespan, given that the latter is a numeric, demographic parameter that contains little information about biological processes or structures to which gene function can readily be related. A complimentary approach is to study age-related pathologies and functional decline in relation to lifespan. As in humans, various senescent pathologies develop in ageing *C. elegans*, including deterioration of the pharynx, intestine, gonad and neurons[3–6]. While some pathologies do not appear to contribute to mortality[7], others may be life limiting. Identification of lethal senescent pathologies may provide us with the missing link between the biochemical function of gene products and their effects on lifespan.

In this study, we use necropsy analysis to investigate the causes of death in *C. elegans* and reveal two distinct modes of death, one that largely occurs earlier in life than the other. Thus interventions that alter lifespan in *C. elegans* reflect effects on timing and/or frequency of one or both types of death. We show how such differential effects can be resolved by mortality deconvolution, involving combined analysis of mortality and necropsy data.

Results

Necropsy analysis reveals two modes of death. What do ageing *C. elegans* die of? To identify possible causes of death, we tracked pathologies in individual wild-type adult hermaphrodites as they aged (Supplementary Fig. 1; Supplementary Table 1) and tested for correlation between pathology severity and age at death. This revealed significant correlations between age at death and several pathologies, including pharyngeal deterioration (Fig. 1a; Supplementary Table 1). This, together with the previous observation that pharyngeal pumping span (that is, the length of time that the pharynx is active) correlates with lifespan[8], suggests that pharyngeal pathology could be life limiting.

Next, necropsy analysis was performed, for which corpses of nematodes that had expired from old age were collected daily and examined. This revealed two distinct types of corpse with respect to pharyngeal pathology (Supplementary Fig. 2). The first showed severe swelling of the posterior pharyngeal bulb, with a 20–120% increase in cross-sectional area (Fig. 1b). The second showed marked atrophy of the posterior bulb, with up to a 70% decrease in cross-sectional area (Fig. 1b). For convenience, we designated these corpse types 'P' ('big P') and 'p' ('small p'), respectively.

Notably, P deaths mainly occurred earlier than p deaths (Fig. 1c), with a median age of death (lifespan) of 12 and 22 days, respectively (Fig. 1d). The distinct timing contributes to the high variance in age at death seen in *C. elegans* populations despite their isogenicity[9,10], where $>50\%$ of the total variance can be explained by the existence of two types of death (Supplementary Table 2). In P deaths, pharyngeal swelling appeared only in the last few days prior to death (Fig. 1e). Swelling was preceded by a major reduction in pharyngeal pumping rate (Fig. 1f), likely contributing to the correlation between pharyngeal pumping span and age of death[8].

As in many animal species (and humans), *C. elegans* mortality rate increases with age. However, there is a hitherto unexplained deceleration of the age increase in mortality rate around day 10–12 (refs 11–13), postulated to reflect population heterogeneity in frailty[14]. The occurrence of this deceleration, which reflects a mid-life surge in death rate, was confirmed in the wild-type populations subjected to necropsy analysis in this study, in which a slope change can be detected, with the most significant change on day 11 of adulthood (Fig. 1g; Supplementary Fig. 3a,b). The surge in mortality in mid-life was also seen in our archive mortality data collected at two locations (Supplementary Fig. 3c,d). In contrast, p mortality showed an exponential increase in mid-to-late life that, combined with the peak of P mortality in mid adulthood, leads to an apparent slowing of the mortality rate acceleration (Fig. 1h).

Pharyngeal swelling is caused by bacterial infection. Next, we explored the possible causes of P deaths, first asking: what is the immediate cause of pharyngeal swelling? The pharynx of immunocompromised *C. elegans* is susceptible to bacterial infection[15] and proliferation of the *Escherichia coli* food source limits worm lifespan[4,16]. Comparison of *E. coli* content in surgically excised pharynxes from live, aged worms found a 42-fold greater number of colony-forming units in swollen pharynxes compared to unswollen ones (Supplementary Fig. 4a), suggesting that the swelling is due to increased bacterial content. To visualize localization of bacteria within pharyngeal tissue, we fed worms with *E. coli* expressing red fluorescent protein (RFP). Red fluorescence was seen throughout the pharyngeal tissue in worms that undergo P death (Fig. 2a), whereas p corpses typically contained no fluorescence or only small fluorescent inclusions in the posterior bulb, perhaps reflecting contained invasions (Fig. 2b; Supplementary Fig. 4b). Live worms in the early stages of bacterial invasion revealed RFP co-localized with green fluorescent protein (GFP) markers of several different pharyngeal cell types but most often with pharyngeal muscle near the grinder (Fig. 2d; Supplementary Fig. 4c,d). Moreover, examination of swollen pharynxes using transmission electron microscopy (TEM) showed them to be filled with bacteria (Fig. 2c), while unswollen pharynxes contained either no invading *E. coli* or small, membrane-bound bacterial inclusions usually near the grinder cuticle (Supplementary Fig. 5). These results suggest a route for initial bacterial invasion through the pharyngeal cuticle in the grinder region.

To test whether pharyngeal swelling is caused by bacterial proliferation, *E. coli* were treated with an antibiotic (carbenicillin) or ultraviolet irradiation. In each case, P death was eliminated (Fig. 2e), and lifespan extended (Supplementary Fig. 6a,b; Supplementary Table 3) as observed previously[4,16]. As expected, blocking bacterial proliferation also removed the mortality rate deceleration seen around day 11 (Fig. 2f); this is also consistent with the absence of mid-life mortality deceleration in populations maintained in the recently described automated systems, including worm corrals[17] and lifespan machines[18], as P death is either eliminated or significantly reduced in both cases (Supplementary Fig. 7). However, elimination of P death did not completely abrogate the correlation between pharyngeal pumping span and lifespan (Supplementary Fig. 6c,d), which could imply that pharyngeal pathology contributes to mortality in additional ways.

High pharyngeal pumping rate promotes P death. Thus P death is associated with pharyngeal invasion and proliferation of bacteria, but why do these deaths occur relatively early, with the majority occurring before day 15? Shifting worms raised on non-proliferating bacteria to proliferating bacteria at time points after day 4 progressively reduced the frequency of P death and reduced early mortality (Fig. 3a,b; Supplementary Fig. 8a–d; Supplementary Table 4), suggesting that a narrow time window exists in early adulthood where worms are susceptible to pharyngeal infection. This, together with initial occurrence of invasion near the grinder, could imply that the high rate of pumping in

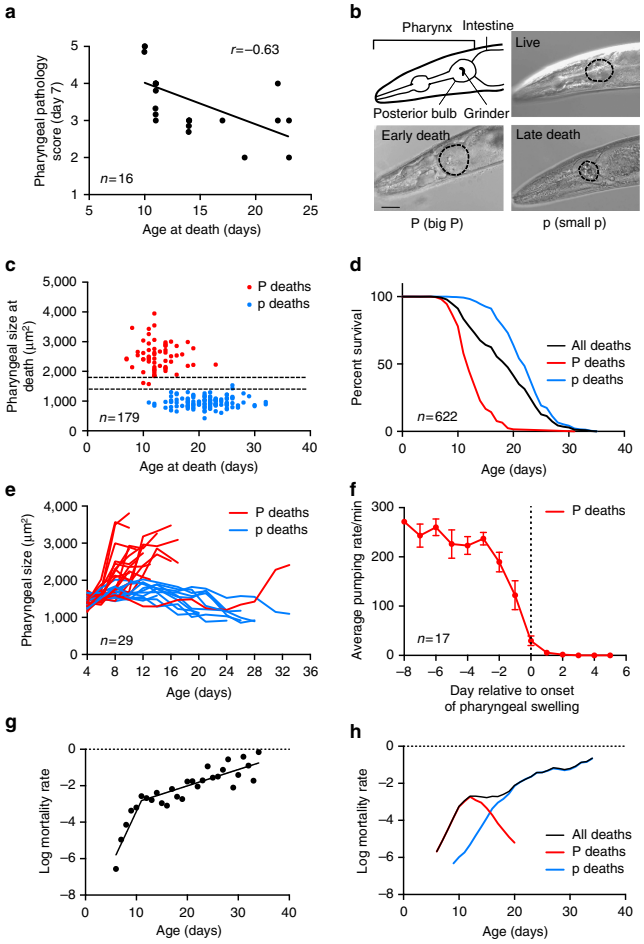

Figure 1 | Two types of corpse in ageing *C. elegans* populations. (**a**) Positive correlation between pharyngeal pathology on day 7 of adulthood and age at death. ($n=16$). (**b**) Corpses with an enlarged or atrophied pharynx. For comparison, the pharynx of a healthy 10-day-old adult worm is shown. The posterior bulb is outlined. Scale bar, 40 µm. (**c**) Age distribution of P and p deaths. *y* Axis shows cross-sectional area of pharynxes on the day of death ($n=179$). Dotted lines represent the size of a healthy pharynx on day 10 (mean ± s.d.). (**d**) Survival curves of all worms (black) or with P and p deaths resolved (red and blue, respectively). Data compiled from 11 independent trials ($n=622$). An additional single large trial ($n=587$) was also performed (Supplementary Fig. 3e). (**e**) Age changes in pharyngeal size in individual worms. Early deaths (mostly pre-day 15) are preceded by a dramatic increase in pharyngeal size. The pharynxes of the remaining worms gradually decrease in size until death ($n=29$). (**f**) Mean pumping rate of worms that die with P. Day 0, first day of swelling. Worms show a major reduction in pumping rate immediately before pharyngeal swelling. Data are mean ± s.e.m. (Trials: 1, $n=17$). (**g**) Segmented linear regression analysis on log mortality rate of wild-type survival under standard conditions (data as in **d**, $X_0=11$). The slopes before and after day 11 are significantly different (slope test $P=2.81\times10^{-9}$). (**h**) Mortality deconvolution of wild-type survival (data as in **d**). Age-specific mortality rates of the whole population (black) or with P and p deaths resolved (red and blue, respectively).

young adults[8] injures the pharyngeal cuticle, perhaps due to mechanical stress, causing cuticular perforations and vulnerability to invasion. If this is correct, then reducing pharyngeal pumping rate should suppress P deaths. We therefore examined a range of pumping defective mutants, including *eat-2(ad1116)* mutants, which have a reduced pumping rate[19]. In most cases, P deaths were reduced or eliminated (Fig. 3c). This suggests that a wild-type, high rate of pharyngeal pumping leads to bacterial invasion of pharyngeal tissue.

The longevity of *eat-2* mutants has previously been attributed to dietary restriction[20]. However, results of mortality and necropsy analysis indicated that the *eat-2* lifespan extension observed was largely attributable to reduction in the frequency of P death, since the lifespans of P and p subpopulations did not

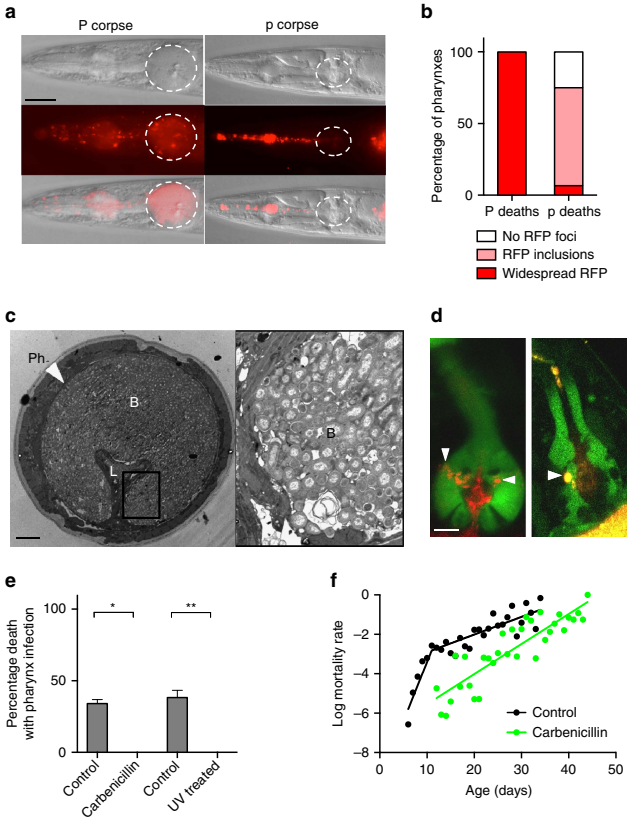

Figure 2 | Swelling in P deaths results from *E. coli* infection. (**a**) Comparison of P and p corpses of worms fed with *E. coli* expressing RFP. Scale bar, 40 μm. (**b**) Proportion of P ($n=70$) and p ($n=75$) corpses with widespread RFP, small intra-pharyngeal RFP inclusions or no detectable RFP foci. (Trials: 2). (**c**) Representative TEM of a swollen pharynx from a live, 8-day-old adult. L, lumen; Ph, pharynx; B, bacteria. The elongated appearance of some bacilli suggests that proliferation occurs within pharyngeal tissue. For TEMs of pharynxes at different stages of infection, see Supplementary Fig. 5. Scale bar, 5 μm. (**d**) Early stages of *E. coli*-RFP invasion of pharynx in transgenic *C. elegans* expressing GFP in selected cell types within the pharynx. Representative images of the muscle (left) and marginal cell marker (right) are shown with nascent intra-pharyngeal infection near the grinder (arrowheads). *E. coli* were noted previously in senescent marginal cells[31]. For gland cell marker image, see Supplementary Fig. 4c. Scale bar, 10 μm. (**e**) Blocking *E. coli* proliferation prevents P death. Proportion of P corpses when worms are grown with or without proliferating *E. coli*. Data are mean ± s.e.m. (Carbenicillin trials: 4; ultraviolet trials: 2, for sample size, see Supplementary Table 3). (**f**) Carbenicillin-treated bacteria remove mortality rate deceleration in mid life. Control wild-type mortality rate (black) as in Fig. 1g. For carbenicillin-treated log mortality rate (green), the slopes of regression are not significantly different when segmented at any point.

significantly differ between N2 and *eat-2* (Fig. 3d; Supplementary Table 5). This suggests, against expectation, that the longevity of *eat-2* mutants is attributable, at least in part, to suppression of P death rather than to dietary restriction.

Wound healing may protect against bacterial infection. Why do only a proportion of worms undergo P death? One possibility is that some worms have a higher pharyngeal pumping rate during early adulthood, resulting in sufficient damage to the cuticle to allow bacterial invasion to occur. However, in early adulthood there was no difference in pumping rate between worms that subsequently underwent P versus p death (Supplementary Fig. 8e). This argues against predisposition due to intrinsic differences in pumping rate. Another possibility suggested by the early adult time window for predisposition to P death is that early mechanical injury to the pharyngeal cuticle subsequently heals, preventing further infection in the majority of worms; the *C. elegans* external cuticle has an efficient wound healing capacity[21]. TEM of the grinder region in older worms revealed major cuticular scars (Supplementary Fig. 9), similar in appearance to cuticular scars described previously[21], consistent with injury and subsequent healing. Together these results suggest that rapid pumping in early adulthood leads to mechanical damage to the pharyngeal cuticle, allowing initial invasion of *E. coli*. In some worms, subsequent proliferation of invading *E. coli* leads to pharyngeal infection and P death, while in others

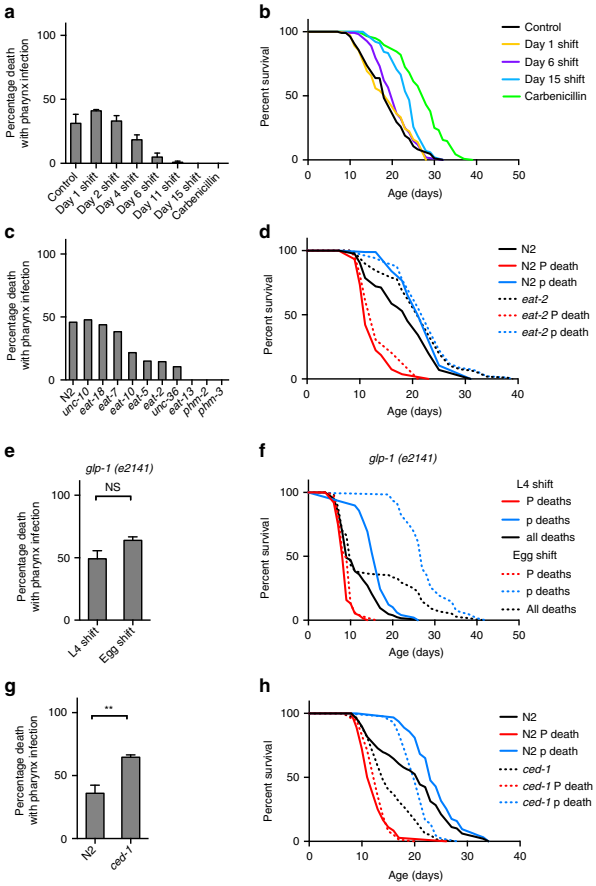

Figure 3 | High pharyngeal pumping rate promotes P death. (**a**) Effect of maintenance on non-proliferating *E. coli* (carbenicillin) during early life on frequency of P deaths. Exposure to proliferating bacteria in early-mid adulthood is required for P death to occur. (Trials: 2, for sample size, see Supplementary Table 4). (**b**) Maintenance on non-proliferating *E. coli* (carbenicillin) during early life reduces early mortality (data as in **a**). (**c**) Effect of pumping-defective mutants on the frequency of P. (Trials: 1–2). (**d**) Effect of *eat-2(ad1116)* on lifespan. Whole population (black) or P and p deaths resolved (red and blue, respectively). Log-rank test between N2 and *eat-2* whole populations $P=0.0007$, P death subpopulations $P=0.1996$, p death subpopulations $P=0.0815$. (Trials: 2, for sample sizes, see Supplementary Table 5). (**e**) Germline defective mutant *glp-1(e2141ts)* increases lifespan without affecting P death frequency when shifted to 25 °C as eggs. (Trials: 2, for sample sizes see Supplementary Table 6). (**f**) Effect of *glp-1* on lifespan, when shifted to 25 °C at either egg (dotted) or L4 larval stage (solid). Median lifespan: L4 shift P deaths 9 days, p deaths 17 days; egg shift P deaths 9 days, p deaths 27 days (data as in **e**). (**g**) *ced-1(e1735)* mutant increases the frequency of P deaths. (Trials: 2, for sample sizes, see Supplementary Table 7). (**h**) Effect of *ced-1* (dotted) on lifespan compared to wild-type (solid). Median lifespan: *ced-1* P deaths 13 days, p deaths 20 days; wild-type P deaths 13 days, p deaths 23 days (data as in **g**).

invasion remains contained after cuticular healing (Supplementary Fig. 10). The reason behind such heterogeneity remains to be discovered but could reflect differences in burden of initial invasion or in the ability to heal or to fight invasion.

Differential effects on P and p in long-lived mutants. In this study, we have shown how combined pathology and mortality analysis allows deconvolution of *C. elegans* mortality profiles, providing a means to understand how interventions alter lifespan in terms of effects on pathology. Examples modelling the effects on mortality and survival due to theoretical alterations in frequency or timing of P and/or p deaths are shown in Fig. 4, many of which resemble real lifespan data observed here and in previous studies (Supplementary Fig. 11). For example, lack of a germline in *glp-1(e2141)* delays p deaths by >10 days but has little effect on either the timing or frequency of P death (Fig. 3e,f;

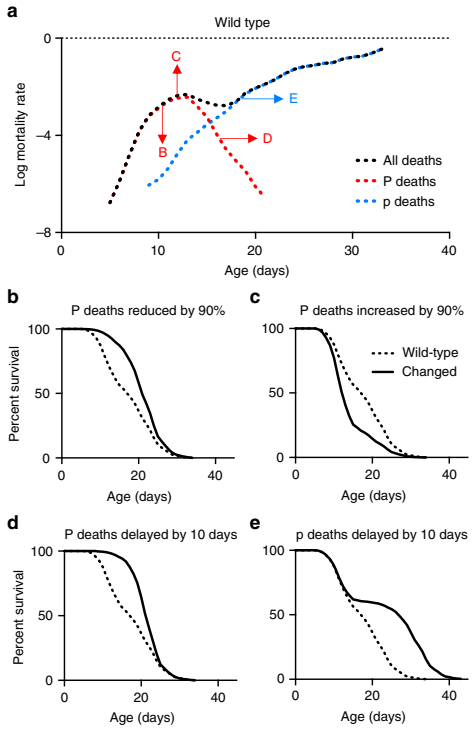

Figure 4 | How mortality deconvolution can decipher survival curves. (**a**) Log mortality rate of an idealized wild-type population. P and p survival were adapted from the P and p death survival calculations in Fig. 1g, and the survival proportions of the whole population were calculated, assuming that P death is 40% of the population and p death is 60%. The resulting survival data were used to calculate the log mortality rate. Arrows show the direction of mortality rate shift by transformations of survival data resulting in lifespan changes shown in (**b**–**e**). Dotted lines, wild-type data; solid lines, data after specified transformation. (**b**) 90% decrease in P deaths. (**c**) 90% increase in P deaths. (**d**) 10-day delay in P deaths. (**e**) No change in P deaths, with 10-day delay in p deaths. For mortality rate plots for (**b**–**e**), see Supplementary Fig. 11.

Supplementary Table 6), which explains the atypical neck-and-shoulder shape of its survival curve[22]. Another example is the short-lived *ced-1(e1735)* mutant, which is hyper-susceptible to pharyngeal invasion by pathogenic bacteria[15]. Its short lifespan on *E. coli* is due to increased frequency (without changes in timing) of P death, as well as faster die-off of p worms (Fig. 3g,h; Supplementary Table 7). In contrast, *eat-2* provides an example of how increased lifespan can result from reduced P death frequency (Fig. 3d). Thus different lifespan-altering interventions can act by differentially affecting different pathologies.

Discussion

As a model organism, *C. elegans* has generated numerous insights and discoveries in the ageing field that have proven to be applicable in higher organisms. However, a long-standing obstacle is that it is difficult to follow the causal chain connecting genes and proteins to demographic parameters, such as lifespan and mortality rate. We argue that to better understand ageing in *C. elegans* requires knowledge not just of genes that influence lifespan but also of the pathologies of ageing and how these cause death. This study describes a novel approach to understanding demographic data in *C. elegans* based on the combined analysis of pathology and mortality (and conceptually similar approaches have been used in human clinical studies, c.f. the competing risks model[23]). This provides a route to discover the biological mechanisms of ageing underlying survival curves and mortality profiles in this powerful model organism.

But is P death attributable to ageing, or is it merely the result of bacterial infection? In order to maximize the contribution of intrinsic determinants of senescence, would it not be better simply to exclude P death, for example, by using antibiotics? Certainly, excluding P death can facilitate analysis of intrinsic determinants of senescence. However, our results suggest that the P subpopulation is itself a useful model for studying the biology of ageing. For example, they suggest that damage incurred early (mechanical damage to the pharyngeal cuticle and contained infections within pharyngeal tissue) lie latent during early–mid adulthood but then recrudesce in later life, potentially due to action of intrinsic determinants of senescence (Supplementary Fig. 8e). Thus the P subpopulation may be used to investigate how early damage can interact with later intrinsic causes of ageing to determine senescent pathology and mortality.

Methods

Culture methods and strains. Standard *C. elegans* maintenance was performed using standard protocol[24]. Strains were grown at 20 °C on nematode growth media (NGM) plates seeded with *E. coli* OP50 to provide a food source. *C. elegans* strains: An N2 hermaphrodite stock recently obtained from the Caenorhabditis Genetics Center was used as wild type (N2 CGCH)[25]. For necropsy analysis: CB3203 *ced-1(e1735) I*, CB4037 *glp-1(e2141) III*, DA597 *phm-2(ad597) I*, DA1116 *eat-2(ad1116) II*, DA493 *phm-3(ad493) III*, DA522 *eat-13(ad522) X*, DA698 *unc-36(ad698) III*, DA521 *egl-4(ad450) IV*, DA606 *eat-10(ad606) IV*, DA464 *eat-5(ad464) I*, DA591 *unc-10(ad591) X*, DA1110 *eat-18(ad1110) I*. For confocal microscopy: BC12677 *dpy-5(e907) I; sIs11111 [rCesC32F10.8::GFP + pCeh361]* (GFP in muscle cells), BC12754 *dpy-5(e907) I; sIs12567[rCesC07H6.3::GFP + pCeh361]* (GFP in marginal cells), BC16329 *dpy-5(e907) I; IsEx16329[rCesF20B10.1::GFP + pCeh361]* (GFP in g1 pharyngeal gland cells).

E. coli OP50 expressing red fluorescent protein (OP50-RFP) was generated by transforming OP50 with plasmid pRZT3 (kindly provided by J.F. Rawls, Duke University, originally from W. Bitter, Vrije University)[26]. pRZT3 contains genes for tetracycline resistance and RFP (DsRed), under the control of a constitutive *lac* promoter. OP50-RFP was grown on lysogeny broth (LB) plates and in LB broth in the presence of 25 μg ml^{-1} tetracycline. However, before NGM plates were seeded, OP50-RFP was resuspended in LB broth without tetracycline. This was to avoid effects of tetracycline on bacterial pathogenicity that might occur even in the presence of the tetracycline-resistance plasmid. Worms were then raised from hatching on OP50-RFP.

To examine the role of proliferating bacteria on pharyngeal swelling, bacterial growth was prevented in two ways. Carbenicillin was added topically onto a 2-day-old bacterial lawn to a final concentration of 4 mM. Unless otherwise specified, worms were transferred from untreated OP50 at L4 stage. For ultraviolet killing, 80 μl of OP50 was added to each NGM plate and left overnight at 20 °C. Plates were then exposed to ultraviolet light for 30 min. Worms were raised on ultraviolet-killed bacteria from aseptic eggs.

Lifespan and Ziehm tables. Lifespan measurements were performed as follows. Trials were conducted at 20 °C unless otherwise specified and without 5-fluoro-2′-deoxyuridine (FUDR). Worms were transferred daily during the reproductive period. Mortality was scored daily to ensure that corpses were fresh and not decomposed, to aid necropsy analysis. Worms that were scored as dead were collected for microscopy. Lifespan measurements were repeated at least twice unless otherwise stated, and survival plots were generated using the combined lifespan data.

In addition to standard presentations of survival data in the form of survival curves and tables of analysed statistics (for example, mean lifespan, comparison statistics), we have also included tables of raw mortality data. The purpose of the latter is to enable future investigators to reanalyse the data, for example, in data mining approaches or for the purpose of resolving discrepancies between different published reports. To this end, we employ a mortality data reporting format developed by M. Ziehm, which applies minimal reporting standards to ensure

inclusion of all essential information about experimental conditions. Data include specification of causes of data censoring, as follows: bag = bag of worms (death from internal hatching of eggs); cont = contaminated (bacterial or fungal infection); dis = disappeared (investigator failed to locate worm); kil = killed (worm accidentally killed during handling); cen = censored (censored without a recorded reason); otw = on the wall (worms climbed wall of Petri dish and died from desiccation); and rup = rupture (internal organs extensively extruded through vulva). We include, for other investigators who choose to take this approach, an unpopulated Ziehm table (Supplementary Data 1).

Survival and mortality analysis. For survival analysis of P or p deaths only (Fig. 1d), all observations from worms with pharynx pathology of the other type were excluded. For mortality analysis (Fig. 1h), log mortality rate of the P and p cohorts were calculated with the other type censored, which allows presentation of the risks in relation to the whole population. Survival and mortality plots were generated using GraphPad Prism with no smoothing.

For the archive data collected at University of Missouri-Columbia (1994–1996) and UCL (1998–2000), mortality plots were generated using SurvCurv[27] using a sliding window smoothing of ±2. Analysis of mortality data revealed that for unknown reasons N2 worms lived 3 days longer at UCL than at UMC. Therefore, we adjusted for this 3-day difference when combining and plotting the mortality data.

Microscopy. Live worms or corpses were mounted onto 2% agar pads. Live worms were anaesthetized by placing them in a drop of 0.2% levamisole. Nomarski images of worms were collected using a Zeiss Axioskop 2 plus microscope with a Hamamatsu ORCA-ER digital camera C4742-95 and Volocity 6.3 software (Macintosh version) for image acquisition. The presence of *E. coli* OP50-RFP in the pharynx was assayed using a rhodamine filter cube (excitation: 540–552 nm; emission: >590 nm).

Before confocal or electron microscopy, aged worms were separated into three groups based on the pattern of red fluorescence from *E. coli* OP50-RFP in their pharynxes: a pharynx full of RFP was taken to be fully infected; a pharynx with medium-sized RFP inclusions was taken to be at an early stage of infection; and a pharynx with no RFP was taken to have no infection. Confocal images were acquired using Zen2009 software driving a LSM-710 confocal station with an inverted Zeiss Axio Observer microscope.

For electron microscopy, worms were prepared using a standard protocol (protocol 8 (ref. 28)). In brief, animals were washed in M9 and then cut in half using 30 G needles. Heads were collected in fixing solution (2.5% glutaraldehyde, 1% paraformaldehyde in 0.1 M sucrose, 0.05 M cacodylate) on ice, rinsed 3 times in 0.2 M cacodylate, fixed in 0.5% OsO_4 and 0.5% $KFe(CN)_6$ in 0.1 M cacodylate on ice and sequentially washed in 0.1 M cacodylate and 0.1 M NaAcetate. Worms were then stained in 1% UAc in 0.1 M NaAcetate (pH 5.2) for 60 min, rinsed 3 times in 0.1 M NaAcetate and rinsed overnight in distilled water. Samples were then embedded in 3% seaplaque agarose, dehydrated and infiltrated through ethanol and propylene-resin series and then cured in 60 °C oven for 3 days. Serial 1 µm sections were taken for light microscopy and at the region of interest ultra-thin sections were cut at 70–80 nm using a diamond knife on a Reichert ultramicrotome. Sections were collected on 300 mesh copper grids and stained with lead citrate before being viewed in a Joel 1010 transition electron microscope. Images were recorded using a Gatan Orius camera. Images were obtained using the Gatan imaging software and then exported into TIFF format.

Measuring *E. coli* content of the pharynx. Worms on day 10 or 11 of adulthood (20 °C) were divided into two groups, those with and without pharyngeal swelling. The posterior bulb of the pharynx was then dissected out using a 31 G needle. These were placed in 120 µl M9 buffer and macerated using the needle. The resulting lysates were vortexed for 30 s and then centrifuged for 1 min at 13,000 r.p.m. Bacterial concentration in supernatants was determined after serial dilution in M9 solution by plating onto LB plates, followed by counts of colony-forming units.

Necropsy analysis. A series of microscope images at ×400 or ×630 magnification were collected along the length of each corpse using Nomarski optics and examined for the presence of any unusual pathologies beyond those typically seen in elderly hermaphrodites[4,5,29]. The pharynx in particular was examined closely to determine whether bacteria was visible within the tissue, and then the area of the posterior bulb was measured using either the Image J or the Volocity 6.3 software.

Measuring pharyngeal pumping rate. Worms were examined *in situ* on NGM agar plates using a Nikon SMZ645 microscope for 15 s, and the number of pharynx pumps was scored manually using a clicker counter. This was repeated three times for each worm, from which mean pumps per minute was calculated.

Longitudinal pathology analysis on individual worms. Worms were cultured individually at 20 °C. On days 4,7,11 and 14 of adulthood, each worm was imaged individually. For imaging, microscope slides were prepared by taping two coverslips on the slide, at each edge, leaving an empty space in the middle for the agarose pad. The worm was then placed on a 2% agarose pad on the slide. Another coverslip was then placed on top but resting on the two side coverslips to reduce the pressure exerted on the worm. The slide was then placed on a PE120 Peltier cooling stage (Linkam Scientific) set to 4 °C. Within a couple of minutes of cooling, the nematodes ceased to move, and images were taken at ×630 magnification using a Zeiss Axioskop. After imaging, each worm was carefully recovered by pipetting 20 µl of M9 buffer between the top coverslip and the agar pad. The coverslip was lifted gently to minimize stress to the worm. The worm was then returned to an NGM plate. Images of pharynxes, distal gonads and uterine tumours were scored on an ordinal scale with scores 1–5 (refs 4,7). Score 1 represents a healthy tissue; score 2 indicates some minor tissue disorder; scores 3/4 are where minor/major pathology has developed and score 5 is where pathology development has reached its maximum. Yolk pools and intestinal atrophy were analysed using semi-quantitative approaches, measuring the area of the yolk pools and intestinal width relative to body area or width, respectively. Lifespans were recorded every day.

Statistics. For lifespan assays, survival and mortality graphs were generated using the Graphpad Prism software, and statistical tests for significant difference between survival curves were performed using the log-rank test. Log-rank tests of both the P cohort versus the p cohort and the P cohort versus all deaths showed highly significant differences ($P<10^{-15}$ and $P<10^{-6}$, respectively), and the p cohort is also significantly different ($P=10^{-3}$) from the cohort of all deaths. For analysis of mortality deceleration, the significance of slope change was tested using GraphPad Prism comparing slopes of linear regression lines[30]. Correlations from single worm, longitudinal pathology analysis were analysed using the Spearman Rank test. The correlation between pumping span and age at death was calculated using a linear regression model, and the comparison of these slopes between worms either on proliferative or non-proliferated bacteria were calculated using a linear model in JMP 11.

Data availability. The data that support the findings of this study are available from the corresponding author upon reasonable request. For the survival assays we have shown, raw data are available in the form of Ziehm tables provided in Supplementary Data 1 of this publication.

References

1. Kenyon, C. J. The genetics of ageing. *Nature* **464,** 504–512 (2010).
2. Lapierre, L. R. & Hansen, M. Lessons from *C. elegans*: signaling pathways for longevity. *Trends Endocrinol. Metab.* **23,** 637–644 (2012).
3. Gems, D. What is an anti-aging treatment? *Exp. Gerontol.* **58,** 14–18 (2014).
4. Garigan, D. *et al.* Genetic analysis of tissue aging in *Caenorhabditis elegans*: a role for heat-shock factor and bacterial proliferation. *Genetics* **161,** 1101–1112 (2002).
5. Herndon, L. A. *et al.* Stochastic and genetic factors influence tissue-specific decline in ageing *C. elegans*. *Nature* **419,** 808–814 (2002).
6. Tank, E. M., Rodgers, K. E. & Kenyon, C. Spontaneous age-related neurite branching in *Caenorhabditis elegans*. *J. Neurosci.* **31,** 9279–9288 (2011).
7. Riesen, M. *et al.* MDL-1, a growth- and tumor-suppressor, slows aging and prevents germline hyperplasia and hypertrophy in *C. elegans*. *Aging* **6,** 98–117 (2014).
8. Huang, C., Xiong, C. & Kornfeld, K. Measurements of age-related changes of physiological processes that predict lifespan of *Caenorhabditis elegans*. *Proc. Natl Acad. Sci. USA* **101,** 8084–8089 (2004).
9. Rea, S. L., Wu, D., Cypser, J. R., Vaupel, J. W. & Johnson, T. E. A stress-sensitive reporter predicts longevity in isogenic populations of *Caenorhabditis elegans*. *Nat. Genet.* **37,** 894–898 (2005).
10. Sanchez-Blanco, A. & Kim, S. K. Variable pathogenicity determines individual lifespan in *Caenorhabditis elegans*. *PLoS Genet.* **7,** e1002047 (2011).
11. Vaupel, J. W., Johnson, T. E. & Lithgow, G. J. Rates of mortality in populations of *Caenorhabditis elegans*. *Science* **266,** 826 (1994).
12. Johnson, T. E., Wu, D., Tedesco, P., Dames, S. & Vaupel, J. W. Age-specific demographic profiles of longevity mutants in *Caenorhabditis elegans* show segmental effects. *J. Gerontol.* **56,** B331–B339 (2001).
13. Brooks, A., Lithgow, G. J. & Johnson, T. E. Mortality rates in a genetically heterogeneous population of *Caenorhabditis elegans*. *Science* **263,** 668–671 (1994).
14. Wu, D., Rea, S. L., Yashin, A. I. & Johnson, T. E. Visualizing hidden heterogeneity in isogenic populations of *C. elegans*. *Exp. Gerontol.* **41,** 261–270 (2006).
15. Haskins, K. A., Russell, J. F., Gaddis, N., Dressman, H. K. & Aballay, A. Unfolded protein response genes regulated by CED-1 are required for *Caenorhabditis elegans* innate immunity. *Dev. Cell* **15,** 87–97 (2008).
16. Gems, D. & Riddle, D. L. Genetic, behavioral and environmental determinants of male longevity in *Caenorhabditis elegans*. *Genetics* **154,** 1597–1610 (2000).
17. Zhang, W. B. *et al.* Extended twilight among isogenic *C. elegans* causes a disproportionate scaling between lifespan and health. *Cell Syst.* **3,** 333–345 (2016).
18. Stroustrup, N. *et al.* The temporal scaling of *Caenorhabditis elegans* ageing. *Nature* **530,** 103–107 (2016).

19. Raizen, D. M., Lee, R. Y. & Avery, L. Interacting genes required for pharyngeal excitation by motor neuron MC in *Caenorhabditis elegans*. *Genetics* **141,** 1365–1382 (1995).
20. Lakowski, B. & Hekimi, S. The genetics of caloric restriction in *Caenorhabditis elegans*. *Proc. Natl Acad. Sci. USA* **95,** 13091–13096 (1998).
21. Pujol, N. *et al.* Distinct innate immune responses to infection and wounding in the *C. elegans* epidermis. *Curr. Biol.* **18,** 481–489 (2008).
22. Arantes-Oliveira, N., Apfeld, J., Dillin, A. & Kenyon, C. Regulation of life-span by germ-line stem cells in *Caenorhabditis elegans*. *Science* **295,** 502–505 (2002).
23. Austin, P. C., Lee, D. S. & Fine, J. P. Introduction to the analysis of survival data in the presence of competing risks. *Circulation* **133,** 601–609 (2016).
24. Brenner, S. The genetics of *Caenorhabditis elegans*. *Genetics* **77,** 71–94 (1974).
25. Gems, D. & Riddle, D. L. Defining wild-type life span in *Caenorhabditis elegans*. *J. Gerontol.* **55,** B215–B219 (2000).
26. van der Sar, A. M. *et al.* Zebrafish embryos as a model host for the real time analysis of *Salmonella typhimurium* infections. *Cell. Microbiol.* **5,** 601–611 (2003).
27. Ziehm, M., Ivanov, D. K., Bhat, A., Partridge, L. & Thornton, J. M. SurvCurv database and online survival analysis platform update. *Bioinformatics* **31,** 3878–3880 (2015).
28. Shaham, S. in *WormBook* (ed. The *C. elegans* Research Community) (2006).
29. Gems, D. & de la Guardia, Y. Alternative perspectives on aging in *Caenorhabditis elegans*: reactive oxygen species or hyperfunction? *Antioxid. Redox Signal* **19,** 321–329 (2013).
30. Zar, J. H. *Biostat. Anal.* (Prentice Hall, Upper Saddle River, NJ, USA, 1999).
31. McGee, M. D. *et al.* Loss of intestinal nuclei and intestinal integrity in aging *C. elegans*. *Aging Cell* **10,** 699–710 (2011).

Acknowledgements

We thank N. Alic, A. Benedetto, F. Cabreiro, N. Pujol (Marseille University) and members of the Gems lab for useful discussion and/or comments on the manuscript; J.F. Rawls (Duke University) and N. Stroustrup (Harvard University) for reagents; and C. Au for technical assistance. We also thank D. Hall and L. Herndon (Albert Einstein College of Medicine) for advice and access to TEM images on WormImage.org, which is supported by NIH (OD 010943). Some strains were provided by the Caenorhabditis Genetics Center, which is funded by NIH Office of Research Infrastructure Programs (P40 OD010440). This work was supported by a Wellcome Trust Strategic Award (098565/Z/12/Z) and an EU grant (FP6-518230, IDEAL).

Author contributions

A.F.G., D.G. and Y.Z. conceived the project. A.F.G., M.E., D.M., L.P., Z.P., H.W., C.Y., W.B.Z. and Y.Z. performed experiments and/or analysed and/or interpreted data. M.T. prepared worms for electron microscopy. G.P. and M.Z. analysed archive lifespan assay data and mortality data. A.F.G., D.G. and Y.Z. wrote the paper.

Additional information

Supplementary Information accompanies this paper at http://www.nature.com/naturecommunications

Competing interests: The authors declare no competing financial interests.

Reprints and permission information is available online at http://npg.nature.com/reprintsandpermissions/

How to cite this article: Zhao, Y. *et al.* Two forms of death in ageing *Caenorhabditis elegans*. *Nat. Commun.* **8,** 15458 doi: 10.1038/ncomms15458 (2017).

Publisher's note: Springer Nature remains neutral with regard to jurisdictional claims in published maps and institutional affiliations.

This work is licensed under a Creative Commons Attribution 4.0 International License. The images or other third party material in this article are included in the article's Creative Commons license, unless indicated otherwise in the credit line; if the material is not included under the Creative Commons license, users will need to obtain permission from the license holder to reproduce the material. To view a copy of this license, visit http://creativecommons.org/licenses/by/4.0/

© The Author(s) 2017

Bibliography

Abrams PA (1993) Does increased mortality favor the evolution of more rapid senescence? *Evolution (N. Y).* 47, 877–887.

Adachi H & Ishii N (2000) Effects of tocotrienols on life span and protein carbonylation in *Caenorhabditis elegans*. *Journals Gerontol.* 55A, 280–285.

Aitlhadj L & Stürzenbaum SR (2010) The use of FUdR can cause prolonged longevity in mutant nematodes. *Mech. Ageing Dev.* 131, 364–5.

Allman E, Johnson D & Nehrke K (2009) Loss of the apical V-ATPase a-subunit VHA-6 prevents acidification of the intestinal lumen during a rhythmic behavior in *C. elegans*. *Am J Physiol Cell Physiol* 297, 1071–1081.

Altun ZF & Hall DH (2009a) Alimentary system, intestine. *WormAtlas*.

Altun ZF & Hall DH (2009b) Alimentary system, pharynx. *WormAtlas*.

Altun ZF & Hall DH (2009c) Introduction. *WormAtlas*.

Angeli S, Klang I & Sivapatham R (2013) A DNA synthesis inhibitor is protective against proteotoxic stressors via modulation of fertility pathways in *Caenorhabditis elegans*. *Aging (Albany. NY).* 5, 759–769.

Baban CK, Cronin M, O'Hanlon D, O'Sullivan GC & Tangney M (2010) Bacteria as vectors for gene therapy of cancer. *Bioeng. Bugs* 1, 385–94.

Barton M & Kimble J (1990) *fog-1*, a regulatory gene required for specification of spermatogenesis in the germ line of *Caenorhabditis elegans*. *Genetics* 125, 29–39.

Beanan MJ & Strome S (1992) Characterization of a germ-line proliferation mutation in *C. elegans*. *Development* 116, 755–66.

Bergquist DC, Williams FM & Fisher CR (2000) Longevity record for deep-sea invertebrate. *Nature* 403, 499–500.

Berset, T, Hoier EF, Battu G, Canevascini S & Hajnal A (2001) Notch inhibition of RAS signaling through MAP kinase phosphatase LIP-1 during *C. elegans* vulval development. *Science* 291, 1055–1058.

Bijnsdorp I V., Comijn EM, Padron JM, Gmeiner WH & Peters GJ (2007) Mechanisms of action of FdUMP[10]: Metabolite activation and thymidylate synthase inhibition. *Oncol. Rep.* 18, 287–291.

Blagosklonny M (2008) Aging: ROS or TOR. *Cell cycle* 7, 3344–3354.

Blagosklonny M (2006) Aging and immortality: quasi-programmed senescence and its pharmacologic inhibition. *Cell Cycle* 5:18, 2087–2102.

Brenner S (1974) The genetics of *Caenorhabditis elegans*. *Genetics* 77, 71–94.

Brooks A, Lithgow GJ & Johnson TE (1994) Mortality rates in a genetically heterogeneous population of *Caenorhabditis elegans*. *Science.* 263, 668–671.

Campion EW, Getahun H, Matteelli A, Chaisson RE & Raviglione M (2015) Latent *Mycobacterium tuberculosis* Infection. *N. Engl. J. Med.* 372, 2127–2135.

Cassada RC & Russell RL (1975) The dauerlarva, a post-embryonic developmental variant of the nematode *Caenorhabditis elegans*. *Dev. Biol.* 46, 326–342.

Chiang WC, Ching TT, Lee HC, Mousigian C & Hsu AL (2012) HSF-1 regulators DDL-1/2 link insulin-like signaling to heat-shock responses and modulation of longevity. *Cell* 148, 322–334.

Chinnaiyan a M, O'Rourke K, Lane BR & Dixit VM (1997) Interaction of CED-4 with CED-3 and CED-9: a molecular framework for cell death. *Science.* 275, 1122–1126.

Chow DK, Glenn CF, Johnston JL, Goldberg IG & Wolkow CA (2006) Sarcopenia in the *Caenorhabditis elegans* pharynx correlates with muscle contraction rate over lifespan. *Exp. Gerontol.* 41, 252–260.

Church DL, Guan KL & Lambie EJ (1995) Three genes of the MAP kinase cascade, *mek-2, mpk-1/sur-1 and let-60 ras*, are required for meiotic cell cycle progression in Caenorhabditis elegans. *Development* 121, 2525–2535.

Clancy DJ, Gems D, Harshman LG, OIdham S, Stocker H, Hafen E, Leevers SJ & Partridge L (2001) Extension of life-span by loss of CHICO, a *Drosophila* insulin receptor substrate protein. *Science.* 292, 104–106.

Coburn C, Allman E, Mahanti P, Benedetto A, Cabreiro F, Pincus Z, Matthijssens F, Araiz C, Mandel A, Vlachos M, Edwards S-A, Fischer G, Davidson A, Pryor RE, Stevens A, Slack FJ, Tavernarakis N, Braeckman BP, Schroeder FC, Nehrke K & Gems D (2013) Anthranilate fluorescence marks a calcium-propagated necrotic wave that promotes organismal death in *C. elegans*. *PLoS Biol.* 11, 1–17.

Condradt B & Horivitz HR (1998) The *C. elegans* protein EGL-1 is required for programmed cell death and interacts with Bcl-2-like protein CED-9. *Cell* 93, 519–529.

The *C. elegans* Sequencing Consortium (1998) Genome sequence of the nematode C. elegans: A platform for investigating biology. *Science.* 282, 2012–2018.

Corski AK, Wightman B & Chalfie MA (2015) A primer on *Caenorhabditis elegans*. *WormBook*. Available at: http://www.wormbook.org.

Cracowski JL, Durand T & Bessard G (2002) Isoprostanes as a biomarker of lipid peroxidation in humans: Physiology, pharmacology and clinical implications. *Trends Pharmacol. Sci.* 23, 360–366.

Cummins J & Tangney M (2013) Bacteria and tumours: causative agents or opportunistic inhabitants? *Infect. Agent. Cancer* 8, 11.

Dambroise E, Monnier L, Ruisheng L, Aguilaniu H, Joly J-S, Tricoire H & Rera M (2016) Two phases of aging separated by the Smurf transition as a public path to death. *Nat. Publ. Gr.*, 1–7.

Davies M, Judge A, Stokes K, Delmestri A, Kemp S, Arden NK & Newton JL (2016) Is rugby playing load predictive of lower limb osteoarthritis in former international rugby players? *Osteoarthr. Cartil.* 24, S533–S534.

DePina AS, Iser WB, Park S-S, Maudsley S, Wilson MA & Wolkow CA (2011) Regulation of *Caenorhabditis elegans* vitellogenesis by DAF-2/IIS through separable transcriptional and posttranscriptional mechanisms. *BMC Physiol.* 11, 11.

Dickinson DJ & Goldstein B (2016) CRISPR-based methods for *Caenorhabditis* elegans genome engineering. *Genetics* 202, 885–901.

Dirksen P, Marsh SA, Braker I, Heitland N, Wagner S, Nakad R, Mader S, Petersen C, Kowallik V, Rosenstiel P, Félix M-A & Schulenburg H (2016) The native microbiome of the nematode *Caenorhabditis elegans*: gateway to a new host-microbiome model. *BMC Biol.* 14, 1–16.

Doonan R, McElwee JJ, Matthijssens F, Walker GA, Houthoofd K, Back P, Matscheski A, Vanfleteren JR & Gems D (2008) Against the oxidative damage theory of aging: superoxide dismutases protect against oxidative stress but have little or no effect on life span in *Caenorhabditis elegans*. *Genes Dev.* 22, 3236–41.

Ellis H & Horvitz HR (1986) Genetic control of programmed cell death in the nematode *C. elegans*. *Cell* 44, 817–829.

Fire A, Xu S, Montgomery MK, Kostas SA, Driver SE & Mello CC (1998) Potent and specific genetice interference by double-stranded RNA in *Caenorhabditis elegans*. *Nature* 391, 806–811.

Francis R, Barton M, Kimble J & Schedl T (1995) *gld-1*, a tumor suppressor gene Required for oocyte development in *Caenorhabditis elegans*. *Genetics* 139, 579–606.

Friedman D & Johnson T (1988) A mutation in the *age-1* gene in *Caenorhabditis elegans* lengthens life and reduces hermaphrodite fertility. *Genetics* 118, 75–86.

Gandhi S, Santelli J, Mitchell DH, Stiles JW & Sanadi DR (1980) A simple method for maintaining large, aging populations of *Caenorhabditis elegans*. *Mech. Ageing Dev.* 12, 137–150.

Garigan D, Hsu A-L, Fraser AG, Kamath RS, Ahringer J & Kenyon C (2002) Genetic analysis of tissue aging in *Caenorhabditis elegans*: a role for heat-shock factor and bacterial proliferation. *Genetics* 161, 1101–12.

Garsin DA (2003) Long-lived *C. elegans daf-2* mutants are resistant to bacterial pathogens. *Science (80-.).* 300, 1921–1921.

Gartner A, Milstein S, Ahmed S, Hodgkin J, Hengartner MO, Brook S & York N (2000) A conserved checkpoint pathway mediates DNA damage–induced apoptosis and cell cycle arrest in *C . elegans*. *Mol. Cell* 5, 435–443.

Gelino S, Chang JT, Kumsta C, She X, Davis A, Nguyen C, Panowski S & Hansen M (2016) Intestinal autophagy improves healthspan and longevity in *C. elegans* during dietary restriction. *PLoS Genet.* 12, 1–24.

Gelino S & Hansen M (2012) Autophagy - an emerging anti-aging mechanism. *J Clin Exp Pathol*, 1–24.

Gems D (2015) The aging-disease false dichotomy: Understanding senescence as pathology. *Front. Genet.* 6, 1–7.

Gems D & Doonan R (2009) Antioxidant defense and aging in *C. elegans*: Is the oxidative damage theory of aging wrong? *Cell Cycle* 8, 1681–7.

Gems D & de la Guardia Y (2013) Alternative perspectives on aging in *Caenorhabditis elegans*: reactive oxygen species or hyperfunction? *Antioxid. Redox Signal.* 19, 321–9.

Gems D & Riddle D (2000) Genetic, behavioral and environmental determinants of male longevity in *Caenorhabditis elegans*. *Genetics* 154, 1597–610.

Gems D & Riddle D (1996) Longevity in *Caenorhabditis elegans* reduced by mating but not gamete production. *Nature* 379, 723–725.

Glantschnig H, Fisher JE, Wesolowski G, Rodan GA & Reszka AA (2003) M-CSF, TNFalpha and RANK ligand promote osteoclast survival by signaling through mTOR/S6 kinase. *Cell Death Differ.* 10, 1165–77.

Golden J & Riddle D (1982) A pheromone influences larval development in the nematode *Caenorhabditis* elegans. *Science (80-.).* 218, 578–580.

Golden J & Riddle D (1984) The *Caenorhabditis elegans* dauer larva: developmental effects of pheromone, food, and temperature. *Dev. Biol.* 78, 368–378.

Golden TR, Beckman KB, Lee AHJ, Dudek N, Hubbard A, Samper E & Melov S (2007) Dramatic age-related changes in nuclear and genome copy number in the nematode *Caenorhabditis elegans*. *Aging Cell* 6, 179–88.

Gumienny TL, Lambie E, Hartwieg E, Horvitz HR & Hengartner MO (1999) Genetic control of programmed cell death in the *Caenorhabditis elegans* hermaphrodite germline. *Development* 126, 1011–22.

Haldane JBS (1941) *News Paths in Genetics*, New York & London: George Allen & Unwin.

Hall-Stoodley L, Costerton JW & Stoodley P (2004) Bacterial biofilms: from the natural environment to infectious diseases. *Nat. Rev. Microbiol.* 2, 95–108.

Hansen M, Chandra A, Mitic LL, Onken B, Driscoll M & Kenyon C (2008) A role for autophagy in the extension of lifespan by dietary restriction in *C. elegans*. *PLoS Genet.* 4.

Hansen M, Taubert S, Crawford D, Libina N, Lee SJ & Kenyon C (2007) Lifespan extension by conditions that inhibit translation in *Caenorhabditis elegans*. *Aging Cell* 6, 95–110.

Harman D (1956) Aging: a theory based on free radical and radiation chemistry. *J. Gerontol.* 11, 298–300.

Harrington L & Harley C (1988) Effect of vitamin E on lifespan and reproduction in *Caenorhabditis elegans*. *Mech. Ageing Dev.* 43, 71–78.

Harrison DE, Strong R, Sharp ZD, Nelson JF, Astle CM, Flurkey K, Nadon NL, Wilkinson JE, Frenkel K, Carter CS, Pahor M, Javors MA, Fernandez E & Miller RA (2010) Rapamycin fed late in life extends lifespan in genetically heterogeneous mice. *Nature* 460, 392–395.

Hars ES, Qi H, Ryazanov AG, Jin S, Cai L, Hu C & Liu LF (2007) Autophagy regulates ageing in *C. elegans*. *Autophagy* 3, 93–95.

Hashimoto Y, Ookuma S & Nishida E (2009) Lifespan extension by suppression of autophagy genes in *Caenorhabditis elegans*. *Genes to Cells* 14, 717–726.

Haskins KA, Russell JF, Gaddis N, Dressman HK & Aballay A (2008) Unfolded Protein Response Genes Regulated by CED-1 Are Required for *Caenorhabditis elegans* Innate Immunity. *Dev. Cell* 15, 87–97.

Hengartner M & Horvitz HR (1994a) *C. elegans* cell survival gene *ced-9* encodes a functional homolog of the mammalian proto-oncogene *bcl-2*. *Cell* 76, 666–676.

Hengartner MO & Horvitz HR (1994b) The ins and outs of programmed cell death during C. elegans development. *Phil. Trans. R. Soc. Lond.* 345, 243–246.

Herndon LA, Schmeissner PJ, Dudaronek JM, Brown PA, Listner KM, Sakano Y, Paupard MC, Hall DH & Driscoll M (2002) Stochastic and genetic factors influence tissue-specific decline in ageing *C. elegans*. *Nature* 419, 808–14.

Herpes Zoster and Functional Decline Consortium (2015) Functional decline and *Herpes zoster* in older people: an interplay of multiple factors. *Aging Clin. Exp. Res.* 27, 757–765.

Hirsch D, Oppenheim D & Klass M (1976) Development of the reproductive system of *Caenorhabditis elegans*. *Dev. Biol.* 49, 200–219.

Hodgkin J (1987) A genetic analysis of the sex-determining gene, *tra-1*, in the nematode *Caenorhabditis elegans*. *Genes Dev.* 1, 731–745.

Hodgkin J (1983) Male phenotypes and mating efficiency in *Caenorhabditis elegans*. *Genetics* 103, 43–64.

Hofmann ER, Milstein S, Boulton SJ, Ye J, Hofmann JJ, Stergiou L, Gartner A, Vidal M & Hengartner MO (2002) *Caenorhabditis elegans* HUS-1 is a DNA damage checkpoint protein required for genome stability and induction of EGL-1. *Curr. Biol.* 12, 1908–1918.

Holzenberger M, Dupont J, Ducos B, Leneuve P, Géloën A, Even PC, Cervera P & Le Bouc Y (2003) IGF-1 receptor regulates lifespan and resistance to oxidative stress in mice. *Nature* 421, 182–187.

Horvitz HR, Chalfie M, Trent C, Sulston JE & Evans PD (1982) Serotonin and octopamine in the nematode *Caenorhabditis elegans*. *Science* 216, 1012–4.

Hosono R (1978) Sterilization and growth inhibition of *Caenorhabditis elegans* by 5-fluorodeoxyuridine. *Exp. Gerontol.* 13, 369–373.

Hosono R, Mitsui Y, Sato Y, Aizawa S & Miwa J (1982) Life span of the wild and mutant nematode *Caenorhabditis elegans*. Effects of sex, sterilization, and temperature. *Exp. Gerontol.* 17, 163–172.

Houthoofd K, Braeckman BP, Lenaerts I, Brys K, De Vreese A, Van Eygen S & Vanfleteren JR (2002) Ageing is reversed, and metabolism is reset to young levels in recovering dauer larvae of *C. elegans*. *Exp. Gerontol.* 37, 1015–1021.

Howes RM (2006) The free radical fantasy: A panoply of paradoxes. *Ann. N. Y. Acad. Sci.* 1067, 22–26.

Hsin H & Kenyon C (1999) Signals from the reproductive system regulate the lifespan of *C. elegans*. *Nature* 399, 362–366.

Hsu A-L, Murphy CT & Kenyon C (2003) Regulation of aging and age-Related disease by DAF-16 and heat-shock factor. *Science.* 300, 1142–1145.

Huang C, Xiong C & Kornfeld K (2004) Measurements of age-related changes of physiological processes that predict lifespan of *Caenorhabditis elegans*. *Proc. Natl. Acad. Sci. U. S. A.* 101, 8084–9.

Hughes SE, Evason K, Xiong C & Kornfeld K (2007) Genetic and pharmacological factors that influence reproductive aging in nematodes. *PLoS Genet.* 3, 0254–0265.

Hughes SE, Huang C & Kornfeld K (2011) Identifcation of mutations that delay somatic or reproductive aging of *Caenorhabditis elegans*. *Genetics* 189, 341–356.

Iwasaki K, James M, Francis R & Schedl T (1996) *emo-1*, a *Caenorhabditis elegans* Sec61py homologue, is required for oocyte development and ovulation. *J. Cell Biol.* 134, 699–714

Jaramillo-Lambert A, Ellefson M, Villeneuve AM & Engebrecht J (2007) Differential timing of S phases, X chromosome replication, and meiotic prophase in the *C. elegans* germ line. *Dev. Biol.* 308, 206–221.

Jia K, Chen D & Riddle D (2004) The TOR pathway interacts with the insulin signaling pathway to regulate *C. elegans* larval development, metabolism and life span. *Development* 131, 3897–906.

Johnson TE, Wu D, Tedesco P, Dames S & Vaupel JW (2001) Age-specific demographic profiles of longevity mutants in Caenorhabditis elegans show segmental effects. *J. Gerontol. A. Biol. Sci. Med. Sci.* 56, B331–B339.

Jud M, Razelun J, Bickel J, Czerwinski M & Schisa JA (2007) Conservation of large foci formation in arrested oocytes of *Caenorhabditis* nematodes. *Dev. Genes Evol.* 217, 221–6.

Jung T, Bader N & Grune T (2007) Lipofuscin: Formation, distribution, and metabolic consequences. *Ann. N. Y. Acad. Sci.* 1119, 97–111.

Kang C & Avery L (2008) To be or not to be, the level of autophagy is the question: Dual roles of autophagy in the survival response to starvation. *Autophagy* 8, 82–84.

Kang C, You NJ & Avery L (2007) Dual roles of autophagy in the survival of *Caenorhabditis elegans* during starvation. *Genes Dev.* 21, 2161–2171.

Kass LR (1985) *Toward a More Natural Science. Biology and Human Affairs.*, New York: The Free Press.

Kenyon C, Chang J, Gensch E, Rudener A & Tabtiang R (1993) A *C. elegans* mutant that lives twice as long as wild type. *Nature* 366, 461–464.

Kenyon CJ (2010) The genetics of ageing. *Nature* 464, 504–12.

Kim JH, Chu SC, Gramlich JL, Pride YB, Babendreier E, Chauhan D, Salgia R, Podar K, Griffin JD & Sattler M (2005) Activation of the PI3K / mTOR pathway by BCR-ABL contributes to increased production of reactive oxygen species. *Blood* 105, 1717–1724.

Kimble J & Sharrock W (1983) Tissue-specific synthesis of yolk proteins in *Caenorhabditis elegans*. *Dev. Biol.* 96, 189–196.

Kimura KD, Tissenbaum HA, Liu Y & Ruvkun G (1997) *daf-2*, an insulin receptor-Like gene that regulates longevity and diapause in *Caenorhabditis elegans*. *Science (80-.).* 277, 942–946.

Kirkwood TBL (1977) Evolution of ageing. *Nature* 270, 301–304.

Kirkwood TBL & Austad SN (2000) Why do we age? *Nature* 408, 233–238.

Klass M (1983) A method for the isolation of longevity mutants in the nematode *Caenorhabditis elegans* and initial results. *Mech. Ageing Dev.* 22, 279–286.

Klass M & Hirsch D (1976) Non-ageing developmental variant of *Caenorhabditis elegans*. *Nature* 260, 523–525.

Klass MR (1977) Aging in the nematode *Caenorhabditis elegans*: major biological and environmental factors influencing lifespan. *Mech. Ageing Dev.* 6, 413–429.

Klionsky DJ (2007) Autophagy: from phenomenology to molecular understanding in less than a decade. *Nat. Rev. Mol. Cell Biol.* 8, 931–937.

Kostic AD, Gevers D, Pedamallu CS, Kostic AD, Gevers D, Pedamallu CS, Michaud M, Duke F, Earl AM, Ojesina AI, Jung J, Bass AJ, Liu C, Shivdasani RA, Ogino S, Tabernero J, Birren BW, Huttenhower C, Garrett WS & Meyerson M (2012) Genomic analysis identifies association of *Fusobacterium* with colorectal carcinoma. *Genome Res.* 22, 292–298.

Kritikou EA, Milstein S, Vidalain PO, Lettre G, Bogan E, Doukoumetzidis K, Gray P, Chappell TG, Vidal M & Hengartner MO (2006) *C. elegans* GLA-3 is a novel component of the MAP kinase MPK-1 signaling pathway required for germ cell survival. *Genes Dev.* 20, 2279–2292.

Kyriakakis E, Markaki M & Tavernarakis N (2016) *Caenorhabditis elegans* as a model for cancer research. *Mol. Cell. Oncol.* 2, e975027-1-11.

L'Hernault SW (1997) *Spermatogenesis. In C. elegans II chapter. 11.*, New York: Cold Spring Harbor Laboratory Press, Cold Spring Harbor.

de la Guardia Y, Gilliat AF, Hellberg J & Rennert P (2016) Run-on of germline apoptosis promotes gonad senescence in *C . elegans*. *Oncotarget* 7, 39082–96.

Lakowski B & Hekimi S (1998) The genetics of caloric restriction in *Caenorhabditis elegans*. *Proc. Natl. Acad. Sci. U. S. A.* 95, 13091–13096.

Lee M-H, Hook B, Lamont LB, Wickens M & Kimble J (2006) LIP-1 phosphatase controls the extent of germline proliferation in *Caenorhabditis elegans*. *EMBO J.* 25, 88–96.

Leiser SF, Jafari G, Primitivo M, Sutphin GL, Dong J, Leonard A, Fletcher M & Kaeberlein M (2016) Age-associated vulval integrity is an important marker of nematode healthspan. *Age (Omaha).* 38, 419–431.

Libina N, Berman JR & Kenyon C (2003) Tissue-specific activities of *C. elegans* DAF-16 in the regulation of lifespan. *Cell* 115, 489–502.

Lin K, Dorman JB, Rodan A & Kenyon C (1997) *daf-16*: An HNF-3/forkhead family member that can function to double the life-span of *Caenorhabditis elegans*. *Science (80-.).* 278, 1319–1322.

Lints R & Hall DH (2009a) Male Introduction. *WormAtlas*, doi:10.3908/wormatlas.2.1.

Lints R & Hall DH (2009b) Male reproductive system, germ line. *WormAtlas*.

Lints R & Hall DH (2009c) Male reproductive system, somatic gonad. *WormAtlas*.

Lints R & Hall DH (2009d) Reproductive system, germ line. *WormAtlas*.

Longley DB, Harkin DP & Johnston PG (2003) 5-Fluorouracil: Mechanisms of Action and Clinical Strategies. *Nat. Rev. Cancer* 3, 330–338.

Luo S, Kleemann GA, Ashraf JM, Shaw WM & Murphy CT (2010) TGF-b and insulin signaling regulate reproductive aging via oocyte and germline quality maintenance. *Cell* 143, 299–312.

Luo S, Shaw WM, Ashraf J & Murphy CT (2009) TGF-?? Sma/Mab signaling mutations uncouple reproductive aging from somatic aging. *PLoS Genet.* 5, 1–15.

Martínez DE (1998) Mortality patterns suggest lack of senescence in hydra. *Exp. Gerontol.* 33, 217–225.

Maures TJ, Booth LN, Benayoun BA, Izrayelit Y, Schroeder FC & Brunet A (2014) Males shorten the life span of *C. elegans* hermaphrodites via secreted compounds. *Science* 343, 541–4.

McCay C, Crowell M & Maynard L (1935) The effect of retarded growth upon the length of life span and upon the ultimate body size. *J. Nutr.* 10, 63–69.

McCulloch D & Gems D (2003) Evolution of male longevity bias in nematodes. *Aging Cell* 2, 165–173.

McElwee JJ, Schuster E, Blanc E, Thomas JH & Gems D (2004) Shared transcriptional signature in *Caenorhabditis elegans* dauer larvae and long-lived *daf-2* mutants implicates detoxification system in longevity assurance. *J. Biol. Chem.* 279, 44533–43.

McGee MD, Day N, Graham J & Melov S (2012) *cep-1*/p53-dependent dysplastic pathology of the aging *C. elegans* gonad. *Aging (Albany. NY).* 4, 256–69.

McGee MD, Weber D, Day N, Vitelli C, Crippen D, Herndon LA, Hall DH & Melov S (2011) Loss of intestinal nuclei and intestinal integrity in aging *C. elegans*. *Aging Cell* 10, 699–710.

McGhee JD (2007) The *C. elegans* Intestine. *WormBook*. Available at: doi/10.1895/wormbook.1.133.1.

McGovern M, Voutev R, Maciejowski J, Corsi AK & Hubbard EJA (2009) A “latent niche” mechanism for tumor initiation. *Proc. Natl. Acad. Sci. U. S. A.* 106, 11617–22.

Medawar PB (1952) *An Unsolved Problem of Biology*, London: H. K. Lewis.

Melendez A & Levine B (2009) Autophagy in *C. elegans*. *WormBook*. Available at: doi/10.1895/wormbook.1.147.1.

Meléndez A, Tallóczy Z, Seaman M, Eskelinen E-L, Hall DH & Levine B (2003) Autophagy genes are essential for dauer development and life-span extension in *C. elegans*. *Science* 301, 1387–91.

Metzstein MM, Stanfield GM & Horvitz HR (1998) Genetics of programmed cell death in *C. elegans*: past, present and future. *Trends Genet.* 14, 410–416.

Michaelson D, Korta DZ, Capua Y & Hubbard EJA (2010) Insulin signaling promotes germline proliferation in *C. elegans*. *Development* 137, 671–80.

Mitchell D & Stiles J (1979) Synchronous growth and aging of *Caenorhabditis elegans* in the presence of fluorodeoxyuridine. *J. Gerontol.* 34, 28–36.

Morris JZ, Tissenbaum HA & Ruvkun G (1996) A phosphatidylinositol-3-OH kinase family member regulating longevity and diapause in *Caenorhabditis elegans*. *Nature* 382, 536–539.

Mukhopadhyay A & Tissenbaum HA (2007) Reproduction and longevity: secrets revealed by *C. elegans*. *Trends Cell Biol.* 17, 65–71.

Murphy CT, McCarroll S a, Bargmann CI, Fraser A, Kamath RS, Ahringer J, Li H & Kenyon C (2003) Genes that act downstream of DAF-16 to influence the lifespan of *Caenorhabditis elegans*. *Nature* 424, 277–283.

Narita M, Young ARJ, Arakawa S, Samarajiwa SA, Nakashima T, Yoshida S, Hong S, Berry LS, Reichelt S, Ferreira M, Tavaré S, Inoki K, Shimizu S & Narita M (2011) Spatial coupling of mTOR and autophagy augments secretory phenotypes. *Science* 332, 966–70.

Naylor R, Richardson SJ & McAllan BM (2008) Boom and bust: A review of the physiology of the marsupial genus Antechinus. *J. Comp. Physiol. B* 178, 545–562.

Nicholas H & Hodgkin J (2004) The ERK MAP kinase cascade mediates tail swelling and a protective response to rectal infection in *C. elegans*. *Curr. Biol.* 14, 1256–1261.

Ogg S, Paradis S, Gottlieb S, Patterson GI, Lee L, Tissenbaum HA & Ruvkun G (1997) The Fork head transcription factor DAF-16 transduces insulin-like metabolic and longevity signals in *C. elegans*. *Nature* 389, 994–9.

Omenn GS, Goodman GE, Thornquist MD, Balmes J, Cullen MR, Glass A, Keogh JP, Meyskens Jr. FL, Valanis B, Williams Jr. JH, Barnhart S, Cherniack MG, Brodkin CA & Hammar S (1996) Risk factors for lung cancer and for intervention effects in CARET, the beta-carotene and retinol efficacy trial. *J. Natl. Cancer Inst.* 88, 1550–1559.

Orr W & Sohal R (1994) Extension of life-span by overexpression of superoxide dismutase and catalase in *Drosophila melanogaster*. *Science.* 263, 1128–1130.

Partridge L & Gems D (2002) Mechanisms of Ageing: Public or Private? *Nat. Rev. Genet.* 3, 165–175.

Pérez VI, Van Remmen H, Bokov A, Epstein CJ, Vijg J & Richardson A (2009) The overexpression of major antioxidant enzymes does not extend the lifespan of mice. *Aging Cell* 8, 73–5.

Peters MA, Teramoto T, White JQ, Iwasaki K & Jorgensen EM (2007) A calcium wave mediated by gap junctions coordinates a rhythmic behavior in *C. elegans*. *Curr. Biol.* 17, 1601–1608.

Pickett CL & Kornfeld K (2013) Age-related degeneration of the egg-laying system promotes matricidal hatching in *Caenorhabditis elegans*. *Aging Cell* 12, 544–553.

Pinkston-Gosse J & Kenyon C (2007) DAF-16/FOXO targets genes that regulate tumor growth in *Caenorhabditis elegans*. *Nat. Genet.* 39, 1403–1409.

Pinkston J, Garigan D, Hansen M & Kenyon C (2006) Mutations that increase the life span of *C. elegans* inhibit tumor growth. *Science.* 313, 971–976.

Podshivalova K, Kerr RA & Kenyon C (2017) How a mutation that slows aging can also disproportionately extend end-of-life decrepitude. *Cell Rep.* 19, 441–450.

Portal-Celhay C, Bradley ER & Blaser MJ (2012) Control of intestinal bacterial proliferation in regulation of lifespan in *Caenorhabditis elegans*. *BMC Microbiol.* 12, 49.

Pujol N, Cypowyj S, Ziegler K, Millet A, Astrain A, Goncharov A, Jin Y, Chisholm AD & Ewbank JJ (2008) Distinct innate immune responses to infection and wounding in the *C. elegans* epidermis. *Curr. Biol.* 18, 481–489.

Van Raamsdonk JM & Hekimi S (2011) FUdR causes a twofold increase in the lifespan of the mitochondrial mutant *gas-1*. *Mech. Ageing Dev.* 132, 519–21.

Van Raamsdonk JM & Hekimi S (2012) Superoxide dismutase is dispensable for normal animal lifespan. *Proc Natl Acad Sci* 109, 5785–5790.

Raizen DM, Lee RYN & Avery L (1995) Interacting genes required for pharyngeal excitation by motor neuron MC in *Caenorhabditis elegans*. *Genetics* 141, 1365–1382.

Reggiori F, Tucker KA, Stromhaug PE & Klionsky DJ (2004) The Atg1-Atg13 complex regulates Atg9 and Atg23 retrieval transport from the pre-autophagosomal structure. *Dev. Cell* 6, 79–90.

Rera M, Bahadorani S, Cho J, Koehler CL, Ulgherait M, Hur JH, Ansari WS, Jr T Lo, Jones DL & Walker DW (2011) Modulation of longevity and tissue homeostasis by the *Drosophila* PGC-1 homolog. *Cell Metab.* 14, 623–634.

Riddle D (1988) *The Nematode Caenorhabditis elegans*, New York: Cold Spring Habour Laboratory Press.

Riddle D, Swanson MM & Albert PS (1981) Interacting genes in nematode dauer larva formation. *Nature* 290, 668–671.

Riesen M, Feyst I, Rattanavirotkul N, Ezcurra M, Tullet JM a, Papatheodorou Y, Ziehm M, Au C, Gilliat AF, Hellberg J, Thornton JM & Gems D (2014) MDL-1, a growth- and tumor-suppressor, slows aging and prevents germline hyperplasia and hypertrophy in *C. elegans*. *Aging (Albany. NY).* 6, 1–20.

Ruckdeschel J, Codish S, Stranahan A & McKneally M (1972) Postoperative empyema improves survival in lung cancer. *N. Engl. J. Med.* 287, 1013–1017.

Rutkowski R, Dickinson R, Stewart G, Craig A, Schimpl M, Keyse SM & Gartner A (2011) Regulation of *Caenorhabditis elegans* p53/*cep-1*-dependent germ cell apoptosis by ras/mapk signaling. *PLoS Genet.* 7, e1002238.

van der Sar AM, Musters RJP, van Eeden FJM, Appelmelk BJ, Vandenbroucke-Grauls CMJE & Bitter W (2003) Zebrafish embryos as a model host for the real time analysis of *Salmonella typhimurium* infections. *Cell. Microbiol.* 5, 601–611.

Schulenburg H, Kurz CL & Ewbank JJ (2004) Evolution of the innate immune system: the worm perspective. *Immunol. Rev.* 198, 36–58.

Schumacher B, Hanazawa M, Lee MH, Nayak S, Volkmann K, Hofmann R, Hengartner M, Schedl T & Gartner A (2005) Translational repression of *C. elegans* p53 by GLD-1 regulates DNA damage-induced apoptosis. *Cell* 120, 357–368.

Schumacher B, Hofmann K, Boulton S & Gartner A (2001) The *C. elegans* homolog of the p53 tumor suppressor is required for DNA damage-induced apoptosis. *Curr. Biol.* 11, 1722–1727.

Schumacher B, Schertel C, Wittenburg N, Tuck S, Mitani S, Gartner A, Conradt B & Shaham S (2005) *C. elegans ced-13* can promote apoptosis and is induced in response to DNA damage. *Cell Death Differ.* 12, 153–61.

Schuster E, McElwee JJ, Tullet JMA, Doonan R, Matthijssens F, Reece-Hoyes JS, Hope IA, Vanfleteren JR, Thornton JM & Gems D (2010) DamID in *C. elegans* reveals longevity-associated targets of DAF-16/FoxO. *Mol. Syst. Biol.* 6, 399.

Seydoux G, Schedl T & Greenwald I (1990) Cell-cell interactions prevent a potential inductive interaction between soma and germline in *C. elegans*. *Cell* 61, 939–951.

Shaham S (2006) Methods in Cell Biology. *WormBook*.

Shapiro MD & Fazio S (2016) From lipids to inflammation: New approaches to reducing atherosclerotic risk. *Circ. Res.* 118, 732–749.

Sharrock WJ, Sutherlin ME, Leske K, Cheng TK & Kim TY (1990) Two distinct yolk lipoprotein complexes from *Caenorhabditis elegans*. *J. Biol. Chem.* 265, 14422–14431.

Shaye DD & Greenwald I (2011) Ortholist: A compendium of *C. elegans* genes with human orthologs. *PLoS One* 6.

Shen M & Hodgkin J (1988) *mab-3*, a gene required for sex-specific yolk protein expression and a male-specific lineage in *C. elegans*. *Cell* 54, 1019–1031.

Shi C & Murphy CT (2014) Mating induces shrinking and death in *Caenorhabditis* mothers. *Science* 343, 536–40.

Shintani T & Klionsky DJ (2004) Autophagy in health and disease: a double-edged sword. *Science (80-.).* 306, 990–995.

Sohal RS, Agarwal S & Sohal BH (1995) Oxidative stress and aging in the Mongolian gerbil (*Meriones unguiculatus*). *Mech Ageing Dev* 81, 15–25.

Sohal RS, Sohal BH & Orr WC (1995) Mitocondrial superoxide and hydrogen peroxide generation, protein oxidative damage, and longevity in different species of flies. *Free Radic. Biol. Med.* 19, 499–504.

Sohal RS & Weindruch R (1996) Oxidative stress, caloric restriction, and aging. *Science (80-.).* 273, 59–63.

Stadtman ER (1992) Protein oxidation and aging. *Science (80-.).* 257, 1220–1224.

Stewart EJ, Madden R, Paul G & Taddei F (2005) Aging and death in an organism that reproduces by morphologically symmetric division. *PLoS Biol.* 3, 295–300.

Sulston JE & Horvitz HR (1977) Post-embryonic cell lineages of the nematode, *Caenorhabditis elegans*. *Dev Biol* 56, 110–156.

Sun J, Folk D, Bradley TJ & Tower J (2002) Induced overexpression of mitochondrial Mn-superoxide dismutase extends the life span of adult *Drosophila melanogaster*. *Genetics* 161, 661–72.

Sun J & Tower J (1999) FLP recombinase-mediated induction of Cu / Zn-superoxide dismutase transgene expression can extend the life span of adult *Drosophila melanogaster* flies. *Mol. Cell. Biol.* 19, 216–228.

Szewczyk NJ, Kozak E & Conley CA (2003) Chemically defined medium and *Caenorhabditis elegans*. *BMC Biotechnol.* 3, 1–7.

Tabara H, Grishok A & Mello CC (1998) RNAi in *C. elegans*: soaking in the genome sequence. *Science (80-.).* 282, 430–431.

Tank EMH, Rodgers KE & Kenyon C (2011) Spontaneous age-related neurite branching in *Caenorhabditis elegans*. *J. Neurosci.* 31, 9279–88.

Tenor JL & Aballay A (2008) A conserved Toll-like receptor is required for *Caenorhabditis elegans* innate immunity. *EMBO Rep.* 9, 103–9.

Tian E, Wang F, Han J & Zhang H (2009) *epg-1* functions in autophagy-regulated processes and may encode a highly divergent Atg13 homolog in *C. elegans*. *Autophagy* 5, 608–615.

Timmons L, Court DL & Fire A (2001) Ingestion of bacterially expressed dsRNAs can produce specific and potent genetic interference in *Caenorhabditis elegans*. *Gene* 263, 103–112.

Timmons L & Fire a (1998) Specific interference by ingested dsRNA. *Nature* 395, 854.

Tower J (2015) Programmed cell death in aging. *Ageing Res. Rev.* 23, 90–100.

Tullet JMA (2015) DAF-16 target identification in *C. elegans*: past, present and future. *Biogerontology* 16, 221–234.

Tullet JMA, Hertweck M, An JH, Baker J, Hwang JY, Liu S, Oliveira RP, Baumeister R & Blackwell TK (2008) Direct inhibition of the longevity-promoting factor SKN-1 by insulin-like signaling in *C. elegans*. *Cell* 132, 1025–1038.

Ulbright TM (2005) Germ cell tumors of the gonads: a selective review emphasizing problems in differential diagnosis, newly appreciated, and controversial issues. *Mod. Pathol.* 18 Suppl 2, S61-79.

Vaupel JW, Johnson TE & Lithgow GJ (1994) Rates of mortality in populations of *Caenorhabditis elegans*. *Science.* 266, 826.

Veal EA, Day AM & Morgan BA (2007) Hydrogen Peroxide Sensing and Signaling. *Mol. Cell* 26, 1–14.

Vellai T, Takacs-Vellai K, Zhang Y, Kovacs AL, Orosz L & Müller F (2003) Genetics: influence of TOR kinase on lifespan in *C. elegans*. *Nature* 426, 620.

Walker G, Houthoofd K, Vanfleteren JR & Gems D (2005) Dietary restriction in *C. elegans*: From rate-of-living effects to nutrient sensing pathways. *Mech. Ageing Dev.* 126, 929–937.

Ward S & Carrel JS (1979) Fertilization and sperm competition in the nematode *Caenorhabditis elegans*. *Dev. Biol.* 73, 304–21.

Williams G (1957) Pleiotropy, natural selection, and the evolution of senescence. *Evolution (N. Y).* 11, 398–411.

Wolke U, Jezuit E a & Priess JR (2007) Actin-dependent cytoplasmic streaming in *C. elegans* oogenesis. *Development* 134, 2227–2236.

Woodruff GC, Knauss CM, Maugel TK & Haag ES (2014) Mating damages the cuticle of *C. elegans* hermaphrodites. *PLoS One* 9, e104456.

Yi W, Ross J & Zarkower D (2000) *mab-3* is a direct *tra-1* target gene regulating diverse aspects of *C. elegans* male sexual development and behavior. *Development* 4480, 4469–4480.

Yuan J, Shaham S, Ledoux S, Ellis HM & Horvitz HR (1993) The *C. elegans* cell death gene *ced-3* encodes aprotein similar to mammalian interleukin-1 beta-converting enzyme. *Cell* 75, 641–652.

Yuan J, Tirabassi R, Bush A & Cole M (1998) The *C. elegans* MDL-1 and MXL-1 proteins can functionally substitute for vertebrate MAD and MAX. *Oncogene* 17, 1109–1118.

Zhao Y, Gilliat AF, Ziehm M, Turmaine M, Wang H, Ezcurra M, Yang C, Phillips G, McBay D, Zhang WB, Partridge L, Pincus Z and Gems D, 2017. Two forms of death in ageing *Caenorhabditis elegans*. Nature Comm. 23,8.

Zhuang JJ & Hunter CP (2011) RNA interference in *Caenorhabditis elegans*: Uptake, mechanism, and regulation. *Parasitology* 139, 560–573.

Zimmerman SM, Hinkson I V, Elias JE & Kim SK (2015) Reproductive aging drives protein accumulation in the uterus and limits lifespan in *C. elegans*. *PLoS Genet.* 11, 1–31.

Zou H, Henzel WJ, Liu X, Lutschg A & Wang X (1997) Apaf-1, a human protein homologous to *C. elegans* CED-4, participates in the cytochrome c-dependent activation of caspase-3. *Cell* 90, 405–413.